SPECIAL REPORT No. 5
GEOLOGICAL SURVEY OF JAPAN

EXPLOSION SEISMIC STUDIES OF THE MATSUSHIRO EARTHQUAKE SWARM AREA

GEOLOGICAL SURVEY OF JAPAN
Hisamoto-cho, Kawasaki-shi, Japan
1969

550.348.436.098.62(521.52)

SPECIAL REPORT No. 5

GEOLOGICAL SURVEY OF JAPAN

Konosuke SATO, Director

EXPLOSION SEISMIC STUDIES OF THE MATSUSHIRO EARTHQUAKE SWARM AREA

CONTENTS

550.343:550.348.436.098.62(521.52)

PART I

EXPLOSION SEISMIC OBSERVATIONS IN THE MATSUSHIRO EARTHQUAKE SWARM AREA

By

Shuzo ASANO, Kanenori ICHIKAWA, Hiroshi OKADA, Susumu KUBOTA, Hiroyoshi SUZUKI, Mitsuo NOGOSHI, Hideo WATANABE, Kiyoshi SEYA, Kazuo NORITOMI and Kyozi TAZIME

Explosion Seismic Observations in the Matsushiro Earthquake Swarm Area

By

Shuzo ASANO*, Kanenori ICHIKAWA**, Hiroshi OKADA***, Susumu KUBOTA*, Hiroyoshi SUZUKI†, Mitsuo NOGOSHI††, Hideo WATANABE†††, Kiyoshi SEYA**, Kazuo NORITOMI†† and Kyozi TAZIME***

Abstract

Explosion seismic observations in the Matsushiro Earthquake Swarm Area were conducted in the period of November 14—December 7, 1967 for two profiles A and B to obtain the velocity structure for the determination of hypocenters, some information on the physical status of the hypocentral region and so on. For the observation, the nineteen parties were organized, the fourteen parties of which made use of magnetic tape recorders and the five parties of which were equipped with 24-element seismic prospecting instruments. Profile A is set up near the western end of the Central Belt of Uplift, one of the geological blocks, and almost parallel to its strike, NE-SW. It is about 65.5 km in length and there are five shot points. Profile B intersects profile A at a point north of Matsushiro, Nagano City with the angle of about 63° and crosses the epicentral area of Matsushiro swarm earthquakes. It is about 47 km in length from Togakushi Village, Kamiminochi Gun to the east of Ueda City and there are four shot points. The dynamite of 171 ~ 499 kg were fired in 1 ~ 4 shot holes with the depth of 30 ~ 45 m and with the inner diameter of 10 cm.

Explosions and their seismic observations were carried out at midnight when the noise level was usually lowest. The Japanese standard time signal (JJY) was used as time signal both at shot points and observation points because lengths of profiles were too long for observation parties to contact with each other. Generally speaking, seismograms obtained are of good quality except for minor parts. Especially most of seismograms obtained by parties with magnetic tape recorders give clear onsets. The time of commencement of initial P wave was classified into three grades, A, B, C by taking the clearness of the onset, time accuracy, etc. into account. In this paper the observations and explosions are described and the data obtained by this experiment are presented.

I. Introduction

The Matsushiro Earthquake Swarm, which took place on August 3, 1965 in Matsushiro, Nagano City, has not come to an end yet in spite of the lapse of time more than three years although the seismic activity has become weaker. First the hypocentral area of this earthquake swarm had been limited to the vicinity of the Seismological Observatory, Japan Meteorological Agency, where the observation by USCGS standard seismometers was just started. Therefore, variation of seismic activity has been observed in quite detail. Since the Matsushiro earthquake swarm has been active for a long time in a limited area on land, almost all kinds of investigations were conducted in cooperation with the institutions and universities concerned[2] as a test field for the earthquake prediction program just started financially. Through those investigations, the following results seem to be especially important:

* Earthquake Research Institute, University of Tokyo. S. Asano was a research associate of Geological Survey of Japan.
** Geological Survey of Japan. K. Seya is now in the Faculty of Science, Okayama University.
*** Hokkaido University. H. Okada and K. Tazime were research associates of Geological Survey of Japan.
† National Research Center for Disaster Prevention, Science and Technology Agency.
†† Akita University. K. Noritomi is a research associate of Geological Survey of Japan.
††† Japan Meteorological Agency.

(1) There are five main stages of seismic activity and the hypocentral region has expanded gradually[3),5),8)].
(2) The hypocentral region has been confined to the Central Belt of Uplift, one of the geological blocks, although the hypocentral region has been expanding[3),10),14)].
(3) The distribution of the initial motion of P waves for almost all felt shocks is of quadrant type and the predominant direction of principal pressure is east-west[7)].
(4) The results from the investigation of earthquake mechanisms agree with those of crustal movement in such measurements as electro-optical[9)], levelling[16)], tilting[4)], etc.
(5) A close relation is observed between the crustal movement and such features of geological structure as the Central Belt of Uplift, earthquake fault, etc[10),11)].

These results contribute to the understanding of the geophysical and geological processes included in the Matsushiro earthquake swarm. Furthermore, as regards the determination of hypocenters, a systematic discrepancy is found to exist between the hypocenters determined by the tripartite stations of Earthquake Research Institute in Sanada, Kamimuroga, Asakawa and those, by the network surrounding the hypocentral area[6),12)].

On the other hand in connection with the underground structure in the swarm area such surveys as gravity[14)], electricity[13)], etc. were carried out by the Geological Survey of Japan and the airborne magnetic survey, by TAKAGI and others[15)]. The data obtained by the former methods are related to fairly shallow structure. In addition to the requirement on the accurate information of velocity structures from the standpoint of hypocenter determination, the necessity to obtain the data on the deeper underground structure had been augmented in order to understand the phenomena of expanding hypocentral region. In the early stage of this earthquake swarm, eager desire had occurred among the scientists concerned to conduct detailed explosion seismic studies in the narrow hypocentral region on land for the purpose of obtaining the data to the relation between the physical process and the underground structure, the physical status in the hypocentral region, the examination of accuracy of hypocenter determination. However, this desire had to be postponed until the seismic activity tends to decay because of the unrest of inhabitants due to numerous felt earthquakes, and of the possibility of masking the explosion seismic signals by the disturbance of natural earthquakes. Since there appeared the tendency of decrease in seismic activity around the end of 1966, cooperative investigation group was organized by the institutions or universities concerned under the sponser of Geological Survey of Japan. Besides Geological Survey of Japan, Japan Meteorological Agency, National Research Center for Disaster Prevention, Hokkaido University, Akita University, and Earthquake Research Institute, University of Tokyo participated in this project. The cooperative experiment was carried out in the period from November 14 to December 7, 1967 under the Adjustment Fund for Promotion of Special Studies, Science and Technology Agency. The boring of shot holes, shooting operations, measurement of shot time, the observation of explosion seismic signals by five 24 element seismic prospecting instruments and survey of positions of shot points and geophones were carried out by Ube Industries, Ltd. by contract.

In this paper, the shooting operations, the system of observations, etc. will be described and the basic data such as the shot time, travel times of the initial P waves, the distance, etc. will be presented. The results of analysis based upon these data will be given in the other paper[1)].

II. Profiles and Shot Points

In Fig. 1 the distribution of hypocenters in the period from October 1965 to October 1967 determined by the temporary network of Earthquake Research Institute, University of Tokyo is presented[3)]. In the so-called 4-th stage the hypocentral region became larger than in the preceding stages, that is, the focal depth had increased and the epicentral area had expanded. Taking the expanded hypocentral region and the geological features in this region into account, two profiles, A and B, were selected. These profiles are shown with the shot points in Fig. 2. Profile A runs in the Central Belt of Uplift and has the length of 65.5 km between Yamanouchi Town, Shimotakai Gun and Shiga Village, Higashichikuma Gun so that the information of the underground structure to the depth of some ten kilometers may be obtained. The profile runs a little west of the central part of hypocentral area, the southern part of which is especially mountainous. Profile B is set up across the strike of the geological structure through the central part of hypocentral area and has the length of about 47 km from Togakushi Village, Kamiminochi Gun to the east of Ueda City. This profile intersects profile A at a point north of Matsushiro with the angle of about 63° and also the density of observation sites becomes sparse around both ends of the profile because of the mountainous topography as profile A.

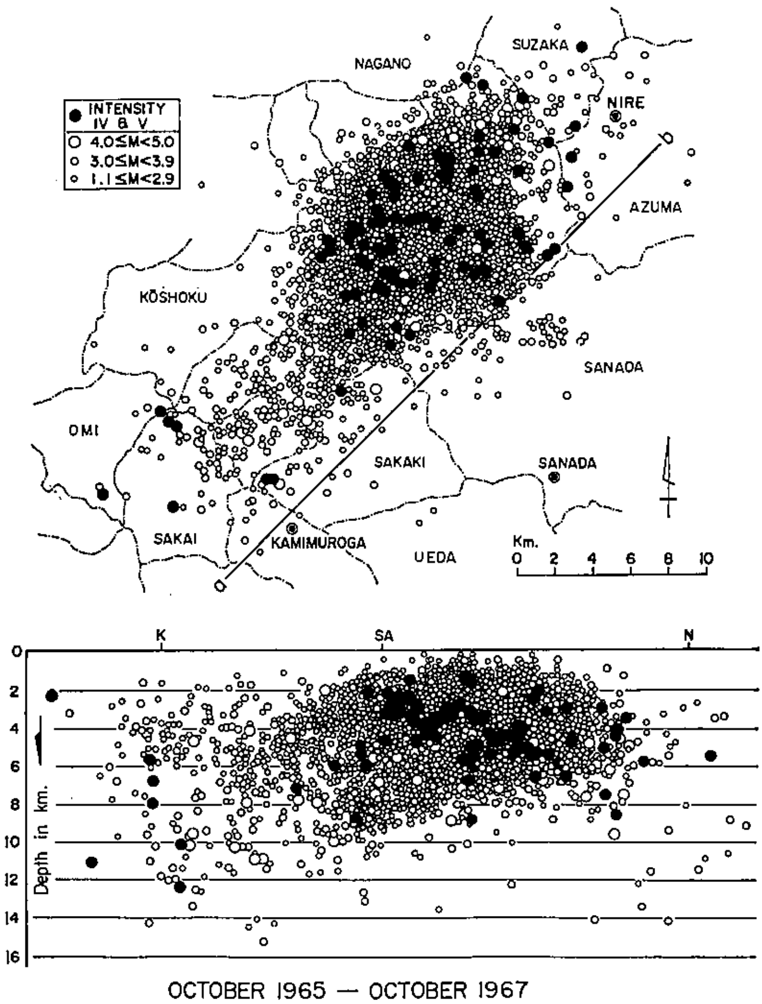

Fig. 1 Distribution of hypocenters of the felt earthquakes in the period October 1965—October 1967. a–b: Plane of projection, K: Kamimuroga, N: Nire, SA: Sanada (After HAGIWARA and IWATA[3])

There are five shot points, I-V, in profile A and four shot points, I-IV, in profile B for long distance. At each shot point, one to four holes with the diameter 10 cm were made depending upon the scheduled amount of explosives. The columnar sections of each shot hole are shown in Fig. 3. The dynamite with the diameter of 85 mm, the length of 668 mm and the weight of 4.5 kg was mainly used and the electric cap for seismic prospecting was used. Effective utilization of small shots for enlarging the bottom of shot hole were made to provide for repetition of shot in case of the obstruction of natural earthquakes or any failure of operations. The shot time, the depth of shot hole, charge size, etc. are given in Table 1. In addition to the data of 13 shots for long distance, the details of explosions for measurement of velocity in the surface layers (9 shots) and for enlarging the bottom of shot holes (17 shots) are also given in Table 1. For measurements of velocity in the surface layers there is one additional shot point in profile A and there are four in profile B. Their locations are shown by small cross marks in Fig. 2.

There are four additional large explosions for the long profiles. Two of them, shots at B-III and at A-V, were fired since one party had some troubles with instruments in the first shots. While shots at A-IV and at B-IV for profile A have special purposes. That is, the shot at B-IV of profile A is a kind of fan shooting in order to find out any possible anomalous travel times; the shot at A-IV was repeated to see the accuracy of measurement of travel times under almost the same conditions. The shot at A-IV was conducted by the Earthquake Research Institute with the cooperation of participating institutions and universities as a first step for future repetition of part of experiment in this region where there was the Hokushin Observatory of Microearthquakes and Crustal Deformation, Earthquake Research Institute.

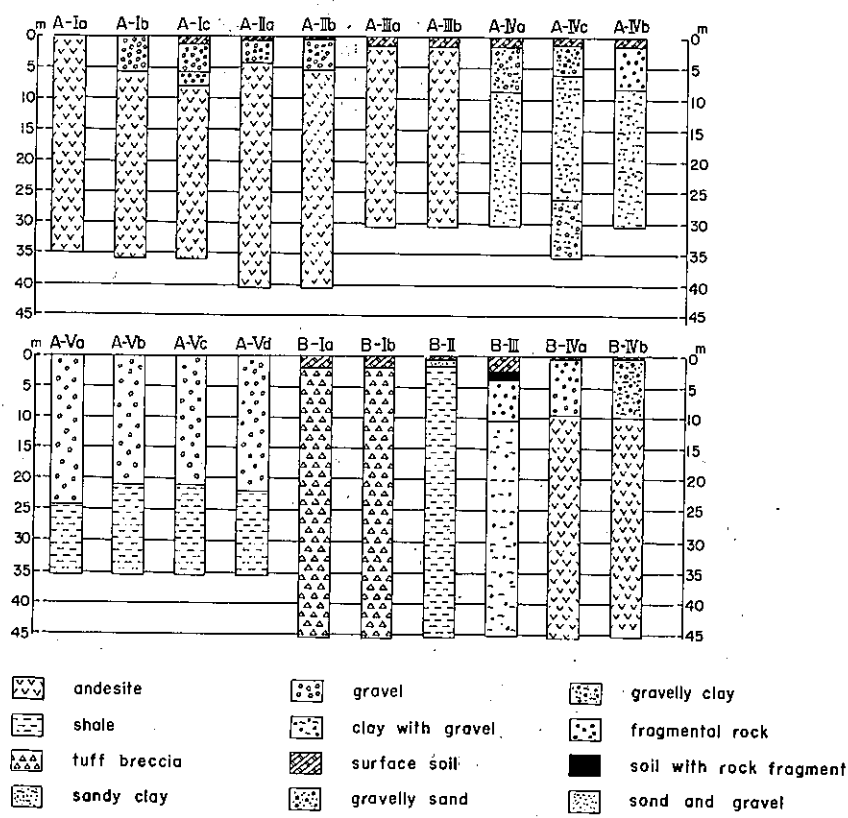

Fig. 3 Columnar sections of shot holes

Table 1 (a) Shot time, depth of shot hole, charge size, etc. for large shots

Date	Shot time			Shot hole	Depth of shot hole	Charge size	Charge length	No. of cap	Total amount of charge
1967	h	m	s		m	kg	m		kg
Nov. 21	1	48	0.111	B-II	45.0	171.0	13.0	1	
Nov. 21	2	48	0.400	B-III	45.0	175.5	4.0	2	
Nov. 23	1	48	0.038	B-I-A	45.0	180.0	15.7	2	} 292.5
Nov. 23	1	48	0.038	B-I-B	45.0	112.5	15.0	2	
Nov. 23	2	48	0.401	B-IV-B	45.0	306.0	17.5	10	
Nov. 24	1	48	0.399	B-III	40.0	171.0	22.5	3	
Nov. 30	1	05	0.098	A-II-A	40.0	144.0	16.5	2	} 288
Nov. 30	1	05	0.098	A-II-B	40.0	144.0	17.0	3	
Nov. 30	2	05	0.138	A-V-B	35.0	139.5	15.0	2	} 499.5
Nov. 30	2	05	0.138	A-V-C	35.0	202.5	12.0	1	
Nov. 30	2	05	0.138	A-V-D	35.0	157.5	13.0	1	
Nov. 30	3	05	0.121	A-III-B	30.0	186.75	15.0	4	
Dec. 2	2	04	59.988	A-I-A	35.0	135.0	19.0	2	} 405
Dec. 2	2	04	59.988	A-I-B	35.0	135.0	26.0	2	
Dec. 2	2	04	59.988	A-I-C	35.0	135.0	24.0	2	
Dec. 2	3	05	0.326	A-IV-B	30.0	166.5	0.5	3	} 324
Dec. 2	3	05	0.326	A-IV-C	35.0	157.5	3.5	2	
Dec. 4	1	04	59.999	A-IV-A	30.0	112.5	9.0	2	} 324
Dec. 4	1	04	59.999	A-IV-B	27.0	67.5	8.0	2	
Dec. 4	1	04	59.999	A-IV-C	29.0	144.0	14.0	2	
Dec. 4	2	05	0.093	A-V-A	30.0	161.0	15.0	3	} 404.5
Dec. 4	2	05	0.093	A-V-B	19.0	121.0	10.0	2	
Dec. 4	2	05	0.093	A-V-C	19.0	122.5	10.0	3	
Dec. 4	3	05	0.010	B-IV-A	45.0	166.5	1.0	2	} 234
Dec. 4	3	05	0.010	B-IV-B	27.5	67.5	12.5	4	

Table 1 (b) Position of shot point

Shot point	Longitude (E)	Latitude (N)	Height (m)
A–I	138°27′02″	36°48′08″	788
II	138 20 34	36 42 12	333
III	138 14 21	36 35 37	347
IV	138 07 59	36 29 32	369
V	137 59 35	36 20 30	609
B–I	138 06 03	36 46 22	1162
II	138 09 40	36 40 21	564
III	138 14 13	36 31 52	524
IV	138 18 50	36 23 16	596

Table 1 (c) Shot time, depth of shot hole, charge size, etc. for shots for measurement of velocity in surface layers

Date	Shot time	Spread	Shot point	Depth of shot hole	Charge size	Charge length	No. of cap
	h m s			m	kg	m	
Nov. 18	12 45 5.429	E_5	B–III	45.0	4.5	0.68	1
Nov. 19	1 48	E_5	E_5–W_1	1.5	2.0	0.2	20
Nov. 24	0 01 0.207	E_1	E_2–W_1	1.5	2.0	0.2	10
Nov. 24	1 01 0.295	E_2, E_3	E_2–W_2	1.5	2.0	0.2	10
Nov. 24	2 01 0.227	E_3, E_4	E_4–W_1	1.5	2.0	0.2	10
Nov. 24	3 01 0.702	E_4, E_5	E_4–W_2	1.5	2.0	0.2	10
Nov. 24	16 41 0.059	E_2	E_2–W_1	1.5	1.0	0.1	5
Nov. 28	13 15 0.096	E_3	A–III	30.0	4.5	0.68	1
Nov. 29	1 04 59.774	E_2, E_3, E_1	E_3–W_1	1.5	2.0	0.2	10

Table 1 (d) Shot time, depth of shot hole, charge size, etc. for shots for enlarging the bottom of shot holes

Date	Shot time	Shot point	Depth of shot hole	Charge size	Charge length	No. of cap
	h m s		m	kg	m	
Nov. 18	12 45 5.429	B–III	45.0	4.5	0.68	1
Nov. 18	13 30	B–I	45.0	4.5	1.40	1
Nov. 19	10 00	B–II	45.0	4.5	0.68	1
Nov. 19	11 00	B–II	45.0	4.5	0.68	1
Nov. 19	11 50	B–II	45.0	4.5	0.68	1
Nov. 19	10 45	B–III	45.0	4.5	0.68	1
Nov. 21	10 05	B–IV–A	45.0	4.5	0.68	1
Nov. 21	16 30	B–IV–B	45.0	4.5	0.68	2
Nov. 22	10 20	B–I–A	45.0	4.5	0.68	1
Nov. 26	13 15	A–V–C	35.0	4.5	0.68	1
Nov. 26	14 00	A–V–D	35.0	4.5	0.68	1
Nov. 28	10 50	A–IV–A	35.0	4.5	0.68	1
Nov. 28	11 40	A–IV–B	30.0	4.5	0.68	1
Nov. 28	13 15 0.096	A–III–B	30.0	4.5	0.68	1
Nov. 28	14 35	A–III–B	30.0	4.5	0.68	1
Nov. 29	10 42	A–III–A	30.0	2.25	0.35	1
Nov. 29	12 30	A–V–B	35.0	4.5	0.68	1

III. Observations

All shots were fired at midnight ($1^h05^m \sim 3^h05^m$ a.m.) when the noise level was usually lowest. Also the schedule of shot was determined by taking the railway schedule into account. To obtain the velocity near each shot point, several geophones were distributed on the line at about 30 m interval and the signals from these geophones were recorded on the same recording paper with the shot instant. In Fig. 4 the positions of geophones are given at each shot point. Since the total length of profile was long, the absolute time, that is, JJY signal was recorded at observation sites as well as at shot points. The accurate crystal clock was always calibrated at each observation site to provide for unexpected fading of JJY signals.

The locations of each observation site are shown in Fig. 2. In this figure, D_1, D_2, ... stand for the parties equipped with magnetic tape recorders (abbreviated as D party) and fourteen D parties were organized by the members of participating institutions or universities. D with smaller suffix means that this observation site is closer to shot point I. That is, D_5 is closer to shot point I than D_8. E_1, E_2, ... stand for the parties of Ube Industries, Ltd. equipped with the seismic prospecting instruments. In Table 2, the magnetic tape recorders used by each observation party and observers are given. Each party tried to select the observation sites with low noise level as close to the scheduled line as possible. However, since it was necessary to have fairly dense distribution of geophones on the profile, the observation sites were sometimes in the rice fields or in the apple orchards with fairly high noise level, especially for seismic prospecting instruments as expected.

In D parties, the same system of observation with that of the Research Group for Explosion Seismology was adopted. Magnetic tape recorders used were mostly of type SONY FMA-23S, MA-33-4S with flat response for D.C.-250 cps. Three geophones were used by each observation party. Two geophones were of vertical type with natural frequency 4 cps and voltage sensitivity about 0.7 volt/kine. One geophone was of vertical type with natural frequency 1 cps and voltage sensitivity about 2.5 volt/kine. The interval of geophones in each observation party was about 400 m. The geophone of 1 cps was put between two 4 cps geophones. Three positions in each party were called point a, b, and c from the side of shot point I. Amplifiers have flat response for $0.5 \sim 200$ cps and have maximum gain about 100 dB. The final frequency characteristics for total system are uniform in velocity for approximate band $4 \sim 100$ cps. Observations were carried out with the gain of $80 \sim 100$ dB and the noise level was several-several 10 μkine. In both profiles on the whole the noise level for the central parts of the profiles was relatively high, and on the both sides, especially on the southern sides of profiles the noise level was lower because of outcrop of rocks. The same way of setting geophones both on the rock and on the ground was adopted through all D parties. When the 4 cps vertical geophone of a cylindrical shape was set on the rock, it was put into the cylinder which was fixed with cement to the rock and stuffing was packed between geophone and cylinder. This device was applied for preventing geophones from vibration of higher order or instability. The 1 cps geophone was simply put on the rock and mostly on the cement-levelled surface of rock. When the ground surface was soft as in the rice field, the hole ($30 \sim 50$ cm in depth) was dug until fairly hard mixture of soil and stone appeared and then the same way mentioned above was applied.

In the beginning of experiment, simultaneous recording of noise and forced vibration caused by weight dropping was carried out by all D parties to obtain relative magnification between each observation system. Also to calibrate all amplifiers by the same instruments, one calibration party visited twice all D parties in each profile.

In addition to the observation of explosion seismic waves, simultaneous continuous observation of microearthquakes with magnetic tape recorders was carried out at midnight, 11^h p.m. $\sim 3^h30^m$ a.m., by D parties to investigate the variation of seismicity through the profile and other problems by using natural earthquakes. This kind of observation was done for 6 days in profile A and for 7 days

A I

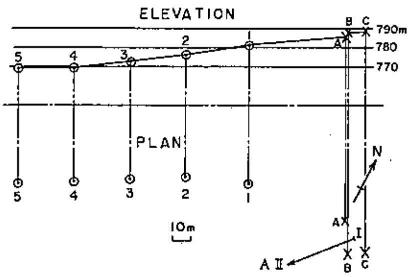

A II

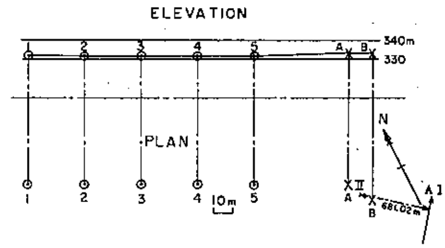

A III

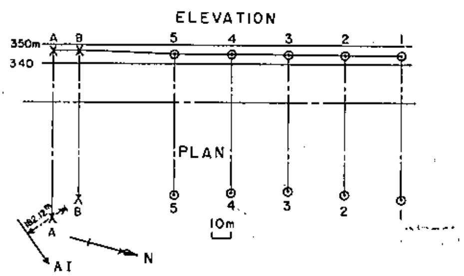

A IV

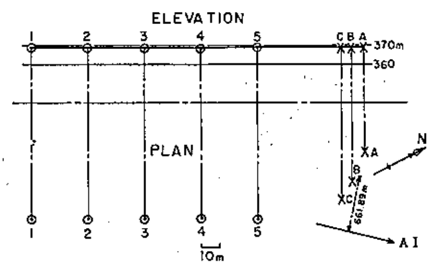

A V

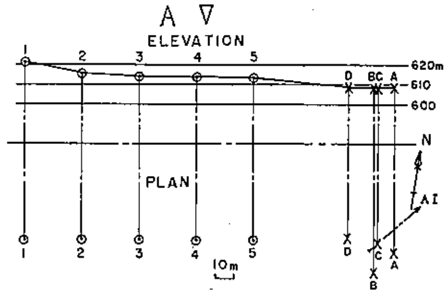

B I

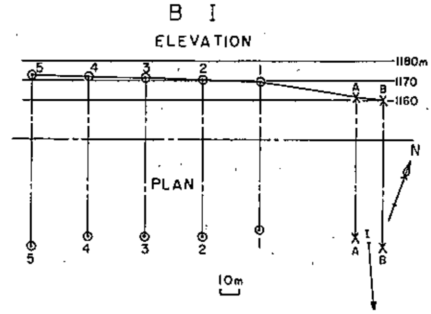

B II

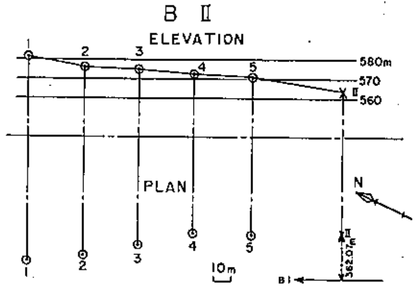

B III

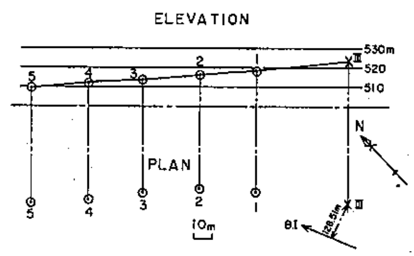

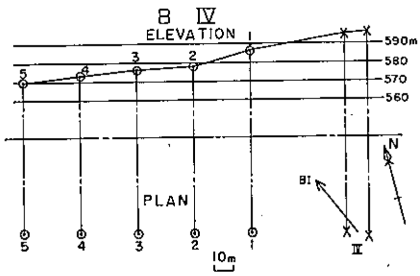

Fig. 4 Geophones near each shot point

in profile B and many microearthquakes, more than one shock per minute in a few observation parties, were registered. The 1 cps vertical geophone was changed by the 1 cps horizontal geophone for observation of natural earthquakes to identify S wave clearly. The investigation by using natural earthquakes will be presented separately in near future.

As mentioned previously, technicians of Ube Industries, Ltd. took observations with five 24 element seismic prospecting instruments in their charge. Vertical geophones of Mark Product Company were used, which have voltage sensitivity about 0.4 volt/kine and natural frequency 4.5 cps. They were put into the ground at every about 100 m. Thus the length of spread by one party of seismic prospecting instrument was about 2.3 km. The seismic prospecting instruments used are shown in the remarks of Table 2. Two seismic prospecting instruments with magnetic tape recording were operated for only five seconds so as to register the initial P wave on the magnetic tape.

Survey of positions of shot and observation points was done by technicians of Ube Industries, Ltd. as shown in Table 2. The positions of shot and observation points were connected to the nearest stations of triangulation and bench marks by the traversing and levelling. In Table 3, the distances from shot point A-I projected to the line connecting shot point A-I with shot point A-V for profile A, the distances from shot point B-I projected to the line connecting shot point B-I with B-IV for profile B, etc. are given.

IV. Results

As mentioned in the introduction, the explosion seismic studies were intended to conduct when the decreasing tendency in the seismic activity appeared. However, it was found through seismic observations with high magnification that a large number of microearthquakes (more than one shock per minute) were still recorded near several observation sites. Therefore, since there was a big anxiety for the explosion seismic signals to be masked by disturbances due to the natural earthquakes, the seismic activity was kept watch on at shot points by the seismic observation with high magnification. However, only twice (shots A-IV, and B-IV) there was a microearthquake near one of observation sites just before the arrival of explosion seismic signals. Fortunately the amplitude of microearthquake was so small in comparison with that of explosion seismic signals that it was unnecessary to repeat explosions. The seismograms obtained with magnetic tape recorders and those with seismic prospecting instruments are given in Figs. 5 and 6 respectively. As seen from these figures, the seismograms obtained are of good quality except for minor portion of them. Particularly most of seismograms obtained by using magnetic tape recorders give distinct first arrivals.

All seismograms were examined by the following procedures:

(1) Only the initials of P waves were picked up this time.

(2) The readings are classified into the following three grades by taking sharpness of commencement, clearness of time signals etc. into account:

Table 2 Observation points, recorders and observers

Obs. Point P-A	Obs. Point P-B	Magnetic Tape Recorder*	Observers***
D_1	D_1	Y	S. IIZUKA (GS), H. KASE (UT)
D_2	D_2	X	K. ITO, I. HASEGAWA (GS)
D_3	D_5	Z_1	H. WATANABE, H. MOCHIZUKI, M. KATSUMATA, M. SEINO (JMA)
D_4	D_6		
D_5	D_4	X	M. NOGOSHI, Y. UEDA (AU)
D_6	D_3	X	H. NABETANI (AU)
D_7	D_7	Y	H. TAKAHASHI, M. TAKAHASHI, H. YASOJIMA, Y. WATANABE, (NRCDP)
D_8	D_8	Y	H. SUZUKI, K. OMURA, T. KUMAGAI (NRCDP)
D_8'	D_7'	X	S. ASANO (ERI), T. MORIYA (HU)
D_9	D_9	X	I. KARAKAMA (ERI), J. CHUJO (GS)
D_{10}	D_{10}	X	T. YOSHII, S. KODOMARI (HU)
D_{11}	D_{11}	Y	K. KAKIICHI, T. HIROTA (HU)
D_{12}	D_{12}	X	S. SUZUKI, T. IGARASHI (HU)
D_{13}	D_{13}	Z_2	Y. ICHINOSE (ERI), S. HASEGAWA, Y. AOKI (UT)
D_{14}	D_{14}	X, Y	S. KUBOTA, H. CHIBA, Y. HIRATA, I. OGINO (ERI)
E_1–E_5		**	Ube Industries, Ltd.; H. OKADA, M. MOTOYAMA, H. MAEKAWA, T. ADACHI (HU)
Shooting Party			Ube Industries, Ltd.
Survey Party			Ube Industries, Ltd.

Staffs of Headquarter	
Chief of Headquarter	K. SEYA (GS)
Chief of Shooting Parties	K. NORITOMI (AU)
	K. ICHIKAWA (GS)
Chief of Parties of Seismic Prospecting Instruments	K. TAZIME (HU)
Chief of Parties of Magnetic Tape Recorders	S. ASANO (ERI)
Calibration Party	T. MORIYA (HU)
	S. ASANO (ERI)

* X: SONY FMA-23S, MA-33-4S
Y: SONY PFM 15
Z_1: TEAC R-500
Z_2: TEAC R-100

** Seismic prospecting instruments used by each observation party are as follows:
E_1: S.I.E. PT 100, PMR 20 type (FM tape recording)
E_5: S.I.E. GA 11, PMR 7 type (AM tape recording)
E_2 E_4: E.T.L. M-3 type
E_3: E.T.L. PRA2, ER64 type

*** The abbreviation of each organization or university is as follows:
GS: Geological Survey of Japan
JMA: Japan Meteorological Agency
AU: Akita University
NRCDP: National Research Center for Disaster Prevention
HU: Hokkaido University
UT: University of Tokyo
ERI: Earthquake Research Institute, University of Tokyo

A: $|\Delta t| \leqq 10^{ms}$,
B: $10^{ms} < |\Delta t| \leqq 30^{ms}$,
C: $30^{ms} < |\Delta t| \leqq 100^{ms}$,

where Δt means ambiguity of time of initials.

(3) Since the waveform of the initial portion of P waves at one observation point was almost the same with that of the adjacent observation point in one station, the arrival time of the initial P with bad SN ratio was estimated from the time difference between clear initial and following clear trough or crest on the seismogram at the adjacent observation point. Then the estimated time in this manner were classified into C and shown with bracket in Tables 5 and 6.

(4) Records with weak initials, especially those of seismic prospecting instruments were sometimes read by referring to the records of adjacent D parties.

(5) Seismograms of repeated shot were compared with those of the first shot if necessary.

Seven members (S. ASANO, K. ICHIKAWA, H. OKADA, S. KUBOTA, H. SUZUKI, M. NOGOSHI, H. WATANABE) examined seismograms and picked the initial P up separately. Then each value of arrival time was re-examined together by seven members and the value as objective as possible was looked for. The arrival times of initial P, travel times thus obtained were given in Table 4 for observation points near shot points, in Table 5 for profile A and in Table 6 for profile B except for the data obtained from shot B–IV for profile A, which are left for future studies.

Acknowledgement

We are much obliged to the following authorities, offices, and organizations: Liaison Council of Hokushin Crustal Movement, Inter-Ministral Liaison Committee in Research Center of Matsushiro Earthquake Swarm; Departments, Sections or Branches concerned of Nagano Prefectural Office, Nagano Police Headquarter and police stations concerned, the following administration authorities:

City: Nagano, Nakano, Suzaka, Ueda, Koshoku,

Town: Sanada, Yamanouchi, Togura, Obuse,

Village: Togakushi, Sakai, Honjo, Shiga;

Nagano Regional Forestry Office; Nagano Railways Control Bureau, Japanese National Railways; Nagano Branch Office, Chubu Electric Power Company; Nagano Electric Railway Company; Nagano Broadcasting Station, Japan Broadcasting Corporation (NHK); Shin-etsu Broadcasting Company; Terao Elementary School, Nagano City; Seismological Observatory, Japan Meteorological Agency; Research Center of Matsushiro Earthquake Swarm; Hokushin Observatory of Microearthquakes and Crustal Deformation, Earthquake Research Institute.

In addition to the above authorities, offices and organizations, we express our hearty thanks to many individuals who supported this experiment.

Our thanks are also due to scientists or technicians who participated in this experiment and placed the data at our disposal.

Our hearty gratitute is expressed to Professor T. HAGIWARA, Earthquake Research Institute, who supported this experiment from the first stage of planning and gavé advices and encouragement through the experiment.

We appreciate the cooperation of the following personnels: Mr. Y. HAYASHI and other participated office staffs of Geological Survey of Japan who dealt with troublesome business; Misses M. KUBOTA, S. INOUE, M. IMAI, and Messrs. I. OGINO, M. SAKA, Y. ICHINOSE for assistance in computations and in making complicated tables and figures.

References

1) ASANO, S., KUBOTA, S., OKADA, H., NOGOSHI, M., SUZUKI, H., ICHIKAWA, K. & WATANABE, H. (1969): Explosion seismic studies of the Matsushiro Earthquake Swarm Area, Part II Underground structure in the Matsushiro Earthquake Swarm Area as derived from explosion seismic data, *Spec. Rep. Geol. Survey of Japan*, no. 5.

2) HAGIWARA, T. (1967): General description of the Matsushiro Swarm Earthquakes, *Zisin*, Ser. II, vol. 20, no. 4, p. 192～200 (in Japanese).

3) HAGIWARA, T. & Iwata, T. (1968): Summary of the seismographic observation of Matsushiro Swarm Earthquakes, *Bull. Earthq. Res. Inst. Univ. of Tokyo*, vol. 46, p. 485～515.

4) HAGIWARA, T., YAMADA, J. & HIRAI, M. (1966): Observation of tilting of the earth's surface due to Matsushiro Earthquakes, Part 1, *Bull. Earthq. Res. Inst. Univ. of Tokyo*, vol. 44, p. 351～361.

5) HAMADA, K. (1968): Ultra micro-earthquakes in the area around Matsushiro, *Bull. Earthq. Res. Inst. Univ. of Tokyo*, vol. 46, p. 271～318.

6) HAMADA, K. & HAGIWARA, T. (1967): High sensitivity tripartite observation of Matsushiro Earthquakes. Part 4, *Bull. Earthq. Res. Inst. Univ. of Tokyo*, vol. 45, p. 159～196.

7) ICHIKAWA, M. (1967): Statistical study of the focal mechanism of Matsushiro Earthquake Swarm, *Zisin*, Ser. II, vol. 20, p. 116～127 (in Japanese).

8) Japan Meteorological Agency (1968): Report on the Matsushiro Earthquake Swarm, Chapter 1 Seismic activity of the Matsushiro Earthquake Swarm, *Technical Report of Japan Meteorological Agency*, no. 62, p. 7～18 (in Japanese).

9) KASAHARA, K. & OKADA, A. (1966): Electro-optical measurement of horizontal strains accumulating in the swarm earthquake area (1), *Bull. Earthq. Res. Inst. Univ. of Tokyo*, vol. 44, p. 335～350.

10) MORIMOTO, R., MURAI, I., MATSUDA, T., NAKAMURA, K., TSUNEISHI, Y. & YOSHIDA, S. (1966): Geological consideration on the Matsushiro Earthquake Swarm since 1965 in Central Japan, *Bull. Earthq. Res. Inst. Univ. of Tokyo*, vol. 44, p. 423～445 (in Japanese).

11) NAKAMURA, K. & TSUNEISHI, Y. (1967): Ground cracks at Matsushiro probably of underlying strike-slip fault origin, II-the Matsushiro Earthquake Fault, *Bull. Earthq. Res. Inst. Univ. of Tokyo*, vol. 45, p. 417～471.

12) OHTAKE, M., CHIBA, H. & HAGIWARA, T. (1967): Ultra microearthquake activity at the southwestern border of the area of Matsushiro Earthquakes, Part 1, *Bull. Earthq. Res. Inst. Univ. of Tokyo*, vol. 45, p. 861～886.

13) ONO, Y. (1967): Electrical sounding at Matsushiro Earthquake district (Report 1), *Notes of Cooperative Research For Disaster Prevention*, no. 5, p. 23～27 (in Japanese).

14) SEYA, K. (1967): Gravity survey in the Matsushiro Earthquake Swarm area, *Notes of Cooperative Research For Disaster Prevention*, no. 5, p. 13～22 (in Japanese).

15) TAKAGI, A., KATO, Y. & MUROI, I. (1968): Features of some earthquake areas from the results of airborne magnetic survey, *Read at the annual meeting of Seismological Society of Japan, June 26.*

16) TSUBOKAWA, I., OKADA, A., TAJIMA, H., MURATA, I., NAGASAWA, K., IZUTUYA, S. & ITO, Y. (1967): Levelling resurvey associated with the area of Matsushiro Earthquake Swarms. (1), *Bull. Earthq. Res. Inst. Univ. of Tokyo*, vol. 45, p. 265～288 (in Japanese).

Table 3 (a) The distance of observation points from the shot point A–I on the line I–V for profile A, the azimuth from each shot point referring to the line I–V and height

Obs. Point		Distance	Height	Azimuth* A–I	A–II	A–III	A–IV	A–V	Deviation** from I–V
		km	m						m
E_1	1	14.741	332	2°40′— —	0°20′— —	1°59′+—	0°03′++	0°50′+—	—651
	2	14.839	332	2 41 — —	0 19 — —	1 59 +—	0 03 ++	0 50 +—	—659
	3	14.942	332	2 40 — —	0 15 — —	1 59 +—	0 03 ++	0 50 +—	—648
	4	15.041	334	2 38 — —	0 08 — —	2 00 +—	0 03 ++	0 50 +—	—644
	5	15.143	335	2 37 — —	0 22 — —	2 00 +—	0 03 ++	0 50 +—	—644
	6	15.242	335	2 35 — —	0 32 — —	1 57 +—	0 02 ++	0 49 +—	—640
	7	15.340	340	2 33 — —	0 39 — —	1 53 +—	0 00	0 48 +—	—636
	8	15.442	343	2 27 — —	2 19 —+	1 50 +—	0 02 ++	0 47 +—	—613
	9	15.540	347	2 19 — —	3 52 —+	1 46 +—	0 04 ++	0 46 +—	—581
	10	15.641	350	2 12 — —	5 07 —+	1 43 +—	0 06 ++	0 45 +—	—553
	11	15.740	353	2 01 — —	7 02 —+	1 32 +—	0 11 ++	0 42 +—	—507
	12	15.833	357	1 50 — —	8 37 —+	1 21 +—	0 16 ++	0 39 +—	—459
	13	15.936	361	1 36 — —	10 27 —+	1 10 +—	0 21 ++	0 36 +—	—397
	14	16.040	364	1 24 — —	11 59 —+	0 51 +—	0 26 ++	0 33 +—	—343
	15	16.139	369	1 24 — —	11 04 —+	0 49 +—	0 30 ++	0 31 +—	—346
	16	16.238	372	1 25 — —	10 08 —+	0 49 +—	0 30 ++	0 31 +—	—353
	17	16.337	376	1 25 — —	9 35 —+	0 49 +—	0 30 ++	0 31 +—	—356
	18	16.436	380	1 23 — —	9 06 —+	0 58 +—	0 30 ++	0 31 +—	—349
	19	16.539	384	— —	8 38 —+	0 58 +—	0 29 ++	0 31 +—	—352
	20	16.638	389	1 22 — —	8 15 —+	0 58 +—	0 29 ++	0 31 +—	—350
	21	16.741	393	— —	7 54 —+	0 58 —+	0 29 ++	0 31 +—	—353
	22	16.839	396	1 31 — —	7 33 —+	0 58 +—	0 29 ++	0 31 +—	—350
	23	16.938	399	1 30 — —	7 15 —+	0 59 +—	0 29 ++	0 31 +—	—348
	24	17.037	401	1 29 — —	6 59 —+	0 59 +—	0 29 ++	0 31 +—	—346
E_2	1	21.887	341	0 57 — —	2 50 —+	1 09 +—	0 22 ++	0 31 +—	—363
	2	21.984	341	0 56 — —	2 48 —+	1 09 +—	1 18 ++	0 31 +—	—358
	3	22.086	340	0 56 — —	2 46 —+	1 10 +—	1 18 ++	0 31 +—	—360
	4	22.188	342	0 56 — —	2 44 —+	1 11 +—	1 18 ++	0 31 +—	—362
	5	22.290	342	0 56 — —	2 42 —+	1 11 +—	1 18 ++	0 31 +—	—364
	6	22.387	342	0 55 — —	2 41 —+	1 12 +—	1 18 ++	0 31 +—	—359
	7	22.489	343	0 55 — —	2 39 —+	1 12 +—	1 18 ++	0 31 +—	—360
	8	22.591	346	0 55 — —	2 37 —+	1 13 +—	1 18 ++	0 31 +—	—362
	9	22.684	346	0 54 — —	2 35 —+	1 14 +—	1 17 ++	0 31 +—	—357
	10	22.789	342	0 54 — —	2 34 —+	1 15 +—	1 17 ++	0 31 +—	—359
	11	22.883	342	0 53 — —	2 33 —+	1 16 +—	1 17 ++	0 31 +—	—354
	12	22.988	340	0 53 — —	2 31 —+	1 16 +—	1 17 ++	0 31 +—	—356
	13	23.084	340	0 52 — —	2 34 —+	1 17 +—	1 17 ++	0 31 +—	—350
	14	23.185	339	0 46 — —	2 37 —+	1 01 +—	1 17 ++	0 31 +—	—325
	15	23.281	339	0 47 — —	2 40 —+	1 01 +—	1 18 ++	0 31 +—	—320
	16	23.377	339	0 46 — —	2 40 —+	1 01 +—	1 18 ++	0 31 +—	—314
	17	23.479	340	0 46 — —	2 37 —+	1 02 +—	1 20 ++	0 31 +—	—316
	18	23.581	339	0 46 — —	2 35 —+	1 03 +—	1 21 ++	0 31 +—	—317
	19	23.683	339	0 46 — —	2 33 —+	1 04 +—	1 22 ++	0 31 +—	—319
	20	23.779	339	0 45 — —	2 32 —+	1 04 +—	1 23 ++	0 31 +—	—313
	21	23.881	338	0 45 — —	2 31 —+	1 04 +—	1 23 ++	0 31 +—	—315
	22	23.983	338	0 45 — —	2 30 —+	1 04 +—	1 23 ++	0 31 +—	—316
	23	24.084	338	0 45 — —	2 29 —+	1 05 +—	1 23 ++	0 31 +—	—318
	24	24.180	338	0 44 — —	2 28 —+	1 06 +—	1 23 ++	0 31 +—	—312

Obs. Point		Distance	Height	A–I	A–II	Azimuth* A–III	A–IV	A–V	Deviation** from I–V
		km	m						m
E_3	1	27.166	340	0°36′−−	2°19′−+	0°14′+−	0°01′++	0°06′+−	−270
	2	27.261	340	0 35 −−	2 18 −+	0 14 +−	0 01 ++	0 06 +−	−263
	3	27.356	340	0 35 −−	2 17 −+	0 13 +−	0 01 ++	0 06 +−	−264
	4	27.462	341	0 35 −−	2 16 −+	0 13 +−	0 00	0 06 +−	−265
	5	27.564	341	0 35 −−	2 15 −+	0 12 +−	0 00	0 06 +−	−266
	6	27.665	341	0 35 −−	2 15 −+	0 12 +−	0 00	0 06 +−	−266
	7	27.766	341	0 35 −−	2 14 −+	0 11 +−	0 00	0 06 +−	−267
	8	27.868	341	0 35 −−	2 13 −+	0 10 +−	0 00	0 06 +−	−268
	9	27.962	343	0 34 −−	2 12 −+	0 10 +−	0 00	0 06 +−	−269
	10	28.064	347	0 34 −−	2 11 −+	0 09 +−	0 00	0 06 +−	−270
	11	28.165	343	0 34 −−	2 10 −+	0 15 +−	0 00	0 06 +−	−270
	12	28.266	343	0 34 −−	2 09 −+	0 21 +−	0 00	0 06 +−	−271
	13	28.367	343	0 34 −−	2 08 −+	0 27 +−	0 01 ++	0 07 +−	−272
	14	28.469	342	0 34 −−	2 07 −+	0 33 +−	0 01 ++	0 07 +−	−273
	15	28.570	343	0 34 −−	2 06 −+	0 40 +−	0 01 ++	0 07 +−	−274
	16	28.671	343	0 34 −−	2 05 −+	0 42 +−	0 01 ++	0 07 +−	−274
	17	28.773	343	0 34 −−	2 04 −+	0 44 +−	0 01 ++	0 07 +−	−275
	18	28.867	343	0 33 −−	2 03 −+	0 45 +−	0 01 ++	0 07 +−	−276
	19	28.968	343	0 33 −−	2 02 −+	0 47 +−	0 01 ++	0 07 +−	−277
	20	29.070	343	0 33 −−	2 01 −+	0 48 +−	0 01 ++	0 07 +−	−278
	21	29.171	344	0 33 −−	2 00 −+	0 56 +−	0 01 ++	0 07 +−	−278
	22	29.272	344	0 33 −−	1 59 −+	1 04 +−	0 01 ++	0 07 +−	−279
	23	29.373	345	0 33 −−	1 58 −+	1 12 +−	0 01 ++	0 07 +−	−280
	24	29.475	345	0 33 −−	1 58 −+	1 19 +−	0 01 ++	0 07 +−	−281
E_4	1	33.402	365	0 59 −+	3 53 −+	11 59 −+	5 12 ++	0 57 ++	+551
	2	33.500	361	1 01 −+	3 56 −+	11 59 −+	5 20 ++	0 59 ++	+572
	3	33.598	361	1 03 −+	3 58 −+	12 00 −+	5 28 ++	1 02 ++	+593
	4	33.697	363	1 05 −+	4 01 −+	12 05 −+	5 33 ++	1 05 ++	+614
	5	33.796	363	1 08 −+	4 05 −+	12 10 −+	5 49 ++	1 08 ++	+646
	6	33.906	363	1 11 −+	4 04 −+	11 53 −+	5 51 ++	1 08 ++	+677
	7	33.995	363	1 08 −+	4 03 −+	11 37 −+	5 53 ++	1 09 ++	+649
	8	34.094	363	1 08 −+	4 02 −+	11 21 −+	5 56 ++	1 09 ++	+651
	9	34.193	362	1 08 −+	4 01 −+	11 07 −+	5 58 ++	1 09 ++	+653
	10	34.300	363	1 07 −+	3 59 −+	10 56 −+	6 00 ++	1 10 ++	+645
	11	34.399	365	1 07 −+	3 58 −+	10 36 −+	6 03 ++	1 10 ++	+647
	12	34.498	368	1 08 −+	3 58 −+	10 27 −+	6 03 ++	1 09 ++	+658
	13	34.597	370	1 08 −+	3 57 −+	10 18 −+	6 11 ++	1 09 ++	+660
	14	34.696	371	1 08 −+	3 56 −+	10 06 −+	6 15 ++	1 08 ++	+662
	15	34.795	372	1 08 −+	3 55 −+	9 54 −+	6 18 ++	1 08 ++	+664
	16	34.895	373	1 08 −+	3 54 −+	9 43 −+	6 21 ++	1 07 ++	+665
	17	35.002	375	1 07 −+	3 53 −+	9 33 −+	6 24 ++	1 07 ++	+657
	18	35.097	374	1 07 −+	3 52 −+	9 21 −+	6 26 ++	1 07 ++	+659
	19	35.196	372	1 07 −+	3 51 −+	9 09 −+	6 28 ++	1 07 ++	+661
	20	35.301	375	1 05 −+	3 49 −+	8 57 −+	6 30 ++	1 07 ++	+642
	21	35.402	374	1 05 −+	3 47 −+	8 45 −+	6 32 ++	1 07 ++	+644
	22	35.497	372	1 05 −+	3 45 −+	8 34 −+	6 34 ++	1 08 ++	+646
	23	35.584	375	1 04 −+	3 43 −+	8 21 −+	6 35 ++	1 09 ++	+637
	24	35.672	377	1 03 −+	3 41 −+	8 08 −+	6 36 ++	1 10 ++	+628
E_5	1	39.146	357	2 38 −−	2 29 −−	9 42 −−	12 21 +−	3 54 +−	−1746
	2	39.246	357	2 37 −−	2 27 −−	9 33 −−	12 31 +−	3 54 +−	−1738
	3	39.347	357	2 36 −−	2 26 −−	9 24 −−	12 41 +−	3 54 +−	−1731
	4	39.447	357	2 35 −−	2 25 −−	9 16 −−	12 53 +−	3 54 +−	−1724

Obs. Point		Distance	Height	Azimuth* A–I	A–II	A–III	A–IV	A–V	Deviation** from I–V
		km	m						m
E_5	5	39.548	357	2°34′ − −	2°23′ − −	9°08′ − −	13°04′ + −	3°54′ + −	−1717
	6	39.649	358	2 33 − −	2 21 − −	9 00 − −	13 15 + −	3 54 + −	−1710
	7	39.750	358	2 32 − −	2 20 − −	8 52 − −	13 26 + −	3 55 + −	−1703
	8	39.851	358	2 31 − −	2 18 − −	8 44 − −	13 29 + −	3 55 + −	−1696
	9	39.952	359	2 30 − −	2 17 − −	8 37 − −	14 52 + −	3 55 + −	−1689
	10	40.053	359	2 29 − −	2 16 − −	8 30 − −	15 05 + −	3 55 + −	−1682
	11	40.154	360	2 28 − −	2 14 − −	8 22 − −	14 18 + −	3 55 + −	−1674
	12	40.255	361	2 27 − −	2 13 − −	8 15 − −	14 33 + −	3 55 + −	−1667
	13	40.356	363	2 26 − −	2 11 − −	8 08 − −	14 48 + −	3 54 + −	−1659
	14	40.456	361	2 25 − −	2 10 − −	8 01 − −	15 02 + −	3 53 + −	−1652
	15	40.557	360	2 24 − −	2 08 − −	7 54 − −	15 18 + −	3 53 + −	−1644
	16	40.657	361	2 23 − −	2 06 − −	7 46 − −	15 34 + −	3 53 + −	−1637
	17	40.759	361	2 22 − −	2 05 − −	7 41 − −	15 51 + −	3 53 + −	−1629
	18	40.860	363	2 21 − −	2 03 − −	7 35 − −	16 11 + −	3 52 + −	−1621
	19	40.961	363	2 20 − −	2 02 − −	7 29 − −	16 32 + −	3 52 + −	−1614
	20	41.062	363	2 19 − −	2 01 − −	7 22 − −	16 47 + −	3 52 + −	−1606
	21	41.163	364	2 18 − −	2 00 − −	7 16 − −	17 07 + −	3 52 + −	−1548
	22	41.264	365	2 17 − −	1 58 − −	7 10 − −	17 28 + −	3 52 + −	−1590
	23	41.364	370	2 16 − −	1 56 − −	7 04 − −	17 50 + −	3 52 + −	−1582
	24	41.464	378	2 15 − −	1 55 − −	6 58 − −	18 13 + −	3 52 + −	−1573
D_1	a	1.070	706	4 50 − −	2 40 + +	0 27 + +	0 59 + +	0 02 + −	− 70
	b	1.541	713	4 00 − −	2 30 + +	0 26 + +	0 58 + +	0 04 + −	− 110
	c	1.925	716	3 20 − −	2 40 + +	0 26 + +	0 58 + +	0 04 + −	− 115
D_2	a	4.800	569	1 45 − −	3 05 + +	0 04 + +	0 05 + +	0 09 + −	− 150
	b	5.149	549	2 55 − −	2 30 + +	0 12 + −	0 05 + +	0 15 + −	− 250
	c	5.539	506	3 35 − −	2 06 + +	0 23 + −	0 12 + +	0 20 + −	− 330
D_3	a	9.425	368	0 30 − −	6 40 + +	0 25 + −	1 00 + +	0 05 + −	− 90
	b	9.625	363	0 05 − +	8 25 + +	0 35 + −	1 15 + +	0 02 + +	+ 41
	c	10.090	353	0 03 − −	8 15 + +	0 30 + −	1 02 + +	0 02 + −	− 40
D_4	a	10.430	344	0 32 − −	7 38 + +	0 06 + −	1 02 + +	0 03 + −	− 110
	b	10.681	344	0 33 − −	7 40 + +	0 05 + −	1 02 + +	0 04 + −	− 150
	c	11.031	341	0 33 − −	8 15 + +	0 02 + −	1 02 + +	0 04 + −	− 159
D_5	a	18.560	386	0 40 − −	6 20 − +	0 01 − −	1 20 + +	0 20 + −	− 245
	b	18.891	375	0 40 − −	5 20 − +	0 01 − −	1 20 + +	0 20 + −	− 264
	c	19.315	366	0 40 − −	5 25 − +	0 00	1 20 + +	0 20 + −	− 251
D_6	a	24.650	340	0 12 − +	4 22 − +	2 54 + +	0 48 + +	0 07 + +	+ 65
	b	25.245	340	0 11 − −	3 15 − +	1 14 + +	0 21 + +	0 04 + −	− 55
	c	25.669	340	0 15 − −	2 56 − +	0 58 + +	0 17 + +	0 09 + −	− 120
D_7	a	30.829	393	2 03 − −	1 30 − −	42 16 − −	3 35 + −	1 50 + −	−1115
	b	31.074	351	1 42 − −	0 50 − −	30 25 − −	2 55 + −	1 31 + −	− 929
	c	31.949	353	1 47 − −	1 04 − −	20 56 − −	3 27 + −	1 42 + −	−1020
D_8	a	35.349	357	1 07 − −	0 11 − −	4 35 − −	1 22 + −	1 10 + −	− 730
	b	35.604	360	0 38 − −	0 48 − −	1 56 − −	1 36 + −	0 44 + −	− 509
	b′	35.709	364	0 32 − −	0 57 − −	1 30 − −	1 40 + +	0 57 + −	− 452
	c	35.895	365	0 31 − −	0 58 − −	1 28 − −	1 40 + +	0 57 + −	− 433
D_9	a	44.750	368	0 51 − −	0 57 − +	1 00 − −	38 30 + −	0 58 + −	− 540
	b	45.160	381	0 32 − −	0 37 − +	0 41 − −	22 30 + −	1 17 + −	− 445
	c	45.470	431	0 13 − −	0 20 − +	0 23 − −	22 29 + −	1 35 + −	− 310

Obs. Point		Distance	Height	Azimuth* A–I	A–II	A–III	A–IV	A–V	Deviation** from I–V
		km	m						m
D_{10}	a	50.320	747	0°37′−−	0°13′−+	1°01′−−	0°40′−+	2°02′+−	− 544
	b	50.575	699	0 36 −−	0 15 −+	0 57 −−	1 30 −+	2 01 +−	− 460
	c	50.960	714	0 41 −−	0 18 −+	1 10 −−	0 40 −+	2 03 +−	− 540
D_{11}	a	52.830	710	0 28 −−	0 24 −+	0 36 −−	2 10 −+	1 54 +−	− 385
	b	53.040	709	0 17 −−	0 38 −+	0 10 −−	3 00 −+	1 08 +−	− 190
	c	53.230	701	0 14 −−	0 42 −+	0 04 −−	3 00 −+	0 58 +−	− 170
D_{12}	a	57.682	817	0 22 −−	0 24 −+	0 24 −−	1 50 −+	2 46 +−	− 369
	b	58.047	755	0 29 −−	0 15 −+	0 37 −−	1 00 −+	3 46 +−	− 500
	c	58.377	716	0 34 −−	0 08 −+	0 48 −−	0 30 −+	4 41 +−	− 577
D_{13}	a	60.835	781	0 58 −−	0 26 −−	1 34 −−	0 50 −−	12 33 +−	−1000
	b	61.155	765	1 07 −−	0 27 −−	1 50 −−	1 30 −−	16 21 +−	−1155
	c	61.400	774	1 11 −−	0 43 −−	1 57 −−	2 00 −−	17 11 +−	−1225
D_{14}	a	64.660	643	0 50 −−	0 15 −+	0 06 −−	0 06 −+	21 00 +−	− 335
	b	64.950	615	0 13 −−	0 30 −+	0 02 −−	0 09 −+	24 00 +−	− 245
	c	64.935	617	0 08 −−	0 36 −+	0 02 −+	0 13 −+	16 00 +−	− 165
	d	65.169	614	0 05 −−	0 38 −+	0 04 −+	0 13 −+	23 00 +−	− 120
	e	65.309	613	0 03 −−	0 39 −+	0 06 −+	0 14 −+	24 00 +−	− 100
	f	65.490	609	0 00	0 41 −+	0 09 −+	0 20 −+	5 00 +−	− 6
S.P.	I	0.000	788						0
	II	14.622	333						− 681
	III	29.814	347						− 182
	IV	44.565	369						− 662
	V	65.504	609						0

* The rectangular coordinate axes x and y are supposed at each shot point. The y-axis is perpendicular to the line connecting A–I with A–V (the line I–V) and the x-axis is parallel to this line. The positive side of x-axis is northward and that of y-axis is eastward. If the geophone is in the third quadrant, the sign −− is given as usual after the value of angle from the line I–V. For example, 2°40′−− means that the angle of the geophone measured at the shot point from the line I–V is 2°40′ and the geophone is in the third quadrant.

** The deviation is measured from the line I–V. The sign − means that the geophone is on the west side to the line I–V.

Table 3 (b) The distance of observation points from the shot point B–I on the line I–IV for profile B, the azimuth from each shot point referring to the line I–IV and height

Obs. Point		Distance	Height	Azimuth* B–I	B–II	B–III	B–IV	Deviation** from I–IV
		km	m					m
E_1	1	16.070	406	0°08′ − +	6°11′ − +	0°42′ − −	0°04′ − −	− 37
	2	16.168	395	0 05 − +	5 50 − +	0 39 − −	0 03 − −	− 24
	3	16.269	387	0 01 − +	5 24 − +	0 35 − −	0 01 − −	− 5
	4	16.367	378	0 02 + +	5 03 − +	0 31 − −	0 01 + −	+ 10
	5	16.466	373	0 05 + +	4 44 − +	0 28 − −	0 03 + −	+ 24
	6	16.565	368	0 02 + +	4 49 − +	0 31 − −	0 01 + −	+ 10
	7	16.662	364	0 03 − +	5 02 − +	0 38 − −	0 02 + −	− 15
	8	16.759	358	0 08 − +	5 15 − +	0 45 − −	0 05 − −	− 39
	9	16.857	361	0 12 − +	5 23 − +	0 51 − −	0 07 − −	− 59
	10	16.956	358	0 15 − +	5 27 − +	0 56 − −	0 09 − −	− 74
	11	17.054	358	0 19 − +	5 35 − +	1 02 − −	0 11 − −	− 94
	12	17.153	357	0 22 − +	5 40 − +	1 20 − −	0 13 − −	−110
	13	17.249	357	0 24 − +	5 40 − +	1 10 − −	0 14 − −	−120
	14	17.353	356	0 25 − +	5 42 − +	1 12 − −	0 15 − −	−126
	15	17.452	356	0 26 − +	5 34 − +	1 14 − −	0 16 − −	−132
	16	17.554	356	0 26 − +	5 29 − +	1 15 − −	0 16 − −	−133
	17	17.679	356	0 26 + +	5 21 − +	1 16 − −	0 16 − −	−134
	18	17.781	356	0 29 − +	5 26 − +	1 22 − −	0 18 − −	−150
	19	17.881	356	0 29 − +	5 21 − +	1 23 − −	0 18 − −	−151
	20	17.980	356	0 29 − +	5 15 − +	1 24 − −	0 18 − −	−152
	21	18.082	356	0 28 − +	5 07 − +	1 23 − −	0 18 − −	−147
	22	18.182	355	0 28 − +	5 02 − +	1 24 − −	0 18 − −	−148
	23	18.282	354	0 28 − +	4 57 − +	1 25 − −	0 18 − −	−149
	24	18.381	353	0 28 − +	4 53 − +	1 26 − −	0 18 − −	−150
E_2	1	19.081	356	1 02 + +	0 09 − +	1 11 + −	0 43 + −	+344
	2	19.182	352	1 02 + +	0 09 − +	1 13 + −	0 43 + −	+346
	3	19.279	351	1 01 + +	0 10 − +	1 12 + −	0 43 + −	+342
	4	19.381	351	1 01 + +	0 10 − +	1 14 + −	0 43 + −	+344
	5	19.482	351	1 01 + +	0 08 − +	1 15 + −	0 44 + −	+346
	6	19.583	351	1 01 + +	0 07 − +	1 17 + −	0 44 + −	+348
	7	19.681	351	1 00 + +	0 09 − +	1 16 + −	0 44 + −	+344
	8	19.781	350	1 00 + +	0 06 − +	1 17 + −	0 44 + −	+345
	9	19.880	350	0 59 + +	0 10 − +	1 17 + −	0 44 + −	+341
	10	19.980	350	0 59 + +	0 09 − +	1 18 + −	0 44 + −	+343
	11	20.081	350	0 59 + +	0 08 − +	1 19 + −	0 45 + −	+345
	12	20.182	350	0 59 + +	0 07 − +	1 21 + −	0 45 + −	+346
	13	20.282	350	0 59 + +	0 06 − +	1 23 + −	0 46 + −	+348
	14	20.381	350	0 58 + +	0 08 − +	1 22 + −	0 45 + −	+344
	15	20.481	349	0 58 + +	0 07 − +	1 23 + −	0 45 + −	+346
	16	20.579	349	0 57 + +	0 09 − +	1 23 + −	0 45 + −	+341
	17	20.680	349	0 57 + +	0 08 − +	1 24 + −	0 45 + −	+343
	18	20.781	349	0 57 + +	0 09 − +	1 26 + −	0 46 + −	+345
	19	20.881	349	0 57 + +	0 06 − +	1 24 + −	0 46 + −	+346
	20	20.982	349	0 57 + +	0 06 − +	1 29 + −	0 47 + −	+348
	21	21.080	349	0 56 + +	0 08 − +	1 29 + −	0 46 + −	+343
	22	21.181	349	0 56 + +	0 07 − +	1 30 + −	0 47 + −	+345
	23	21.281	349	0 56 + +	0 06 − +	1 32 + −	0 47 + −	+347
	24	21.382	349	0 56 + +	0 05 − +	1 48 + −	0 47 + −	+348

Obs. Point		Distance	Height	Azimuth* B–I	B–II	B–III	B–IV	Deviation** from I–IV
		km	m					m
E_3	1	21.812	343	0°32′ − +	3°26′ − +	2°29′ − −	0°28′ − −	−203
	2	21.913	345	0 40 − +	3 42 − +	2 54 − −	0 35 − −	−255
	3	22.011	344	0 47 − +	3 57 − +	3 18 − −	0 42 − −	−301
	4	22.114	345	0 53 − +	4 08 − +	3 39 − −	0 48 − −	−341
	5	22.212	345	1 00 − +	4 22 − +	4 05 − −	0 55 − −	−388
	6	22.314	345	1 06 − +	4 33 − +	4 27 − −	1 00 − −	−428
	7	22.412	348	1 06 − +	4 31 − +	4 32 − −	1 01 − −	−430
	8	22.514	346	1 01 − +	4 18 − +	4 21 − −	0 57 − −	−400
	9	22.612	346	0 59 − +	4 12 − +	4 19 − −	0 55 − −	−388
	10	22.713	345	0 56 − +	4 03 − +	4 14 − −	0 53 − −	−370
	11	22.812	344	0 54 − +	3 57 − +	3 20 − −	0 52 − −	−358
	12	22.914	345	0 51 − +	3 49 − +	4 06 − −	0 49 − −	−340
	13	23.012	346	0 52 − +	3 49 − +	4 14 − −	0 51 − −	−348
	14	23.113	346	0 52 − +	3 48 − +	4 19 − −	0 51 − −	−350
	15	23.214	346	0 52 − +	3 46 − +	4 23 − −	0 51 − −	−351
	16	23.314	346	0 52 − +	3 45 − +	4 29 − −	0 52 − −	−353
	17	23.412	346	0 53 − +	3 45 − +	4 38 − −	0 53 − −	−361
	18	23.511	346	0 53 − +	3 46 − +	4 47 − −	0 55 − −	−363
	19	23.614	347	0 53 − +	3 42 − +	4 49 − −	0 54 − −	−364
	20	23.713	347	0 54 − +	3 43 − +	4 59 − −	0 56 − −	−372
	21	23.812	348	0 54 − +	3 41 − +	5 05 − −	0 56 − −	−374
	22	23.913	348	0 54 − +	3 40 − +	5 12 − −	0 57 − −	−376
	23	24.010	348	0 55 − +	3 40 − +	5 22 − −	0 58 − −	−384
	24	24.113	350	0 54 − +	3 40 − +	5 25 − −	0 58 − −	−379
E_4	1	24.146	361	0 46 + +	0 11 − +	2 06 + −	0 49 + −	+323
	2	24.244	352	0 40 + +	0 23 − +	1 42 + −	0 43 + −	+282
	3	24.345	349	0 35 + +	0 33 − +	1 21 + −	0 38 + −	+248
	4	24.446	348	0 30 + +	0 42 − +	0 58 + −	0 33 + −	+213
	5	24.544	348	0 24 + +	0 54 − +	0 30 + −	0 27 + −	+171
	6	24.644	348	0 19 + +	0 03 − +	0 06 + −	0 21 + −	+136
	7	24.744	349	0 14 + +	1 11 − +	0 15 + −	0 17 + −	+108
	8	24.843	349	0 11 + +	1 18 − +	0 36 − −	0 13 + −	+ 79
	9	24.944	349	0 09 + +	1 21 − +	0 48 − −	0 10 + −	+ 65
	10	25.046	350	0 07 + +	1 24 − +	1 00 − −	0 08 + −	+ 51
	11	25.144	351	0 04 + +	1 30 − +	1 19 − −	0 05 + −	+ 29
	12	25.245	352	0 02 + +	1 33 − +	1 32 − −	0 02 + −	+ 15
	13	25.346	352	0 00	1 36 − +	1 47 − −	0 00	0
	14	25.444	353	0 03 − +	1 41 − +	2 08 − −	0 04 − −	− 22
	15	25.544	355	0 03 − +	1 40 − +	2 12 − −	0 04 − −	− 22
	16	25.644	391	0 03 − +	1 40 − +	2 15 − −	0 04 − −	− 22
	17	25.744	360	0 02 − +	1 37 − +	2 12 − −	0 03 − −	− 15
	18	25.846	362	0 00	1 32 − +	2 02 − −	0 00	0
	19	25.948	366	0 01 + +	1 30 − +	1 58 − −	0 01 + −	+ 8
	20	26.045	369	0 02 + +	1 35 − +	1 54 − −	0 03 + −	+ 15
	21	26.153	373	0 03 + +	1 25 − +	1 49 − −	0 04 + −	+ 23
	22	26.244	376	0 04 + +	1 22 − +	1 45 − −	0 04 + −	+ 31
	23	26.347	387	0 06 + +	1 18 − +	1 31 − −	0 08 + −	+ 46
	24	26.446	409	0 07 + +	1 15 − +	1 25 − −	0 09 + −	+ 54
E_5	1	27.563	461	0 44 + +	0 02 − +	6 47 + −	1 03 + −	+353
	2	27.664	453	0 44 + +	0 02 − +	7 12 + −	1 04 + −	+354
	3	27.761	451	0 43 + +	0 03 − +	7 22 + −	1 03 + −	+347

Obs. Point		Distance	Height	Azimuth* B–I	B–II	B–III	B–IV	Deviation** from I–IV
		km	m					m
E_5	4	27.861	449	0°43′++	0°03′−+	7°52′+−	1°04′+−	+349
	5	27.962	451	0 43 ++	0 03 −+	8 25 +−	1 04 +−	+350
	6	28.062	451	0 43 ++	0 03 −+	9 06 +−	1 05 +−	+351
	7	28.163	493	0 43 ++	0 02 −+	9 50 +−	1 05 +−	+352
	8	28.263	488	0 43 ++	0 02 −+	10 44 +−	1 06 +−	+354
	9	28.361	482	0 39 ++	0 09 −+	10 03 +−	1 00 +−	+322
	10	28.463	478	0 35 ++	0 15 −+	9 16 +−	0 55 +−	+290
	11	28.558	473	0 29 ++	0 26 −+	7 11 +−	0 46 +−	+241
	12	28.663	468	0 26 ++	0 31 −+	6 25 +−	0 41 +−	+217
	13	28.762	470	0 20 ++	0 41 −+	3 13 +−	0 32 +−	+167
	14	28.862	473	0 20 ++	0 40 −+−	3 52 +−	0 32 +−	+168
	15	28.963	478	0 20 ++	0 40 −+	4 38 +−	0 33 +−	+169
	16	29.062	482	0 20 ++	0 40 −+	5 56 +−	0 33 +−	+169
	17	29.163	488	0 23 ++	0 34 −+	3 51 +−	0 38 +−	+195
	18	29.262	494	0 29 ++	0 23 −+	31 32 +−	0 49 +−	+247
	19	29.363	500	0 32 ++	0 18 −+	57 20 +−	0 54 +−	+273
	20	29.463	512	0 34 ++	0 14 −+	86 30 −+	0 58 +−	+291
	21	29.560	520	0 40 ++	0 04 −+	63 39 −+	0 09 +−	+344
	22	29.653	521	0 49 ++	0 14 −+	55 47 −+	1 25 +−	+423
	23	29.751	538	0 54 ++	0 21 −+	48 41 −+	1 35 +−	+467
	24	29.852	559	1 00 ++	0 31 −+	44 34 −+	1 47 +−	+521
D_1	a	−0.300	1201	72 02 −−	5 34 −−	2 02 −−	1 08 −−	−924
	b	0.040	1179	86 51 −+	5 01 −−	1 39 −−	0 53 −−	−722
	c	−0.067	1166	8 44 −−	1 43 −−	0 16 −−	0 00	− 10
D_2	a	0.215	1175	66 43 −+	4 03 −−	1 14 −−	0 37 −−	−500
	b	0.449	1195	24 36 −+	2 43 −−	0 40 −−	2 33 −−	−205
	b	0.560	1186	42 24 −+	4 14 −−	1 16 −−	0 38 −−	−512
	c	0.798	1225	1 55 −+	1 55 −−	0 19 −−	0 02 −−	− 27
	c	0.806	1194	36 22 −+	4 43 −−	1 27 −−	0 45 −−	−593
D_3	a	7.445	1125	2 48 ++	0 02 +−	0 37 +−	0 32 +−	+364
	b	7.892	1085	3 08 ++	0 53 +−	0 48 +−	0 38 +−	+432
	c	8.303	1082	3 47 ++	2 37 +−	1 08 +−	0 49 +−	+549
D_4	a	8.729	1054	3 11 ++	1 56 +−	0 59 +−	0 44 +−	+485
	b	9.027	1051	2 53 ++	1 35 +−	0 55 +−	0 41 +−	+455
	c	9.344	1035	3 49 ++	4 55 +−	1 25 +−	0 58 +−	+623
D_5	a	11.499	701	2 49 ++	12 52 +−	1 23 +−	0 55 +−	+566
	b	11.746	667	2 47 ++	18 00 +−	1 26 +−	0 56 +−	+571
	c	11.939	626	2 32 ++	20 16 +−	1 18 +−	0 52 +−	+528
D_6	a	12.241	601	2 24 ++	45 20 +−	1 17 +−	0 51 +−	+513
	b	12.516	593	2 34 ++	57 33 ++	1 28 +−	0 57 +−	+561
	c	12.806	647	2 46 ++	31 41 ++	1 41 +−	1 03 +−	+619
D_7	a	26.734	412	1 23 ++	1 17 ++	11 34 +−	1 58 +−	+685
	b	27.261	448	1 27 ++	1 16 ++	14 22 +−	2 02 +−	+690
	b′	27.250	448	1 17 ++	1 16 ++	14 17 +−	2 02 +−	+690
	c	27.475	463	1 27 ++	0 58 ++	13 50 +−	1 54 +−	+616
D_8	a	30.486	625	0 42 ++	0 02 ++	13 18 ++	1 19 +−	+372
	b	30.756	671	0 26 ++	0 24 −+	4 34 ++	0 50 +−	+233
	c	31.097	732	0 13 ++	0 45 −+	0 23 −+	0 26 +−	+118

Obs. Point		Distance	Height	Azimuth B–I	B–II	B–III	B–IV	Deviation from I–IV
		km	m					m
D_9	a	33.368	936	0°36′−+	1°57′−+	6°58′−+	1°30′−−	−349
	b	33.818	918	1 09 −+	2 47 −+	10 29 −+	3 01 −−	−679
	c	34.155	860	1 31 −+	3 20 −+	12 23 −+	4 08 −−	−904
D_{10}	a	34.485	864	1 20 −+	3 01 −+	10 29 −+	3 46 −−	−803
	b	34.808	821	1 22 −+	3 03 −+	10 09 −+	4 01 −−	−830
	c	35.135	822	1 09 −+	2 57 −+	9 22 −+	4 01 −−	−808
D_{11}	a	36.448	765	1 16 −+	2 47 −+	7 37 −+	4 31 −−	−806
	b	36.640	761	1 04 −+	2 28 −+	6 26 −+	0 24 −−	−682
	c	37.062	764	0 43 −+	1 55 −+	4 27 −+	2 46 −−	−464
D_{12}	a	38.274	706	0 26 ++	0 47 ++	1 03 ++	1 58 +−	+289
	b	38.801	694	0 43 ++	0 16 ++	2 12 ++	3 32 +−	+485
	c	39.066	704	0 47 ++	0 22 ++	2 25 +−	4 01 +−	+534
D_{13}	a	41.510	738	0 44 ++	0 20 ++	1 55 ++	5 53 +−	+531
	b	41.804	651	0 38 ++	0 12 ++	1 33 ++	5 26 +−	+462
	c	42.052	598	0 26 ++	0 05 ++	0 52 ++	3 57 +−	+318
D_{14}	a	45.545	577	0 10 −+	0 51 −+	0 56 −+	6 45 −−	−133
	b	45.672	577	0 14 −+	0 57 −+	1 07 −+	10 36 −−	−186
	c	45.923	586	0 09 −+	0 50 −+	0 52 −+	9 12 −−	−120
	d	46.210	584	0 05 −+	0 44 −+	0 40 −+	8 22 −−	− 67
	e	46.431	576	0 03 −+	0 41 −+	0 34 −+	9 47 −−	− 40
	f	46.655	593	0 01 −+	0 35 −+	0 26 −+	51 04 −−	0
S.P.	I	0.000	1162					0
	II	12.390	564					+362
	III	29.453	524					+129
	IV	46.666	596					0

* The rectangular coordinate axes x and y are supposed at B–II and B–III. The x-axis is perpendicular to the line connecting B–I with B–IV (the line I–IV) and the y-axis is parallel to this line. The positive side of x-axis is eastward and that of y-axis is southward. If the geophone is in the third quadrant at the shot point, the sign −− is given as usual after the value of angle from the line I–IV. For example, 2°40′−− means that the angle of the geophone measured at the shot point from the line I–IV is 2°40′ and the geophone is in the third quadrant. In the case of B–I, if the geophone is on the lefthand side from B–I to the line I–IV, the sign ++ is given and if the geophone is on the righthand side to the line I–IV, the sign −− is given. While in the case of B–IV, if the geophone is on the lefthand side from B–IV to the line I–IV, the sign +− is given and if the geophone is on the righthand side to the line I–IV, the sign +− is given.

** The deviation is measured from the line I–IV. The sign − means that the geophone is on the west side to the line I–IV.

Table 4 Travel time data for observation points near the shot point

Shot Point	Obs. Point	Distance	Class	Travel Time
		m		s
A–I	1	54.5	A	0.039
	2	87.0	A	0.062
	3	115.2	A	0.071
	4	144.3	A	0.097
A–II	1	169.7	C	0.061
	2	139.7	A	0.046
	3	109.8	A	0.038
	5	49.8	A	0.028
A–III	2	139.7	C	0.090
	3	109.7	A	0.080
	4	80.1	B	0.064
	5	50.1	B	0.055
A–IV	1	171.2	A	0.089
	2	141.3	C	0.070
	3	111.9	A	0.061
	4	82.3	A	0.049
	5	53.5	B	0.036
A–V	1	170.0	A	0.070
	2	140.0	A	0.059
	3	109.9	A	0.050
	4	80.0	A	0.039
	5	49.8	A	0.030
B–I	1	50	A	0.044
	2	80	A	0.054
	3	110	A	0.068
	4	140	A	0.079
	5	170	C	0.095
B–II	1	167	C	0.101
	2	137	A	0.086
	3	108	A	0.068
	4	79	A	0.055
	5	48	A	0.041
B–III	1	48	A	0.033
	2	78	A	0.045
	3	108	C	0.055
	4	137	A	0.065
	5	167	A	0.070
B–IV	1	62	A	0.034
	2	92	A	0.049
	3	122	B	0.058
	4	152	A	0.070
	5	182	A	0.084

Table 5 (1) Travel time data for shot A–I

Observation Point		Geophone*	Δ** (km)	Class	Phase***	Arrival† Time	Travel Time	Corrected†† Travel time
						h m 2 05		
						s	s	s
E_1	1	4.5 V	14.741	A	P_1	3.130+	3.142	3.139
	2	4.5 V	14.839	B	P_1	3.142+	3.154	3.151
	3	4.5 V	14.942	B	P_1	3.140+	3.152	3.149
	4	4.5 V	15.041	C	P_1	(3.16)+	(3.17)	(3.17)
	5	4.5 V	15.143	B	P_1	3.190+	3.202	3.199
	6	4.5 V	15.242	C	P_1	(3.20)+	(3.321)	(3.21)
	7	4.5 V	15.340	B	P_1	3.210+	3.222	3.219
	8	4.5 V	15.442	B	P_1	3.230+	3.242	3.239
	9	4.5 V	15.540	B	P_1	3.250+	3.262	3.259
	10	4.5 V	15.641	B	P_1	3.289+	3.301	3.299
	11	4.5 V	15.740	B	P_1	3.292+	3.304	3.302
	12	4.5 V	15.833	B	P_1	3.295+	3.307	3.305
	13	4.5 V	15.936	B	P_1	3.320	3.332	3.331
	14	4.5 V	16.040	B	P_1	3.328+	3.340	3.339
	15	4.5 V	16.139	B	P_1	3.347+	3.359	3.358
	16	4.5 V	16.238	A	P_1	3.352+	3.364	3.363
	18	4.5 V	16.436	B	P_1	3.390+	3.402	3.401
	19	4.5 V	16.539	B	P_1	3.409+	3.421	3.420
	20	4.5 V	16.638	B	P_1	3.442+	3.454	3.453
	21	4.5 V	16.741	B	P_1	3.456+	3.468	3.467
	22	4.5 V	16.839	B	P_1	3.467+	3.479	3.478
	23	4.5 V	16.938	B	P_1	3.489+	3.501	3.500
	24	4.5 V	17.037	B	P_1	3.500+	3.512	3.511
E_2	1	4.5 V	21.887	C	P_1	(4.41) +	(4.42)	
	2	4.5 V	21.984	C	P_1	(4.43) +	(4.44)	
	3	4.5 V	22.086	B	P_1	4.443 +	4.455	4.454
	4	4.5 V	22.188	B	P_1	4.452 +	4.464	4.463
	5	4.5 V	22.290	C	P_1	(4.46) +	(4.47)	
	6	4.5 V	22.387	C	P_1	((4.47)) +	((4.48))	
	7	4.5 V	22.489	C	P_1	(4.49) +	(4.50)	
	8	4.5 V	22.591	C	P_1	(4.49) +	(4.50)	
	9	4.5 V	22.684	C	P_1	(4.52) +	(4.53)	
	10	4.5 V	22.789	C	P_1	(4.53) +	(4.54)	
	11	4.5 V	22.883	B	P_1	4.543 +	4.555	4.554
	12	4.5 V	22.988	B	P_1	4.558 +	4.570	4.569
	13	4.5 V	23.084	C	P_1	4.59 +	4.60	
	14	4.5 V	23.185	C	P_1	((4.59)) +	((4.60))	
	15	4.5 V	23.281	C	P_1	((4.61)) +	((4.62))	
	17	4.5 V	23.479	C	P_1	(4.62) +	(4.63)	
	18	4.5 V	23.581	A	P_1	4.628 +	4.640	4.640
	20	4.5 V	23.779	C	P_1	(4.66) +	(4.67)	
	21	4.5 V	23.881	C	P_1	(4.66) +	(4.67)	
	22	4.5 V	23.983	C	P_1	(4.67) +	(4.68)	
	23	4.5 V	24.084	B	P_1	4.669 +	4.681	4.681
	24	4.5 V	24.180	C	P_1	(4.67) +	(4.68)	
E_3	13	4.5 V	28.367	C	P_1	(5.30) +	(5.31)	
	14	4.5 V	28.469	C	P_1	(5.33) +	(5.34)	

Observation Point		Geophone*	Δ** (km)	Class	Phase***	Arrival† Time	Travel Time	Corrected†† Travel time
						s	s	
E_3	15	4.5 V	28.570	C	P_1	(5.34) +	(5.35)	
	16	4.5 V	28.671	B	P_1	5.366+	5.378	
	17	4.5 V	28.773	C	P_1	(5.36) +	(5.37)	
	18	4.5 V	28.867	C	P_1	(5.38) +	(5.39)	
	19	4.5 V	28.968	C	P_1	(5.39) +	(5.40)	
	20	4.5 V	29.070	C	P_1	(5.41) +	(5.42)	
	22	4.5 V	29.272	C	P_1	(5.42) +	(5.43)	
	23	4.5 V	29.373	C	P_1	(5.44) +	(5.45)	
	24	4.5 V	29.475	B	P_1	5.445+	5.457	
E_4	2	4.5 V	33.500	C	P_1	6.25 +	6.26	
	3	4.5 V	33.598	C	P_1	6.27 +	6.28	
	4	4.5 V	33.697	C	P_1	6.27 +	6.28	
	5	4.5 V	33.796	C	P_1	6.30 +	6.31	
	7	4.5 V	33.995	C	P_1	6.33 +	6.34	
	8	4.5 V	34.094	C	P_1	6.35 +	6.36	
	9	4.5 V	34.193	C	P_1	6.36 +	6.37	
	10	4.5 V	34.300	C	P_1	6.37 +	6.38	
	12	4.5 V	34.498	C	P_1	6.41 +	6.42	
	13	4.5 V	34.597	C	P_1	6.44 +	6.45	
	14	4.5 V	34.696	C	P_1	6.46 +	6.47	
	15	4.5 V	34.795	C	P_1	6.49 +	6.50	
	16	4.5 V	34.895	C	P_1	6.50 +	6.51	
	17	4.5 V	35.002	C	P_1	6.51 +	6.52	
	18	4.5 V	35.097	C	P_1	6.52 +	6.53	
	19	4.5 V	35.196	C	P_1	6.53 +	6.54	
	20	4.5 V	35.301	C	P_1	6.54 +	6.55	
								s
E_5	3	4.5 V	39.347	C	P_1	7.19 +	7.20	7.19
	5	4.5 V	39.548	C	P_1	7.20 +	7.21	7.20
	6	4.5 V	39.649	C	P_1	(7.17)	(7.18)	(7.17)
	7	4.5 V	39.750	C	P_1	7.21 +	7.22	7.21
	8	4.5 V	39.851	B	P_1	7.237+	7.249	7.242
	9	4.5 V	39.952	C	P_1	7.25 +	7.26	7.25
	10	4.5 V	40.053	C	P_1	7.29 +	7.30	7.29
	16	4.5 V	40.657	C	P_1	7.38 +	7.39	7.38
	19	4.5 V	40.961	C	P_1	7.42 +	7.43	7.42
	20	4.5 V	41.062	C	P_1	7.43 +	7.44	7.43
	21	4.5 V	41.163	C	P_1	7.45 +	7.46	7.45
	24	4.5 V	41.464	C	P_1	7.49 +	7.50	7.49
D_1	a	4 V	1.070	A	P_1	0.497+	0.509	0.507
	b	1 V	1.541	A	P_1	0.619+	0.631	0.629
	c	4 V	1.925	A	P_1	0.704+	0.716	0.715
D_2	a	4 V	4.800	A	P_1	1.427+	1.439	1.438
	b	1 V	5.149	A	P_1	1.493+	1.505	1.503
	c	4 V	5.539	A	P_1	1.532+	1.544	1.541
D_3	a	1 V	9.425	A	P_1	2.137+	2.149	
	b	4 V	9.625	A	P_1	2.171+	2.183	
	c	2 V	10.090	A	P_1	2.305+	2.317	
D_4	a	4 V	10.430	A	P_1	2.360+	2.372	
	b	2 V	10.681	A	P_1	2.415+	2.427	
	c	4 V	11.031	A	P_1	2.452+	2.464	

Observation Point		Geophone*	Δ** (km)	Class	Phase***	Arrival† Time	Travel Time	Corrected†† Travel time
						s	s	s
D_5	a	1 V	18.560	A	P_1	3.788+	3.800	
	b	1 V	18.891	A	P_1	3.871+	3.883	
	c	1 V	19.315	A	P_1	3.952+	3.964	
D_6	a	1 V	24.650	C	P_1	4.68 +	4.69	
	b	1 V	25.245	C	P_1	4.81 +	4.82	
	c	1 V	25.669	A	P_1	4.951+	4.963	
D_7	b	1 V	31.074	C	P_1	5.621+	5.63	
	c	4 V	31.949	C	P_1	5.89 +	5.91	
D_8	a	4 V	35.349	B	P_1	6.439+	6.451	6.450
	b	1 V	35.604	B	P_1	6.463+	6.475	
	c	4 V	35.895	A	P_1	6.528+	6.540	
	b′	4 V	35.709	B	P_1	6.496+	6.508	6.503
	b	$1H_{//}$	35.604	A	P_1	6.527+	6.539	
	b	$1H_{\angle R}$	35.604	C	P_1	6.55 +	6.56	
D_9	a	4 V	44.750	C	P_1	(8.08) +	(8.09)	
	b	1 V	45.160	B	P_1	8.080+	8.092	
	c	4 V	45.470	C	P_1	8.17 +	8.18	
D_{10}	a	4 V	50.320	B	P_1	8.983+	8.995	8.994
	b	1 V	50.575	B	P_1	8.996+	9.008	
	c	4 V	50.960	B	P_1	9.080+	9.092	9.091
D_{11}	a	4 V	52.830	C	P_1	(9.38) +	(9.39)	
	b	1 V	53.040	B	P_1	9.399+	9.411	
	c	4 V	53.230	C	P_1	(9.42) +	(9.43)	
D_{12}	a	4 V	57.682	B	P_1	10.144+	10.156	
	b	1 V	58.047	A	P_1	10.162+	10.174	
	c	4 V	58.377	C	P_1	10.248+	10.260	10.259
D_{13}	a	4 V	60.835	B	P_1	10.716+	10.728	10.726
	b	1 V	61.155	B	P_1	10.800+	10.812	10.810
	c	4 V	61.400	C	P_1	10.88 +	10.89	
D_{14}	a	1 V	64.660	B	P_1	11.443+	11.455	11.454
	c	4 V	64.935	C	P_1	(11.51) +	(11.52)	
	d	4 V	65.169	C	P_1	11.55 +	11.56	
	e	4 V	65.309	C	P_1	11.57 +	11.58	
	f	4 V	65.490	C	P_1	11.59 +	11.60	

* 4.5 V means that the vertical geophone with the natural frequency of 4.5 cps. 1 $H_{//}$ means that the horizontal geophone with the natural frequency of 1 cps is set up for registration of longitudinal component of ground motion. While 1 $H_{\angle R}$ means that it is set up for registration of transversal componett of ground motion. 1 H means that the horizontal geophone is set up to record east-west somponent of ground motion.

** Δ means the distance projected to the line I–V.

*** P_1 means the initial of P waves.

† The number with brackct shows that the arrival time is estimated from the time difference between clear initial and clear trough or crest at the adjacent observation points when the correlation between these troughs or crests is good. The sign + means that the direction of initial ground motion is upwards for the vertial geophones, to righthand side from the shot point for the transversal component, to push from the shot point for the longitudinal component and westwards for the horizontal component.

†† The corrected travel time means the travel time projected to the line I–V. This is derived by multiplying observed travel time with cosine of azimuth given in Table 3. If there is no difference between observed and corrected travel time because of small azimuth, the space is left blank and the value of Travel Time in this table should be used.

The above explanations are common for all tables in Tables 5 and 6 except for I–V which must be replaced by I–IV in Table 6.

Table 5 (2) Travel time data for shot A–II

Observation Point		Geophone	Δ (km)	Class	Phase	Arrival Time	Travel Time	Corrected Travel time
						1h 05m		
E_1	2	4.5 V	0.218	A	P_1	0.210s+	0.112s	
	3	4.5 V	0.320	A	P_1	0.222+	0.124	
	4	4.5 V	0.419	A	P_1	0.251+	0.153	
	5	4.5 V	0.521	A	P_1	0.287+	0.189	
	6	4.5 V	0.620	A	P_1	0.311+	0.213	
	7	4.5 V	0.718	A	P_1	0.309+	0.211	
	8	4.5 V	0.820	A	P_1	0.328+	0.230	
	9	4.5 V	0.918	A	P_1	0.352+	0.254	0.253s
	10	4.5 V	1.019	A	P_1	0.389+	0.291	0.290
	11	4.5 V	1.118	A	P_1	0.422+	0.324	0.324
	12	4.5 V	1.211	A	P_1	0.430+	0.332	0.328
	13	4.5 V	1.314	A	P_1	0.452+	0.354	0.348
	14	4.5 V	1.418	A	P_1	0.481+	0.383	0.375
	15	4.5 V	1.517	A	P_1	0.513+	0.415	0.407
	16	4.5 V	1.616	A	P_1	0.520+	0.422	0.415
	17	4.5 V	1.715	A	P_1	0.554+	0.456	0.450
	19	4.5 V	1.917	B	P_1	0.603+	0.505	0.499
	20	4.5 V	2.016	B	P_1	0.634+	0.536	0.530
	21	4.5 V	2.119	A	P_1	0.671+	0.573	0.568
	22	4.5 V	2.218	B	P_1	0.675+	0.577	0.572
	23	4.5 V	2.316	B	P_1	0.710+	0.612	0.607
	24	4.5 V	2.415	B	P_1	0.728+	0.630	0.625
E_2	1	4.5 V	7.265	A	P_1	1.810+	1.712	1.710
	2	4.5 V	7.362	A	P_1	1.830+	1.732	1.730
	3	4.5 V	7.464	A	P_1	1.839+	1.741	1.739
	4	4.5 V	7.566	A	P_1	1.847+	1.749	1.747
	5	4.5 V	7.668	B	P_1	1.860+	1.762	1.760
	6	4.5 V	7.765	A	P_1	1.877+	1.779	1.777
	7	4.5 V	7.867	A	P_1	1.892+	1.794	1.792
	8	4.5 V	7.969	A	P_1	1.912+	1.814	1.812
	9	4.5 V	8.062	A	P_1	1.930+	1.832	1.830
	10	4.5 V	8.168	A	P_1	1.952+	1.854	1.852
	11	4.5 V	8.261	A	P_1	1.975+	1.877	1.875
	12	4.5 V	8.366	A	P_1	2.000+	1.902	1.900
	13	4.5 V	8.463	B	P_1	2.021+	1.923	1.921
	14	4.5 V	8.563	B	P_1	2.045+	1.947	1.945
	15	4.5 V	8.659	A	P_1	2.052+	1.954	1.952
	16	4.5 V	8.756	B	P_1	2.061+	1.963	1.961
	17	4.5 V	8.857	A	P_1	2.067+	1.969	1.967
	18	4.5 V	8.960	A	P_1	2.081+	1.983	1.981
	19	4.5 V	9.061	B	P_1	2.092+	1.994	1.992
	21	4.5 V	9.259	A	P_1	2.104+	2.006	2.004
	22	4.5 V	9.361	B	P_1	2.106+	2.008	2.006
	23	4.5 V	9.463	B	P_1	2.113+	2.015	2.013
	24	4.5 V	9.558	B	P_1	2.115+	2.017	2.015
E_3	1	4.5 V	12.544	A	P_1	2.564+	2.466	2.464
	2	4.5 V	12.639	A	P_1	2.583+	2.485	2.483
	3	4.5 V	12.735	A	P_1	2.621+	2.523	2.521

Observation Point		Geophone	Δ (km)	Class	Phase	Arrival Time	Travel Time	Corrected Travel time
						s	s	s
E_3	4	4.5 V	12.841	B	P_1	2.640+	2.542	2.540
	5	4.5 V	12.942	B	P_1	2.626+	2.528	2.526
	6	4.5 V	13.043	A	P_1	2.640+	2.542	2.540
	7	4.5 V	13.144	B	P_1	2.640+	2.542	2.540
	8	4.5 V	13.246	A	P_1	2.670+	2.572	2.570
	9	4.5 V	13.341	A	P_1	2.706+	2.608	2.606
	10	4.5 V	13.442	A	P_1	2.738+	2.640	2.638
	11	4.5 V	13.543	A	P_1	2.742+	2.644	2.642
	13	4.5 V	13.745	A	P_1	2.779+	2.681	2.679
	14	4.5 V	13.847	A	P_1	2.799+	2.701	2.699
	15	4.5 V	13.948	A	P_1	2.820+	2.722	2.720
	16	4.5 V	14.050	A	P_1	2.835+	2.737	2.735
	17	4.5 V	14.151	A	P_1	2.853+	2.755	2.753
	18	4.5 V	14.245	A	P_1	2.860+	2.762	2.760
	19	4.5 V	14.347	A	P_1	2.873+	2.775	2.773
	20	4.5 V	14.448	B	P_1	2.890+	2.792	2.790
	22	4.5 V	14.650	B	P_1	2.900+	2.802	2.800
	23	4.5 V	14.752	A	P_1	2.910+	2.812	2.810
	24	4.5 V	14.853	A	P_1	2.913+	2.815	2.813
E_4	1	4.5 V	18.781	C	P_1	(3.58)+	(3.48)	(3.47)
	2	4.5 V	18.879	C	P_1	(3.61)+	(3.51)	(3.50)
	3	4.5 V	18.977	C	P_1	(3.64)+	(3.54)	(3.53)
	4	4.5 V	19.075	C	P_1	(3.65)+	(3.55)	(3.54)
	5	4.5 V	19.175	C	P_1	(3.68)+	(3.58)	(3.57)
	6	4.5 V	19.284	C	P_1	(3.70)+	(3.60)	(3.59)
	7	4.5 V	19.373	C	P_1	(3.78)+	(3.68)	(3.67)
	8	4.5 V	19.472	C	P_1	3.73 +	3.63	3.62
	9	4.5 V	19.571	C	P_1	(3.75)+	(3.65)	(3.64)
	10	4.5 V	19.678	C	P_1	(3.76)+	(3.66)	(3.65)
	11	4.5 V	19.777	C	P_1	3.77 +	3.67	3.66
	12	4.5 V	19.876	C	P_1	(3.79)+	(3.69)	(3.68)
	13	4.5 V	19.975	C	P_1	(3.83)+	(3.73)	(3.72)
	14	4.5 V	20.074	C	P_1	(3.86)+	(3.76)	(3.75)
	15	4.5 V	20.174	C	P_1	(3.89)+	(3.79)	(3.78)
	16	4.5 V	20.273	C	P_1	(3.90)+	(3.80)	(3.79)
	17	4.5 V	20.380	C	P_1	(3.91)+	(3.81)	(3.80)
	18	4.5 V	20.475	C	P_1	(3.91)+	(3.81)	(3.80)
	19	4.5 V	20.574	C	P_1	(3.90)+	(3.80)	(3.79)
	20	4.5 V	20.679	C	P_1	(3.92)+	(3.82)	(3.81)
	22	4.5 V	20.875	C	P_1	(3.95)+	(3.85)	(3.84)
	23	4.5 V	20.963	C	P_1	(3.95)+	(3.85)	(3.84)
	24	4.5 V	21.050	C	P_1	(3.96)+	(3.86)	(3.85)
E_5	1	4.5 V	24.524	C	P_1	(4.57) +	(4.47)	
	2	4.5 V	24.624	B	P_1	4.600+	4.502	4.498
	3	4.5 V	24.725	B	P_1	4.616+	4.518	4.514
	4	4.5 V	24.826	B	P_1	4.620+	4.522	4.518
	6	4.5 V	25.028	C	P_1	(4.60) +	(4.50)	
	7	4.5 V	25.128	B	P_1	4.635+	4.537	4.534
	8	4.5 V	25.229	C	P_1	(4.67) +	(4.57)	
	9	4.5 V	25.330	B	P_1	4.716+	4.618	4.614
	10	4.5 V	25.431	C	P_1	(4.73) +	(4.63)	

Observation Point		Geophone	Δ (km)	Class	Phase	Arrival Time	Travel Time	Corrected Travel time
						s	s	
E_5	11	4.5 V	25.532	C	P_1	4.78 +	4.68	
	12	4.5 V	25.633	C	P_1	(4.80) +	(4.70)	
	13	4.5 V	25.734	C	P_1	(4.81) +	(4.71)	
	14	4.5 V	25.835	C	P_1	(4.81) +	(4.71)	s
	15	4.5 V	25.936	B	P_1	4.817+	4.719	4.716
	16	4.5 V	26.036	C	P_1	(4.81) +	(4.71)	
	17	4.5 V	26.137	C	P_1	(4.81) +	(4.71)	
	18	4.5 V	26.238	C	P_1	(4.81) +	(4.71)	
	19	4.5 V	26.339	C	P_1	(4.84) +	(4.74)	
	20	4.5 V	26.440	C	P_1	(4.85) +	(4.75)	
	21	4.5 V	26.541	C	P_1	4.86 +	4.76	
	22	4.5 V	26.642	C	P_1	4.88 +	4.78	
	24	4.5 V	26.843	C	P_1	4.90 +	4.80	
D_1	a	4 V	13.552	A	P_1	2.995+	2.897	2.894
	b	1 V	13.081	B	P_1	2.875+	2.777	2.774
	c	4 V	12.697	B	P_1	2.756+	2.658	2.655
D_2	a	4 V	9.822	A	P_1	2.218+	2.120	2.117
	b	1 V	9.473	A	P_1	2.167+	2.069	2.067
	c	4 V	9.082	A	P_1	2.109+	2.011	2.010
D_3	a	1 V	5.197	A	P_1	1.254+	1.156	1.148
	b	4 V	4.996	A	P_1	1.211+	1.113	1.101
	c	2 V	4.532	A	P_1	1.180+	1.082	1.071
D_4	a	4 V	4.192	A	P_1	1.141+	1.043	1.034
	b	2 V	3.941	A	P_1	1.108+	1.010	1.001
	c	4 V	3.591	A	P_1	0.985+	0.887	0.878
D_5	a	1 V	3.938	A	P_1	1.153	1.055	1.049
	b	1 V	4.269	A	P_1	1.159+	1.061	1.056
	c	1 V	4.693	A	P_1	1.156+	1.058	1.053
D_6	a	1 V	10.029	A	P_1	2.137+	2.039	2.033
	b	1 V	10.623	A	P_1	2.268+	2.170	2.167
	c	1 V	11.047	A	P_1	2.414+	2.316	2.313
D_7	a	4 V	16.207	A	P_1	3.127+	3.029	3.028
	b	1 H	16.452	A	P_1	3.193+	3.095	
	c	4 V	17.327	A	P_1	3.310+	3.212	3.211
D_8	a	4 V	20.727	B	P_1	3.901+	3.803	
	b	1 V	20.982	A	P_1	3.937+	3.839	
	c	4 V	21.273	B	P_1	3.988+	3.890	3.889
D_9	a	4 V	30.128	A	P_1	5.538+	5.440	5.439
	b	1 V	30.539	A	P_1	5.557+	5.459	
	c	4 V	30.848	A	P_1	5.624+	5.526	
D_{10}	a	4 V	35.698	B	P_1	6.463+	6.365	
	b	1 V	35.953	A	P_1	6.491+	6.393	
	c	4 V	36.338	B	P_1	6.564+	6.466	
D_{11}	a	4 V	38.208	B	P_1	6.848+	6.750	
	b	1 V	38.418	B	P_1	6.870+	6.772	
	c	4 V	38.609	B	P_1	6.919+	6.821	6.820

Observation Point		Geophone	Δ (km)	Class	Phase	Arrival Time	Travel Time	Corrected Travel time
						s	s	
D_{12}	a	4 V	43.060	B	P_1	7.659+	7.561	
	b	1 V	43.425	C	P_1	7.70 +	7.60	
	c	4 V	43.755	B	P_1	7.768+	7.670	
D_{13}	a	4 V	46.213	C	P_1	8.10 +	8.00	
	b	1 V	46.533	C	P_1	(8.20) +	(8.10)	
	c	4 V	46.778	C	P_1	(8.34) +	(8.24)	
D_{14}	a	4 V	50.038	B	P_1	8.962+	8.864	
	c	1 V	50.313	C	P_1	9.026+	8.928	
	c	1 H	50.313	C	P_1	9.02 +	8.92	
	d	4 V	50.547	C	P_1	9.04 +	8.94	
	e	4 V	50.688	C	P_1	9.07 +	8.97	
	f	4 V	50.869	C	P_1	9.12 +	9.02	

Table 5 (3) Travel time data for shot A–III

Observation Point		Geophone	Δ (km)	Class	Phase	Arrival Time	Travel Time	Corrected Travel time
						3h 05m		
						s	s	s
E_1	1	4.5 V	15.074	B	P_1	2.958+	2.837	2.835
	2	4.5 V	14.975	A	P_1	2.938+	2.817	2.815
	3	4.5 V	14.872	B	P_1	2.910+	2.789	2.787
	4	4.5 V	14.774	C	P_1	2.900+	2.779	2.777
	5	4.5 V	14.671	B	P_1	2.876+	2.755	2.753
	6	4.5 V	14.573	B	P_1	2.871+	2.750	2.748
	7	4.5 V	14.474	B	P_1	2.837+	2.716	2.715
	8	4.5 V	14.372	B	P_1	2.806+	2.685	2.684
	9	4.5 V	14.275	B	P_1	2.796+	2.675	2.674
	10	4.5 V	14.174	B	P_1	2.795+	2.674	2.673
	11	4.5 V	14.074	C	P_1	2.774+	2.653	2.652
	12	4.5 V	13.982	B	P_1	2.756+	2.635	2.634
	13	4.5 V	13.878	B	P_1	2.735+	2.614	2.613
	14	4.5 V	13.774	B	P_1	2.718+	2.597	
	15	4.5 V	13.676	B	P_1	2.706+	2.585	
	16	4.5 V	13.576	B	P_1	2.687+	2.566	
	21	4.5 V	13.074	B	P_1	2.609+	2.488	
	22	4.5 V	12.975	C	P_1	2.598+	2.477	
	24	4.5 V	12.778	C	P_1	2.582+	2.461	
E_2	1	4.5 V	7.927	B	P_1	1.842+	1.721	
	2	4.5 V	7.831	B	P_1	1.821+	1.700	
	3	4.5 V	7.729	A	P_1	1.803+	1.682	
	4	4.5 V	7.627	B	P_1	1.776+	1.655	
	5	4.5 V	7.524	B	P_1	1.746+	1.625	
	6	4.5 V	7.428	B	P_1	1.730+	1.609	
	7	4.5 V	7.326	A	P_1	1.714+	1.593	

Observation Point		Geophone	Δ (km)	Class	Phase	Arrival Time	Travel Time	Corrected Travel time
E_2	8	4.5 V	7.224	A	P_1	1.699+ s	1.578 s	
	9	4.5 V	7.131	A	P_1	1.693+	1.572	
	10	4.5 V	7.025	A	P_1	1.676+	1.555	
	11	4.5 V	6.931	A	P_1	1.656+	1.535	
	12	4.5 V	6.827	A	P_1	1.638+	1.517	
	13	4.5 V	6.730	A	P_1	1.605+	1.484	
	14	4.5 V	6.630	C	P_1	1.582+	1.461	
	15	4.5 V	6.533	B	P_1	1.558+	1.437	
	16	4.5 V	6.437	A	P_1	1.539+	1.418	
	17	4.5 V	6.335	A	P_1	1.515+	1.394	
	18	4.5 V	6.233	A	P_1	1.493+	1.372	
	19	4.5 V	6.132	A	P_1	1.466+	1.345	
	20	4.5 V	6.035	B	P_1	1.454+	1.333	
	21	4.5 V	5.934	A	P_1	1.418+	1.297	
	22	4.5 V	5.832	A	P_1	1.395+	1.274	
	23	4.5 V	5.730	A	P_1	1.367+	1.246	
	24	4.5 V	5.634	A	P_1	1.345+	1.224	
E_3	1	4.5 V	2.648	A	P_1	0.791+	0.670	
	2	4.5 V	2.533	A	P_1	0.798+	0.677	
	3	4.5 V	2.458	A	P_1	0.775+	0.654	
	4	4.5 V	2.352	A	P_1	0.740+	0.619	
	5	4.5 V	2.250	A	P_1	0.713+	0.592	
	6	4.5 V	2.149	A	P_1	0.692+	0.571	
	7	4.5 V	2.048	A	P_1	0.676+	0.555	
	8	4.5 V	1.946	A	P_1	0.669+	0.548	
	9	4.5 V	1.852	A	P_1	0.673+	0.552	
	10	4.5 V	1.750	A	P_1	0.663+	0.542	
	11	4.5 V	1.649	A	P_1	0.641+	0.520	
	12	4.5 V	1.548	A	P_1	0.633+	0.512	
	13	4.5 V	1.447	A	P_1	0.619+	0.498	
	14	4.5 V	1.345	A	P_1	0.590+	0.469	
	15	4.5 V	1.244	A	P_1	0.561+	0.440	
	16	4.5 V	1.143	A	P_1	0.540+	0.419	
	17	4.5 V	1.041	A	P_1	0.517+	0.396	
	18	4.5 V	0.947	A	P_1	0.488+	0.367	
	19	4.5 V	0.846	A	P_1	0.454+	0.333	
	20	4.5 V	0.744	A	P_1	0.426+	0.305	
	21	4.5 V	0.643	A	P_1	0.391+	0.270	
	22	4.5 V	0.542	A	P_1	0.360+	0.239	
	23	4.5 V	0.441	A	P_1	0.327+	0.206	
	24	4.5 V	0.339	A	P_1	0.295+	0.174	
E_4	1	4.5 V	3.588	A	P_1	0.909+	0.788	0.771 s
	2	4.5 V	3.686	B	P_1	0.934+	0.813	0.795
	3	4.5 V	3.784	A	P_1	0.961+	0.840	0.822
	4	4.5 V	3.883	A	P_1	0.988+	0.867	0.848
	5	4.5 V	3.982	A	P_1	1.002+	0.881	0.861
	6	4.5 V	4.092	A	P_1	1.042+	0.921	0.901
	7	4.5 V	4.181	A	P_1	1.049+	0.928	0.909
	8	4.5 V	4.280	B	P_1	1.064+	0.943	0.925
	9	4.5 V	4.379	A	P_1	1.076+	0.955	0.937
	10	4.5 V	4.486	A	P_1	1.085+	0.964	0.947

Observation Point		Geophone	Δ (km)	Class	Phase	Arrival Time	Travel Time	Corrected Travel time
						s	s	s
E_4	11	4.5 V	4.585	A	P_1	1.105+	0.984	0.967
	12	4.5 V	4.684	A	P_1	1.135+	1.014	0.997
	13	4.5 V	4.783	A	P_1	1.172+	1.051	1.034
	14	4.5 V	4.882	A	P_1	1.205+	1.084	1.067
	15	4.5 V	4.981	A	P_1	1.235+	1.114	1.097
	16	4.5 V	5.081	A	P_1	1.254+	1.133	1.117
	17	4.5 V	5.188	A	P_1	1.264+	1.143	1.127
	18	4.5 V	5.283	B	P_1	1.259+	1.138	1.123
	19	4.5 V	5.382	A	P_1	1.267+	1.146	1.131
	20	4.5 V	5.487	A	P_1	1.281+	1.160	1.146
	22	4.5 V	5.683	A	P_1	1.310+	1.189	1.176
	23	4.5 V	5.770	A	P_1	1.318+	1.197	1.184
	24	4.5 V	5.858	A	P_1	1.330+	1.209	1.197
E_5	1	4.5 V	9.332	A	P_1	1.954+	1.833	1.807
	2	4.5 V	9.432	A	P_1	1.987+	1.866	1.840
	3	4.5 V	9.533	A	P_1	2.000+	1.879	1.854
	4	4.5 V	9.633	A	P_1	2.001+	1.880	1.855
	5	4.5 V	9.734	A	P_1	2.001+	1.880	1.856
	6	4.5 V	9.835	A	P_1	1.985+	1.864	1.841
	7	4.5 V	9.936	A	P_1	2.022+	1.901	1.878
	8	4.5 V	10.037	A	P_1	2.061+	1.940	1.917
	9	4.5 V	10.138	A	P_1	2.096+	1.975	1.952
	10	4.5 V	10.239	A	P_1	2.124+	2.003	1.981
	11	4.5 V	10.340	A	P_1	2.160+	2.039	2.017
	12	4.5 V	10.441	A	P_1	2.201+	2.080	2.058
	13	4.5 V	10.542	A	P_1	2.208+	2.087	2.066
	14	4.5 V	10.642	A	P_1	2.212+	2.091	2.070
	15	4.5 V	10.743	A	P_1	2.209+	2.088	2.068
	16	4.5 V	10.843	A	P_1	2.209+	2.088	2.069
	17	4.5 V	10.945	A	P_1	2.202+	2.081	2.062
	18	4.5 V	11.046	B	P_1	2.202+	2.081	2.062
	19	4.5 V	11.147	B	P_1	2.240+	2.119	2.101
	20	4.5 V	11.248	A	P_1	2.250+	2.129	2.111
	21	4.5 V	11.349	A	P_1	2.273+	2.152	2.134
	22	4.5 V	11.450	B	P_1	2.281+	2.160	2.143
	24	4.5 V	11.650	A	P_1	2.314+	2.193	2.177
D_1	a	4 V	28.744	B	P_1	5.415+	5.294	
	b	1 V	28.274	C	P_1	5.292+	5.171	
	c	4 V	27.889	C	P_1	5.187+	5.066	
D_2	a	4 V	25.015	B	P_1	4.672+	4.551	
	b	1 V	24.666	B	P_1	4.611+	4.490	
	c	4 V	24.275	B	P_1	4.568+	4.447	
D_3	a	1 V	20.389	C	P_1	3.74 +	3.62	
	b	4 V	20.189	C	P_1	3.69 +	3.57	
	c	2 V	19.724	C	P_1	3.64 +	3.52	
D_4	a	4 V	19.384	B	P_1	3.656+	3.535	
	b	2 V	19.134	B	P_1	3.629+	3.508	
	c	4 V	18.784	B	P_1	3.527+	3.406	

Observation Point		Geophone	Δ (km)	Class	Phase	Arrival Time	Travel Time	Corrected Travel time
D_5	a	1 V	11.254	B	P_1	2.336+ s	2.215 s	
	b	1 V	10.924	B	P_1	2.333+	2.212	
	c	1 V	10.499	A	P_1	2.326+	2.205	
D_6	a	1 V	5.164	A	P_1	1.179+	1.058	1.057 s
	b	1 V	4.569	A	P_1	1.172+	1.051	
	c	1 V	4.145	A	P_1	1.116+	0.995	
D_7	a	4 V	1.015	A	P_1	0.453+	0.332	0.246
	b	1 V	1.259	A	P_1	0.462+	0.341	0.294
	c	4 V	2.135	A	P_1	0.638+	0.517	0.483
D_8	a	4 V	5.535	A	P_1	1.259+	1.138	1.134
	b	1 V	5.790	A	P_1	1.287+	1.166	1.165
	c	4 V	6.081	A	P_1	1.333+	1.212	1.212
	b	4 V	5.895	A	P_1	1.293+	1.172	1.172
	b	1 $H_{//}$	5.790	A	P_1	1.274+	1.153	1.152
	b	1 $H_{\angle R}$	5.790	A	P_1	1.275+	1.154	1.153
D_9	a	4 V	14.936	A	P_1	2.953+	2.832	
	b	1 V	15.346	A	P_1	2.970+	2.849	
	c	4 V	15.656	A	P_1	3.043+	2.922	
D_{10}	a	4 V	20.505	A	P_1	3.911+	3.790	3.789
	b	1 V	20.761	A	P_1	3.935+	3.814	3.813
	c	4 V	21.146	A	P_1	4.012+	3.891	3.890
D_{11}	a	4 V	23.015	B	P_1	4.303+	4.182	
	b	1 V	23.226	A	P_1	4.320+	4.199	
	c	4 V	23.416	B	P_1	4.347+	4.226	
D_{12}	a	4 V	27.867	A	P_1	5.116+	4.995	
	b	1 V	28.233	A	P_1	5.151+	5.030	
	c	4 V	28.563	A	P_1	5.233+	5.112	
D_{13}	a	4 V	31.021	A	P_1	5.662+	5.541	5.539
	b	1 V	31.341	A	P_1	5.744+	5.623	5.620
	c	4 V	31.586	A	P_1	5.854+	5.733	5.730
D_{14}	a	1 V	34.846	A	P_1	6.433+	6.312	
	c	4 V	35.121	B	P_1	6.490+	6.369	
	c	1 H	35.121	B	P_1	6.510+	6.389	
	d	4 V	35.354	A	P_1	6.542+	6.421	
	e	4 V	35.495	A	P_1	6.558+	6.437	
	f	4 V	35.676	C	P_1	6.63 +	6.51	

Table 5 (4) Travel time data for shot A–IV_1

Observation Point		Geophone	Δ (km)	Class	Phase	Arrival Time	Travel Time	Corrected Travel time
						3^h05^m		
						s	s	
E_1	1	4.5 V	29.824	A	P_1	5.729+	5.403	
	2	4.5 V	29.726	A	P_1	5.707+	5.381	
	3	4.5 V	29.623	B	P_1	5.698+	5.372	
	4	4.5 V	29.524	B	P_1	5.680+	5.354	
	5	4.5 V	29.422	B	P_1	5.676+	5.350	
	6	4.5 V	29.323	A	P_1	5.648+	5.322	
	7	4.5 V	29.225	B	P_1	5.620+	5.294	
	8	4.5 V	29.123	B	P_1	5.596+	5.270	
	9	4.5 V	29.025	A	P_1	5.583+	5.257	
	10	4.5 V	28.924	B	P_1	5.599+	5.273	
	11	4.5 V	28.825	B	P_1	5.560+	5.234	
	12	4.5 V	28.732	B	P_1	5.539+	5.213	
	13	4.5 V	28.629	B	P_1	5.529+	5.203	
	14	4.5 V	28.525	B	P_1	5.510+	5.184	
	15	4.5 V	28.426	A	P_1	5.484+	5.158	
	16	4.5 V	28.327	A	P_1	5.461+	5.135	
	18	4.5 V	28.129	B	P_1	5.453+	5.127	
	19	4.5 V	28.026	B	P_1	5.444+	5.118	
	20	4.5 V	27.927	A	P_1	5.438+	5.112	
	21	4.5 V	27.824	A	P_1	5.415+	5.089	
	22	4.5 V	27.726	B	P_1	5.406+	5.080	
	23	4.5 V	27.627	B	P_1	5.382+	5.056	
	24	4.5 V	27.528	B	P_1	5.360+	5.034	
E_2	1	4.5 V	22.678	A	P_1	4.626+	4.300	
	2	4.5 V	22.581	A	P_1	4.613+	4.287	4.286 (s)
	3	4.5 V	22.479	B	P_1	4.598+	4.272	4.271
	4	4.5 V	22.377	A	P_1	4.575+	4.249	4.248
	5	4.5 V	22.275	A	P_1	4.560+	4.234	4.233
	6	4.5 V	22.178	B	P_1	4.526+	4.200	4.199
	7	4.5 V	22.076	B	P_1	4.500+	4.174	4.173
	8	4.5 V	21.974	A	P_1	4.502+	4.176	4.175
	9	4.5 V	21.881	B	P_1	4.497+	4.171	4.170
	10	4.5 V	21.776	B	P_1	4.463+	4.137	4.136
	17	4.5 V	21.086	A	P_1	4.320+	3.994	3.993
	18	4.5 V	20.984	A	P_1	4.300+	3.974	3.973
	19	4.5 V	20.882	A	P_1	4.278+	3.952	3.951
	21	4.5 V	20.684	A	P_1	4.232+	3.906	3.905
	22	4.5 V	20.582	A	P_1	4.205+	3.879	3.878
	23	4.5 V	20.481	A	P_1	4.175+	3.849	3.848
	24	4.5 V	20.385	B	P_1	4.149+	3.823	3.822
E_3	1	4.5 V	17.399	B	P_1	3.652+	3.326	
	2	4.5 V	17.304	A	P_1	3.651+	3.325	
	3	4.5 V	17.209	A	P_1	3.635+	3.309	
	4	4.5 V	17.103	A	P_1	3.600+	3.274	
	5	4.5 V	17.001	A	P_1	3.583+	3.257	
	6	4.5 V	16.900	A	P_1	3.558+	3.232	
	7	4.5 V	16.799	A	P_1	3.548+	3.222	
	8	4.5 V	16.697	A	P_1	3.536+	3.210	

Observation Point		Geophone	Δ (km)	Class	Phase	Arrival Time	Travel Time	Corrected Travel time
E_3	9	4.5 V	16.603	B	P_1	3.540+ s	3.214 s	
	10	4.5 V	16.501	A	P_1	3.538+	3.212	
	11	4.5 V	16.400	B	P_1	3.505+	3.179	
	12	4.5 V	16.299	A	P_1	3.507+	3.181	
	13	4.5 V	16.198	A	P_1	3.484+	3.158	
	14	4.5 V	16.096	B	P_1	3.474+	3.148	
	15	4.5 V	15.995	B	P_1	3.450+	3.124	
	16	4.5 V	15.894	B	P_1	3.425+	3.099	
	17	4.5 V	15.792	A	P_1	3.409+	3.083	
	18	4.5 V	15.698	A	P_1	3.388+	3.062	
	19	4.5 V	15.597	A	P_1	3.368+	3.042	
	20	4.5 V	15.495	A	P_1	3.350+	3.024	
	21	4.5 V	15.394	B	P_1	3.315+	2.989	
	22	4.5 V	15.293	A	P_1	3.295+	2.969	
	23	4.5 V	15.192	A	P_1	3.270+	2.944	
	24	4.5 V	15.090	A	P_1	3.237+	2.911	
E_4	1	4.5 V	11.163	A	P_1	2.561+	2.235	2.226 s
	2	4.5 V	11.065	A	P_1	2.568+	2.242	2.232
	3	4.5 V	10.967	B	P_1	2.530+	2.204	2.194
	4	4.5 V	10.868	A	P_1	2.522+	2.196	2.186
	5	4.5 V	10.769	B	P_1	2.508+	2.182	2.171
	6	4.5 V	10.659	B	P_1	2.487+	2.161	2.150
	7	4.5 V	10.570	B	P_1	2.474+	2.148	2.137
	8	4.5 V	10.471	A	P_1	2.450+	2.124	2.113
	9	4.5 V	10.372	B	P_1	2.420+	2.094	2.083
	10	4.5 V	10.265	A	P_1	2.408+	2.082	2.071
	11	4.5 V	10.166	A	P_1	2.397+	2.071	2.059
	12	4.5 V	10.067	B	P_1	2.384+	2.058	2.047
	13	4.5 V	9.968	B	P_1	2.400+	2.074	2.062
	14	4.5 V	9.869	B	P_1	2.370+	2.044	2.032
	15	4.5 V	9.770	A	P_1	2.358+	2.032	2.020
	16	4.5 V	9.670	A	P_1	2.337+	2.011	1.999
	17	4.5 V	9.563	A	P_1	2.306+	1.980	1.968
	18	4.5 V	9.468	A	P_1	2.274+	1.948	1.936
	19	4.5 V	9.369	A	P_1	2.236+	1.910	1.898
	20	4.5 V	9.264	A	P_1	2.213+	1.887	1.875
	21	4.5 V	9.163	A	P_1	2.182+	1.856	1.844
	22	4.5 V	9.068	B	P_1	2.172+	1.846	1.834
	23	4.5 V	8.981	A	P_1	2.146+	1.820	1.808
	24	4.5 V	8.893	A	P_1	2.124+	1.798	1.786
E_5	1	4.5 V	5.419	A	P_1	1.589+	1.263	1.234
	2	4.5 V	5.319	A	P_1	1.580+	1.254	1.224
	3	4.5 V	5.218	A	P_1	1.569+	1.243	1.213
	4	4.5 V	5.118	A	P_1	1.532+	1.206	1.175
	5	4.5 V	5.017	A	P_1	1.499+	1.173	1.143
	6	4.5 V	4.916	A	P_1	1.451+	1.125	1.095
	7	4.5 V	4.815	A	P_1	1.459+	1.133	1.102
	8	4.5 V	4.714	A	P_1	1.460+	1.134	1.103
	9	4.5 V	4.613	A	P_1	1.471+	1.145	1.107
	10	4.5 V	4.512	A	P_1	1.483+	1.157	1.117
	11	4.5 V	4.411	A	P_1	1.470+	1.144	1.109

Observation Point		Geophone	Δ (km)	Class	Phase	Arrival Time	Travel Time	Corrected Travel time
						s	s	s
E_5	12	4.5 V	4.310	A	P_1	1.444+	1.118	1.082
	13	4.5 V	4.209	A	P_1	1.413+	1.087	1.051
	14	4.5 V	4.109	A	P_1	1.371+	1.045	1.009
	15	4.5 V	4.008	B	P_1	1.337+	1.011	0.975
	16	4.5 V	3.908	B	P_1	1.286+	0.960	0.925
	17	4.5 V	3.806	B	P_1	1.264+	0.938	0.901
	18	4.5 V	3.705	B	P_1	1.232+	0.906	0.870
	19	4.5 V	3.604	B	P_1	1.228+	0.902	0.865
	20	4.5 V	3.503	A	P_1	1.219+	0.893	0.855
	21	4.5 V	3.402	A	P_1	1.168+	0.842	0.805
	22	4.5 V	3.301	A	P_1	1.168+	0.842	0.803
	23	4.5 V	3.201	A	P_1	1.144+	0.818	0.779
	24	4.5 V	3.101	A	P_1	1.118+	0.792	0.752
D_1	a	4 V	43.495	A	P_1	8.152+	7.826	7.825
	b	1 V	43.025	A	P_1	8.068+	7.742	7.741
	c	4 V	42.640	B	P_1	7.968+	7.642	7.641
D_2	a	4 V	39.766	B	P_1	7.409+	7.083	
	b	1 V	39.417	B	P_1	7.335+	7.009	
	c	4 V	39.026	B	P_1	7.289+	6.963	
D_3	a	1 V	35.140	A	P_1	6.504+	6.178	6.177
	b	4 V	34.940	B	P_1	6.446+	6.120	6.119
	c	2 V	34.475	B	P_1	6.442+	6.116	6.115
D_4	a	4 V	34.135	C	P_1	6.40 +	6.07	6.07
	b	2 V	33.885	B	P_1	6.374+	6.048	6.047
	c	4 V	33.534	A	P_1	6.299+	5.973	5.972
D_5	a	1 V	26.005	A	P_1	5.239+	4.913	4.912
	b	1 V	25.675	A	P_1	5.189+	4.863	4.862
	c	1 V	25.250	A	P_1	5.116+	4.790	4.789
D_6	a	1 V	19.915	B	P_1	3.985+	3.659	
	b	1 V	19.320	B	P_1	3.973+	3.647	
	c	1 V	18.896	B	P_1	3.924+	3.598	
D_7	a	4 V	13.736	A	P_1	3.011+	2.685	2.680
	b	1 V	13.491	A	P_1	2.932+	2.606	2.603
	c	4 V	12.616	A	P_1	2.795+	2.469	2.465
D_8	a	4 V	9.216	A	P_1	2.185+	1.859	1.858
	b	1 V	8.961	A	P_1	2.107+	1.781	1.780
	c	4 V	8.670	A	P_1	2.054+	1.728	1.727
	b′	4 V	8.856	A	P_1	2.083+	1.757	1.756
	b	1 $H_{//}$	8.961	A	P_1	2.120+	1.794	1.793
	b	1 $H_{\angle R}$	8.961	A	P_1	2.133−	1.807	1.806
D_9	a	4 V	0.185	A	P_1	0.428+	0.102	0.080
	b	1 V	0.595	A	P_1	0.555+	0.229	0.212
D_{10}	a	4 V	5.755	A	P_1	1.595+	1.269	
	b	1 V	6.010	A	P_1	1.641+	1.315	
	c	4 V	6.395	B	P_1	1.733+	1.407	
D_{11}	a	4 V	8.265	A	P_1	2.032+	1.706	1.705
	b	1 V	8.475	A	P_1	2.045+	1.719	1.717
	c	4 V	8.665	A	P_1	2.097+	1.771	1.769

Observation Point		Geophone	Δ (km)	Class	Phase	Arrival Time	Travel Time	Corrected Travel time
						s	s	s
D_{12}	a	4 V	13.116	B	P_1	2.867+	2.541	2.540
	b	1 V	13.482	A	P_1	2.913+	2.587	
	c	4 V	13.812	A	P_1	2.996+	2.670	
D_{13}	a	4 V	16.270	A	P_1	3.452+	3.126	
	b	1 V	16.590	A	P_1	3.537+	3.211	3.210
	c	4 V	16.835	A	P_1	3.619+	3.293	3.292
D_{14}	a	1 V	20.095	A	P_1	4.233+	3.907	
	b	1 H	20.384	B	P_1	4.297−	3.971	
	c	4 V	20.370	A	P_1	4.291+	3.965	
	d	4 V	20.604	A	P_1	4.330+	4.004	
	e	4 V	20.744	A	P_1	4.359+	4.033	
	f	4 V	20.925	A	P_1	4.411+	4.085	

Table 5 (5) Travel time data for shot A–IV_2

Observation Point		Geophone	Δ (km)	Class	Phase	Arrival Time	Travel Time	Corrected Travel time
						h m 1 05		
						s	s	
E_1	1	4.5 V	29.824	B	P_1	5.430+	5.431	
	2	4.5 V	29.726	A	P_1	5.390+	5.391	
	3	4.5 V	29.623	A	P_1	5.377+	5.378	
	4	4.5 V	29.524	A	P_1	5.363+	5.364	
	5	4.5 V	29.422	A	P_1	5.355+	5.356	
	6	4.5 V	29.323	A	P_1	5.324+	5.325	
	7	4.5 V	29.225	B	P_1	5.292+	5.293	
	8	4.5 V	29.123	A	P_1	5.280+	5.281	
	9	4.5 V	29.025	A	P_1	5.270+	5.271	
	10	4.5 V	28.924	A	P_1	5.278+	5.279	
	11	4.5 V	28.825	A	P_1	5.242+	5.243	
	12	4.5 V	28.732	A	P_1	5.219+	5.220	
	13	4.5 V	28.629	A	P_1	5.210+	5.211	
	14	4.5 V	28.525	A	P_1	5.188+	5.189	
	15	4.5 V	28.426	A	P_1	5.167+	5.168	
	16	4.5 V	28.327	A	P_1	5.147+	5.148	
	17	4.5 V	28.228	A	P_1	5.132+	5.133	
	18	4.5 V	28.129	A	P_1	5.136+	5.137	
	19	4.5 V	28.026	A	P_1	5.130+	5.131	
	20	4.5 V	27.927	B	P_1	5.100+	5.101	
	21	4.5 V	27.824	A	P_1	5.098+	5.099	
	22	4.5 V	27.726	A	P_1	5.084+	5.085	
	23	4.5 V	27.627	A	P_1	5.068+	5.069	
	24	4.5 V	27.528	A	P_1	5.056+	5.057	

Observation Point		Geophone	Δ (km)	Class	Phase	Arrival Time	Travel Time	Corrected Travel time
						s	s	s
E_2	1	4.5 V	22.678	B	P_1	4.315+	4.316	4.316
	2	4.5 V	22.581	B	P_1	4.295+	4.296	4.295
	3	4.5 V	22.479	A	P_1	4.283+	4.284	4.283
	4	4.5 V	22.377	B	P_1	4.263+	4.264	4.263
	5	4.5 V	22.275	B	P_1	4.237+	4.238	4.237
	6	4.5 V	22.178	B	P_1	4.212+	4.213	4.212
	7	4.5 V	22.076	A	P_1	4.196+	4.197	4.196
	8	4.5 V	21.974	A	P_1	4.180+	4.181	4.180
	9	4.5 V	21.881	B	P_1	4.175+	4.176	4.175
	10	4.5 V	21.776	A	P_1	4.154+	4.155	4.154
	11	4.5 V	21.682	A	P_1	4.129+	4.130	4.129
	12	4.5 V	21.577	A	P_1	4.117+	4.118	4.117
	13	4.5 V	21.481	B	P_1	4.090+	4.091	4.090
	14	4.5 V	21.380	C	P_1	4.06 +	4.06	4.06
	15	4.5 V	21.284	A	P_1	4.040+	4.041	4.040
	16	4.5 V	21.188	C	P_1	4.01 +	4.01	4.01
	17	4.5 V	21.086	B	P_1	3.998+	3.999	3.998
	18	4.5 V	20.984	A	P_1	3.980+	3.981	3.980
	19	4.5 V	20.882	A	P_1	3.956+	3.957	3.956
	20	4.5 V	20.786	A	P_1	3.924+	3.925	3.924
	21	4.5 V	20.684	A	P_1	3.900+	3.901	3.900
	22	4.5 V	20.582	A	P_1	3.884+	3.885	3.884
	23	4.5 V	20.481	A	P_1	3.860+	3.861	3.860
	24	4.5 V	20.385	A	P_1	3.836+	3.837	3.836
E_3	2	4.5 V	17.304	A	P_1	3.326+	3.327	
	3	4.5 V	17.209	A	P_1	3.313+	3.314	
	4	4.5 V	17.103	A	P_1	3.284+	3.285	
	5	4.5 V	17.001	A	P_1	3.256+	3.257	
	6	4.5 V	16.900	A	P_1	3.236+	3.237	
	7	4.5 V	16.799	A	P_1	3.221+	3.222	
	8	4.5 V	16.697	A	P_1	3.215+	3.216	
	9	4.5 V	16.603	A	P_1	3.224+	3.225	
	10	4.5 V	16.501	A	P_1	3.210+	3.211	
	11	4.5 V	16.400	A	P_1	3.186+	3.187	
	12	4.5 V	16.299	A	P_1	3.185+	3.186	
	13	4.5 V	16.198	A	P_1	3.168+	3.169	
	14	4.5 V	16.096	A	P_1	3.146+	3.147	
	16	4.5 V	15.894	A	P_1	3.106+	3.107	
	17	4.5 V	15.792	A	P_1	3.081+	3.082	
	18	4.5 V	15.698	A	P_1	3.064+	3.065	
	19	4.5 V	15.597	A	P_1	3.043+	3.044	
	20	4.5 V	15.495	A	P_1	3.031+	3.032	
	21	4.5 V	15.394	A	P_1	2.999+	3.000	
	22	4.5 V	15.293	A	P_1	2.975+	2.976	
	23	4.5 V	15.192	A	P_1	2.949+	2.950	
	24	4.5 V	15.090	A	P_1	2.923+	2.924	
E_4	1	4.5 V	11.163	A	P_1	2.233+	2.234	2.225
	2	4.5 V	11.065	A	P_1	2.240+	2.241	2.231
	3	4.5 V	10.967	A	P_1	2.216+	2.217	2.207
	5	4.5 V	10.769	A	P_1	2.192+	2.193	2.182
	6	4.5 V	10.659	A	P_1	2.184+	2.185	2.174

Observation Point		Geophone	Δ (km)	Class	Phase	Arrival Time	Travel Time	Corrected Travel time
						s	s	s
E_4	7	4.5 V	10.570	A	P_1	2.159+	2.160	2.149
	8	4.5 V	10.471	A	P_1	2.134+	2.135	2.124
	9	4.5 V	10.372	A	P_1	2.110+	2.111	2.100
	10	4.5 V	10.265	A	P_1	2.085+	2.086	2.075
	11	4.5 V	10.166	A	P_1	2.072+	2.073	2.061
	12	4.5 V	10.067	A	P_1	2.073+	2.074	2.063
	13	4.5 V	9.968	A	P_1	2.077+	2.078	2.066
	14	4.5 V	9.869	A	P_1	2.052+	2.053	2.041
	15	4.5 V	9.770	A	P_1	2.033+	2.034	2.022
	16	4.5 V	9.670	A	P_1	2.011+	2.012	2.000
	17	4.5 V	9.563	B	P_1	1.980+	1.981	1.969
	18	4.5 V	9.468	B	P_1	1.952+	1.953	1.941
	19	4.5 V	9.369	A	P_1	1.911+	1.912	1.900
	20	4.5 V	9.264	A	P_1	1.885+	1.886	1.874
	21	4.5 V	9.163	A	P_1	1.858+	1.859	1.847
	22	4.5 V	9.068	A	P_1	1.843+	1.844	1.832
	23	4.5 V	8.981	A	P_1	1.821+	1.822	1.810
	24	4.5 V	8.893	A	P_1	1.801+	1.802	1.790
E_5	1	4.5 V	5.419	A	P_1	1.260+	1.261	1.232
	2	4.5 V	5.319	B	P_1	1.225+	1.226	1.197
	3	4.5 V	5.218	A	P_1	1.190+	1.191	1.161
	4	4.5 V	5.118	B	P_1	1.140+	1.141	1.110
	5	4.5 V	5.017	B	P_1	1.136+	1.137	1.108
	6	4.5 V	4.916	A	P_1	1.125+	1.126	1.096
	7	4.5 V	4.815	A	P_1	1.126+	1.127	1.096
	8	4.5 V	4.714	A	P_1	1.137+	1.138	1.107
	9	4.5 V	4.613	A	P_1	1.139+	1.140	1.102
	10	4.5 V	4.512	A	P_1	1.120+	1.121	1.082
	11	4.5 V	4.411	A	P_1	1.116+	1.117	1.082
	12	4.5 V	4.310	A	P_1	1.107+	1.108	1.072
	13	4.5 V	4.209	A	P_1	1.081+	1.082	1.046
	14	4.5 V	4.109	A	P_1	1.041+	1.042	1.006
	15	4.5 V	4.008	A	P_1	1.012+	1.013	0.977
	16	4.5 V	3.908	A	P_1	0.972+	0.973	0.938
	17	4.5 V	3.806	A	P_1	0.930+	0.931	0.894
	18	4.5 V	3.705	A	P_1	0.899+	0.900	0.864
	19	4.5 V	3.604	A	P_1	0.903+	0.904	0.867
	20	4.5 V	3.503	A	P_1	0.892+	0.893	0.855
	22	4.5 V	3.301	A	P_1	0.843+	0.844	0.805
	23	4.5 V	3.201	B	P_1	0.818+	0.819	0.780
	24	4.5 V	3.101	A	P_1	0.792+	0.793	0.753
D_1	a	4 V	43.495	A	P_1	7.829+	7.830	7.829
	b	1 V	43.025	B	P_1	7.740+	7.741	7.740
	c	4 V	42.640	B	P_1	7.645+	7.646	7.645
D_2	a	4 V	39.766	B	P_1	7.079+	7.080	
	b	1 V	39.417	B	P_1	7.034+	7.035	
	c	4 V	39.026	C	P_1	(6.97) +	(6.970)	

Observation Point		Geophone	Δ (km)	Class	Phase	Arrival Time	Travel Time	Corrected Travel time
						s	s	s
D_3	a	1 V	35.140	A	P_1	6.184+	6.185	6.184
	b	4 V	34.940	A	P_1	6.142+	6.143	6.142
	c	2 V	34.475	A	P_1	6.130+	6.131	6.130
D_4	a	4 V	34.135	A	P_1	6.104+	6.105	6.104
	b	2 V	33.885	A	P_1	6.079+	6.080	6.079
	c	4 V	33.534	A	P_1	5.977+	5.978	5.977
D_5	a	1 V	26.005	A	P_1	4.936+	4.937	4.936
	b	1 V	25.675	A	P_1	4.880+	4.881	4.880
	c	1 V	25.250	A	P_1	4.796+	4.797	4.796
D_6	a	1 V	19.915	A	P_1	3.668+	3.669	
	b	1 V	19.320	A	P_1	3.663+	3.664	
	c	1 V	18.896	A	P_1	3.611+	3.612	
D_7	a	4 V	13.736	A	P_1	2.689+	2.690	2.685
	b	1 V	13.491	A	P_1	2.607+	2.608	2.605
	c	4 V	12.616	A	P_1	2.476+	2.477	2.473
D_8	a	4 V	9.216	A	P_1	1.865+	1.866	1.865
	b	1 V	8.961	A	P_1	1.791+	1.792	1.791
	c	4 V	8.670	A	P_1	1.744+	1.745	1.744
	b′	4 V	8.856	A	P_1	1.764+	1.765	1.764
	b	1 H∠R	8.961	A	P_1	1.794−	1.795	1.794
	b	1 H//	8.961	A	P_1	1.794+	1.795	1.794
D_9	a	4 V	0.185	A	P_1	0.105+	0.106	0:083
	b	1 V	0.595	A	P_1	0.232+	0.233	0.215
	c	4 V	0.905	A	P_1	0.328+	0.329	0.304
D_{10}	a	4 V	5.755	A	P_1	1.270+	1.271	
	b	1 V	6.010	A	P_1	1.315+	1.316	
	c	4 V	6.395	A	P_1	1.405+	1.406	
D_{11}	a	4 V	8.265	A	P_1	1.712+	1.713	1.712
	b	1 V	8.475	A	P_1	1.725+	1.726	1.724
	c	4 V	8.665	A	P_1	1.768+	1.769	1.767
D_{12}	a	4 V	13.116	A	P_1	2.541+	2.542	2.541
	b	1 V	13.482	A	P_1	2.590+	2.591	
	c	4 V	13.812	A	P_1	2.673+	2.674	
D_{13}	a	4 V	16.270	A	P_1	3.124+	3.125	
	b	1 V	16.590	A	P_1	3.197+	3.198	3.197
	c	4 V	16.835	B	P_1	3.285+	3.286	3.285
D_{14}	a	1 V	20.095	A	P_1	3.905+	3.906	
	b	1 V	20.384	A	P_1	3.964+	3.965	
	c	1 H	20.370	A	P_1	3.966+	3.967	
	d	4 V	20.604	A	P_1	3.994+	3.995	
	e	4 V	20.744	A	P_1	4.024+	4.025	
	f	4 V	20.925	A	P_1	4.086+	4.087	

Table 5 (6) Travel time data for shot A–V_1

Observation Point		Geophone	Δ (km)	Class	Phase	Arrival Time	Travel Time	Corrected Travel time
						$2^h 05^m$		
						s	s	
D_1	a	4 V	64.434	B	P_1	11.612+	11.474	
	b	1 V	63.964	B	P_1	11.516+	11.378	
	c	4 V	63.579	B	P_1	11.428+	11.290	
D_2	a	4 V	60.705	C	P_1	10.84 +	10.70	
	b	1 V	60.356	C	P_1	10.78 +	10.64	
D_3	a	4 V	56.079	B	P_1	9.940+	9.802	
	b	2 V	55.879	C	P_1	9.91 +	9.77	
	c	4 V	55.414	C	P_1	9.85 +	9.71	
D_4	a	4 V	55.074	C	P_1	9.85 +	9.71	
	b	2 V	54.823	C	P_1	9.84 +	9.70	
D_6	a	1 V	40.854	C	P_1	7.48 +	7.34	
	b	1 V	40.259	B	P_1	7.467+	7.329	
	c	1 V	39.835	B	P_1	7.402+	7.264	
D_7	a	4 V	34.675	A	P_1	6.514+	6.376	6.373 s
	b	1 V	34.430	A	P_1	6.445+	6.307	6.305
	c	4 V	33.555	A	P_1	6.310+	6.172	6.169
D_8	a	4 V	30.155	A	P_1	5.737+	5.599	5.598
	b	1 V	29.900	A	P_1	5.668+	5.530	
	c	4 V	29.609	A	P_1	5.624+	5.486	5.485
	b′	4 V	29.795	A	P_1	5.628+	5.490	5.489
	b	1 $H_{//}$	29.900	A	P_1	5.661+	5.523	5.522
D_9	a	4 V	20.754	A	P_1	4.179+	4.041	4.040
	b	1 V	20.344	A	P_1	4.095+	3.957	3.956
	c	4 V	20.034	A	P_1	4.054+	3.916	3.914
D_{10}	a	4 V	15.184	A	P_1	3.264+	3.126	3.124
	b	1 V	14.929	A	P_1	3.186+	3.048	3.046
	c	4 V	14.544	B	P_1	3.136+	2.998	2.996
D_{11}	a	4 V	12.674	A	P_1	2.790+	2.652	2.651
	b	1 V	12.464	A	P_1	2.720+	2.582	2.581
	c	4 V	12.274	A	P_1	2.690+	2.552	
D_{12}	a	4 V	7.823	A	P_1	1.954+	1.816	1.814
	b	1 V	7.457	A	P_1	1.879+	1.741	1.737
	c	4 V	7.127	A	P_1	1.867+	1.729	1.723
D_{13}	a	4 V	4.669	A	P_1	1.504+	1.366	1.333
	b	1 V	4.349	A	P_1	1.434+	1.296	1.243
	c	4 V	4.104	A	P_1	1.376+	1.238	1.183
D_{14}	a	4 V	0.844	A	P_1	0.487+	0.349	0.326
	c	1 V	0.569	A	P_1	0.346+	0.208	0.200
	c	1 H	0.569	A	P_1	0.343+	0.205	0.197
	d	4 V	0.335	A	P_1	0.264+	0.126	0.116
	f	4 V	0.014	A	P_1	0.161+	0.023	0.023

Table 5 (7) Travel time data for shot A–V_2

Observation Point		Geophone	Δ (km)	Class	Phase	Arrival Time	Travel Time	Corrected Travel time
						$2^h 05^m$ s	s	
E_1	1	4.5 V	50.763	C	P_1	(9.14) +	(9.05)	
	2	4.5 V	50.665	C	P_1	(9.11) +	(9.02)	
	3	4.5 V	50.562	C	P_1	(9.09) +	(9.00)	
	4	4.5 V	50.463	C	P_1	(9.08) +	(8.99)	
	5	4.5 V	50.361	C	P_1	(9.05) +	(8.96)	
	6	4.5 V	50.262	C	P_1	9.04 +	8.95	
	7	4.5 V	50.164	C	P_1	(9.01) +	(8.92)	
	8	4.5 V	50.062	C	P_1	(9.00) +	(8.91)	s
	9	4.5 V	49.964	B	P_1	8.976+	8.883	8.882
	10	4.5 V	49.863	C	P_1	(8.97) +	(8.88)	
	11	4.5 V	49.764	C	P_1	(8.96) +	(8.87)	
	12	4.5 V	49.671	C	P_1	(8.93) +	(8.84)	
	13	4.5 V	49.568	B	P_1	8.907+	8.814	8.813
	14	4.5 V	49.464	B	P_1	8.891+	8.798	
	15	4.5 V	49.365	C	P_1	(8.88) +	(8.79)	
	16	4.5 V	49.266	B	P_1	8.856+	8.763	
	17	4.5 V	49.167	C	P_1	(8.85) +	(8.76)	
	18	4.5 V	49.068	C	P_1	8.83 +	8.74	
	19	4.5 V	48.965	C	P_1	(8.83) +	(8.74)	
	20	4.5 V	48.866	C	P_1	(8.82) +	(8.73)	
	21	4.5 V	48.763	B	P_1	8.790+	8.697	
	22	4.5 V	48.665	C	P_1	(8.79) +	(8.70)	
	23	4.5 V	48.566	C	P_1	(8.78) +	(8.69)	
	24	4.5 V	48.467	C	P_1	(8.77) +	(8.68)	
E_2	1	4.5 V	43.617	C	P_1	(8.06) +	(7.97)	
	2	4.5 V	43.520	C	P_1	(8.04) +	(7.95)	
	3	4.5 V	43.418	C	P_1	(8.03) +	(7.94)	
	4	4.5 V	43.316	C	P_1	8.00 +	7.91	
	5	4.5 V	43.214	C	P_1	(7.99) +	(7.90)	
	8	4.5 V	42.913	C	P_1	7.91 +	7.82	
	9	4.5 V	42.820	C	P_1	7.90 +	7.81	
	10	4.5 V	42.715	C	P_1	7.88 +	7.79	
	11	4.5 V	42.621	C	P_1	(7.87) +	(7.78)	
	12	4.5 V	42.516	C	P_1	(7.85) +	(7.76)	
	13	4.5 V	42.420	C	P_1	(7.84) +	(7.75)	
	14	4.5 V	42.319	C	P_1	(7.79) +	(7.70)	
	15	4.5 V	42.223	C	P_1	(7.77) +	(7.68)	
	16	4.5 V	42.127	C	P_1	(7.76) +	(7.67)	
	17	4.5 V	42.025	C	P_1	(7.73) +	(7.64)	
	18	4.5 V	41.923	C	P_1	7.71 +	7.62	
	19	4.5 V	41.821	C	P_1	(7.68) +	(7.59)	
	20	4.5 V	41.725	B	P_1	7.663+	7.570	
	21	4.5 V	41.623	B	P_1	7.640+	7.547	
	22	4.5 V	41.521	C	P_1	7.62 +	7.53	
	23	4.5 V	41.420	C	P_1	7.60 +	7.51	
	24	4.5 V	41.324	C	P_1	7.57 +	7.48	

Observation Point		Geophone	Δ (km)	Class	Phase	Arrival Time	Travel Time	Corrected Travel time
						s	s	
E_3	2	4.5 V	38.243	C	P_1	(7.08) +	(6.99)	
	3	4.5 V	38.148	C	P_1	(7.07) +	(6.98)	
	4	4.5 V	38.042	B	P_1	7.041 +	6.948	
	5	4.5 V	37.940	B	P_1	7.025+	6.932	
	6	4.5 V	37.839	C	P_1	(6.99) +	(6.90)	
	7	4.5 V	37.738	C	P_1	(7.00) +	(6.91)	
	8	4.5 V	37.636	C	P_1	(6.98) +	(6.89)	
	9	4.5 V	37.542	C	P_1	6.99 +	6.90	
	10	4.5 V	37.440	C	P_1	(6.97) +	(6.88)	
	11	4.5 V	37.339	B	P_1	6.951 +	6.858	
	12	4.5 V	37.238	B	P_1	6.950+	6.857	
	13	4.5 V	37.137	B	P_1	6.936+	6.843	
	14	4.5 V	37.035	B	P_1	6.912+	6.819	
	16	4.5 V	36.833	B	P_1	6.876+	6.783	
	17	4.5 V	36.731	B	P_1	6.863+	6.770	
	18	4.5 V	36.637	A	P_1	6.829+	6.736	
	19	4.5 V	36.536	A	P_1	6.812+	6.719	
	20	4.5 V	36.434	A	P_1	6.788+	6.695	
	21	4.5 V	36.333	B	P_1	6.782+	6.689	
	22	4.5 V	36.232	C	P_1	6.77 +	6.68	
	23	4.5 V	36.131	B	P_1	6.727+	6.634	
	24	4.5 V	36.029	A	P_1	6.698+	6.605	
E_4	2	4.5 V	32.004	C	P_1	6.00 +	5.91	
	3	4.5 V	31.906	B	P_1	5.997+	5.904	5.903 s
	5	4.5 V	31.708	B	P_1	5.971+	5.878	5.877
	6	4.5 V	31.598	C	P_1	(5.97) +	(5.88)	
	8	4.5 V	31.410	B	P_1	5.925+	5.832	5.831
	9	4.5 V	31.311	B	P_1	5.910+	5.817	5.816
	10	4.5 V	31.204	C	P_1	(5.89) +	(5.80)	
	11	4.5 V	31.105	C	P_1	(5.88) +	(5.79)	
	12	4.5 V	31.006	B	P_1	5.885+	5.792	5.791
	13	4.5 V	30.907	B	P_1	5.866+	5.773	5.772
	14	4.5 V	30.808	B	P_1	5.860+	5.767	5.766
	15	4.5 V	30.709	B	P_1	5.830+	5.737	5.736
	16	4.5 V	30.609	B	P_1	5.812+	5.719	5.718
	17	4.5 V	30.502	B	P_1	5.787+	5.694	5.693
	18	4.5 V	30.407	B	P_1	5.746+	5.653	5.652
	19	4.5 V	30.308	B	P_1	5.716+	5.623	5.622
	20	4.5 V	30.203	B	P_1	5.690+	5.597	5.596
	21	4.5 V	30.102	B	P_1	5.660+	5.567	5.566
	22	4.5 V	30.007	B	P_1	5.670+	5.577	5.576
	23	4.5 V	29.920	C	P_1	(5.65) +	(5.56)	
	24	4.5 V	29.832	B	P_1	5.637+	5.544	5.543
E_5	1	4.5 V	26.358	C	P_1	(5.13) +	(5.04)	(5.03)
	2	4.5 V	26.258	C	P_1	(5.13) +	(5.04)	(5.03)
	3	4.5 V	26.157	C	P_1	(5.12) +	(5.03)	(5.02)
	4	4.5 V	26.057	C	P_1	5.08 +	4.99	4.98
	5	4.5 V	25.956	C	P_1	5.05 +	4.96	4.95
	6	4.5 V	25.855	B	P_1	5.000+	4.907	4.896
	7	4.5 V	25.754	B	P_1	5.015+	4.922	4.910
	8	4.5 V	25.653	B	P_1	5.012+	4.919	4.907

Observation Point		Geophone	Δ (km)	Class	Phase	Arrival Time	Travel Time	Corrected Travel time
						s	s	s
E_5	9	4.5 V	25.552	B	P_1	5.026+	4.933	4.921
	10	4.5 V	25.451	B	P_1	5.031+	4.938	4.926
	11	4.5 V	25.350	B	P_1	5.015+	4.922	4.910
	12	4.5 V	25.249	A	P_1	4.990+	4.897	4.885
	13	4.5 V	25.148	B	P_1	4.960+	4.867	4.856
	14	4.5 V	25.048	B	P_1	4.927+	4.834	4.823
	15	4.5 V	24.947	A	P_1	4.892+	4.799	4.788
	16	4.5 V	24.847	A	P_1	4.874+	4.781	4.770
	17	4.5 V	24.745	C	P_1	(4.82) +	(4.73)	(4.72)
	18	4.5 V	24.644	C	P_1	(4.78) +	(4.69)	(4.68)
	19	4.5 V	24.543	B	P_1	4.792+	4.699	4.688
	20	4.5 V	24.442	B	P_1	4.795+	4.702	4.691
	21	4.5 V	24.341	B	P_1	4.782+	4.689	4.678
	22	4.5 V	24.240	B	P_1	4.758+	4.665	4.654
	24	4.5 V	24.040	B	P_1	4.708+	4.615	4.604
D_1	a	4 V	64.434	B	P_1	11.556+	11.463	
	b	1 V	63.964	B	P_1	11.477+	11.384	
	c	4 V	63.579	B	P_1	11.374+	11.281	
D_2	a	4 V	60.705	B	P_1	10.810+	10.717	
	b	1 V	60.356	A	P_1	10.761+	10.668	
	c	4 V	59.965	B	P_1	10.712+	10.619	
D_3	a	1 V	56.079	C	P_1	9.900+	9.807	
	b	4 V	55.879	C	P_1	9.857+	9.764	
	c	2 V	55.414	C	P_1	9.84 +	9.75	
D_4	a	4 V	55.074	C	P_1	9.81 +	9.72	
	b	2 V	54.823	C	P_1	9.77 +	9.68	
	c	4 V	54.473	C	P_1	9.70 +	9.61	
D_5	a	1 V	46.944	A	P_1	8.668+	8.575	
	b	1 V	46.613	A	P_1	8.604+	8.511	
	c	1 V	46.189	A	P_1	8.530+	8.437	
D_6	a	1 V	40.854	C	P_1	7.39 +	7.30	
	b	1 V	40.259	B	P_1	7.417+	7.324	
	c	1 V	39.835	C	P_1	7.33 +	7.24	
D_7	a	4 V	34.675	A	P_1	6.474+	6.381	6.378
	b	1 V	34.430	A	P_1	6.394+	6.301	6.299
	c	4 V	33.555	A	P_1	6.256+	6.163	6.160
D_8	a	4 V	30.155	A	P_1	5.688+	5.595	5.594
	b	1 V	29.900	A	P_1	5.613+	5.520	
	c	4 V	29.609	A	P_1	5.573+	5.480	5.479
	b′	4 V	29.795	A	P_1	5.586+	5.493	5.492
	b	1 $H_{\angle R}$	29.900	B	P_1	5.614−	5.521	5.520
	b	1 $H_{//}$	29.900	A	P_1	5.610+	5.517	5.516
D_9	a	4 V	20.754	B	P_1	4.142+	4.049	4.048
	b	1 V	20.344	A	P_1	4.053+	3.960	3.959
	c	4 V	20.034	A	P_1	4.010+	3.917	3.915
D_{10}	a	4 V	15.184	A	P_1	3.214+	3.121	3.119
	b	1 V	14.929	A	P_1	3.134+	3.041	3.039
	c	4 V	14.544	B	P_1	3.086+	2.993	2.991

Observation Point		Geophone	Δ (km)	Class	Phase	Arrival Time	Travel Time	Corrected Travel time
						s	s	s
D_{11}	a	4 V	12.674	B	P_1	2.837+	2.744	2.743
	b	1. V	12.464	A	P_1	2.760+	2.667	2.666
	c	4 V	12.274	A	P_1	2.733+	2.640	
D_{12}	a	4 V	7.823	A	P_1	1.919+	1.826	1.824
	b	1 V	7.457	A	P_1	1.835+	1.742	1.738
	c	4 V	7.127	A	P_1	1.825+	1.732	1.726
D_{13}	a	4 V	4.669	A	P_1	1.454+	1.361	1.328
	b	1 V	4.349	A	P_1	1.388+	1.295	1.243
	c	4 V	4.104	A	P_1	1.332+	1.239	1.184
D_{14}	a	1 V	0.844	A	P_1	0.442+	0.349	0.326
	c	1 V	0.569	A	P_1	0.306+	0.213	0.205
	c	1 H	0.569	A	P_1	0.300+	0.207	0.199
	d	4 V	0.335	A	P_1	0.223+	0.130	0.120
	e	1 V	0.195	A	P_1	0.180+	0.087	0.079
	f	4 V	0.014	A	P_1	0.115+	0.022	0.022

Table 5 (8) Travel time data for shot enlarging the bottom of shot holle A–III

Observation Point		Geophone	Δ (km)	Class	Phase	Arrival Time	Travel Time	Corrected Travel time
						$13^h 15^m$ s	s	
E_3	12	4.5 V	1.548	B	P_1	0.618+	0.519	
	13	4.5 V	1.447	A	P_1	0.601+	0.502	
	14	4.5 V	1.345	A	P_1	0.573+	0.474	
	15	4.5 V	1.244	A	P_1	0.545+	0.446	
	16	4.5 V	1.143	A	P_1	0.521+	0.422	
	17	4.5 V	1.041	A	P_1	0.499+	0.400	
	18	4.5 V	0.947	A	P_1	0.468+	0.369	
	19	4.5 V	0.846	A	P_1	0.437+	0.338	
	20	4.5 V	0.744	A	P_1	0.410+	0.311	
	21	4.5 V	0.643	A	P_1	0.375+	0.276	
	22	4.5 V	0.542	A	P_1	0.342+	0.243	
	23	4.5 V	0.441	A	P_1	0.309+	0.210	
	24	4.5 V	0.339	A	P_1	0.278+	0.179	

Table 5 (9) Travel time data for shot E_3–W_1

Observation Point		Geophone	Δ (km)	Class	Phase	Arrival Time	Travel Time	Corrected Travel time
						1^h 05^m		
E_2	1	4.5 V	4.666	B	P_1	0.974+	1.205	
	2	4.5 V	4.569	B	P_1	0.955+	1.186	
	3	4.5 V	4.467	B	P_1	0.940+	1.171	
	4	4.5 V	4.365	B	P_1	0.914+	1.145	
	5	4.5 V	4.263	C	P_1	0.89 +	1.12	
	6	4.5 V	4.166	B	P_1	0.855+	1.086	
	7	4.5 V	4.064	B	P_1	0.854+	1.085	
	8	4.5 V	3.962	B	P_1	0.832+	1.063	
	9	4.5 V	3.869	B	P_1	0.810+	1.041	
	10	4.5 V	3.764	A	P_1	0.802+	1.033	
	11	4.5 V	3.670	A	P_1	0.778+	1.009	
	12	4.5 V	3.565	A	P_1	0.750+	0.981	
	13	4.5 V	3.469	B	P_1	0.712+	0.943	
	15	4.5 V	3.272	B	P_1	0.667+	0.898	
	17	4.5 V	3.074	B	P_1	0.615+	0.846	
	18	4.5 V	2.972	A	P_1	0.593+	0.824	
	19	4.5 V	2.870	A	P_1	0.567+	0.798	
	20	4.5 V	2.774	B	P_1	0.531+	0.762	
	21	4.5 V	2.672	B	P_1	0.500+	0.731	
	22	4.5 V	2.570	B	P_1	0.476+	0.707	
	23	4.5 V	2.469	B	P_1	0.452+	0.683	
	24	4.5 V	2.373	C	P_1	(0.42) +	(0.65)	
E_3	1	4.5 V	0.613	B	P_1	0.036+	0.267	
	2	4.5 V	0.708	B	P_1	0.055+	0.286	
	3	4.5 V	0.803	A	P_1	0.092+	0.323	
	4	4.5 V	0.909	A	P_1	0.133+	0.364	
	5	4.5 V	1.011	B	P_1	0.150+	0.381	
	6	4.5 V	1.112	A	P_1	0.158+	0.389	
	7	4.5 V	1.213	A	P_1	0.172+	0.403	
	8	4.5 V	1.315	A	P_1	0.194+	0.425	
	9	4.5 V	1.409	A	P_1	0.230+	0.461	
	10	4.5 V	1.511	B	P_1	0.268+	0.499	
	11	4.5 V	1.612	A	P_1	0.291+	0.522	
	12	4.5 V	1.713	A	P_1	0.317+	0.548	
	13	4.5 V	1.814	A	P_1	0.338+	0.569	
	14	1.5 V	1.916	A	P_1	0.364+	0.595	
	15	4.5 V	2.017	A	P_1	0.387+	0.618	
	16	4.5 V	2.118	A	P_1	0.405+	0.636	
	17	4.5 V	2.220	A	P_1	0.436+	0.667	
	18	4.5 V	2.314	A	P_1	0.442+	0.673	
	19	4.5 V	2.415	A	P_1	0.457+	0.688	
	20	4.5 V	2.517	A	P_1	0.468+	0.699	
	22	4.5 V	2.719	B	P_1	0.498+	0.729	
	23	4.5 V	2.820	A	P_1	0.507+	0.738	
	24	4.5 V	2.922	A	P_1	0.520+	0.751	

Table 6 (1) Travel time data for shot B–I

Observation Point	Geophone	Δ (km)	Class	Phase	Arrival Time	Travel Time	Corrected Travel time
					$1^{h}\,48^{m}$ s	s	s
E_1 1	4.5 V	16.070	C				(4.61)
2	4.5 V	16.168	C	P_1	4.65 +	4.61	4.61
3	4.5 V	16.269	C	P_1	4.66 +	4.62	4.62
4	4.5 V	16.367	C	P_1	4.67 +	4.63	4.63
5	4.5 V	16.466	C	P_1			(4.66)
6	4.5 V	16.565	C	P_1	4.70 +	4.67	4.67
7	4.5 V	16.662	C	P_1			(4.67)
8	4.5 V	16.759	C	P_1	4.70 +	4.67	4.67
9	4.5 V	16.857	C	P_1	4.74 +	4.71	4.71
10	4.5 V	16.956	C	P_1	4.77 +	4.73	4.73
11	4.5 V	17.054	C	P_1	4.78 +	4.74	4.74
12	4.5 V	17.153	C	P_1	4.78 +	4.75	4.75
13	4.5 V	17.249	C	P_1	4.81 +	4.78	4.78
14	4.5 V	17.353	C	P_1	4.80 +	4.76	4.76
15	4.5 V	17.452	C	P_1			(4.77)
16	4.5 V	17.554	C	P_1	4.81 +	4.78	4.78
17	4.5 V	17.679	C	P_1	4.81 +	4.78	4.78
18	4.5 V	17.781	C	P_1	4.81 +	4.77	4.77
19	4.5 V	17.881	C	P_1	4.83 +	4.79	4.79
20	4.5 V	17.980	C	P_1	4.83 +	4.79	4.79
21	4.5 V	18.082	C	P_1	4.85 +	4.81	4.81
22	4.5 V	18.182	C	P_1	4.86 +	4.83	4.83
23	4.5 V	18.282	C	P_1	4.87 +	4.83	4.83
24	4.5 V	18.381	C	P_1	4.88 +	4.84	4.84
E_2 1	4.5 V	19.081	C	P_1	4.96 +	4.92	4.92
2	4.5 V	19.182	C	P_1	4.97 +	4.93	4.93
3	4.5 V	19.279	C	P_1	4.98 +	4.94	4.94
4	4.5 V	19.381	C	P_1	5.00 +	4.96	4.96
5	4.5 V	19.482	C	P_1	5.03 +	4.99	4.99
6	4.5 V	19.583	C	P_1			(5.01)
7	4.5 V	19.681	C	P_1	5.06 +	5.02	5.02
8	4.5 V	19.781	C	P_1	5.06 +	5.02	5.02
9	4.5 V	19.880	C	P_1	5.08 +	5.04	5.03
10	4.5 V	19.980	C	P_1	5.10 +	5.06	5.05
11	4.5 V	20.081	C	P_1	5.10 +	5.06	5.06
12	4.5 V	20.182	C	P_1	5.10 +	5.06	5.06
13	4.5 V	20.282	C	P_1	5.11 +	5.07	5.07
14	4.5 V	20.381	C	P_1	5.12 +	5.08	5.08
15	4.5 V	20.481	C	P_1	5.13 +	5.09	5.09
16	4.5 V	20.579	C	P_1			(5.10)
17	4.5 V	20.680	C	P_1	5.16 +	5.12	5.12
18	4.5 V	20.781	C	P_1	5.16 +	5.12	5.12
19	4.5 V	20.881	C	P_1	5.18 +	5.14	5.14
20	4.5 V	20.982	C	P_1	5.19 +	5.15	5.15
21	4.5 V	21.080	C	P_1	5.20 +	5.17	5.16
22	4.5 V	21.181	C	P_1	5.22 +	5.18	5.17
23	4.5 V	21.281	C	P_1	5.22 +	5.18	5.18
24	4.5 V	21.382	C	P_1	5.23 +	5.19	5.18

Observation Point		Geophone	Δ (km)	Class	Phase	Arrival Time	Travel Time	Corrected Travel time
						s	s	s
E_3	1	4.5 V	21.812	C	P_1	5.30 +	5.26	5.26
	2	4.5 V	21.913	C	P_1	5.33 +	5.29	5.29
	3	4.5 V	22.011	C	P_1	5.35 +	5.31	5.31
	4	4.5 V	22.114	C	P_1	5.34 +	5.30	5.30
	5	4.5 V	22.212	C	P_1	5.36 +	5.32	5.32
	6	4.5 V	22.314	C	P_1	5.37 +	5.33	5.33
	7	4.5 V	22.412	C	P_1	5.38 +	5.34	5.34
	8	4.5 V	22.514	C	P_1	5.39 +	5.35	5.35
	9	4.5 V	22.612	C	P_1	5.39 +	5.35	5.35
	10	4.5 V	22.713	C	P_1			(5.35)
	11	4.5 V	22.812	C	P_1			(5.36)
	12	4.5 V	22.914	C	P_1	5.41 +	5.37	5.37
	13	4.5 V	23.012	C	P_1	5.43 +	5.39	5.39
	14	4.5 V	23.113	C	P_1	5.44 +	5.40	5.40
	15	4.5 V	23.214	C	P_1	5.46 +	5.42	5.42
	16	4.5 V	23.314	C	P_1	5.47 +	5.43	5.43
	17	4.5 V	23.412	C	P_1	5.46 +	5.42	5.42
	18	4.5 V	23.511	C	P_1			(5.43)
	20	4.5 V	23.713	C	P_1	5.51 +	5.47	5.47
	22	4.5 V	23.913	C	P_1	5.53 +	5.49	5.49
	23	4.5 V	24.010	C	P_1	5.55 +	5.51	5.51
	24	4.5 V	24.113	C	P_1	5.51 +	5.47	5.47
E_4	3	4.5 V	24.345	C	P_1	5.58 +	5.54	5.54
	4	4.5 V	24.446	C	P_1	5.60 +	5.56	5.56
	5	4.5 V	24.544	C	P_1			(5.58)
	6	4.5 V	24.644	C	P_1	5.64 +	5.60	5.60
	7	4.5 V	24.744	C	P_1	5.66 +	5.63	5.63
	8	4.5 V	24.843	C	P_1	5.69 +	5.65	5.65
	9	4.5 V	24.944	C	P_1	5.70 +	5.66	5.66
	12	4.5 V	25.245	C	P_1	5.73 +	5.69	5.69
	13	4.5 V	25.346	C	P_1	5.75 +	5.71	5.71
	14	4.5 V	25.444	C	P_1	5.78 +	5.74	5.74
	15	4.5 V	25.544	C	P_1	5.80 +	5.77	5.77
	16	4.5 V	25.644	C	P_1			(5.78)
	17	4.5 V	25.744	C	P_1			(5.79)
	18	4.5 V	25.846	C	P_1	5.84 +	5.80	5.80
	19	4.5 V	25.948	C	P_1			(5.82)
	20	4.5 V	26.045	C	P_1			(5.85)
	21	4.5 V	26.153	C	P_1	5.92 +	5.88	5.88
E_5	1	4.5 V	27.563	C	P_1	6.22 +	6.18	6.18
	2	4.5 V	27.664	C	P_1	6.21 +	6.17	6.17
	3	4.5 V	27.761	C	P_1			(6.16)
	4	4.5 V	27.861	C	P_1			(6.15)
	5	4.5 V	27.962	C	P_1	6.19 +	6.15	6.15
	6	4.5 V	28.062	C	P_1	6.19 +	6.15	6.15
	7	4.5 V	28.163	C	P_1	6.18 +	6.14	6.14
	8	4.5 V	28.263	C	P_1	6.18 +	6.14	6.14
	9	4.5 V	28.361	C	P_1	6.18 +	6.14	6.14
	10	4.5 V	28.463	C	P_1	6.20 +	6.16	6.16
	11	4.5 V	28.558	C	P_1	6.23 +	6.19	6.19
	12	4.5 V	28.663	C	P_1	6.26 +	6.22	6.22

Observation Point		Geophone	Δ (km)	Class	Phase	Arrival Time	Travel Time	Corrected Travel time
						s	s	s
E_5	13	4.5 V	28.762	C	P_1	6.27 +	6.23	6.23
	14	4.5 V	28.862	C	P_1	6.28 +	6.24	6.24
	15	4.5 V	28.963	C	P_1	6.29 +	6.25	6.25
	16	4.5 V	29.062	C	P_1	6.30 +	6.26	6.26
	17	4.5 V	29.163	C	P_1	6.32 +	6.28	6.28
	18	4.5 V	29.262	C	P_1	6.34 +	6.30	6.30
	19	4.5 V	29.363	C	P_1	6.36 +	6.32	6.32
	20	4.5 V	29.463	C	P_1	6.37 +	6.33	6.33
	21	4.5 V	29.560	C	P_1	6.39 +	6.36	6.35
	22	4.5 V	29.653	C	P_1	6.42 +	6.38	6.38
	23	4.5 V	29.751	C	P_1			(6.40)
	24	4.5 V	29.852	C	P_1			(6.42)
D_1	a	4 V	0.300	A	P_1	0.472+	0.434	0.134
	b	1 V	0.040	A	P_1	0.372+	0.334	0.018
	c	4 V	0.067	A	P_1	0.080+	0.042	0.042
D_2	a	4 V	0.215	A	P_1	0.302+	0.264	0.104
	b	1 V	0.449	A	P_1	0.268+	0.230	0.209
	c	4 V	0.798	A	P_1	0.395+	0.357	0.357
D_3	b	1 V	7.892	C	P_1	2.56 −	2.52	2.52
	c	1 V	8.303	B	P_1	2.797−	2.759	2.753
D_4	a	1 V	8.729	A	P_1	2.860+	2.822	2.818
	b	1 V	9.027	A	P_1	2.870+	2.832	2.828
	c	1 V	9.344	A	P_1	2.950+	2.912	2.906
D_5	a	4 V	11.499	C	P_1	3.48 −	3.44	3.44
	b	2 V	11.746	C	P_1	3.55 −	3.51	3.51
	c	4 V	11.939	B	P_1	3.579−	3.541	3.537
D_6	a	2 V	12.241	B	P_1	3.607−	3.569	3.566
	b	2 V	12.516	B	P_1	3.678−	3.640	3.636
	c	4 V	12.806	B	P_1	3.780−	3.742	3.738
D_7	a	4 V	26.734	C	P_1	6.13 +	6.09	6.09
	b	1 V	27.261	C	P_1	6.17 +	6.13	6.13
	c	4 V	27.475	B	P_1	6.218+	6.190	6.188
D_8	a	4 V	30.486	C	P_1	6.49 +	6.45	6.45
	b	1 V	30.756	B	P_1	6.579+	6.541	6.541
	c	4 V	31.097	B	P_1	6.618+	6.580	6.580
D_9	a	4 V	33.368	B	P_1	6.965+	6.927	6.926
	b	1 V	33.818	C	P_1			(7.01)
	c	4 V	34.155	C	P_1			(7.07)
D_{10}	a	4 V	34.485	C	P_1	7.17 −	7.13	7.13
	b	1 V	34.808	C	P_1	7.23 −	7.19	7.19
	c	4 V	35.135	B	P_1	7.278−	7.240	7.239
D_{11}	a	4 V	36.448	C	P_1	7.50 +	7.46	7.46
	b	1 V	36.640	C	P_1	7.51 +	7.47	7.47
	c	4 V	37.062	B	P_1	7.578+	7.540	7.539
D_{12}	a	4 V	38.274	C	P_1	7.70 −	7.66	7.66
	b	1 V	38.801	C	P_1	7.84 −	7.80	7.80
	c	4 V	39.066	C	P_1	7.89 −	7.85	7.85

Observation Point		Geophone	Δ (km)	Class	Phase	Arrival Time	Travel Time	Corrected Travel time
						s	s	s
D_{13}	a	4 V	41.510	C	P_1	8.29 +	8.25	8.25
	b	1 V	41.804	C	P_1	8.32 +	8.28	8.28
	c	4 V	42.052	C	P_1	8.38 +	8.34	8.34
D_{14}	a	4 V	45.545	B	P_1	9.480+	9.442	9.442
	c	1 V	45.923	B	P_1	9.591+	9.553	9.553
	e	4 V	46.431	B	P_1	9.665+	9.627	9.627
	f	4 V	46.655	B	P_1	9.750+	9.712	9.712

Table 6 (2) Travel time data for shot B–II

Observation Point		Geophone	Δ (km)	Class	Phase	Arrival Time	Travel Time	Corrected Travel time
						2h 48m		
						s	s	s
E_1	1	4.5 V	3.680	B	P_1	1.528+	1.417	1.409
	2	4.5 V	3.778	B	P_1	1.546+	1.435	1.428
	3	4.5 V	3.879	B	P_1	1.585+	1.474	1.468
	4	4.5 V	3.977	B	P_1	1.606+	1.495	1.489
	5	4.5 V	4.076	B	P_1	1.649+	1.538	1.533
	6	4.5 V	4.175	B	P_1	1.655+	1.544	1.539
	7	4.5 V	4.232	B	P_1	1.684+	1.573	1.567
	8	4.5 V	4.369	B	P_1	1.726+	1.615	1.608
	9	4.5 V	4.467	B	P_1	1.729+	1.618	1.611
	10	4.5 V	4.566	B	P_1	1.764+	1.653	1.646
	11	4.5 V	4.664	B	P_1	1.780+	1.669	1.661
	12	4.5 V	4.763	B	P_1	1.799+	1.688	1.680
	13	4.5 V	4.859	B	P_1	1.830+	1.719	1.711
	14	4.5 V	4.963	B	P_1	1.832+	1.721	1.713
	15	4.5 V	5.062	B	P_1	1.872+	1.761	1.753
	16	4.5 V	5.164	B	P_1	1.909+	1.798	1.790
	17	4.5 V	5.289	B	P_1	1.928+	1.817	1.809
	18	4.5 V	5.391	B	P_1	1.934+	1.823	1.815
	19	4.5 V	5.491	B	P_1	1.969+	1.858	1.850
	20	4.5 V	5.590	C	P_1	1.98 +	1.87	1.86
	21	4.5 V	5.692	B	P_1	2.000+	1.889	1.881
	22	4.5 V	5.792	C	P_1	2.04 +	1.93	1.92
	23	4.5 V	5.892	C	P_1	2.08 +	1.97	1.96
	24	4.5 V	5.991	C	P_1			(2.00)
E_2	1	4.5 V	6.691	C	P_1	2.36 +	2.24	2.24
	2	4.5 V	6.792	C	P_1	2.37 +	2.26	2.26
	3	4.5 V	6.889	C	P_1	2.38 +	2.27	2.27
	4	4.5 V	6.991	C	P_1	2.39 +	2.28	2.28
	5	4.5 V	7.092	C	P_1	2.41 +	2.30	2.30
	6	4.5 V	7.463	C	P_1			(2.32)
	7	4.5 V	7.291	C	P_1	2.44 +	2.33	2.33

Observation Point		Geophone	Δ (km)	Class	Phase	Arrival Time	Travel Time	Corrected Travel time
						s	s	s
E_2	8	4.5 V	7.391	C	P_1	2.45 +	2.34	2.34
	9	4.5 V	7.490	B	P_1	2.47 +	2.36	2.36
	10	4.5 V	7.590	B	P_1	2.49 +	2.38	2.38
	11	4.5 V	7.691	B	P_1	2.51 +	2.39	2.39
	12	4.5 V	7.792	A	P_1	2.52 +	2.41	2.41
	13	4.5 V	7.892	A	P_1	2.54 +	2.43	2.43
	14	4.5 V	7.991	A	P_1	2.56 +	2.45	2.45
	15	4.5 V	8.091	A	P_1	2.57 +	2.45	2.45
	16	4.5 V	8.189	B	P_1	2.60 +	2.48	2.48
	17	4.5 V	8.290	B	P_1	2.61 +	2.50	2.50
	18	4.5 V	8.391	B	P_1	2.62 +	2.50	2.50
	19	4.5 V	8.491	B	P_1	2.63 +	2.52	2.52
	20	4.5 V	8.592	A	P_1	2.63 +	2.52	2.52
	21	4.5 V	8.690	A	P_1	2.65 +	2.54	2.54
	22	4.5 V	8.791	B	P_1	2.66 +	2.54	2.54
	23	4.5 V	8.891	A	P_1	2.67 +	2.56	2.56
	24	4.5 V	8.992	B	P_1	2.68 +	2.57	2.57
E_3	1	4.5 V	9.422	C	P_1	2.70 +	2.59	2.59
	2	4.5 V	9.523	B	P_1	2.720+	2.609	2.604
	3	4.5 V	9.621	B	P_1	2.742+	2.631	2.625
	4	4.5 V	9.724	A	P_1	2.773+	2.662	2.655
	5	4.5 V	9.822	A	P_1	2.781+	2.670	2.662
	6	4.5 V	9.924	A	P_1	2.790+	2.679	2.671
	7	4.5 V	10.022	B	P_1	2.801+	2.690	2.682
	8	4.5 V	10.124	A	P_1	2.811+	2.700	2.692
	9	4.5 V	10.222	B	P_1	2.813+	2.702	2.695
	10	4.5 V	10.323	B	P_1	2.821+	2.710	2.703
	11	4.5 V	10.422	C	P_1	2.84 +	2.73	2.72
	12	4.5 V	10.524	C	P_1			(2.74)
	13	4.5 V	10.622	B	P_1	2.875+	2.764	2.758
	14	4.5 V	10.723	A	P_1	2.891+	2.780	2.774
	15	4.5 V	10.824	A	P_1	2.891+	2.780	2.774
	16	4.5 V	10.924	C	P_1	2.90 +	2.79	2.786
	17	4.5 V	11.022	B	P_1	2.914+	2.803	2.797
	18	4.5 V	10.621	B	P_1	2.920+	2.809	2.803
	19	4.5 V	10.624	B	P_1	2.920+	2.809	2.803
	20	4.5 V	11.323	B	P_1	2.932+	2.821	2.815
	21	4.5 V	11.422	B	P_1	2.939+	2.828	2.822
	22	4.5 V	11.523	B	P_1	2.953+	2.842	2.836
	23	4.5 V	11.620	C	P_1	2.96 +	2.85	2.84
	24	4.5 V	11.723	C	P_1	2.97 +	2.86	2.85
E_4	2	4.5 V	11.854	C	P_1			(2.88)
	3	4.5 V	11.955	C	P_1			(2.91)
	4	4.5 V	12.056	C	P_1			(2.92)
	5	4.5 V	12.154	C	P_1			(2.92)
	8	4.5 V	12.453	C	P_1			(2.94)
	10	4.5 V	12.656	C	P_1			(2.95)
	11	4.5 V	12.754	C	P_1			(2.98)
	12	4.5 V	12.855	C	P_1			(2.99)
	13	4.5 V	12.956	C	P_1			(3.01)
	14	4.5 V	13.054	C	P_1			(3.02)

Observation Point		Geophone	Δ (km)	Class	Phase	Arrival Time	Travel Time	Corrected Travel time
						s	s	s
E_4	15	4.5 V	13.154	C	P_1	3.17 +	3.06	3.05
	16	4.5 V	13.254	C				(3.04)
	17	4.5 V	13.354	C	P_1	3.18 +	3.07	3.07
	18	4.5 V	13.456	C	P_1	3.19 +	3.08	3.08
	19	4.5 V	13.558	C	P_1	3.20 +	3.09	3.08
	20	4.5 V	13.655	C	P_1	3.21 +	3.10	3.10
	21	4.5 V	13.763	C	P_1	3.22 +	3.11	3.11
	24	4.5 V	14.056	C	P_1			(3.14)
E_5	1	4.5 V	15.173	C	P_1			(3.46)
	2	4.5 V	15.274	C	P_1	3.59 +	3.48	3.48
	3	4.5 V	15.371	C	P_1	3.62 +	3.51	3.51
	4	4.5 V	15.471	C	P_1			(3.52)
	5	4.5 V	15.572	C	P_1	3.65 +	3.54	3.54
	6	4.5 V	15.672	C	P_1	3.69 +	3.57	3.57
	7	4.5 V	15.773	C	P_1	3.70 +	3.59	3.59
	8	4.5 V	15.873	B	P_1	3.714+	3.603	3.603
	9	4.5 V	15.971	B	P_1	3.729+	3.618	3.618
	10	4.5 V	16.073	B	P_1	3.743+	3.632	3.632
	11	4.5 V	16.168	B	P_1	3.747+	3.636	3.636
	12	4.5 V	16.273	B	P_1	3.738+	3.627	3.627
	13	4.5 V	16.372	B	P_1	3.755+	3.644	3.644
	14	4.5 V	16.472	B	P_1	3.793+	3.682	3.682
	15	4.5 V	16.573	C	P_1	3.82 +	3.70	3.70
	16	4.5 V	16.672	B	P_1	3.815+	3.704	3.704
	17	4.5 V	16.773	C	P_1	3.85 +	3.74	3.74
	18	4.5 V	16.872	C	P_1	3.86 +	3.74	3.74
	19	4.5 V	16.973	C	P_1	3.85 +	3.74	3.74
	20	4.5 V	17.073	C	P_1	3.88 +	3.76	3.76
	21	4.5 V	17.170	C	P_1	3.90 +	3.79	3.79
	22	4.5 V	17.263	C	P_1	3.91 +	3.80	3.80
	23	4.5 V	17.361	C	P_1	3.92 +	3.80	3.80
	24	4.5 V	17.462	C	P_1	3.93 +	3.82	3.82
D_1	a	4 V	12.690	C	P_1	3.89 +	3.78	3.76
	b	1 V	12.350	B	P_1	3.831+	3.720	3.706
	c	4 V	12.457	C	P_1	3.81 +	3.70	3.70
D_2	a	4 V	12.175	B	P_1	3.792+	3.681	3.672
	b	1 V	11.941	B	P_1	3.746+	3.635	3.631
	c	4 V	11.592	B	P_1	3.610+	3.499	3.497
D_3	a	1 V	4.945	A	P_1	1.890+	1.779	1.779
	b	1 V	4.498	B	P_1	1.750+	1.639	1.639
	c	1 H	4.087	C	P_1	1.68 +	1.57	1.57
D_4	a	1 V	3.661	B	P_1	1.580+	1.469	1.468
	b	1 V	3.363	B	P_1	1.492+	1.381	1.380
	c	1 V	3.046	B	P_1	1.435+	1.324	1.319
D_5	a	4 V	0.893	A	P_1	0.560+	0.449	0.438
	b	2 V	0.644	A	P_1	0.474+	0.363	0.345
	c	4 V	0.449	A	P_1	0.368+	0.257	0.241
D_6	a	2 V	0.149	A	P_1	0.228+	0.117	0.082
	b	2 V	0.126	A	P_1	0.230+	0.119	0.064
	c	4 V	0.410	A	P_1	0.375+	0.264	0.247

Observation Point		Geophone	Δ (km)	Class	Phase	Arrival Time	Travel Time	Corrected Travel time
						s	s	s
D_7	a	4 V	14.344	A	P_1	3.458+	3.347	3.346
	b	1 V	14.271	B	P_1	3.565+	3.454	3.453
	c	4 V	15.085	C	P_1	3.59 +	3.48	3.48
D_8	a	4 V	17.820	B	P_1	4.100+	3.989	3.989
	b	1 V	18.107	B	P_1	4.147+	4.036	4.032
	c	4 V	18.446	A	P_1	4.191+	4.080	4.080
D_9	a	4 V	20.978	B	P_1	4.546+	4.435	4.432
	b	1 V	21.428	B	P_1	4.577+	4.466	4.461
	c	4 V	21.765	B	P_1	4.624+	4.513	4.505
D_{10}	a	4 V	21.495	C	P_1	4.67 +	4.56	4.55
	b	1 V	22.418	B	P_1	4.740+	4.629	4.623
	c	4 V	22.745	B	P_1	4.790+	4.679	4.673
D_{11}	a	4 V	24.058	B	P_1	5.023+	4.912	4.906
	b	1 V	24.250	B	P_1	5.027+	4.916	4.912
	c	4 V	24.672	A	P_1	5.090+	4.979	4.976
D_{12}	a	4 V	25.884	A	P_1	5.287+	5.176	5.175
	b	1 V	26.411	B	P_1	5.351+	5.240	5.240
	c	4 V	26.676	A	P_1	5.431+	5.320	5.320
D_{13}	a	4 V	29.120	A	P_1	5.936+	5.825	5.825
	b	1 V	29.414	A	P_1	5.960+	5.849	5.849
	c	4 V	29.662	A	P_1	6.016+	5.905	5.905
D_{14}	a	4 V	33.155	C	P_1	6.95 +	6.84	6.84
	b	4 V	33.282	C	P_1	6.94 +	6.83	6.83
	c	1 V	33.533	B	P_1	7.033+	6.922	6.921
	d	4 V	33.820	C	P_1	7.07 +	6.96	6.96
	e	4 V	34.041	C	P_1	7.15 +	7.04	7.04
	f	4 V	34.265	C	P_1	7.05 +	6.94	6.94

Table 6 (3) Travel time data for shot B–III_1

Observation Point		Geophone	Δ (km)	Class	Phase	Arrival Time	Travel Time	Corrected Travel time
						2h 48m		
						s	s	s
E_2	1	4.5 V	10.372	A	P_1	2.722+	2.322	2.322
	2	4.5 V	10.271	B	P_1	2.699+	2.299	2.299
	3	4.5 V	10.174	B	P_1	2.677+	2.277	2.277
	4	4.5 V	10.072	B	P_1	2.659+	2.259	2.259
	5	4.5 V	9.971	A	P_1	2.640+	2.240	2.240
	6	4.5 V	9.600	B	P_1	2.606+	2.206	2.206
	7	4.5 V	9.772	B	P_1	2.591+	2.191	2.191
	8	4.5 V	9.672	B	P_1	2.584+	2.184	2.184
	9	4.5 V	9.573	B	P_1	2.562+	2.162	2.162
	10	4.5 V	9.473	A	P_1	2.524+	2.124	2.123
	11	4.5 V	9.372	A	P_1	2.493+	2.093	2.092

Observation Point		Geophone	Δ (km)	Class	Phase	Arrival Time	Travel Time	Corrected Travel time
						s	s	s
E_2	12	4.5 V	9.271	A	P_1	2.469+	2.069	2.068
	13	4.5 V	9.171	B	P_1	2.435+	2.035	2.034
	14	4.5 V	9.072	B	P_1	2.433+	2.033	2.032
	15	4.5 V	8.972	A	P_1	2.416+	2.016	2.015
	16	4.5 V	8.874	A	P_1	2.393+	1.993	1.992
	17	4.5 V	8.773	A	P_1	2.372+	1.972	1.971
	18	4.5 V	8.672	A	P_1	2.347+	1.947	1.946
	19	4.5 V	8.572	A	P_1	2.318+	1.918	1.917
	20	4.5 V	8.471	A	P_1	2.306+	1.906	1.905
	21	4.5 V	8.373	A	P_1	2.287+	1.887	1.886
	22	4.5 V	8.272	A	P_1	2.256+	1.856	1.855
	23	4.5 V	8.172	A	P_1	2.238+	1.838	1.837
	24	4.5 V	8.071	A	P_1	2.203+	1.803	1.802
E_3	1	4.5 V	7.641	A	P_1	2.100+	1.700	1.698
	2	4.5 V	7.540	A	P_1	2.090+	1.690	1.688
	3	4.5 V	7.442	A	P_1	2.080+	1.680	1.677
	4	4.5 V	7.342	A	P_1	2.031+	1.631	1.628
	5	4.5 V	7.241	A	P_1	2.002+	1.602	1.598
	6	4.5 V	7.139	A	P_1	1.979+	1.579	1.574
	7	4.5 V	7.041	A	P_1	1.970+	1.570	1.565
	8	4.5 V	6.939	A	P_1	1.949+	1.549	1.545
	9	4.5 V	6.841	A	P_1	1.921+	1.521	1.517
	10	4.5 V	6.740	A	P_1	1.901+	1.501	1.497
	11	4.5 V	6.641	A	P_1	1.871+	1.471	1.468
	12	4.5 V	6.539	A	P_1	1.856+	1.456	1.452
	13	4.5 V	6.441	A	P_1	1.826+	1.426	1.422
	14	4.5 V	6.340	A	P_1	1.803+	1.403	1.399
	15	4.5 V	6.239	A	P_1	1.773+	1.373	1.369
	16	4.5 V	6.139	A	P_1	1.749+	1.349	1.345
	17	4.5 V	6.041	A	P_1	1.736+	1.336	1.332
	18	4.5 V	5.942	A	P_1	1.719+	1.319	1.314
	19	4.5 V	5.839	A	P_1	1.690+	1.290	1.285
	20	4.5 V	5.740	A	P_1	1.672+	1.272	1.267
	21	4.5 V	5.641	A	P_1	1.649+	1.249	1.244
	22	4.5 V	5.540	A	P_1	1.631+	1.231	1.226
	23	4.5 V	5.443	A	P_1	1.625+	1.225	1.220
	24	4.5 V	5.340	A	P_1	1.563+	1.163	1.158
E_4	1	4.5 V	5.306	A	P_1	1.564+	1.164	1.163
	2	4.5 V	5.209	A	P_1	1.542+	1.142	1.142
	3	4.5 V	5.108	A	P_1	1.550+	1.150	1.150
	4	4.5 V	5.007	A	P_1	1.547+	1.147	1.147
	5	4.5 V	4.859	B	P_1	1.561+	1.161	1.161
	6	4.5 V	4.809	A	P_1	1.537+	1.137	1.137
	7	4.5 V	4.709	C	P_1	1.52 +	1.12	1.12
	8	4.5 V	4.610	A	P_1	1.502+	1.102	1.102
	9	4.5 V	4.509	A	P_1	1.497+	1.097	1.097
	10	4.5 V	4.407	B	P_1	1.436+	1.036	1.036
	11	4.5 V	4.309	B	P_1	1.435+	1.035	1.035
	12	4.5 V	4.208	B	P_1	1.371+	0.971	0.971
	13	4.5 V	4.107	A	P_1	1.347+	0.947	0.947
	14	4.5 V	4.009	A	P_1	1.332+	0.932	0.931

Observation Point		Geophone	Δ (km)	Class	Phase	Arrival Time	Travel Time	Corrected Travel time
						s	s	s
E_4	15	4.5 V	3.909	A	P_1	1.316+	0.916	0.915
	16	4.5 V	3.809	A	P_1	1.292+	0.892	0.891
	17	4.5 V	3.709	A	P_1	1.284+	0.884	0.883
	18	4.5 V	3.607	A	P_1	1.297+	0.897	0.896
	19	4.5 V	3.505	B	P_1	1.282+	0.882	0.881
	20	4.5 V	3.408	A	P_1	1.300+	0.900	0.900
	21	4.5 V	3.300	A	P_1	1.284+	0.884	0.884
	23	4.5 V	3.106	B	P_1	1.251+	0.851	0.851
	24	4.5 V	3.007	A	P_1	1.242+	0.842	0.842
E_5	1	4.5 V	1.890	A	P_1	0.959+	0.559	0.555
	2	4.5 V	1.789	A	P_1	0.903+	0.503	0.499
	3	4.5 V	1.692	A	P_1	0.844+	0.444	0.440
	4	4.5 V	1.592	A	P_1	0.795+	0.395	0.391
	5	4.5 V	1.491	A	P_1	0.774+	0.374	0.370
	6	4.5 V	1.391	A	P_1	0.737+	0.337	0.333
	7	4.5 V	1.290	A	P_1	0.735+	0.335	0.330
	8	4.5 V	1.190	A	P_1	0.708+	0.308	0.303
	9	4.5 V	1.092	A	P_1	0.696+	0.296	0.291
	10	4.5 V	0.990	A	P_1	0.665+	0.265	0.262
	11	4.5 V	0.895	A	P_1	0.643+	0.243	0.241
	12	4.5 V	0.790	A	P_1	0.605+	0.205	0.204
	13	4.5 V	0.691	B	P_1	0.585+	0.185	0.185
	14	4.5 V	0.591	B	P_1	0.562+	0.162	0.162
	15	4.5 V	0.490	A	P_1	0.548+	0.148	0.148
	16	4.5 V	0.391	A	P_1	0.527+	0.127	0.126
	17	4.5 V	0.290	A	P_1	0.503+	0.103	0.103
	18	4.5 V	0.191	A	P_1	0.476+	0.076	0.065
	19	4.5 V	0.090	A	P_1	0.467+	0.067	0.036
	20	4.5 V	0.010	A	P_1	0.480+	0.080	0.005
	21	4.5 V	0.107	A	P_1	0.496+	0.096	0.043
	22	4.5 V	0.200	A	P_1	0.530+	0.130	0.073
	23	4.5 V	0.298	A	P_1	0.546+	0.146	0.096
	24	4.5 V	0.399	A	P_1	0.584+	0.184	0.131
D_1	a	4 V	29.753	B	P_1	6.856−	6.456	6.452
	b	4 V	29.413	C	P_1	6.78 −	6.38	6.38
	c	1 V	29.520	C	P_1	6.79 −	6.39	6.39
D_2	a	4 V	29.238	C	P_1	6.66 +	6.26	6.26
	b	1 V	29.004	C	P_1	6.60 +	6.20	6.20
	c	4 V	28.655	C	P_1	6.55 +	6.15	6.15
D_4	a	1 V	20.724	B	P_1	5.065+	4.665	4.665
	b	1 V	20.414	C	P_1	5.01 +	4.61	4.61
	c	1 V	20.109	C	P_1	5.00 +	4.60	4.60
D_5	a	4 V	17.954	B	P_1	4.403+	4.003	4.002
	b	2 V	17.707	C	P_1	4.37 +	3.97	3.97
	c	4 V	17.514	B	P_1	4.255+	3.855	3.854
D_6	a	2 V	17.212	B	P_1	4.130+	3.730	3.729
	c	4 V	16.647	A	P_1	4.098+	3.698	3.697
D_7	a	4 V	2.719	A	P_1	1.137+	0.737	0.722
	b	1 V	2.192	A	P_1	1.025+	0.625	0.605
	c	4 V	1.978	A	P_1	0.968+	0.568	0.552

Observation Point		Geophone	Δ (km)	Class	Phase	Arrival Time	Travel Time	Corrected Travel time
D_8	a	4 V	0.757	A	P_1	0.727+ s	0.327 s	0.318 s
	b	1 V	1.044	A	P_1	0.770+	0.370	0.369
	c	4 V	1.383	A	P_1	0.840+	0.440	0.440
D_9	a	4 V	3.915	A	P_1	1.342+	0.942	0.935
	b	4 V	4.364	A	P_1	1.443+	1.043	1.026
	c	4 V	4.702	A	P_1	1.506+	1.106	1.080
D_{10}	a	4 V	5.032	A	P_1	1.566+	1.166	1.147
	b	1 V	5.355	A	P_1	1.636+	1.236	1.217
	c	4 V	5.682	A	P_1	1.676+	1.276	1.259
D_{11}	a	4 V	6.995	A	P_1	1.886+	1.486	1.473
	b	1 V	7.187	A	P_1	1.906+	1.506	1.497
	c	4 V	7.609	A	P_1	1.971+	1.571	1.566
D_{12}	a	4 V	8.821	A	P_1	2.166+	1.766	1.766
	b	1 V	9.348	A	P_1	2.276+	1.876	1.875
	c	4 V	9.613	A	P_1	2.326+	1.926	1.924
D_{13}	a	4 V	12.057	A	P_1	2.864+	2.464	2.463
	b	1 V	12.351	A	P_1	2.887+	2.487	2.486
	c	4 V	12.599	A	P_1	2.947+	2.547	2.547
D_{14}	a	4 V	16.092	A	P_1	3.934+	3.534	3.534
	b	4 V	16.219	A	P_1	3.976+	3.576	3.575
	c	1 V	16.470	A	P_1	4.046+	3.646	3.646
	c	1 H	16.470	B	P_1	4.080−	3.680	3.680
	e	4.5 V	16.978	A	P_1	4.164+	3.764	3.764
	f	4 V	17.202	A	P_1	4.220+	3.820	3.820

Table 6 (4) Travel time data for shot B–III_2

Observation Point		Geophone	Δ (km)	Class	Phase	Arrival Time	Travel Time	Corrected Travel time
E_1	1	4.5 V	13.383	C		1 h 48 m		(2.98) s
	2	4.5 V	13.285	B	P_1	3.361+ s	2.962 s	2.962
	3	4.5 V	13.184	A	P_1	3.343+	2.944	2.944
	4	4.5 V	13.086	A	P_1	3.319+	2.920	2.920
	5	4.5 V	12.987	A	P_1	3.299+	2.900	2.900
	6	4.5 V	12.888	B	P_1	3.276+	2.877	2.877
	7	4.5 V	12.831	B	P_1	3.268+	2.869	2.869
	8	4.5 V	12.694	B	P_1	3.236+	2.837	2.837
	9	4.5 V	12.596	A	P_1	3.224+	2.825	2.825
	10	4.5 V	12.497	A	P_1	3.202+	2.803	2.803
	11	4.5 V	12.399	A	P_1	3.166+	2.767	2.766
	12	4.5 V	12.300	A	P_1	3.158+	2.759	2.758
	13	4.5 V	12.204	A	P_1	3.135+	2.736	2.735
	14	4.5 V	12.100	A	P_1	3.121+	2.722	2.721
	15	4.5 V	12.001	A	P_1	3.095+	2.696	2.695

Observation Point		Geophone	Δ (km)	Class	Phase	Arrival Time	Travel Time	Corrected Travel time
						s	s	s
E_1	16	4.5 V	11.899	A	P_1	3.077+	2.678	2.677
	17	4.5 V	11.774	A	P_1	3.054+	2.655	2.654
	18	4.5 V	11.672	A	P_1	3.014+	2.615	2.614
	19	4.5 V	11.572	A	P_1	2.998+	2.599	2.598
	20	4.5 V	11.473	A	P_1	2.970+	2.571	2.570
	21	4.5 V	11.371	A	P_1	2.946+	2.547	2.546
	22	4.5 V	11.271	A	P_1	2.924+	2.525	2.524
	23	4.5 V	11.171	A	P_1	2.899+	2.500	2.499
	24	4.5 V	11.072	A	P_1	2.878+	2.479	2.478
E_2	1	4.5 V	10.372	B	P_1	2.737+	2.338	2.338
	2	4.5 V	10.271	A	P_1	2.703+	2.304	2.304
	3	4.5 V	10.174	A	P_1	2.678+	2.279	2.279
	4	4.5 V	10.072	A	P_1	2.659+	2.260	2.260
	5	4.5 V	9.971	A	P_1	2.642+	2.243	2.243
	6	4.5 V	9.600	B	P_1	2.618+	2.219	2.219
	7	4.5 V	9.772	A	P_1	2.592+	2.193	2.193
	8	4.5 V	9.672	A	P_1	2.562+	2.163	2.163
	9	4.5 V	9.573	A	P_1	2.555+	2.156	2.156
	10	4.5 V	9.473	B	P_1	2.524+	2.125	2.124
	11	4.5 V	9.372	A	P_1	2.494+	2.095	2.094
	12	4.5 V	9.271	B	P_1	2.472+	2.073	2.073
	13	4.5 V	9.171	B	P_1	2.466+	2.067	2.067
	14	4.5 V	9.072	A	P_1	2.433+	2.034	2.033
	15	4.5 V	8.972	A	P_1	2.414+	2.015	2.014
	16	4.5 V	8.874	A	P_1	2.394+	1.995	1.994
	17	4.5 V	8.773	A	P_1	2.371+	1.972	1.971
	18	4.5 V	8.672	A	P_1	2.336+	1.937	1.936
	19	4.5 V	8.572	A	P_1	2.315+	1.916	1.915
	20	4.5 V	8.471	A	P_1	2.303+	1.904	1.903
	21	4.5 V	8.373	A	P_1	2.283+	1.884	1.883
	22	4.5 V	8.272	A	P_1	2.260+	1.861	1.860
	23	4.5 V	8.172	A	P_1	2.233+	1.834	1.833
	24	4.5 V	8.071	A	P_1	2.219+	1.820	1.819
E_3	1	4.5 V	7.641	A	P_1	2.101+	1.702	1.700
	2	4.5 V	7.540	A	P_1	2.086+	1.687	1.685
	3	4.5 V	7.442	C	P_1			(1.66)
	4	4.5 V	7.342	A	P_1	2.036+	1.637	1.634
	5	4.5 V	7.241	A	P_1	2.008+	1.609	1.605
	6	4.5 V	7.139	A	P_1	1.980+	1.581	1.576
	7	4.5 V	7.041	A	P_1	1.968+	1.569	1.564
	8	4.5 V	6.939	A	P_1	1.949+	1.550	1.546
	9	4.5 V	6.841	A	P_1	1.919+	1.520	1.516
	10	4.5 V	6.740	A	P_1	1.888+	1.489	1.485
	11	4.5 V	6.641	A	P_1	1.859+	1.460	1.458
	12	4.5 V	6.539	A	P_1	1.837+	1.438	1.434
	13	4.5 V	6.441	A	P_1	1.826+	1.427	1.423
	14	4.5 V	6.340	A	P_1	1.798+	1.399	1.395
	15	4.5 V	6.239	A	P_1	1.777+	1.378	1.374
	16	4.5 V	6.139	A	P_1	1.750+	1.351	1.347
	17	4.5 V	6.041	A	P_1	1.736+	1.337	1.333
	18	4.5 V	5.942	A	P_1	1.717+	1.318	1.313

Observation Point		Geophone	Δ (km)	Class	Phase	Arrival Time	Travel Time	Corrected Travel time
						s	s	s
E_3	19	4.5 V	5.839	A	P_1	1.697+	1.298	1.293
	20	4.5 V	5.740	A	P_1	1.678+	1.279	1.274
	21	4.5 V	5.641	A	P_1	1.665+	1.266	1.261
	22	4.5 V	5.540	A	P_1	1.625+	1.226	1.221
	23	4.5 V	5.443	A	P_1	1.617+	1.218	1.213
	24	4.5 V	5.340	A	P_1	1.566+	1.167	1.162
E_4	1	4.5 V	5.306	A	P_1	1.552+	1.153	1.152
	2	4.5 V	5.209	B	P_1	1.535+	1.136	1.136
	3	4.5 V	5.108	A	P_1	1.535+	1.136	1.136
	4	4.5 V	5.007	A	P_1	1.541+	1.142	1.142
	5	4.5 V	4.859	C	P_1	1.56 +	1.16	1.16
	6	4.5 V	4.809	A	P_1	1.535+	1.136	1.136
	7	4.5 V	4.709	B	P_1	1.541+	1.142	1.142
	8	4.5 V	4.610	A	P_1	1.484+	1.085	1.085
	9	4.5 V	4.509	B	P_1	1.480+	1.081	1.081
	10	4.5 V	4.407	B	P_1	1.422+	1.023	1.023
	11	4.5 V	4.309	B	P_1	1.422+	1.023	1.023
	12	4.5 V	4.208	A	P_1	1.370+	0.971	0.971
	13	4.5 V	4.107	A	P_1	1.344+	0.945	0.945
	14	4.5 V	4.009	A	P_1	1.319+	0.920	0.919
	15	4.5 V	3.909	A	P_1	1.315+	0.916	0.915
	16	4.5 V	3.809	A	P_1	1.284+	0.885	0.884
	17	4.5 V	3.709	A	P_1	1.271+	0.872	0.871
	18	4.5 V	3.607	A	P_1	1.289+	0.890	0.889
	19	4.5 V	3.505	C	P_1	1.27 +	0.87	0.87
	20	4.5 V	3.408	A	P_1	1.287+	0.888	0.888
	21	4.5 V	3.300	A	P_1	1.275+	0.876	0.876
	22	4.5 V	3.209	A	P_1	1.264+	0.865	0.865
	23	4.5 V	3.106	A	P_1	1.244+	0.845	0.845
	24	4.5 V	3.007	A	P_1	1.234+	0.835	0.835
E_5	1	4.5 V	1.890	A	P_1	0.948+	0.549	0.545
	2	4.5 V	1.789	A	P_1	0.897+	0.498	0.494
	3	4.5 V	1.692	A	P_1	0.846+	0.447	0.443
	4	4.5 V	1.592	A	P_1	0.801+	0.402	0.398
	5	4.5 V	1.491	A	P_1	0.777+	0.378	0.374
	6	4.5 V	1.391	A	P_1	0.737+	0.338	0.334
	7	4.5 V	1.290	A	P_1	0.739+	0.340	0.335
	8	4.5 V	1.190	A	P_1	0.707+	0.308	0.303
	9	4.5 V	1.092	A	P_1	0.697+	0.298	0.293
	10	4.5 V	0.990	A	P_1	0.667+	0.268	0.265
	11	4.5 V	0.895	A	P_1	0.644+	0.245	0.243
	12	4.5 V	0.790	A	P_1	0.608+	0.209	0.208
	13	4.5 V	0.691	B	P_1	0.586+	0.187	0.187
	14	4.5 V	0.591	B	P_1	0.566+	0.168	0.168
	15	4.5 V	0.490	A	P_1	0.548+	0.149	0.149
	16	4.5 V	0.391	A	P_1	0.528+	0.129	0.128
	17	4.5 V	0.290	A	P_1	0.504+	0.105	0.105
	18	4.5 V	0.191	A	P_1	0.478+	0.079	0.067
	19	4.5 V	0.090	A	P_1	0.467+	0.068	0.037
	20	4.5 V	0.010	A	P_1	0.479+	0.080	0.005
	21	4.5 V	0.107	A	P_1	0.498+	0.099	0.044
	22	4.5 V	0.200	A	P_1	0.527+	0.128	0.072

Observation Point		Geophone	Δ (km)	Class	Phase	Arrival Time	Travel Time	Corrected Travel time
						s	s	s
E_5	23	4.5 V	0.298	A	P_1	0.547−	0.148	0.098
	24	4.5 V	0.399	A	P_1	0.586+	0.187	0.133
D_1	a	4 V	29.753	B	P_1	6.810+	6.411	6.407
	b	1 V	29.413	C	P_1	6.68 +	6.28	6.28
	c	4 V	29.520	C	P_1	6.75 +	6.35	6.35
D_2	a	4 V	29.238	A	P_1	6.648+	6.249	6.248
	b	1 V	29.004	B	P_1	6.594+	6.195	6.195
	c	4 V	28.655	B	P_1	6.524+	6.125	6.125
D_3	a	1 V	22.008	B	P_1	5.510+	5.111	5.110
	b	1 V	21.561	A	P_1	5.413+	5.014	5.013
	c	1 V	21.150	A	P_1	5.350+	4.951	4.950
D_4	a	1 V	20.724	A	P_1	5.210+	4.811	4.811
	b	1 V	20.414	A	P_1	5.145+	4.746	4.746
	c	1 V	20.109	A	P_1	5.040+	4.641	4.640
D_5	a	4 V	17.954	A	P_1	4.400+	4.001	4.000
	b	2 V	17.707	A	P_1	4.332+	3.933	3.932
	c	4 V	17.514	A	P_1	4.255+	3.856	3.855
D_6	a	2 V	17.212	A	P_1	4.232+	3.833	3.832
	b	2 V	16.937	A	P_1	4.125+	3.726	3.725
	c	4 V	16.647	A	P_1	4.117+	3.718	3.717
D_7	a	4 V	2.719	A	P_1	1.137+	0.738	0.723
	b	1 V	2.192	A	P_1	1.022+	0.623	0.604
	c	4 V	1.978	A	P_1	0.958+	0.559	0.543
D_8	a	4 V	0.757	A	P_1	0.725+	0.326	0.317
	b	1 V	1.044	A	P_1	0.766+	0.367	0.366
	c	4 V	1.383	A	P_1	0.841+	0.442	0.442
D_9	a	4 V	3.915	A	P_1	1.344+	0.945	0.938
	b	1 V	4.364	A	P_1	1.442+	1.043	1.026
	c	4 V	4.702	A	P_1	1.500+	1.101	1.075
D_{10}	a	4 V	5.032	A	P_1	1.568+	1.169	1.149
	b	1 V	5.355	A	P_1	1.629+	1.230	1.211
	c	4 V	5.682	A	P_1	1.676+	1.277	1.260
D_{11}	a	4 V	6.995	A	P_1	1.892+	1.493	1.480
	b	1 V	7.187	A	P_1	1.911+	1.512	1.502
	c	4 V	7.609	A	P_1	1.973+	1.574	1.569
D_{12}	a	4 V	8.821	A	P_1	2.161+	1.762	1.762
	b	1 V	9.348	A	P_1	2.270+	1.871	1.870
	c	4 V	9.613	A	P_1	2.320+	1.921	1.919
D_{13}	a	4 V	12.057	A	P_1	2.868+	2.469	2.468
	b	1 V	12.351	A	P_1	2.886+	2.487	2.486
	c	4 V	12.599	A	P_1	2.952+	2.553	2.553
D_{14}	a	4 V	16.092	A	P_1	3.945+	3.546	3.546
	b	4 V	16.219	A	P_1	3.972+	3.573	3.572
	c	1 V	16.470	A	P_1	4.045+	3.646	3.646
	e	4 V	16.978	A	P_1	4.164+	3.765	3.765
	f	4 V	17.202	A	P_1	4.215+	3.816	3.816

Table 6 (5) Travel time data for shot B–IV

Observation Point		Geophone	Δ (km)	Class	Phase	Arrival Time	Travel Time	Corrected Travel time
						$2^h 48^m$		
E_1	1	4.5 V	30.596	C				$(6.38)^s$
	2	4.5 V	30.498	C	P_1	6.74^s +	6.34^s	6.34
	3	4.5 V	30.397	C	P_1			(6.31)
	4	4.5 V	30.299	C	P_1			(6.29)
	5	4.5 V	30.200	C	P_1			(6.27)
	6	4.5 V	30.101	C	P_1			(6.25)
	7	4.5 V	30.044	C	P_1			(6.22)
	8	4.5 V	29.907	C	P_1	6.60 +	6.20	6.20
	9	4.5 V	29.809	C	P_1			(6.17)
	10	4.5 V	29.710	C	P_1	6.55 +	6.15	6.15
	11	4.5 V	29.612	C	P_1			(6.13)
	12	4.5 V	29.513	C	P_1			(6.10)
	13	4.5 V	29.417	C	P_1			(6.08)
	14	4.5 V	29.313	C	P_1			(6.06)
	15	4.5 V	29.214	C	P_1			(6.03)
	16	4.5 V	29.112	C	P_1	6.42 +	6.02	6.02
	17	4.5 V	28.987	C	P_1			(5.99)
	18	4.5 V	28.885	C	P_1			(5.97)
	19	4.5 V	28.785	C	P_1	6.35 +	5.95	5.95
	20	4.5 V	28.686	C	P_1			(5.92)
	21	4.5 V	28.584	C	P_1			(5.89)
	22	4.5 V	28.484	C	P_1			(5.86)
	23	4.5 V	28.384	C	P_1			(5.84)
	24	4.5 V	28.285	C	P_1	6.21 +	5.81	5.81
E_2	1	4.5 V	27.585	C	P_1	6.10 +	5.70	5.70
	2	4.5 V	27.484	C	P_1	6.09 +	5.69	5.69
	3	4.5 V	27.387	C	P_1			(5.68)
	4	4.5 V	27.285	C	P_1			(5.67)
	5	4.5 V	27.184	C	P_1	6.06 +	5.66	5.65
	6	4.5 V	26.813	C	P_1			(5.64)
	7	4.5 V	26.985	C	P_1	6.04 +	5.64	5.63
	8	4.5 V	26.885	C	P_1			(5.62)
	9	4.5 V	26.786	B	P_1	6.011+	5.610	5.609
	10	4.5 V	26.686	B	P_1	5.989+	5.588	5.587
	11	4.5 V	26.585	B	P_1	5.973+	5.572	5.571
	12	4.5 V	26.484	C	P_1	5.94 +	5.54	5.54
	13	4.5 V	26.384	B	P_1	5.930+	5.529	5.528
	14	4.5 V	26.285	B	P_1	5.882+	5.481	5.480
	15	4.5 V	26.185	B	P_1	5.877+	5.476	5.475
	16	4.5 V	26.087	B	P_1	5.854+	5.453	5.452
	17	4.5 V	25.986	C	P_1	5.82 +	5.42	5.42
	18	4.5 V	25.885	B	P_1	5.797+	5.396	5.395
	19	4.5 V	25.785	B	P_1	5.778+	5.377	5.376
	20	4.5 V	25.684	B	P_1	5.766+	5.365	5.364
	21	4.5 V	25.586	B	P_1	5.750+	5.349	5.348
	22	4.5 V	25.485	B	P_1	5.733+	5.332	5.331
	23	4.5 V	25.385	C	P_1	5.72 +	5.32	5.31
	24	4.5 V	25.284	C	P_1	5.70 +	5.30	5.30

Observation Point		Geophone	Δ (km)	Class	Phase	Arrival Time	Travel Time	Corrected Travel time
						s	s	s
E_3	1	4.5 V	24.854	B	P_1	5.590+	5.189	5.189
	2	4.5 V	24.753	B	P_1	5.579+	5.179	5.179
	3	4.5 V	24.655	C	P_1			(5.16)
	4	4.5 V	24.552	B	P_1	5.535+	5.134	5.133
	5	4.5 V	24.454	B	P_1	5.506+	5.105	5.104
	6	4.5 V	24.352	B	P_1	5.475+	5.074	5.073
	7	4.5 V	24.254	B	P_1	5.457+	5.056	5.055
	8	4.5 V	24.152	B	P_1	5.433+	5.032	5.031
	9	4.5 V	24.054	B	P_1	5.413+	5.012	5.011
	10	4.5 V	23.953	B	P_1	5.395+	4.994	4.994
	11	4.5 V	23.854	B	P_1	5.358+	4.957	4.957
	12	4.5 V	23.752	A	P_1	5.340+	4.939	4.939
	13	4.5 V	23.654	A	P_1	5.317+	4.916	4.916
	14	4.5 V	23.553	B	P_1	5.295+	4.894	4.894
	15	4.5 V	23.452	A	P_1	5.283+	4.882	4.882
	16	4.5	23.352	A	P_1	5.251+	4.850	4.850
	17	4.5 V	23.254	B	P_1	5.222+	4.821	4.821
	18	4.5 V	23.155	A	P_1	5.217+	4.816	4.816
	19	4.5 V	23.052	C	P_1			(4.80)
	20	4.5 V	22.953	A	P_1	5.186+	4.785	4.785
	21	4.5 V	22.854	B	P_1	5.175+	4.774	4.774
	22	4.5 V	22.753	A	P_1	5.170+	4.769	4.769
	23	4.5 V	22.656	B	P_1	5.138+	4.737	4.737
	24	4.5 V	22.553	A	P_1	5.088+	4.687	4.687
E_4	1	4.5 V	22.519	B	P_1	5.092+	4.691	4.691
	3	4.5 V	22.321	B	P_1	5.073+	4.672	4.672
	4	4.5 V	22.220	B	P_1	5.078+	4.677	4.677
	5	4.5 V	22.122	C	P_1	5.10 +	4.70	4.70
	6	4.5 V	22.022	B	P_1	5.070+	4.669	4.669
	7	4.5 V	21.922	B	P_1	5.072+	4.671	4.671
	8	4.5 V	21.823	B	P_1	5.038+	4.637	4.637
	9	4.5 V	21.722	C	P_1	5.01 +	4.61	4.61
	10	4.5 V	21.620	C	P_1	4.97 +	4.56	4.56
	11	4.5 V	21.522	C	P_1	4.97 +	4.57	4.57
	12	4.5 V	21.421	C	P_1	4.91 +	4.51	4.51
	13	4.5 V	21.320	C	P_1	4.89 +	4.49	4.49
	14	4.5 V	21.222	B	P_1	4.876+	4.475	4.475
	15	4.5 V	21.122	B	P_1	4.865+	4.464	4.464
	16	4.5 V	21.022	B	P_1	4.852+	4.451	4.451
	17	4.5 V	20.922	C	P_1	4.85 +	4.44	4.44
	18	4.5 V	20.820	B	P_1	4.843+	4.442	4.442
	20	4.5 V	20.621	C	P_1	4.83 +	4.43	4.43
	21	4.5 V	20.513	C	P_1	4.82 +	4.42	4.42
	23	4.5 V	20.319	B	P_1	4.819+	4.418	4.418
	24	4.5 V	20.220	B	P_1	4.814+	4.413	4.413
E_5	1	4.5 V	19.103	A	P_1	4.596+	4.195	4.194
	2	4.5 V	19.002	A	P_1	4.549+	4.148	4.147
	3	4.5 V	18.905	A	P_1	4.510	4.109	4.108
	4	4.5 V	18.805	A	P_1	4.478+	4.077	4.076
	5	4.5 V	18.704	A	P_1	4.447+	4.046	4.045
	6	4.5 V	18.604	B	P_1	4.416+	4.015	4.014
	7	4.5 V	18.503	A	P_1	4.428+	4.027	4.026

Observation Point		Geophone	Δ (km)	Class	Phase	Arrival Time	Travel Time	Corrected Travel time
						s	s	s
E_5	8	4.5 V	18.403	A	P_1	4.410+	4.009	4.008
	9	4.5 V	18.305	A	P_1	4.401+	4.000	4.000
	10	4.5 V	18.203	A	P_1	4.377+	3.976	3.976
	11	4.5 V	18.108	A	P_1	4.368+	3.967	3.967
	12	4.5 V	18.003	B	P_1	4.335+	3.934	3.934
	13	4.5 V	17.904	B	P_1	4.315+	3.914	3.914
	14	4.5 V	17.804	B	P_1	4.296+	3.895	3.895
	15	4.5 V	17.703	B	P_1	4.296+	3.895	3.895
	16	4.5 V	17.604	B	P_1	4.274+	3.873	3.873
	17	4.5 V	17.503	B	P_1	4.262+	3.861	3.861
	18	4.5 V	17.404	B	P_1	4.249+	3.848	3.848
	19	4.5 V	17.303	A	P_1	4.235+	3.834	3.834
	20	4.5 V	17.203	A	P_1	4.220+	3.819	3.819
	21	4.5 V	17.106	A	P_1	4.200+	3.799	3.799
	22	4.5 V	17.013	A	P_1	4.181+	3.780	3.779
	23	4.5	16.915	B	P_1	4.158+	3.757	3.755
	24	4.5 V	16.814	A	P_1	4.150+	3.749	3.747
D_1	a	4 V	46.966	B	P_1	10.200+	9.799	9.797
	b	1 V	46.626	B	P_1	10.137+	9.736	9.735
	c	4 V	46.733	B	P_1	10.124+	9.723	9.723
D_2	a	4 V	46.451	C	P_1	10.00 +	9.60	9.60
	b	1 V	46.217	C	P_1	9.95 +	9.55	9.54
	c	4 V	45.868	C	P_1	9.81 +	9.41	9.41
D_3	b	1 V	38.774	C	P_1	8.81 −	8.41	8.41
	c	1 V	38.363	C	P_1	8.68 −	8.28	8.28
D_4	a	1 V	37.937	C	P_1	8.56 −	8.16	8.16
	b	1 V	37.639	B	P_1	8.560−	8.159	8.158
	c	1 V	37.322	B	P_1	8.472−	8.071	8.070
D_5	a	4 V	35.167	B	P_1	7.831−	7.430	7.429
	b	2 V	34.920	C	P_1	7.72 +	7.32	7.32
	c	4 V	34.727	C	P_1	7.64 +	7.24	7.24
D_6	a	2 V	34.425	C	P_1	7.55 +	7.15	7.15
	b	2 V	34.150	C	P_1	7.47 +	7.07	7.07
	c	4 V	33.860	C	P_1	7.40 +	7.00	7.00
D_7	a	4 V	19.932	B	P_1	4.700+	4.299	4.296
	b	1 V	19.405	A	P_1	4.643+	4.242	4.239
	c	4 V	19.191	A	P_1	4.597+	4.196	4.194
D_8	a	4 V	16.456	A	P_1	4.036+	3.635	3.634
	b	1 V	16.169	A	P_1	3.984+	3.583	3.583
	c	4 V	15.830	A	P_1	3.923+	3.522	3.522
D_9	a	4 V	13.298	A	P_1	3.546+	3.145	3.142
	b	1 V	12.848	A	P_1	3.473+	3.072	3.068
	c	4 V	12.511	A	P_1	3.388+	2.987	2.979
D_{10}	a	4 V	12.181	A	P_1	3.338+	2.937	2.931
	b	1 V	11.858	A	P_1	3.255+	2.854	2.847
	c	4 V	11.531	A	P_1	3.218+	2.817	2.810

Observation Point		Geophone		Δ (km)	Class	Phase	Arrival Time	Travel Time	Corrected Travel time
							s	s	s
D_{11}	a	4	V	10.218	A	P_1	2.991+	2.590	2.582
	b	1	V	10.026	A	P_1	2.941+	2.540	2.540
	c	4	V	9.604	A	P_1	2.878+	2.477	2.474
D_{12}	a	4	V	8.392	A	P_1	2.726+	2.325	2.324
	b	1	V	7.865	A	P_1	2.668+	2.267	2.263
	c	4	V	7.600	A	P_1	2.623+	2.222	2.216
D_{13}	a	4	V	5.156	A	P_1	2.158+	1.757	1.748
	b	1	V	4.862	A	P_1	2.046+	1.645	1.638
	c	4	V	4.614	A	P_1	2.012+	1.611	1.607
D_{14}	a	4	V	1.121	A	P_1	0.885+	0.484	0.481
	b	4	V	0.994	A	P_1	0.833+	0.432	0.425
	c	1	V	0.743	A	P_1	0.728+	0.327	0.325
	c	1	H	0.743	A	P_1	0.730	0.329	0.327
	e	4	V	0.235	A	P_1	0.515+	0.114	0.112
	f	4	V	0.011	A	P_1	0.424+	0.023	0.014

Table 6 (6) Travel time data for shot E_2–W_1

Observation Point		Geophone	Δ (km)	Class	Phase	Arrival Time	Travel Time	Corrected Travel time
						s	s	s
E_1	2	4.5 V	2.833	C	P_1	1.60 +	1.54	1.53
	3	4.5 V	2.733	C	P_1	1.58 +	1.52	1.51
	4	4.5 V	2.634	C	P_1	1.56 +	1.50	1.49
	5	4.5 V	2.535	C	P_1	1.49 +	1.43	1.42
	6	4.5 V	2.436	C	P_1			(1.37)
	7	4.5 V	2.339	C	P_1			(1.33)
	8	4.5 V	2.243	B	P_1	1.353+	1.294	1.280
	9	4.5 V	2.145	B	P_1	1.299+	1.240	1.223
	10	4.5 V	2.045	B	P_1	1.253+	1.194	1.174
	11	4.5 V	1.948	B	P_1	1.212+	1.153	1.130
	12	4.5 V	1.849	A	P_1	1.170+	1.111	1.085
	13	4.5 V	1.752	A	P_1	1.137+	1.078	1.048
	14	4.5 V	1.649	A	P_1	1.037+	0.978	0.947
	15	4.5 V	1.549	A	P_1	1.007+	0.948	0.914
	16	4.5 V	1.448	A	P_1	0.975+	0.916	0.878
	17	4.5 V	1.323	B	P_1	0.916+	0.857	0.814
	18	4.5 V	1.220	A	P_1	0.878+	0.819	0.772
	19	4.5 V	1.121	B	P_1	0.780+	0.721	0.671
	20	4.5 V	1.021	B	P_1	0.768+	0.709	0.651
	21	4.5 V	0.919	B	P_1	0.718+	0.659	0.597
	22	4.5 V	0.819	A	P_1	0.685+	0.626	0.553
	23	4.5 V	0.720	A	P_1	0.648+	0.589	0.507
	24	4.5 V	0.620	B	P_1	0.618+	0.559	0.463
E_2	1	4.5 V	0.080	A	P_1	0.097+	0.038	
	2	4.5 V	0.181	A	P_1	0.131+	0.072	
	3	4.5 V	0.278	A	P_1	0.181+	0.122	
	4	4.5 V	0.380	A	P_1	0.217+	0.158	
	5	4.5 V	0.480	B	P_1	0.268+	0.209	
	6	4.5 V	0.581	B	P_1	0.312+	0.253	
	7	4.5 V	0.679	A	P_1	0.378+	0.319	
	8	4.5 V	0.780	B	P_1	0.398+	0.339	
	9	4.5 V	0.878	B	P_1	0.463+	0.404	
	10	4.5 V	0.979	B	P_1	0.509+	0.450	
	11	4.5 V	1.080	B	P_1	0.567+	0.508	
	12	4.5 V	1.180	B	P_1	0.613+	0.554	
	13	4.5 V	1.281	C	P_1	0.68 +	0.62	
	14	4.5 V	1.379	C	P_1	0.72 +	0.66	
	15	4.5 V	1.480	C	P_1	0.75 +	0.69	
	16	4.5 V	1.578	C	P_1	0.78 +	0.72	
	17	4.5 V	1.678	C	P_1	0.85 +	0.80	
	18	4.5 V	1.779	C	P_1	0.92 +	0.86	
	20	4.5 V	1.980	C	P_1	1.00 +	0.94	

Table 6 (7) Travel time data for shot E_2–W_2

Observation Point		Geophone	Δ (km)	Class	Phase	Arrival Time	Travel Time	Corrected Travel time
E_2	1	4.5 V	2.255	B	P_1	1.322+ s	1.026 s	
	2	4.5 V	2.154	B	P_1	1.303+	1.007	
	3	4.5 V	2.057	C	P_1	1.27 +	0.97	
	4	4.5 V	1.955	B	P_1	1.223+	0.927	
	5	4.5 V	1.855	B	P_1	1.191+	0.895	
	7	4.5 V	1.656	C	P_1	1.10 +	0.81	
	8	4.5 V	1.555	B	P_1	1.049+	0.753	
	9	4.5 V	1.457	B	P_1	1.002+	0.706	
	10	4.5 V	1.357	B	P_1	0.960+	0.664	
	11	4.5 V	1.257	B	P_1	0.915+	0.619	
	12	4.5 V	1.157	B	P_1	0.869+	0.573	
	13	4.5 V	1.054	B	P_1	0.790+	0.494	
	14	4.5 V	0.956	B	P_1	0.763+	0.467	
	15	4.5 V	0.855	B	P_1	0.718+	0.422	
	16	4.5 V	0.757	A	P_1	0.675+	0.379	
	17	4.5 V	0.657	A	P_1	0.632+	0.336	
	18	4.5 V	0.556	A	P_1	0.584+	0.288	
	19	4.5 V	0.455	A	P_1	0.539+	0.243	
	20	4.5 V	0.354	A	P_1	0.493+	0.197	
	21	4.5 V	0.256	A	P_1	0.448+	0.152	
	22	4.5 V	0.156	A	P_1	0.402+	0.106	
	24	4.5 V	0.046	A	P_1	0.337+	0.041	
E_3	1	4.5 V	0.731	A	P_1	0.646+	0.350	
	2	4.5 V	0.838	A	P_1	0.691+	0.395	
	3	4.5 V	0.940	B	P_1	0.770+	0.474	
	4	4.5 V	1.043	A	P_1	0.808+	0.512	
	5	4.5 V	1.148	A	P_1	0.855+	0.559	
	6	4.5 V	1.252	A	P_1	0.900+	0.604	
	7	4.5 V	1.332	A	P_1	0.918+	0.622	
	8	4.5 V	1.400	A	P_1	0.941+	0.645	
	9	4.5 V	1.477	A	P_1	0.958+	0.662	
	10	4.5 V	1.558	A	P_1	0.978+	0.682	
	11	4.5 V	1.641	A	P_1	0.978+	0.682	
	12	4.5 V	1.727	A	P_1	1.003+	0.707	
	13	4.5 V	1.820	A	P_1	1.029+	0.733	
	14	4.5 V	1.914	A	P_1	1.056+	0.760	
	15	4.5 V	2.008	A	P_1	1.071+	0.775	
	16	4.5 V	2.104	A	P_1	1.086+	0.790	
	17	4.5 V	2.199	A	P_1	1.087+	0.791	
	18	4.5 V	2.294	A	P_1	1.098+	0.802	
	19	4.5 V	2.392	B	P_1	1.125+	0.829	
	20	4.5 V	2.489	A	P_1	1.148+	0.852	
	21	4.5 V	2.585	B	P_1	1.151+	0.855	
	22	4.5 V	2.682	B	P_1	1.161+	0.865	
	23	4.5 V	2.778	B	P_1	1.191+	0.894	
	24	4.5 V	2.876	A	P_1	1.164+	0.868	

Table 6 (8) Travel time data for shot E_4–W_1

Observation Point		Geophone	Δ (km)	Class	Phase	Arrival Time	Travel Time	Corrected Travel time
						s	s	
E_3	1	4.5 V	2.439	A	P_1	0.962+	0.735	
	2	4.5 V	2.352	A	P_1	0.947+	0.720	
	3	4.5 V	2.269	A	P_1	0.949+	0.722	
	4	4.5 V	2.181	A	P_1	0.924+	0.697	
	5	4.5 V	2.103	A	P_1	0.897+	0.670	
	6	4.5 V	2.023	A	P_1	0.874+	0.647	
	7	4.5 V	1.931	A	P_1	0.858+	0.631	
	8	4.5 V	1.826	A	P_1	0.831+	0.604	
	9	4.5 V	1.731	A	P_1	0.800+	0.573	
	10	4.5 V	1.632	A	P_1	0.773+	0.546	
	11	4.5 V	1.537	A	P_1	0.731+	0.504	
	12	4.5 V	1.437	A	P_1	0.717+	0.490	
	13	4.5 V	1.355	A	P_1	0.689+	0.462	
	14	4.5 V	1.268	A	P_1	0.664+	0.437	
	15	4.5 V	1.185	A	P_1	0.635+	0.408	
	16	4.5 V	1.103	A	P_1	0.603+	0.376	
	17	4.5 V	1.032	A	P_1	0.580+	0.353	
	18	4.5 V	0.960	A	P_1	0.563+	0.336	
	19	4.5 V	0.891	A	P_1	0.552+	0.325	
	20	4.5 V	0.836	A	P_1	0.520+	0.293	
	21	4.5 V	0.784	A	P_1	0.513+	0.286	
	22	4.5 V	0.742	A	P_1	0.511+	0.284	
	24	4.5 V	0.694	A	P_1	0.435+	0.208	
E_4	1	4.5 V	0.050	A	P_1	0.323+	0.096	
	2	4.5 V	0.052	C	P_1	0.36 +	0.13	
	3	4.5 V	0.153	C	P_1	0.41 +	0.18	
	4	4.5 V	0.250	C	P_1	0.46 +	0.23	
	5	4.5 V	0.347	B	P_1	0.528+	0.301	
	6	4.5 V	0.448	A	P_1	0.537+	0.310	
	7	4.5 V	0.548	A	P_1	0.569+	0.342	
	8	4.5 V	0.646	A	P_1	0.574+	0.347	
	9	4.5 V	0.747	A	P_1	0.620+	0.393	
	10	4.5 V	0.849	A	P_1	0.606+	0.379	
	11	4.5 V	0.946	A	P_1	0.606+	0.379	
	12	4.5 V	1.049	A	P_1	0.635+	0.408	
	13	4.5 V	1.150	A	P_1	0.652+	0.425	
	14	4.5 V	1.248	A	P_1	0.673+	0.446	
	15	4.5 V	1.348	A	P_1	0.697+	0.470	
	16	4.5 V	1.448	A	P_1	0.710+	0.483	
	17	4.5 V	1.547	A	P_1	0.724+	0.497	
	18	4.5 V	1.650	B	P_1	0.753+	0.526	
	20	4.5 V	1.849	B	P_1	0.843+	0.616	
	21	4.5 V	1.957	B	P_1	0.888+	0.661	
	22	4.5 V	2.048	B	P_1	0.919+	0.692	
	23	4.5 V	2.150	C	P_1	0.95 +	0.73	
	24	4.5 V	2.250	B	P_1	0.971+	0.744	
D_7	a	4 V	2.538	B	P_1	0.910+	0.683	0.677
	b	1 V	3.065	B	P_1	1.058+	0.831	0.825
	c	4 V	3.278	A	P_1	1.110+	0.883	0.870

Table 6 (9) Travel time data for E_4–W_2

Observation Point		Geophone	Δ (km)	Class	Pbase	Arrival Time	Travel Time	Corrected Travel time
E_4	1	4.5 V	2.148	C	P_1	$1\overset{s}{.}37$ +	$0\overset{s}{.}67$	$0\overset{s}{.}67$
	3	4.5 V	1.949	B	P_1	1.363+	0.661	0.661
	4	4.5 V	1.848	C	P_1	1.34 +	0.63	0.63
	6	4.5 V	1.650	C	P_1	1.31 +	0.61	0.61
	7	4.5 V	1.550	C	P_1	1.30 +	0.60	0.59
	8	4.5 V	1.452	C	P_1	1.25 +	0.55	0.54
	10	4.5 V	1.249	B	P_1	1.179+	0.477	0.474
	11	4.5 V	1.151	B	P_1	1.171+	0.469	0.465
	12	4.5 V	1.049	B	P_1	1.116+	0.414	0.410
	13	4.5 V	0.948	B	P_1	1.085+	0.383	0.378
	14	4.5 V	0.850	A	P_1	1.064+	0.362	0.356
	15	4.5 V	0.750	A	P_1	1.051+	0.349	0.343
	16	4.5 V	0.650	A	P_1	1.021+	0.319	0.309
	17	4.5 V	0.551	A	P_1	0.994+	0.292	0.286
	18	4.5 V	0.448	A	P_1	0.948+	0.246	0.240
	19	4.5 V	0.347	A	P_1	0.901+	0.199	0.195
	20	4.5 V	0.249	A	P_1	0.849+	0.147	0.144
	21	4.5 V	0.141	A	P_1	0.798+	0.096	0.094
	22	4.5 V	0.050	A	P_1	0.745+	0.043	0.043
	23	4.5 V	0.053	A	P_1	0.768+	0.066	0.064
	24	4.5 V	0.152	A	P_1	0.837+	0.135	0.132
E_5	1	4.5 V	1.269	B	P_1	1.324+	0.622	0.602
	2	4.5 V	1.370	A	P_1	1.338+	0.636	0.618
	3	4.5 V	1.467	B	P_1	1.350+	0.648	0.631
	4	4.5 V	1.567	B	P_1	1.352+	0.650	0.636
	5	4.5 V	1.667	B	P_1	1.345+	0.643	0.631
	6	4.5 V	1.768	B	P_1	1.350+	0.648	0.638
	7	4.5 V	1.868	B	P_1	1.390+	0.688	0.678
	8	4.5 V	1.969	B	P_1	1.396+	0.694	0.685
	9	4.5 V	2.067	B	P_1	1.415+	0.713	0.706
	10	4.5 V	2.169	B	P_1	1.421+	0.719	0.714
	11	4.5 V	2.264	C	P_1			(0.71)
	12	4.5 V	2.369	C	P_1			(0.73)
	13	4.5 V	2.468	C	P_1			(0.75)
	14	4.5 V	2.568	C	P_1			(0.78)
	15	4.5 V	2.669	C	P_1			(0.79)
	16	4.5 V	2.768	C	P_1			(0.81)
	17	4.5 V	2.869	C	P_1			(0.83)
	18	4.5 V	2.968	C	P_1			(0.84)
	19	4.5 V	3.069	C	P_1			(0.87)
	20	4.5 V	3.169	C	P_1			(0.91)
	21	4.5 V	3.266	C	P_1			(0.92)
	22	4.5 V	3.359	C	P_1			(0.94)
	23	4.5 V	3.457	C	P_1			(0.94)
	24	4.5 V	3.558	C	P_1			(0.97)
D_7	a	4 V	0.440	A	P_1	1.049+	0.347	0.202
	b	1 V	0.967	A	P_1	1.246+	0.544	0.448
	c	4 V	1.180	A	P_1	1.298+	0.596	0.537

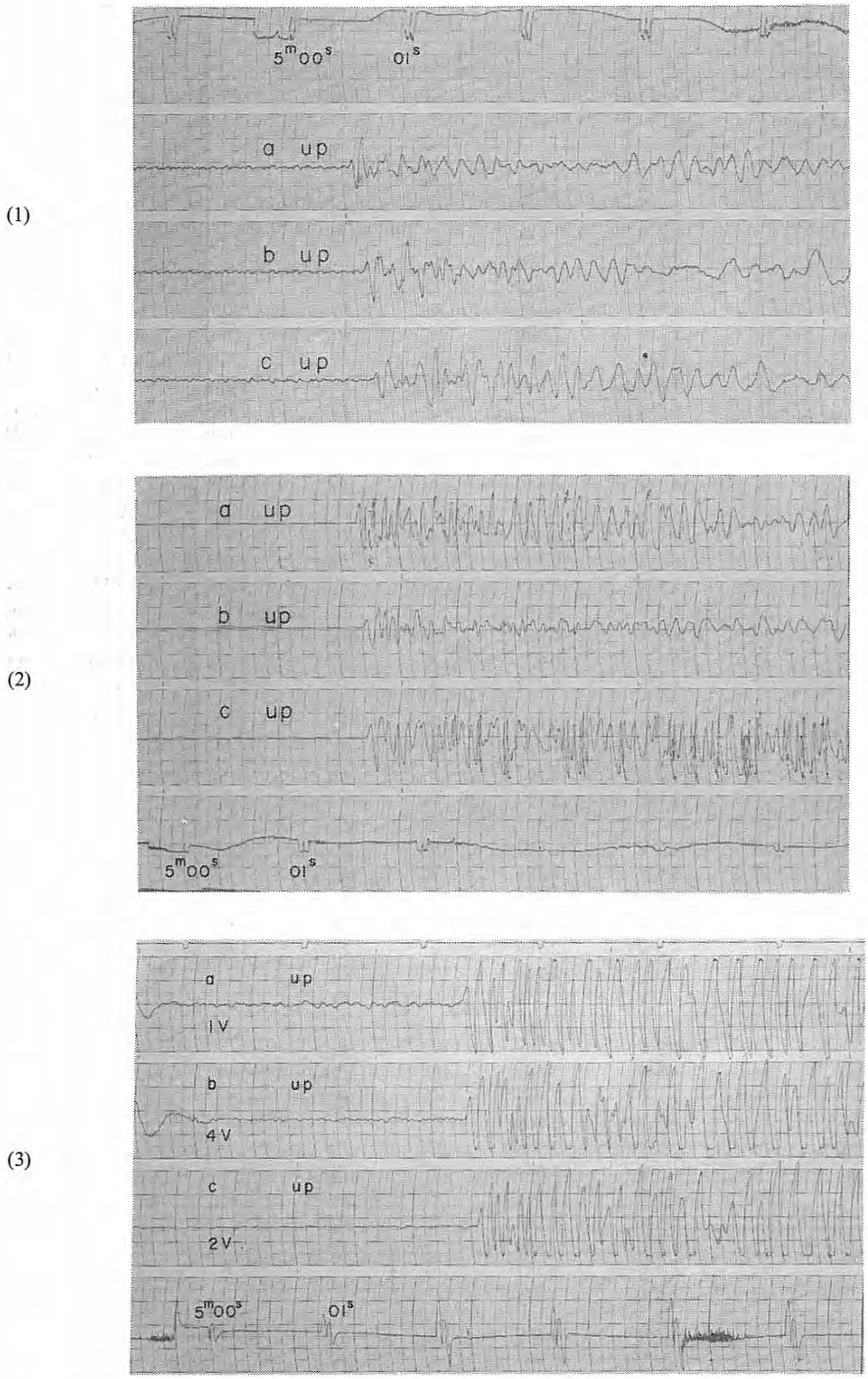

Fig. 5–1 Seismograms obtained (1) at D_1, (2) at D_2 and (3) at D_3 from the shot A–I

(4)

(5)

(6)

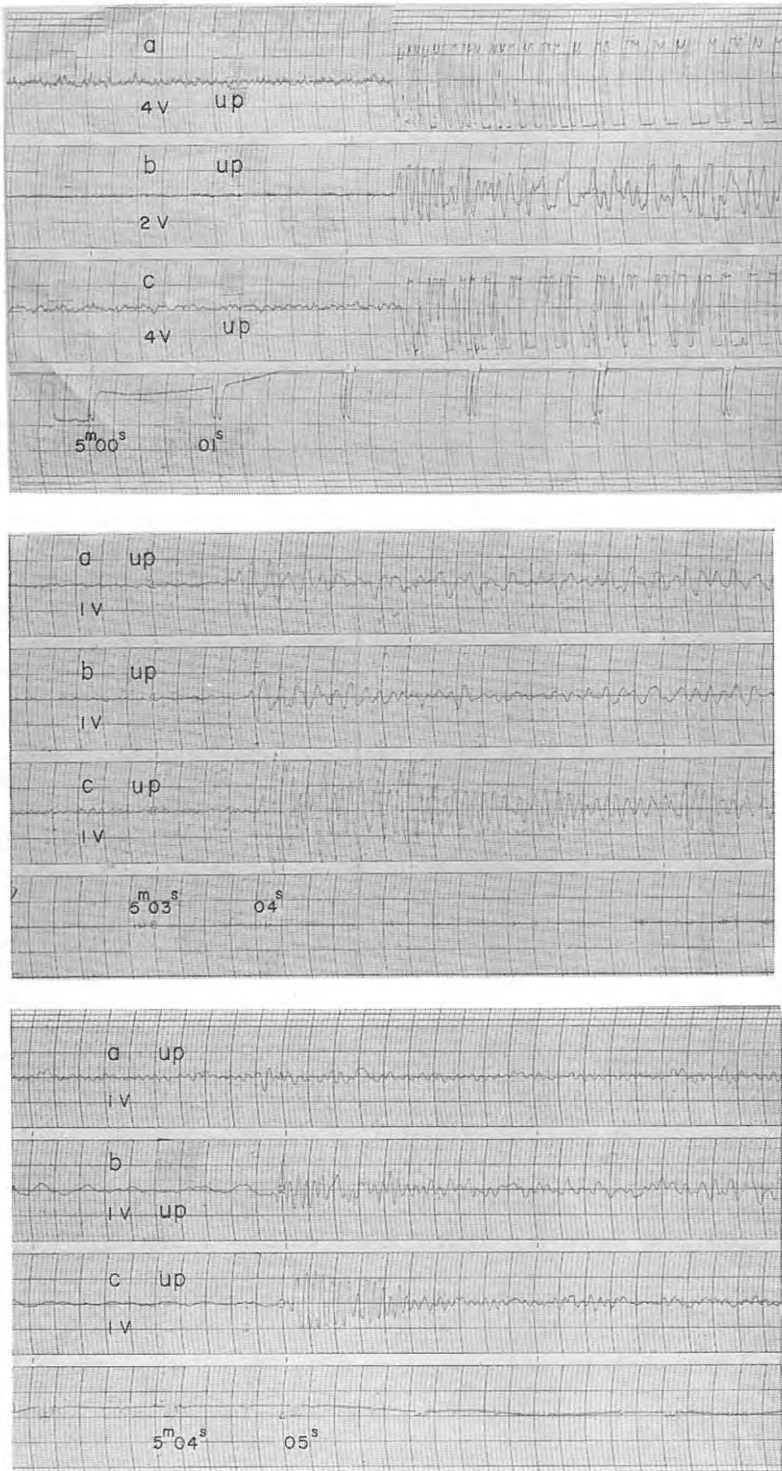

Fig. 5–2 Seismograms obtained (4) at D_4, (5) at D_5 and (6) at D_6 from the shot A–I

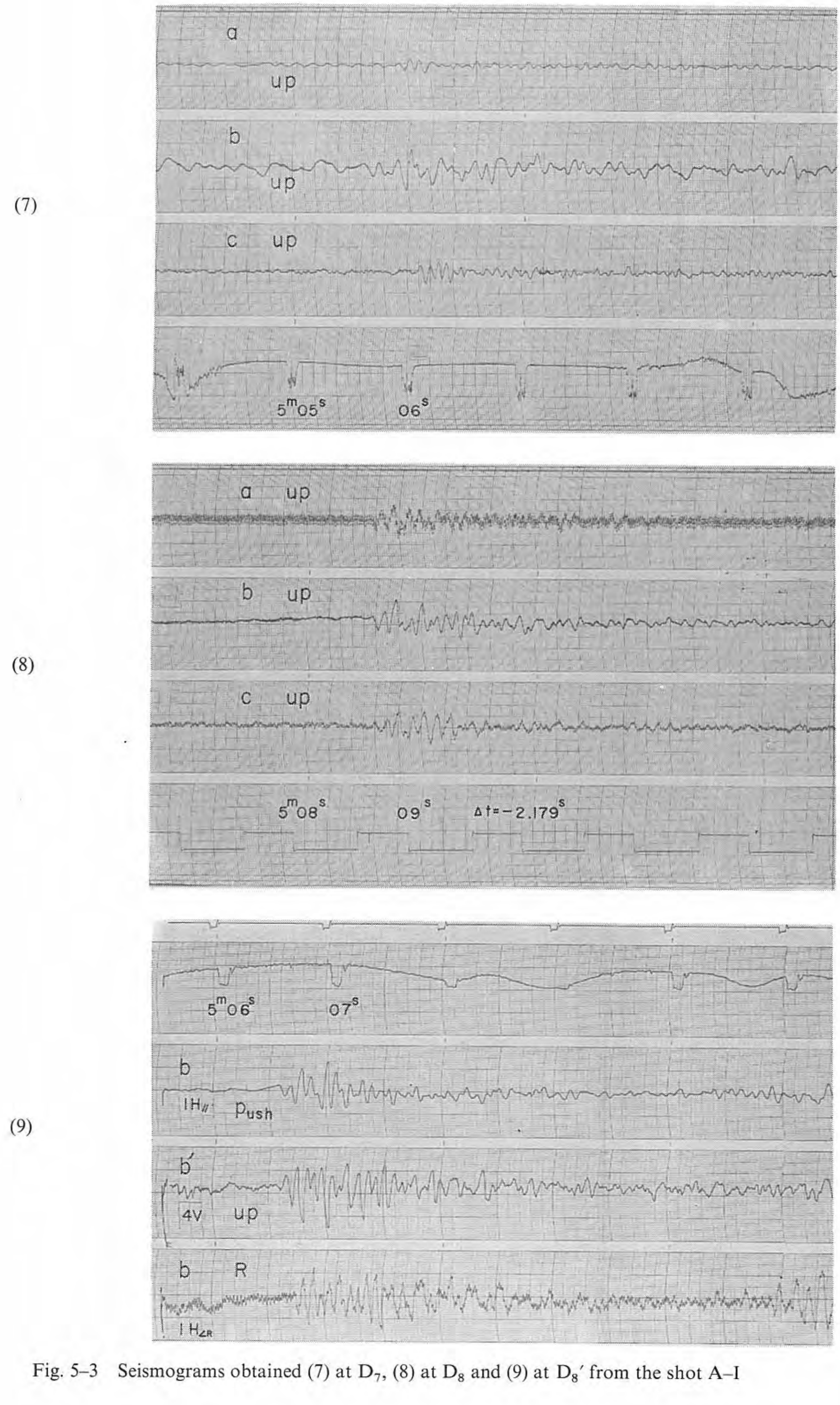

Fig. 5–3 Seismograms obtained (7) at D_7, (8) at D_8 and (9) at D_8' from the shot A–I

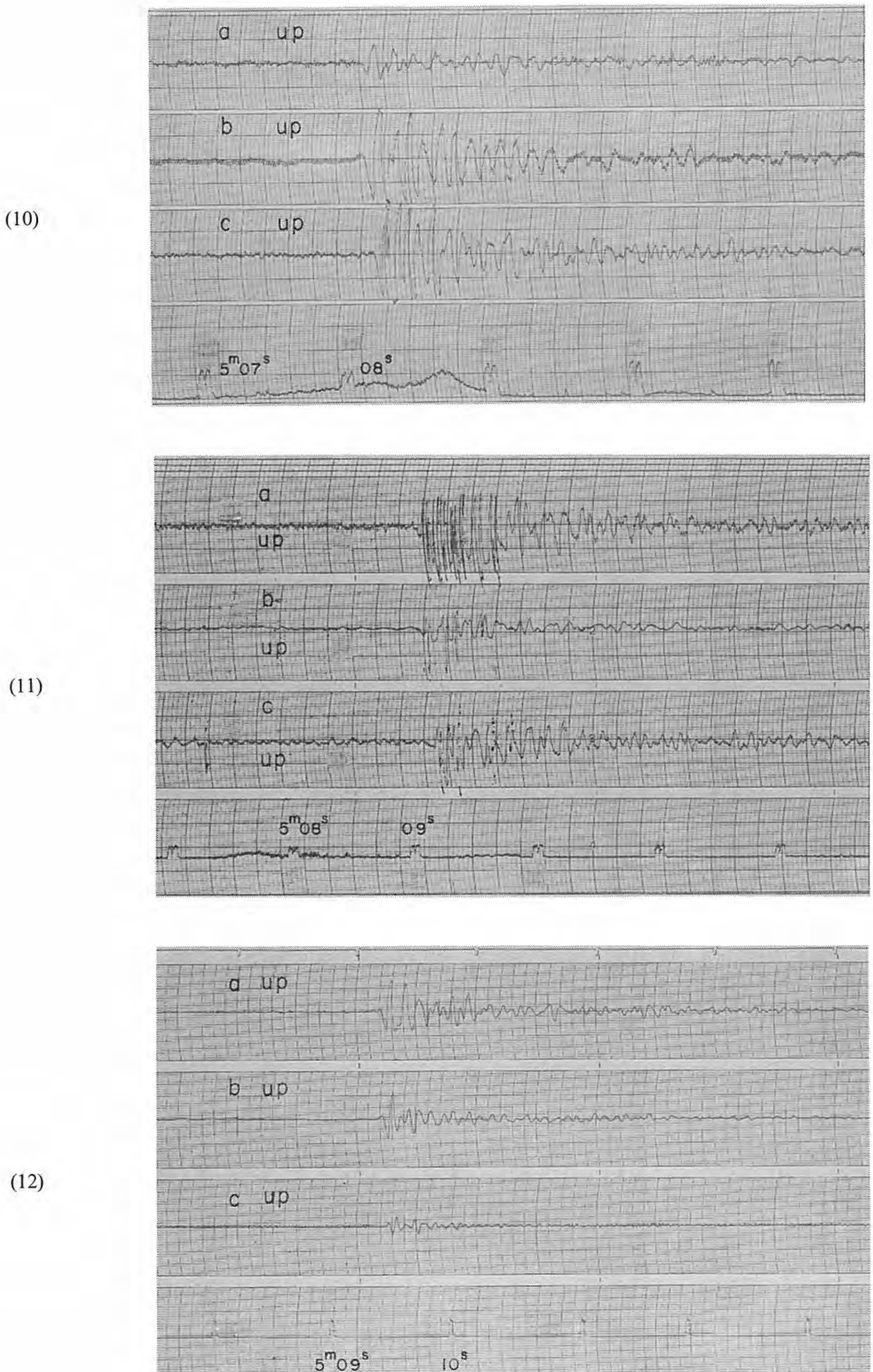

Fig. 5–4 Seismograms obtained (10) at D_9, (11) at D_{10} and (12) at D_{11} from the shot A–I

(13)

(14)

(15)

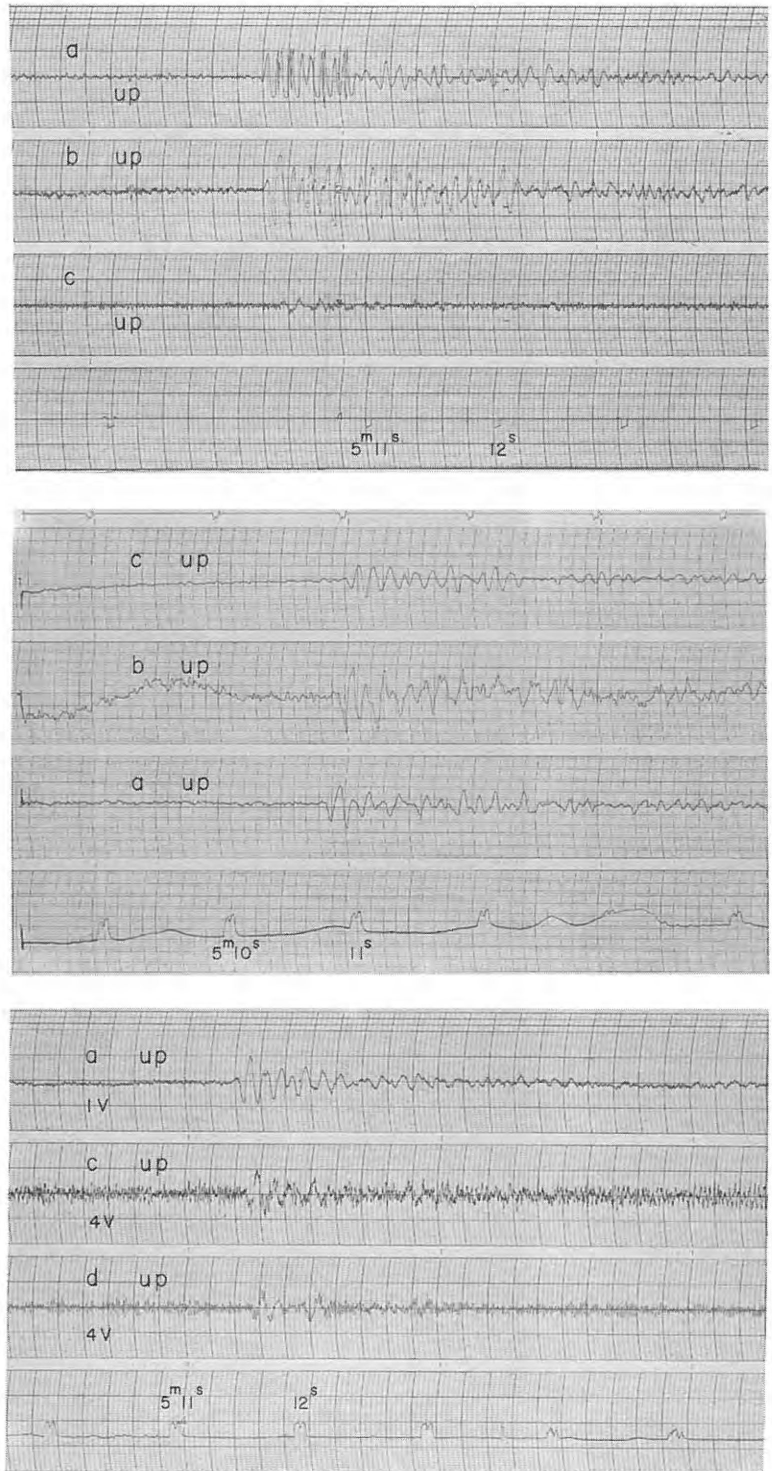

Fig. 5–5 Seismograms obtained (13) at D_{12}, (14) at D_{13} and (15) at D_{14} from the shot A–I

(16)

(17)

(18)

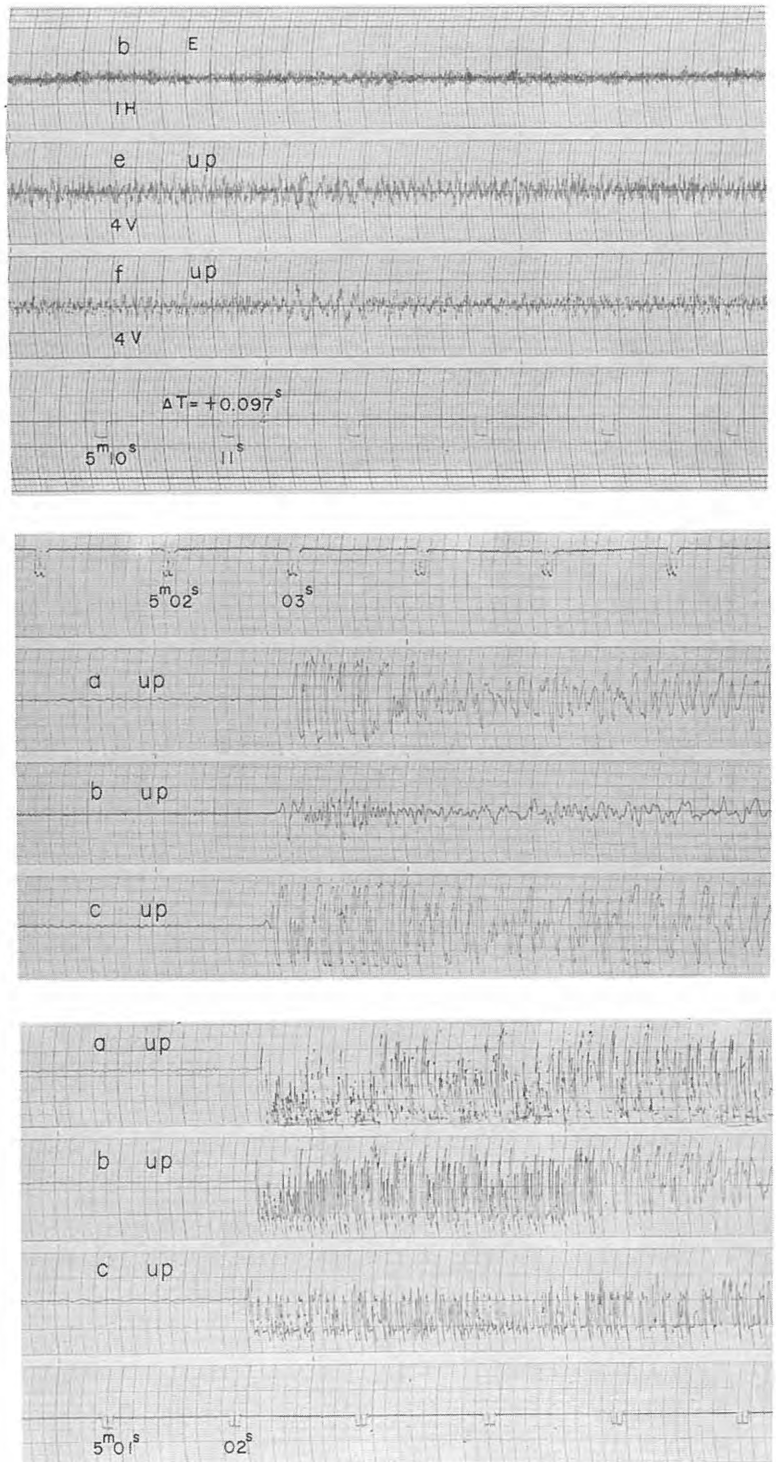

Fig. 5–6 Seismograms obtained (16) at D_{14} from the shot A–I, and (17) at D_1 and (18) at D_2 from the shot A–II

(19)

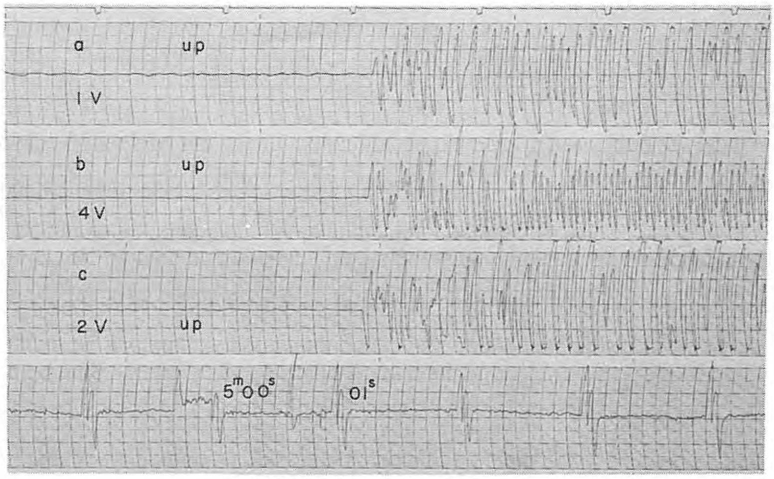

(20)

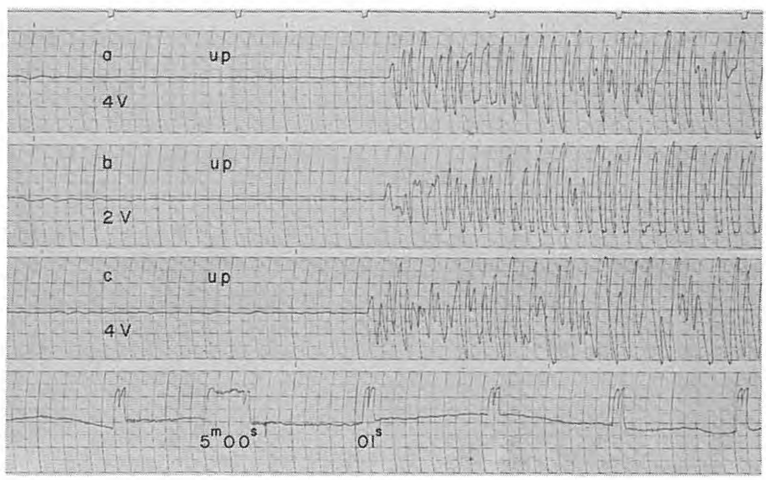

(21)

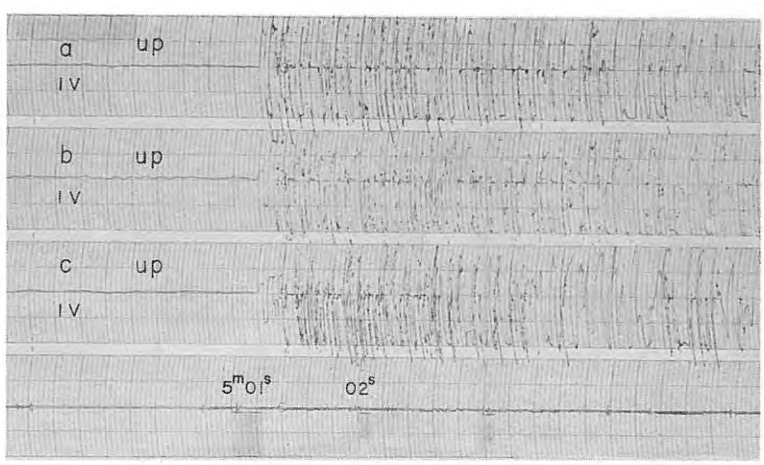

Fig. 5–7 Seismograms obtained (19) at D_3, (20) at D_4 and (21) at D_5 from the shot A–II

(22)

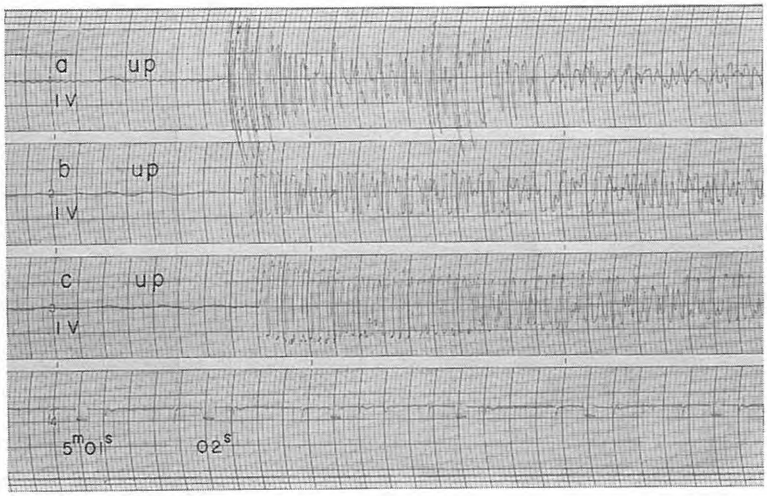

(23)

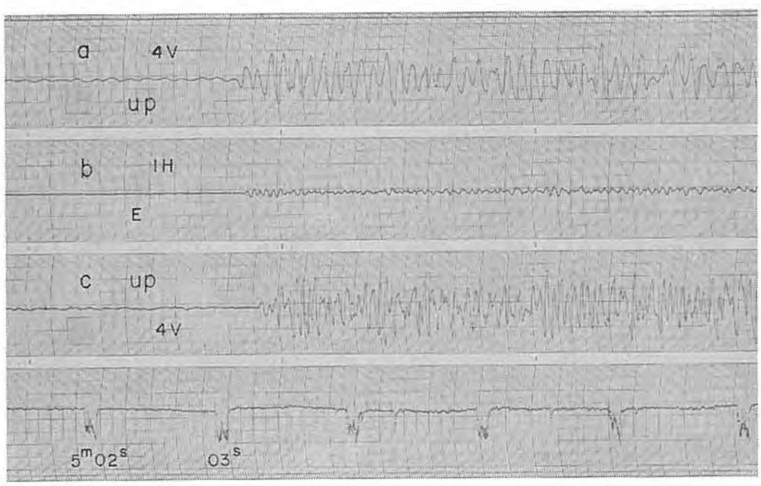

(24)

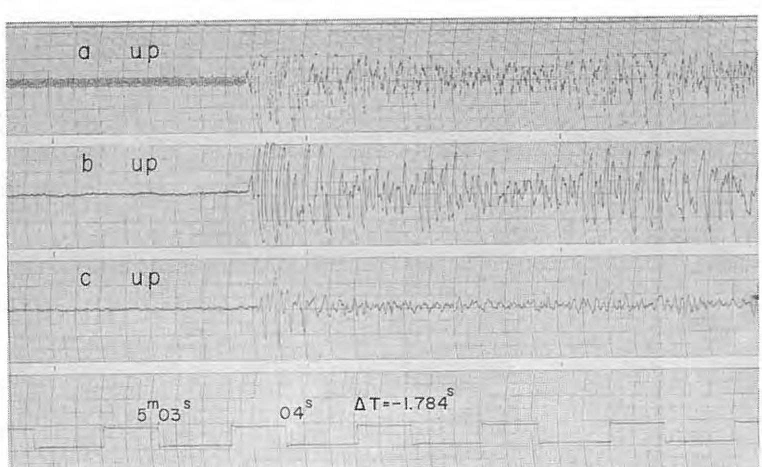

Fig. 5–8 Seismograms obtained (22) at D_6, (23) at D_7 and (24) at D_8 from the shot A–II

(25)

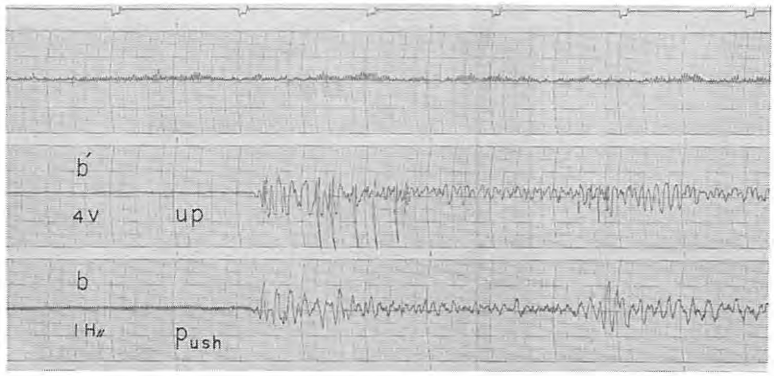

(26)

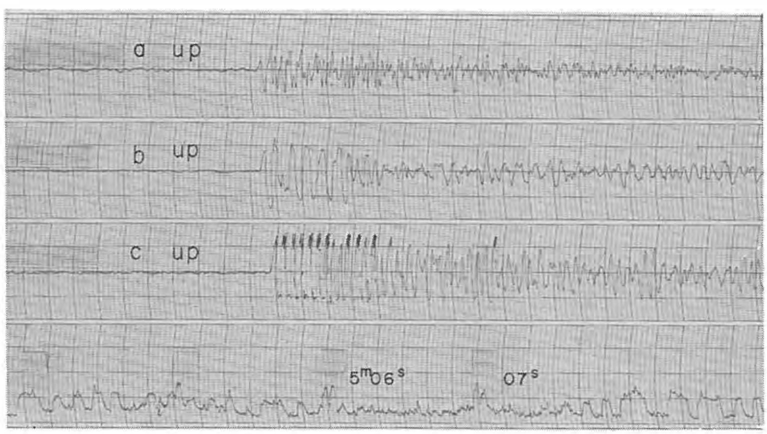

(27)

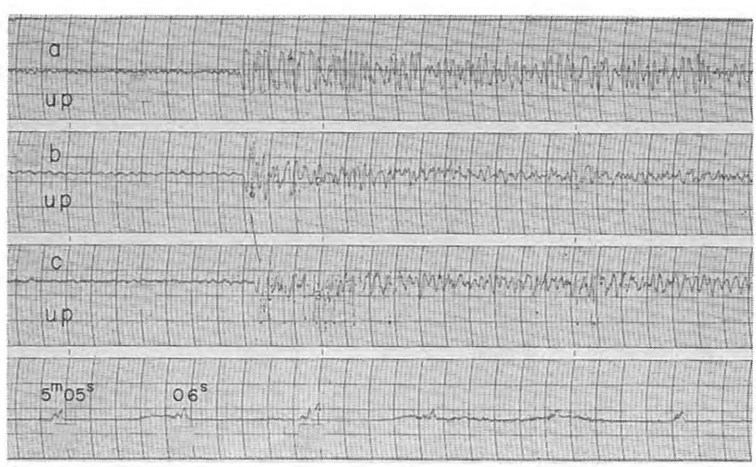

Fig. 5–9 Seismograms obtained (25) at D_8', (26) at D_9 and (27) at D_{10} from the shot A–II

(28)

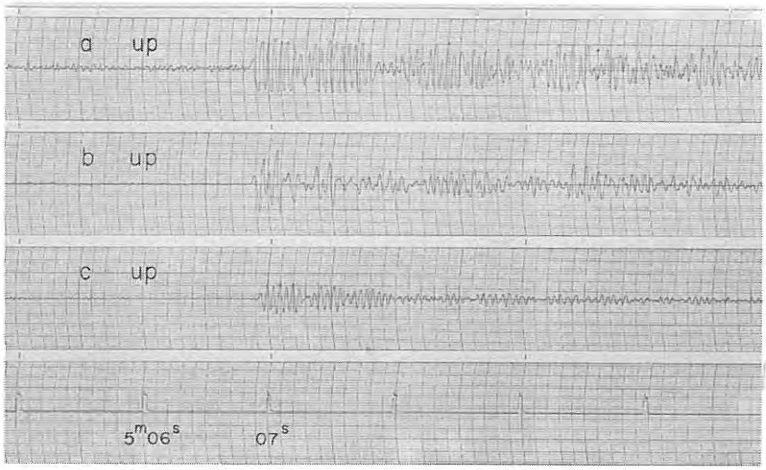

(29)

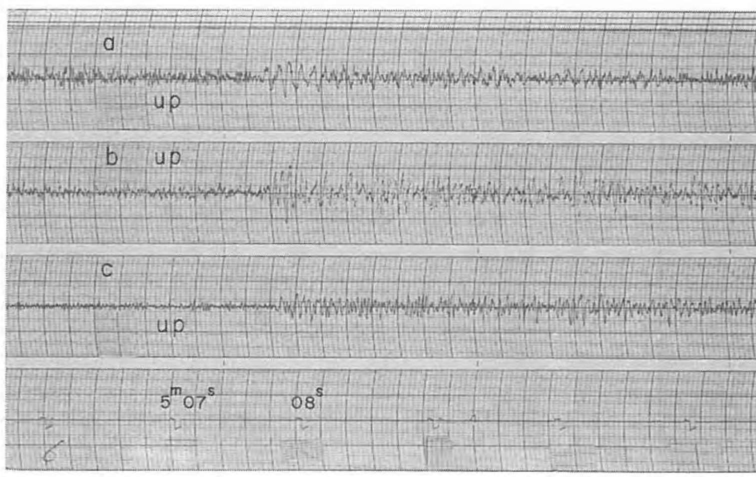

(30)

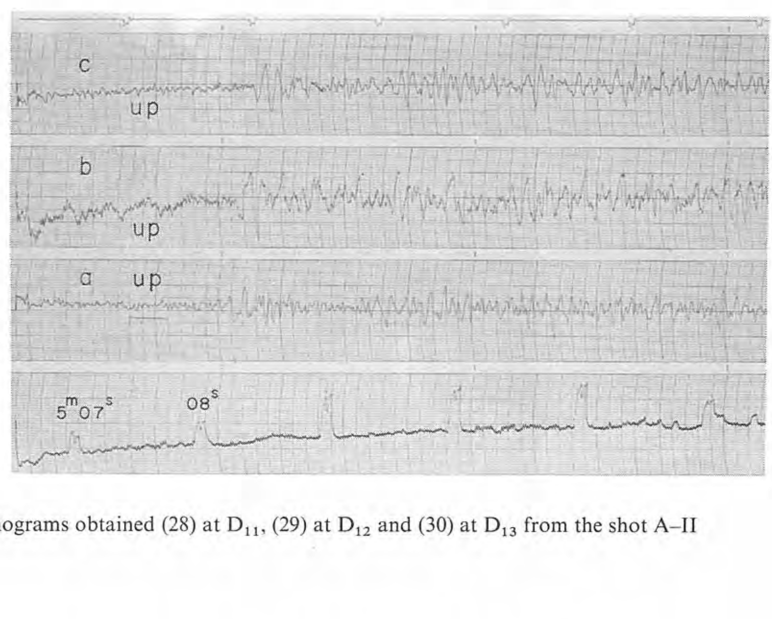

Fig. 5–10 Seismograms obtained (28) at D_{11}, (29) at D_{12} and (30) at D_{13} from the shot A–II

(31)
(32)
(33)

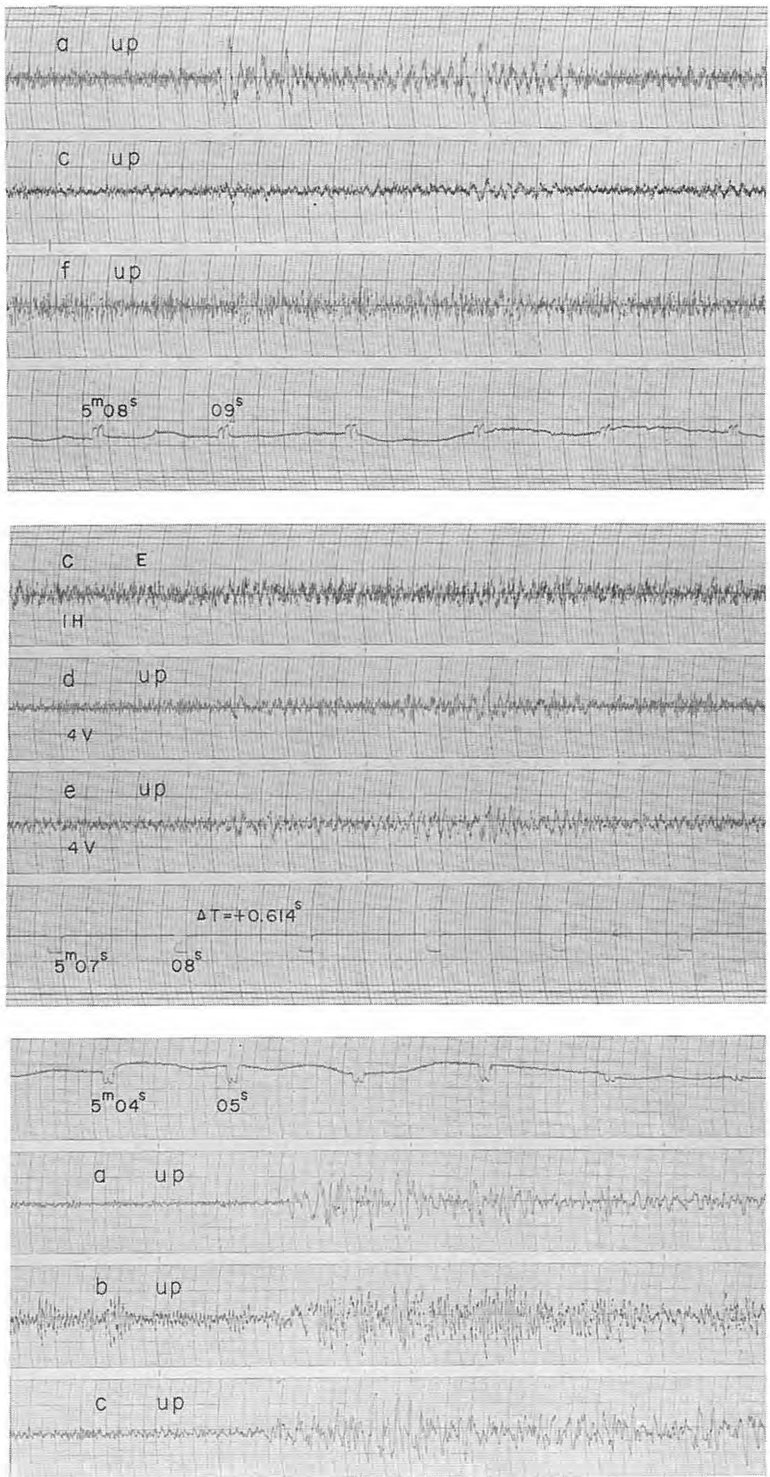

Fig. 5–11 Seismograms obtained (31), (32) at D_{14} from the shot A–II, and (33) at D_1 from the shot A–III

(34)

(35)

(36)

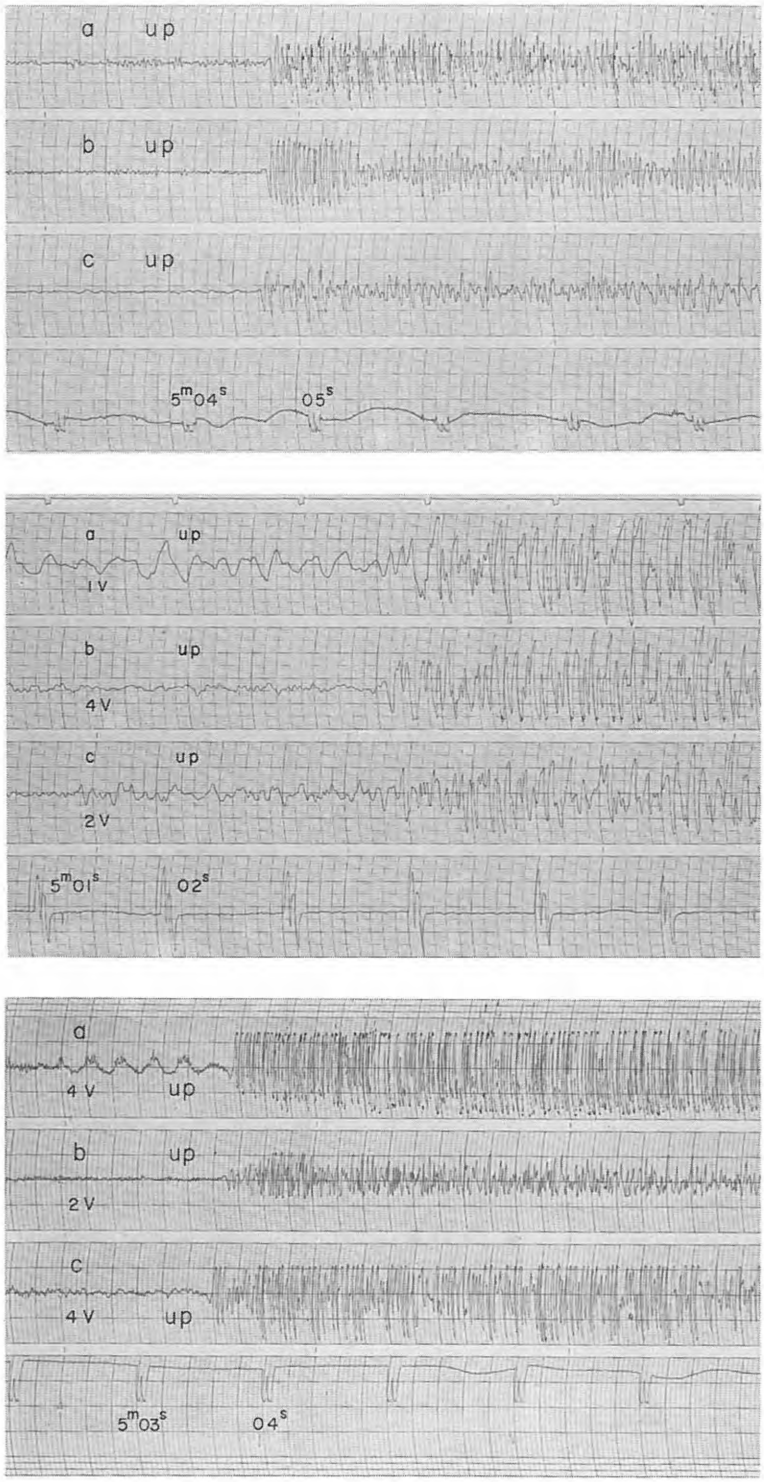

Fig. 5–12 Seismograms obtained (34) at D_2, (35) at D_3 and (36) at D_4 from the shot A–III

(37)

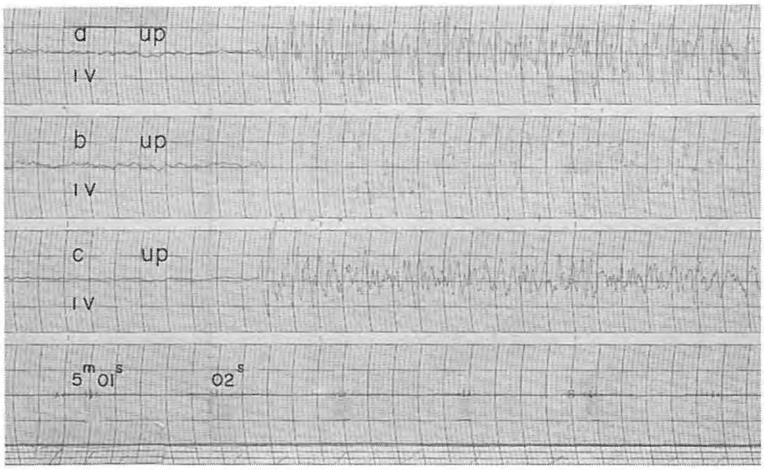

(38)

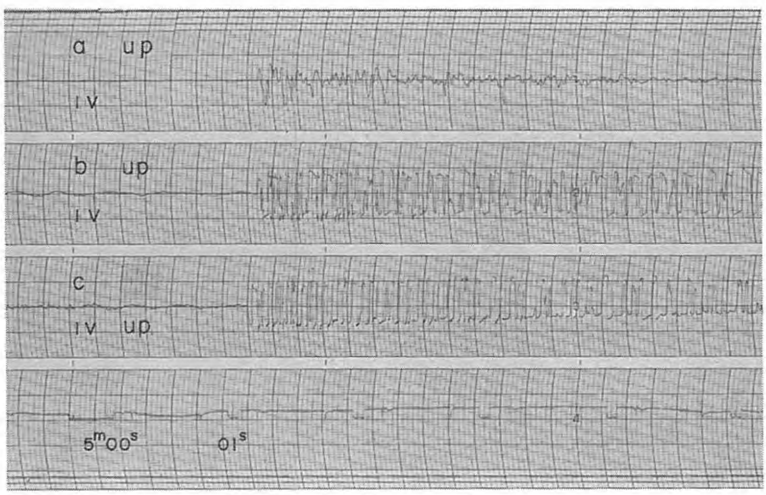

(39)

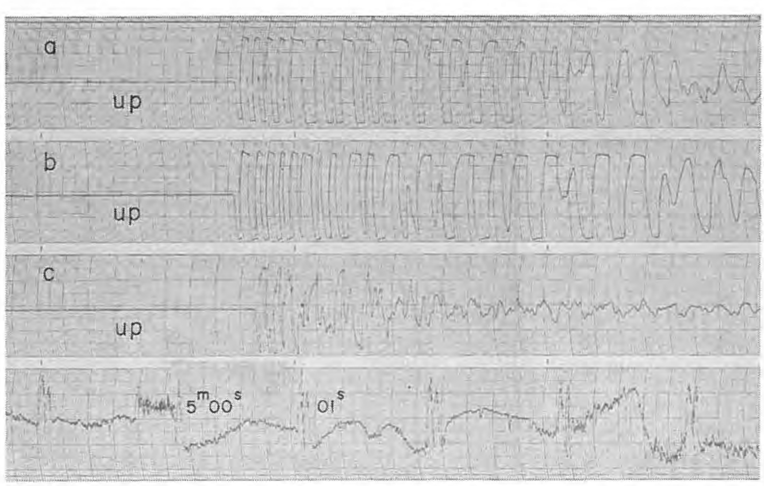

Fig. 5–13 Seismograms obtained (37) at D_5, (38) at D_6 and (39) at D_7 from the shot A–III

(40)

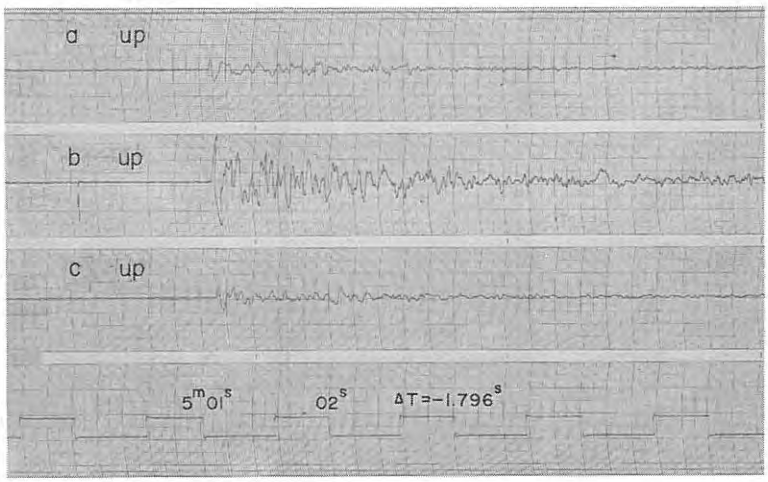

(41)

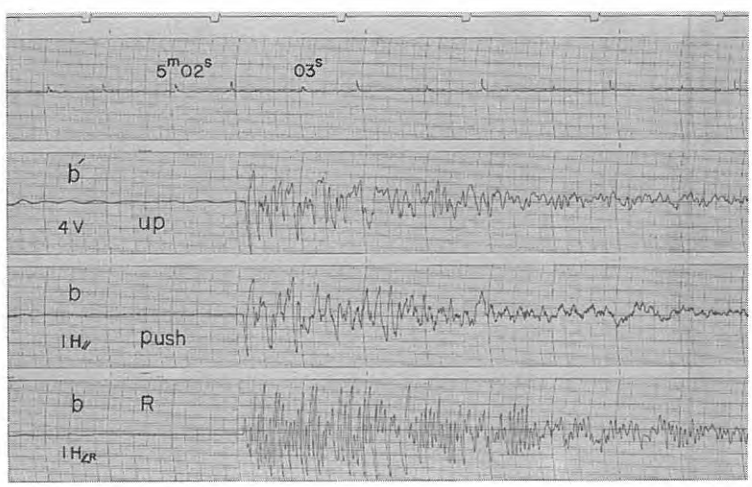

(42)

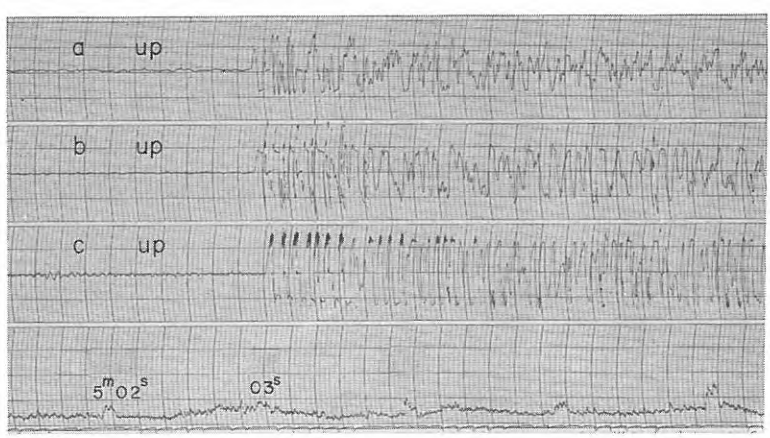

Fig. 5–14 Seismograms obtained (40) at D_8, (41) at D_8' and (42) at D_9 from the shot A–III

(43)

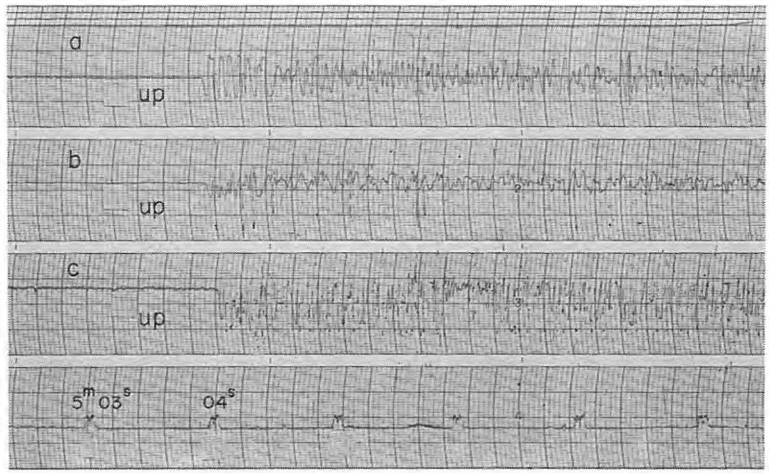

(44)

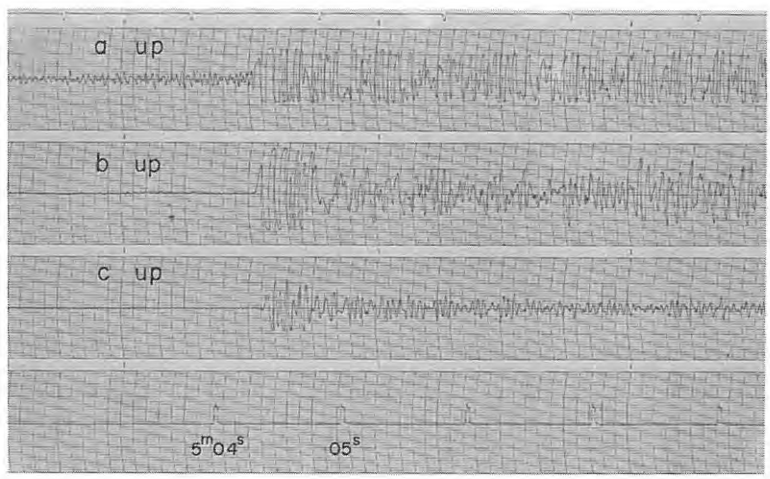

(45)

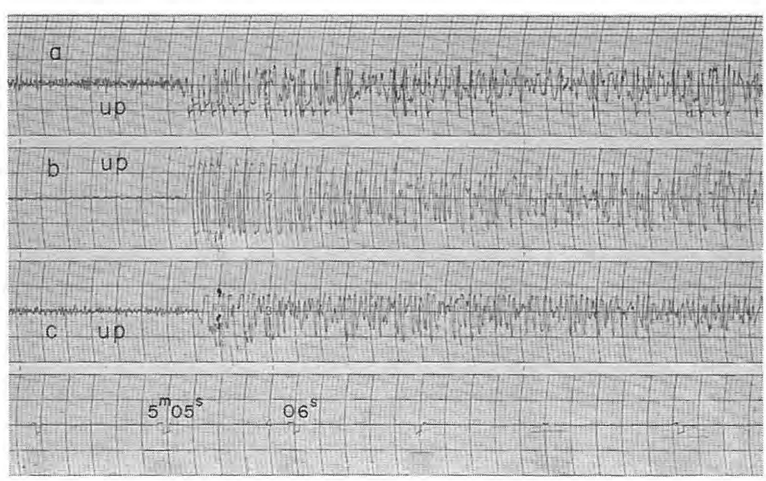

Fig. 5–15 Seismograms obtained (43) at D_{10}, (44) at D_{11} and (45) at D_{12} from the shot A–III

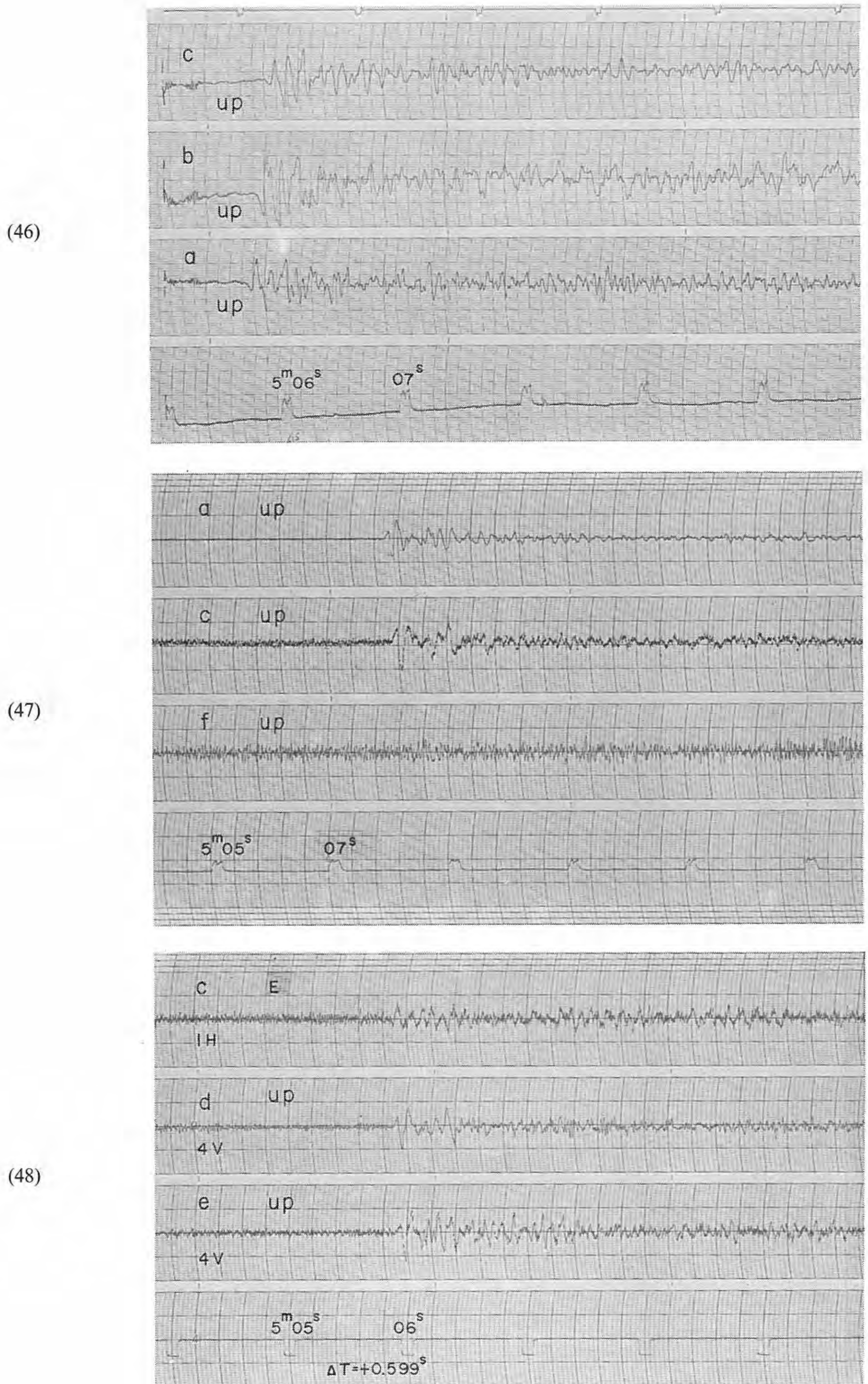

Fig. 5–16 Seismograms obtained (46) at D_{13}, (47), (48) at D_{14} from the shot A–III

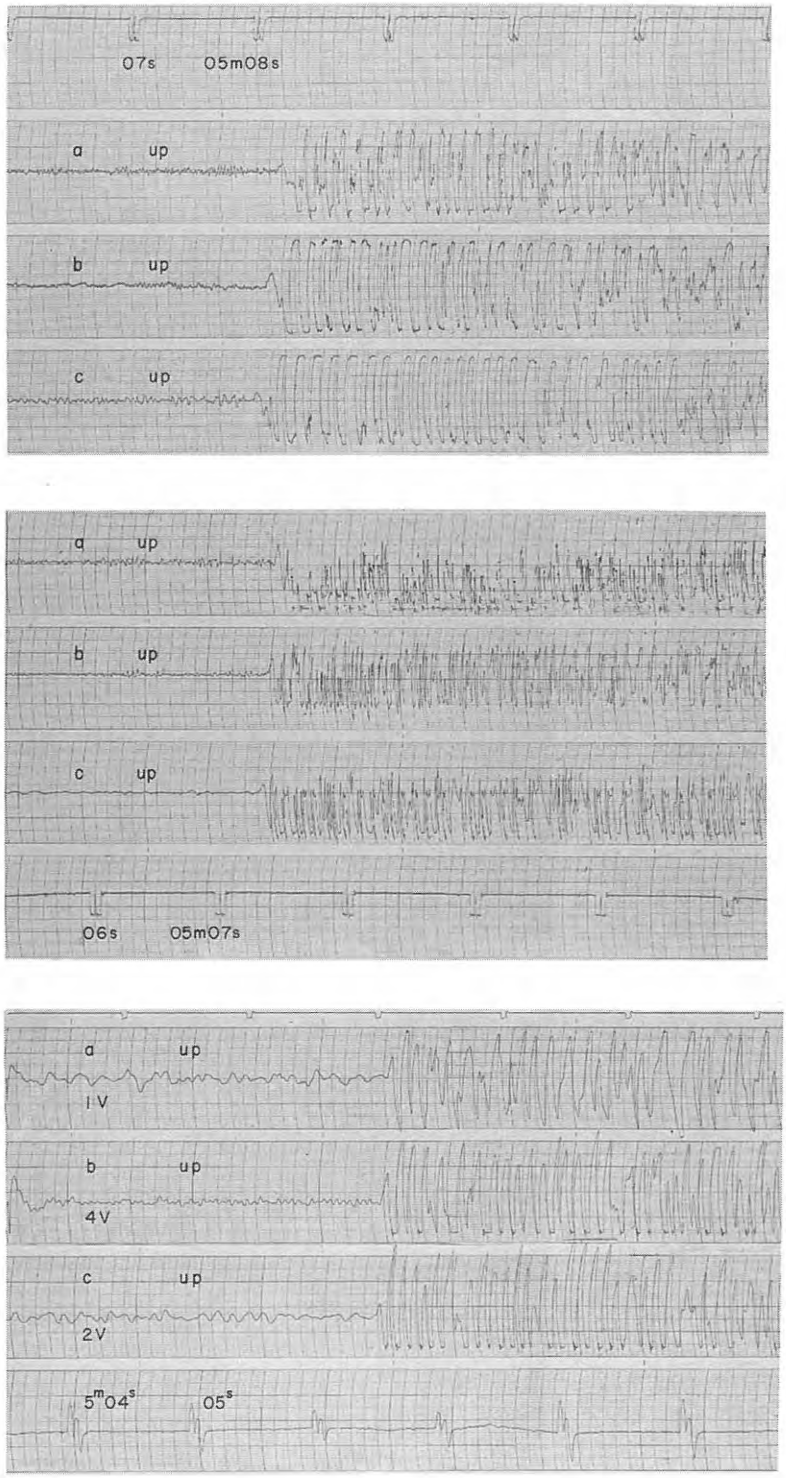

Fig. 5–17 Seismograms obtained (49) at D_1, (50) at D_2 and (51) at D_3 from the shot A–IV_1

(52)

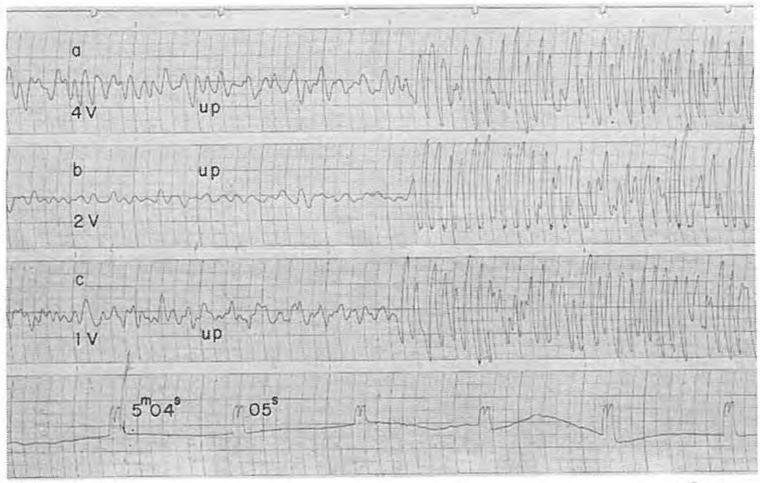

(53)

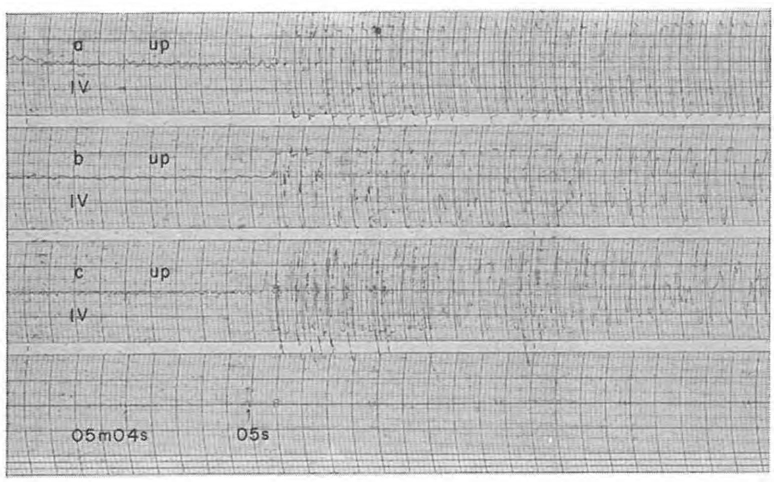

(54)

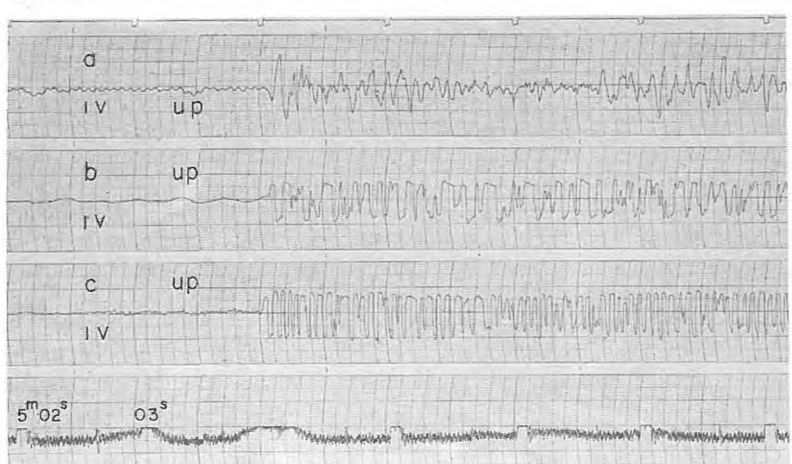

Fig. 5–18 Seismograms obtained (52) at D_4, (53) at D_5 and (54) at D_6 from the shot A–IV_1

(55)

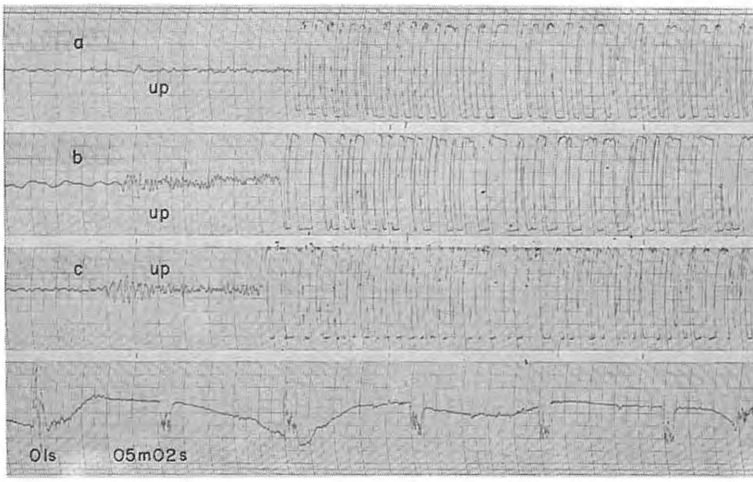

(56)

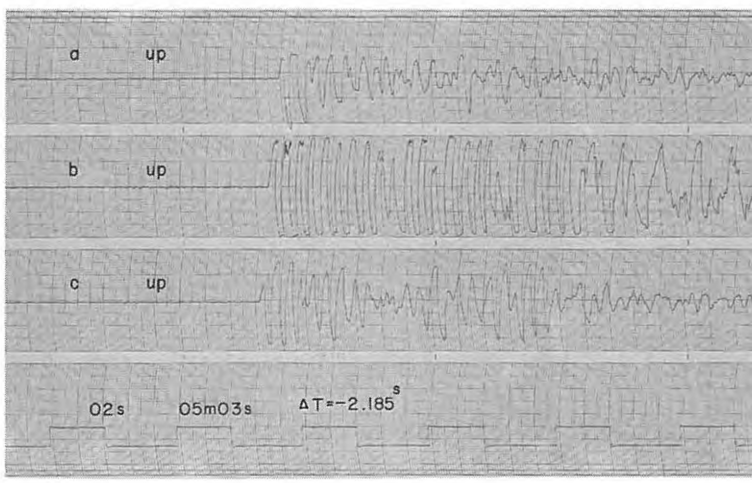

(57)

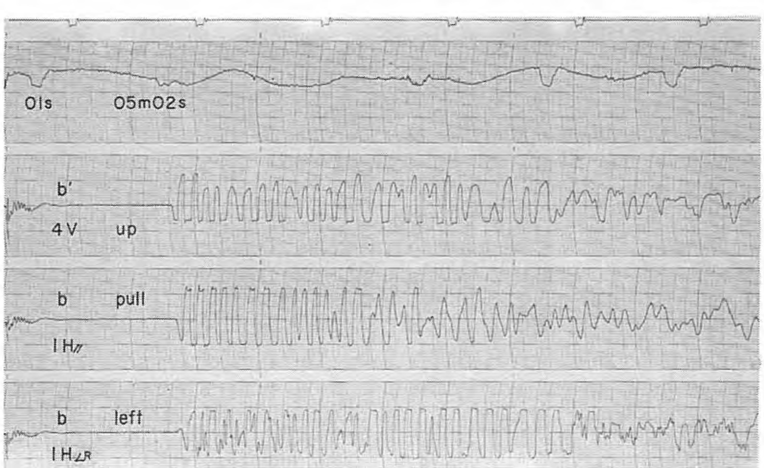

Fig. 5–19 Seismograms obtained (55) at D_7, (56) at D_8 and (57) at D_8' from the shot A–IV_1

(58)

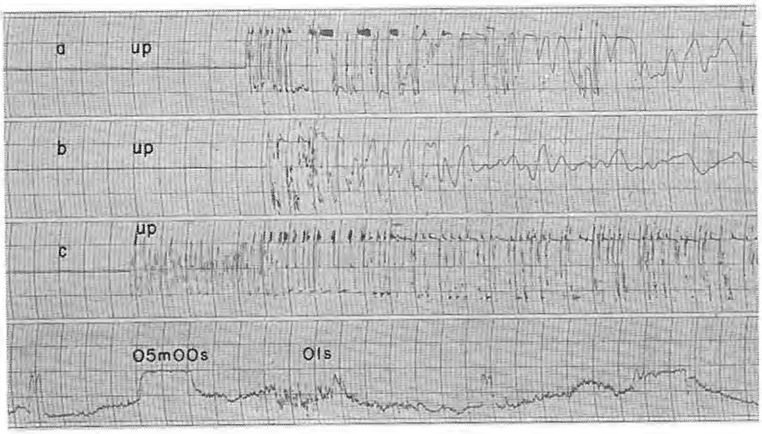

(59)

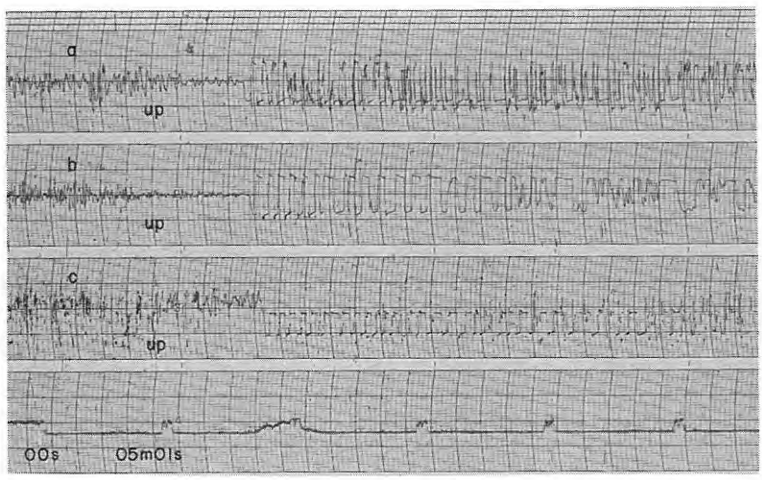

(60)

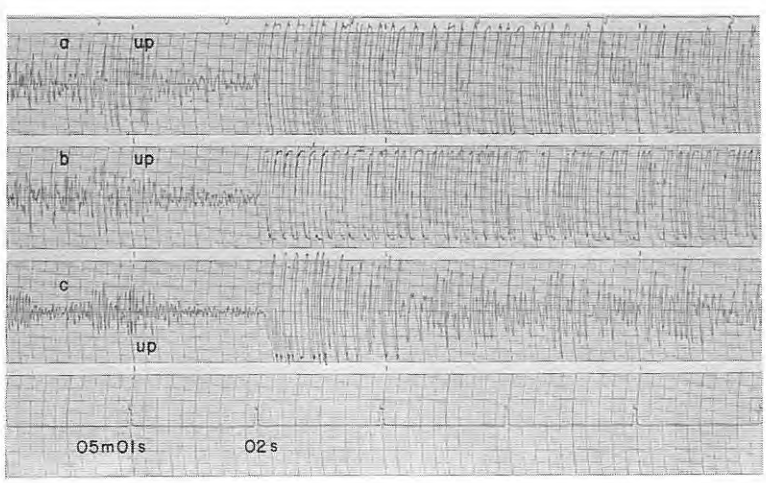

Fig. 5–20 Seismograms obtained (58) at D_9, (59) at D_{10} and (60) at D_{11} from the shot A–IV_1

(61)

(62)

(63)

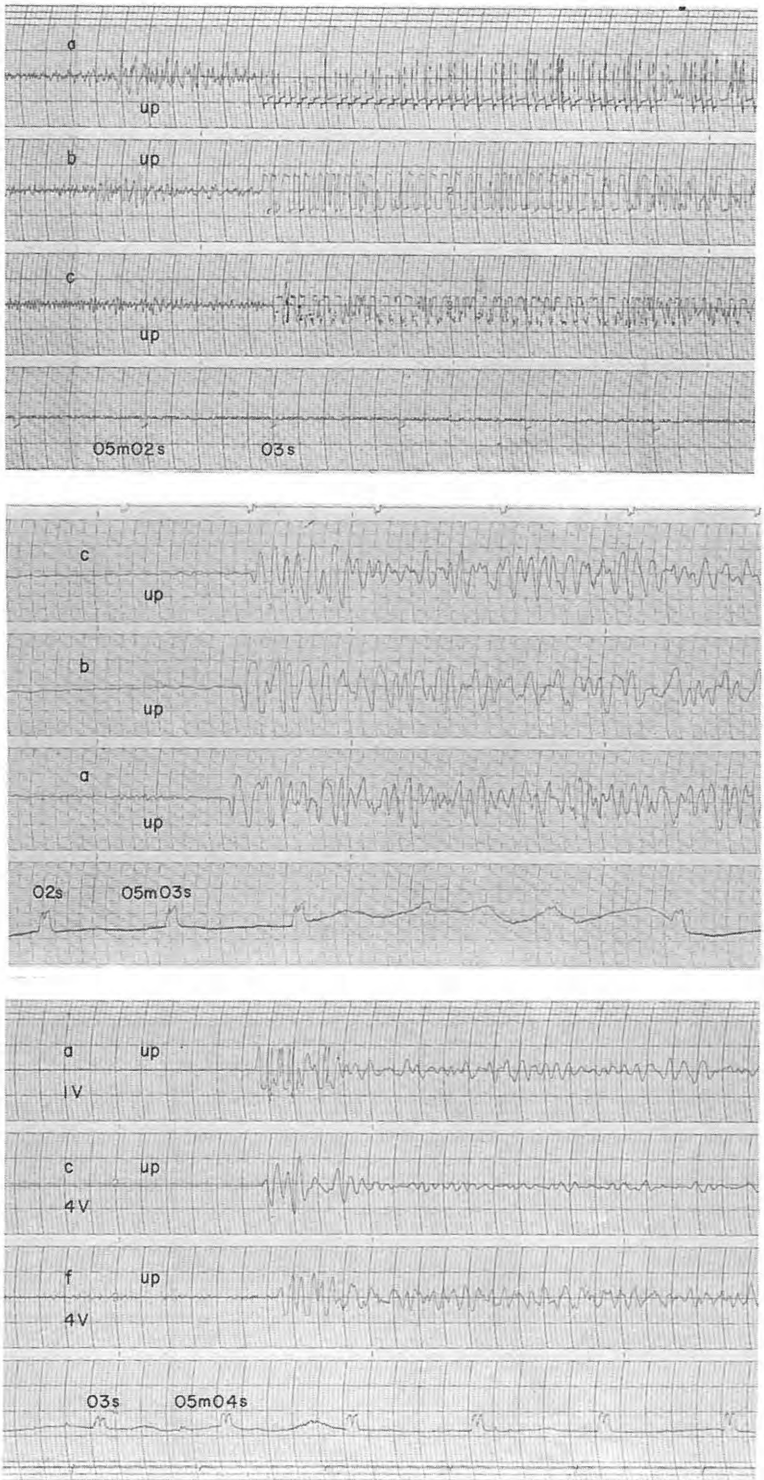

Fig. 5–21 Seismograms obtained (61) at D_{12}, (62) at D_{13} and (63) at D_{14} from the shot A–IV_1

(64)

(65)

(66)

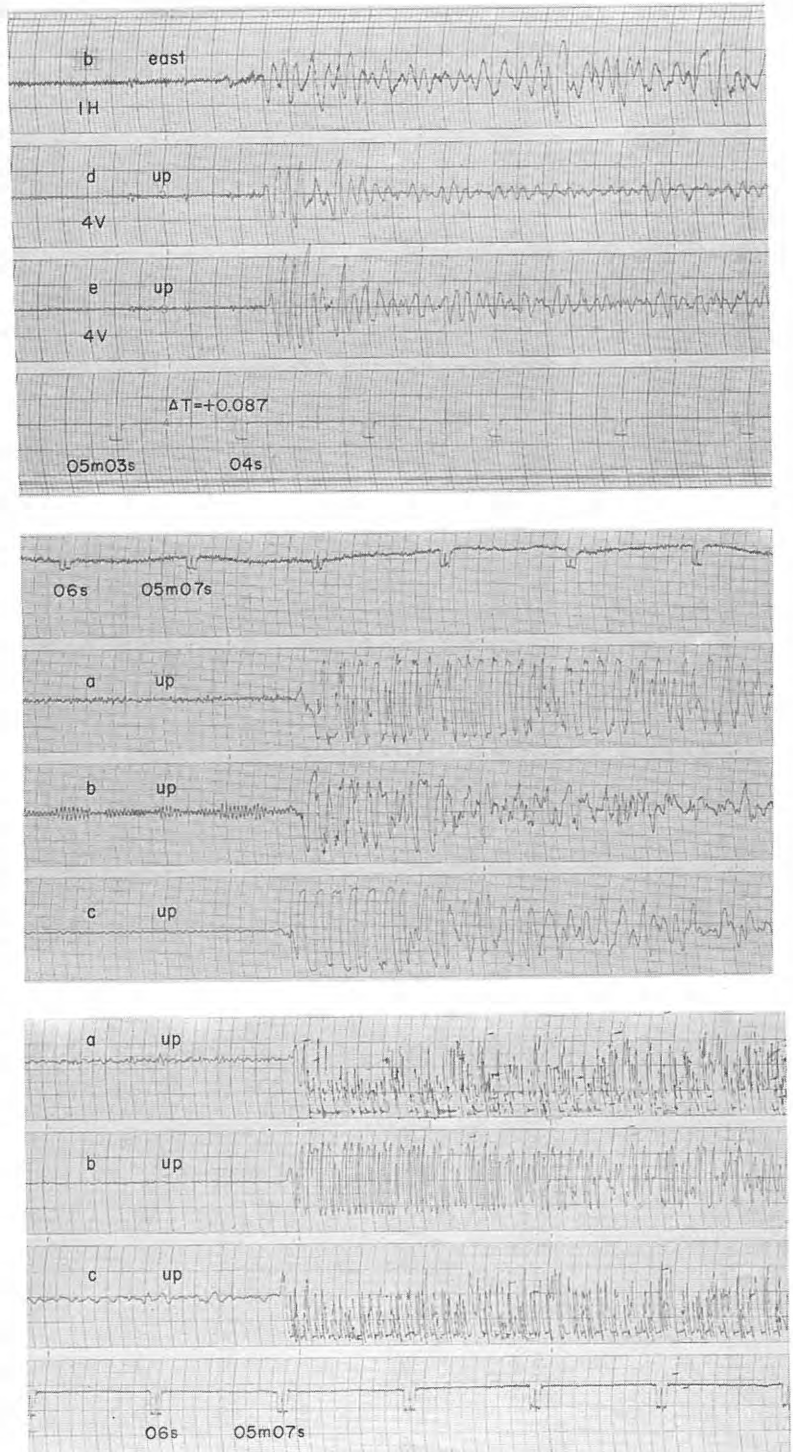

Fig. 5–22 Seismograms obtained (64) at D_{14} from the shot A–IV_1, and (65) at D_1 and (66) at D_2 from the shot A–IV_2

(67)

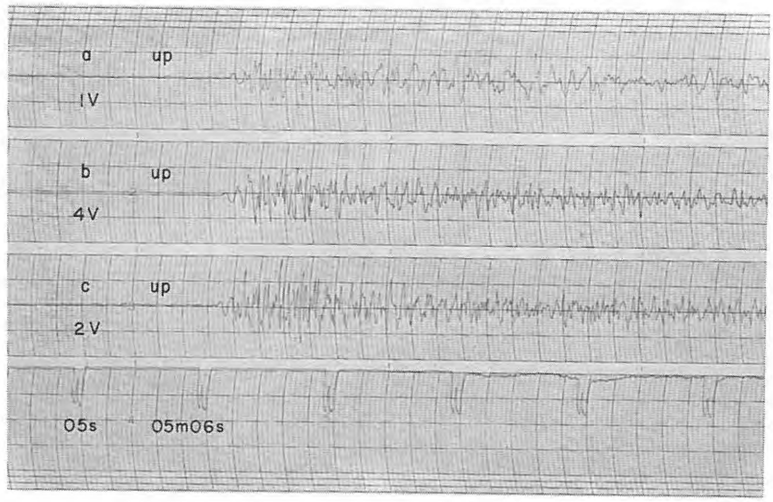

(68)

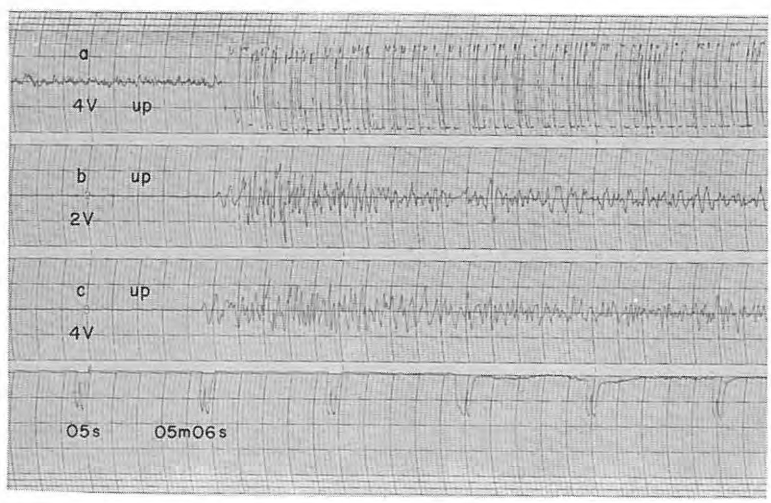

(69)

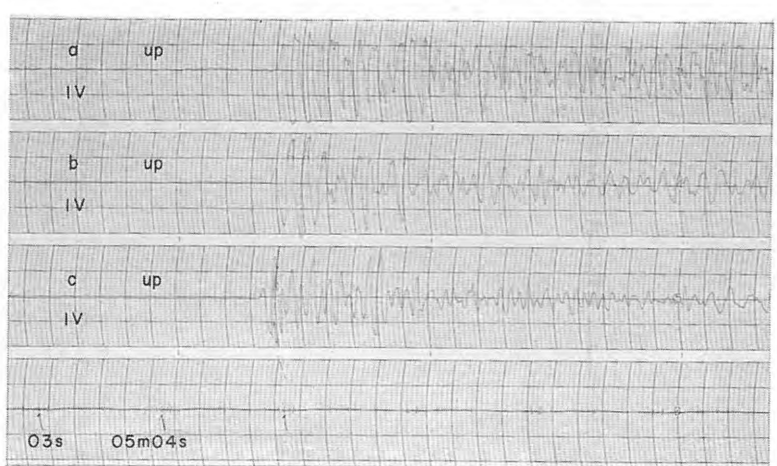

Fig. 5–23 Seismograms obtained (67) at D_3, (68) at D_4 and (69) at D_5 from the shot A–IV_2

(70)

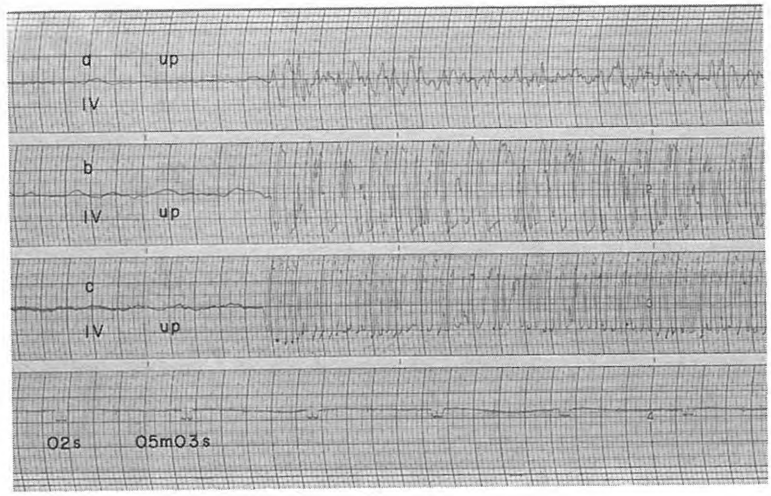

(71)

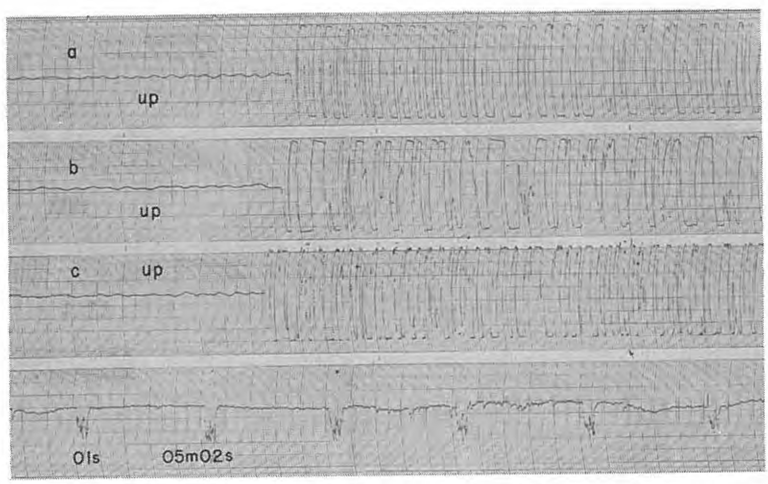

(72)

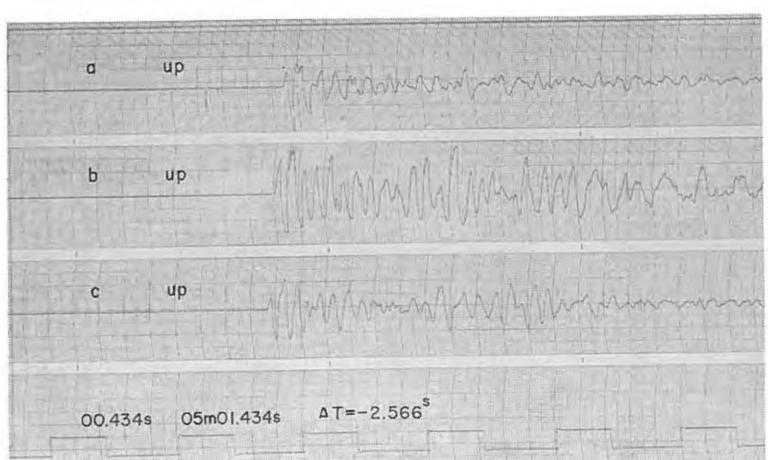

Fig. 5–24 Seismograms obtained (70) at D_6, (71) at D_7 and (72) at D_8 from the shot A–IV_2

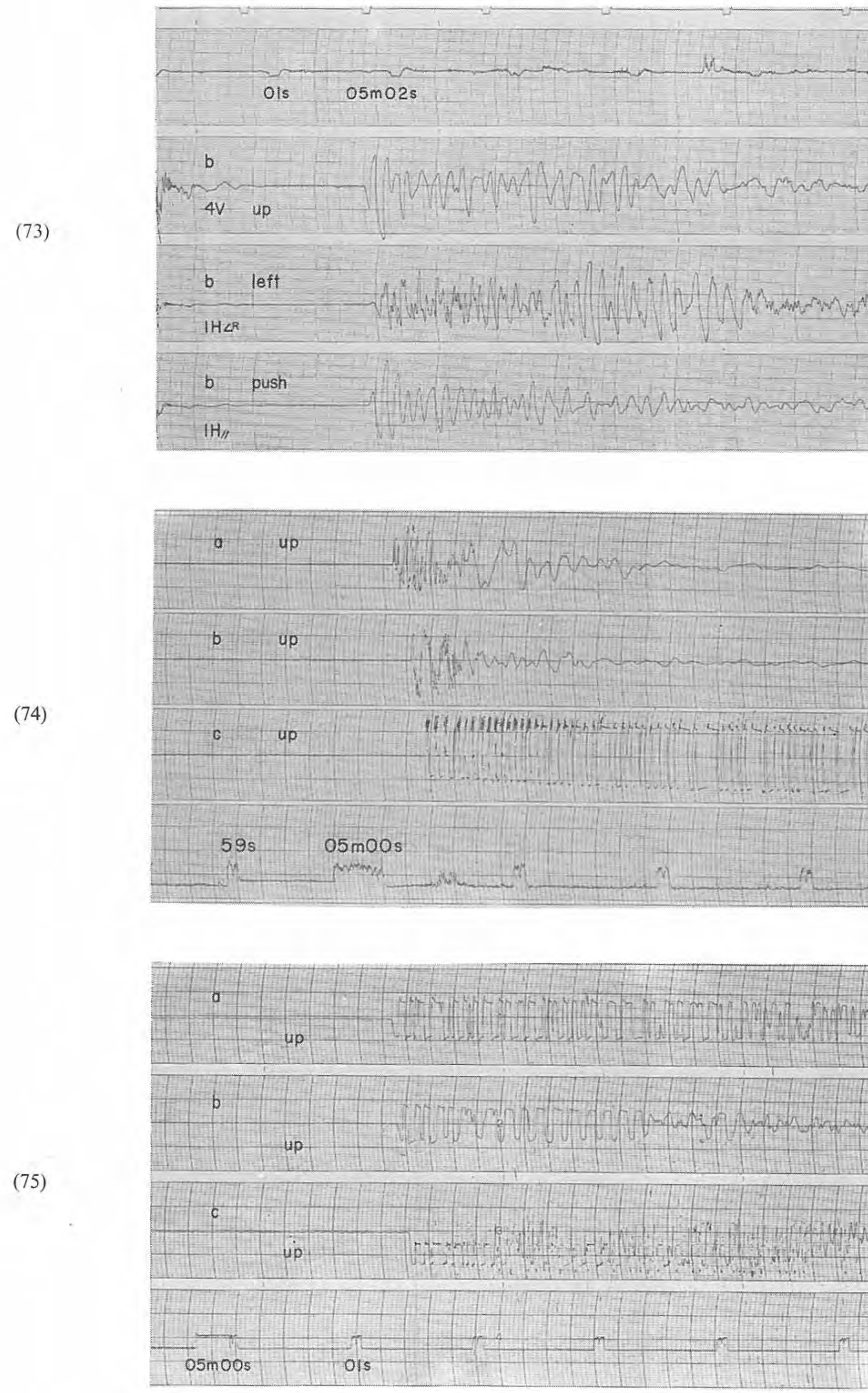

Fig. 5–25 Seismograms obtained (73) at D_8', (74) at D_9 and (75) at D_{10} from the shot A–IV_2

(76)

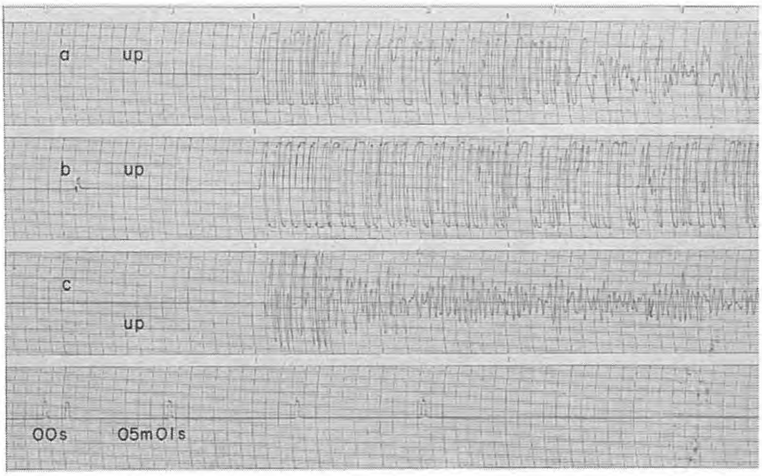

(77)

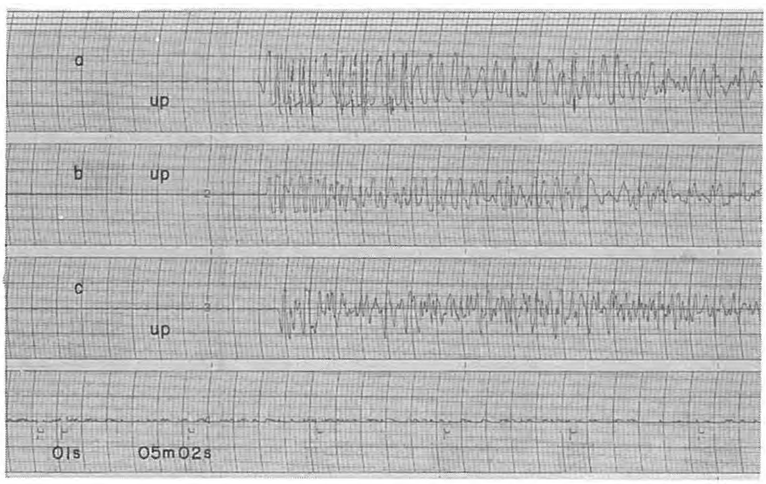

(78)

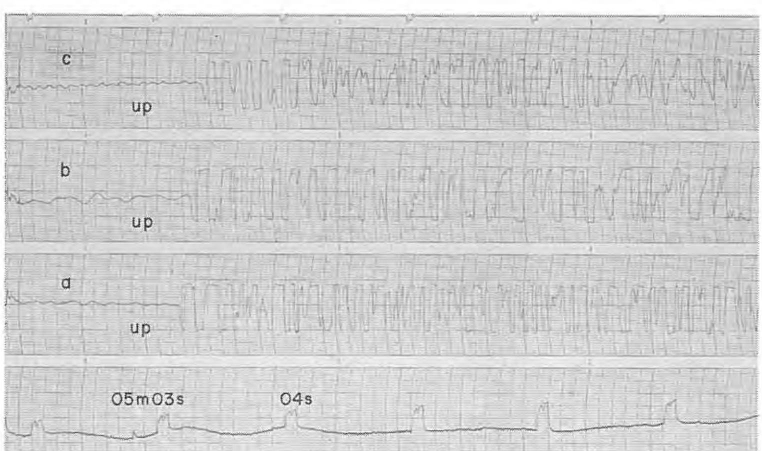

Fig. 5–26 Seismograms obtained (76) at D_{11}, (77) at D_{12} and (78) at D_{13} from the shot A–IV_2

(79)

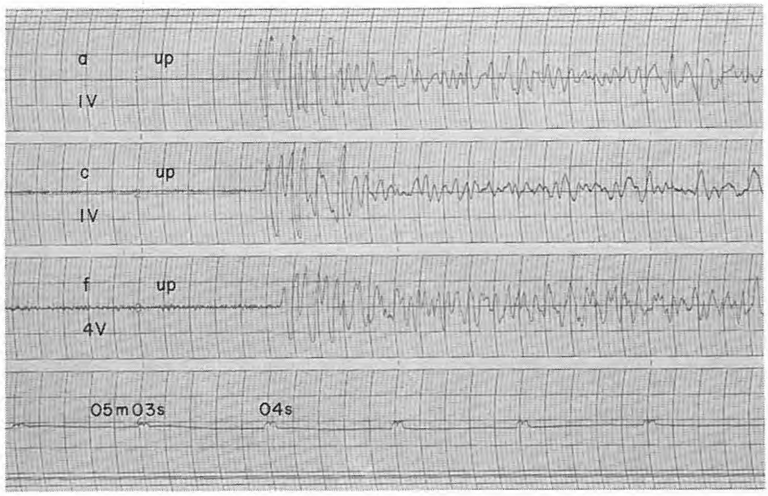

(80)

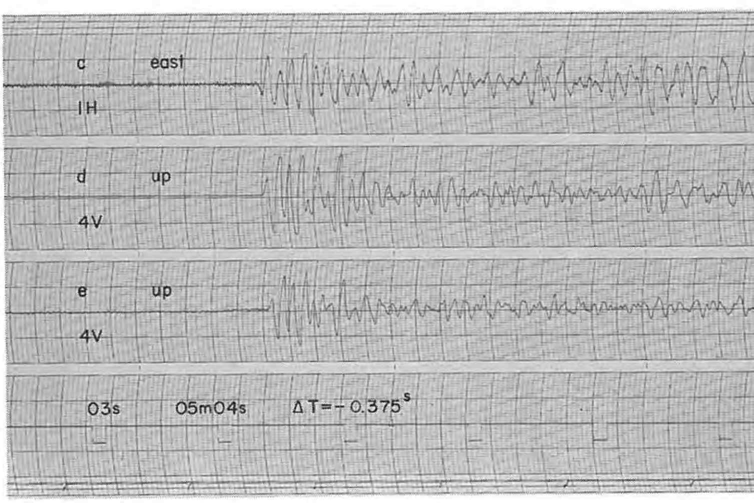

(81)

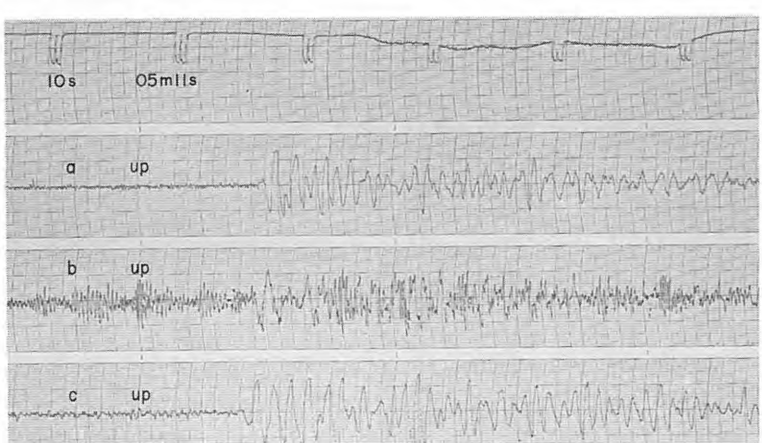

Fig. 5–27 Seismograms obtained (79), (80) at D_{14} from the shot A–IV_2, and (81) at D_1 from the shot A–V_1

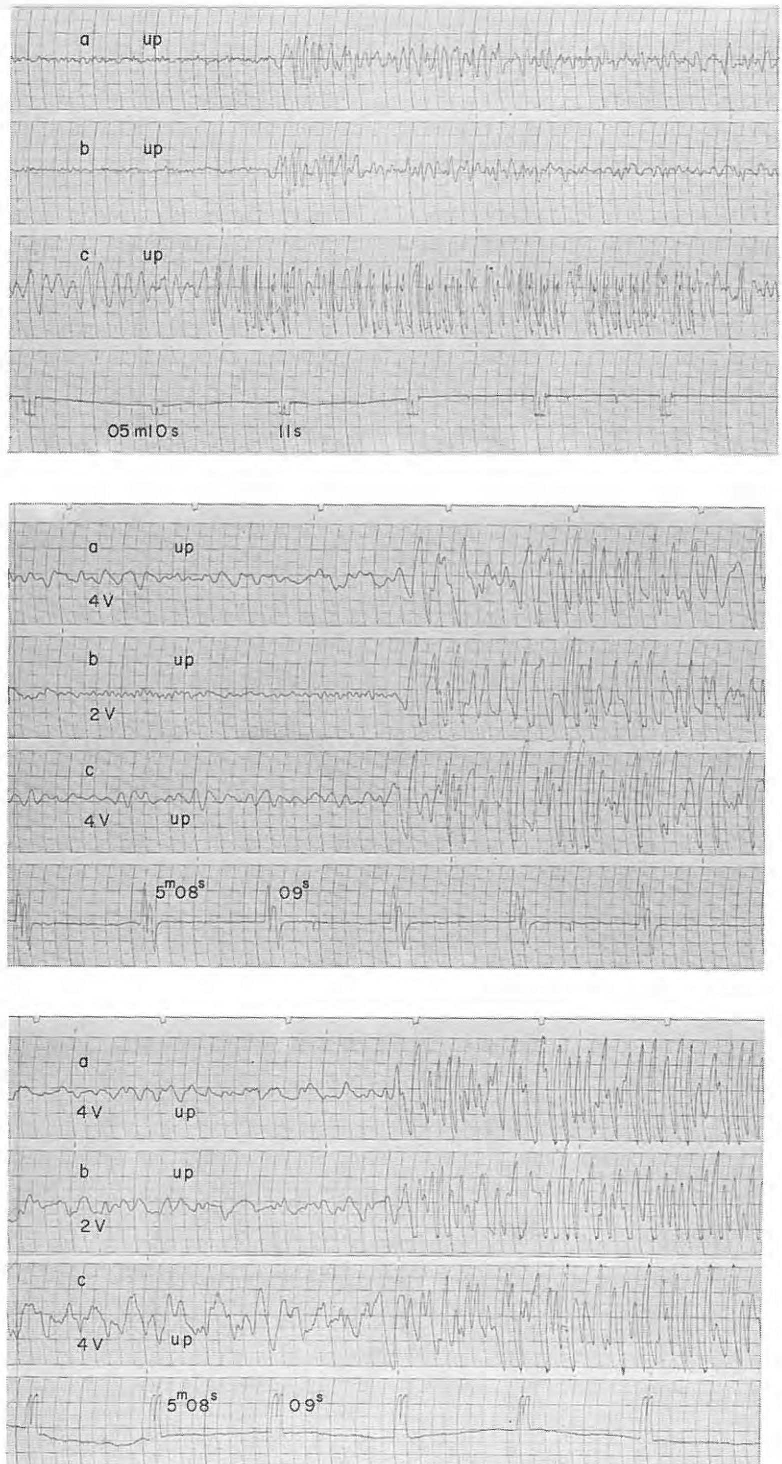

Fig. 5–28 Seismograms obtained (82) at D_2, (83) at D_3 and (84) at D_4 from the shot A–V_1

(85)

(86)

(87)

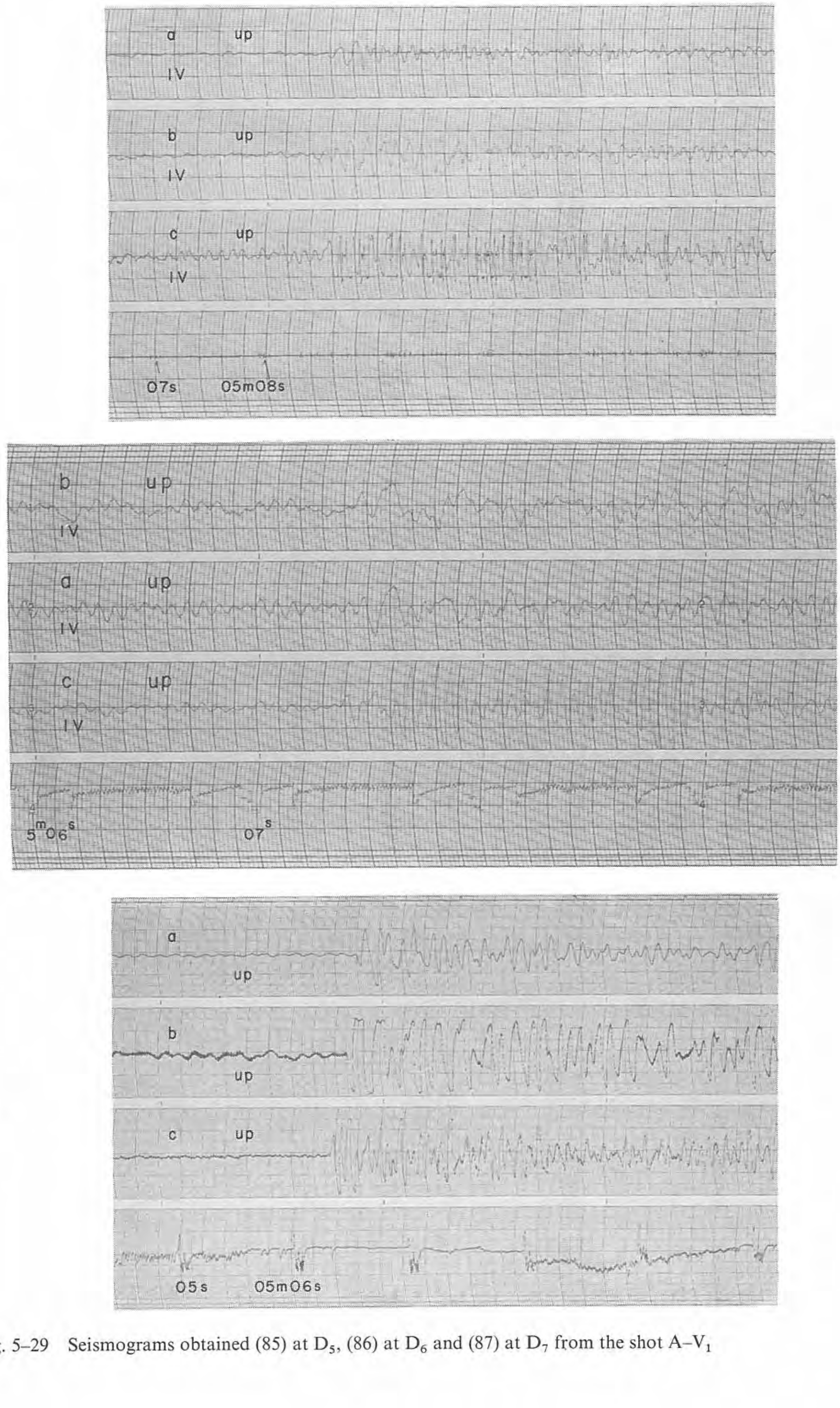

Fig. 5–29 Seismograms obtained (85) at D_5, (86) at D_6 and (87) at D_7 from the shot $A–V_1$

(88)

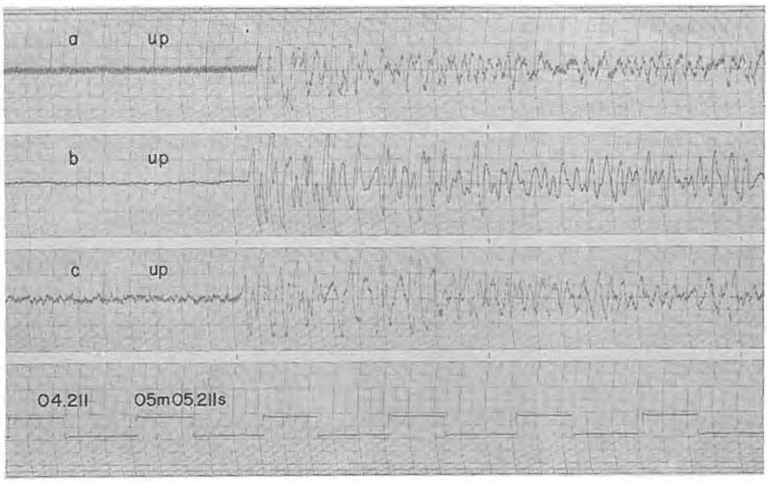

(89)

(90)

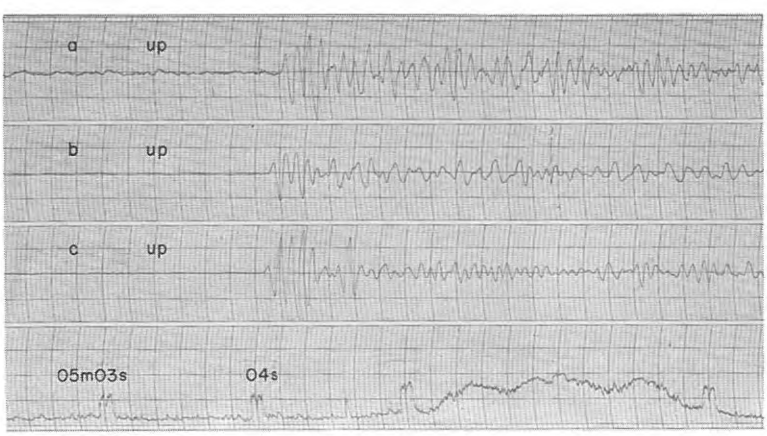

Fig. 5–30 Seismograms obtained (88) at D_8, (89) at D_8' and (90) at D_9 from the shot A–V_1

(91)

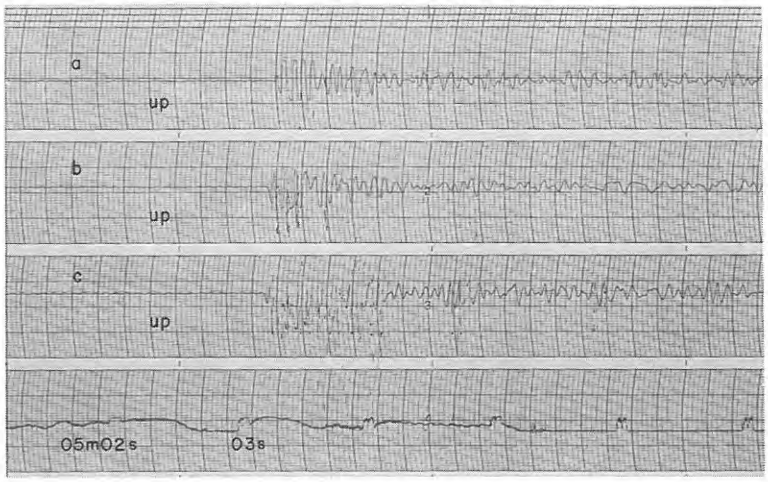

(92)

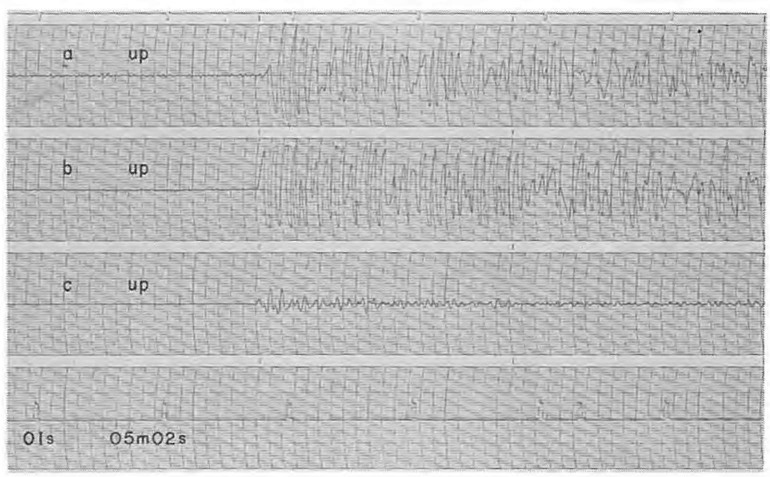

(93)

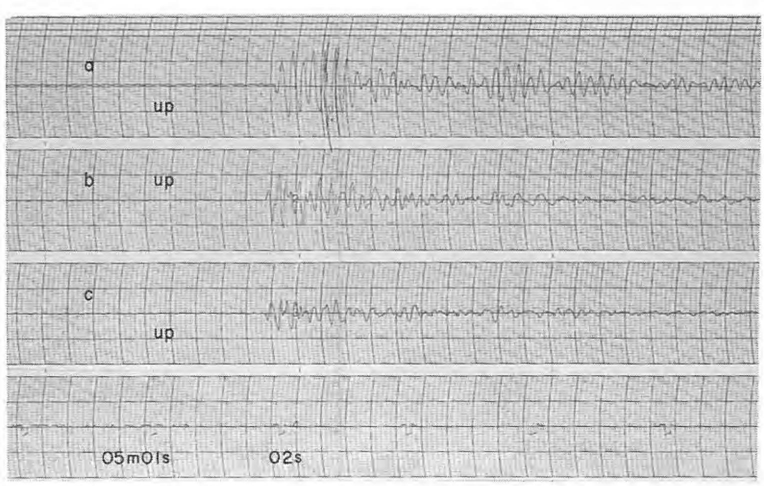

Fig. 5–31 Seismograms obtained (91) at D_{10}, (92) at D_{11} and (93) at D_{12} from the shot A–V_1

(94)

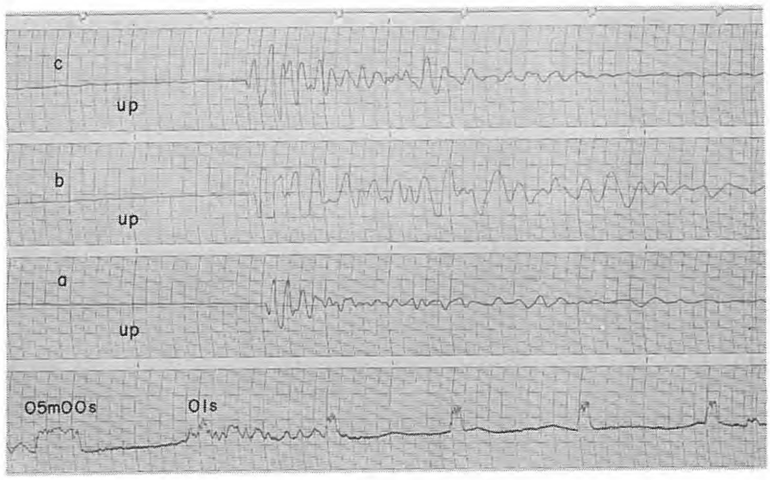

(95)

(96)

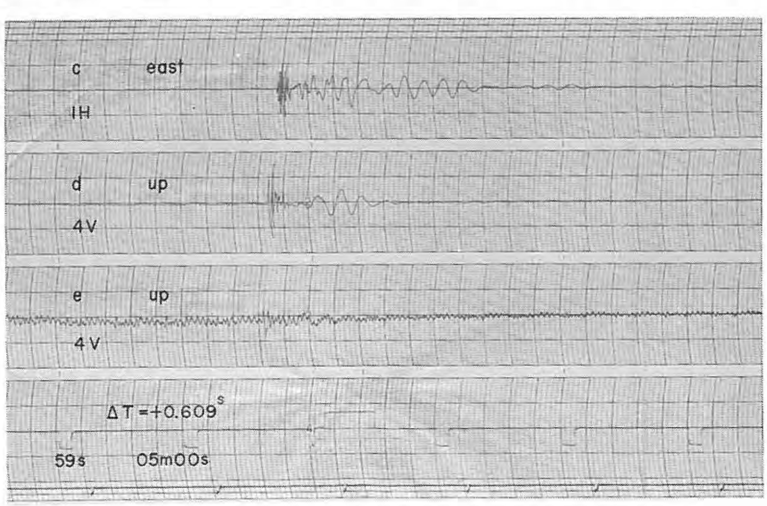

Fig. 5–32 Seismograms obtained (94) at D_{13}, (95), (96) at D_{14} from the shot A–V_1

(97)

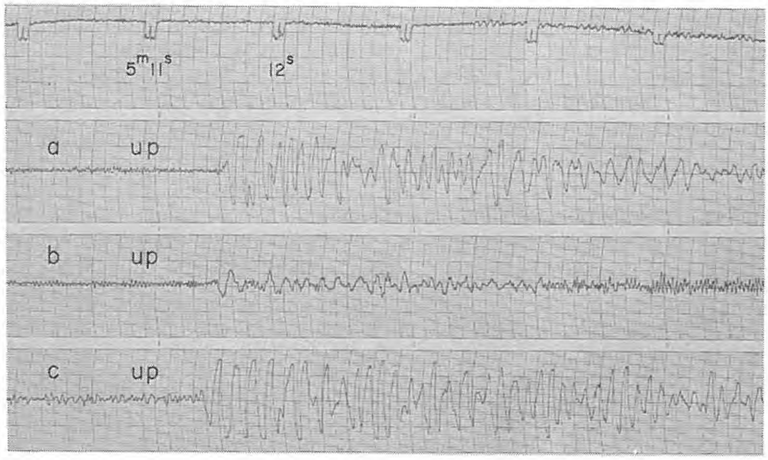

(98)

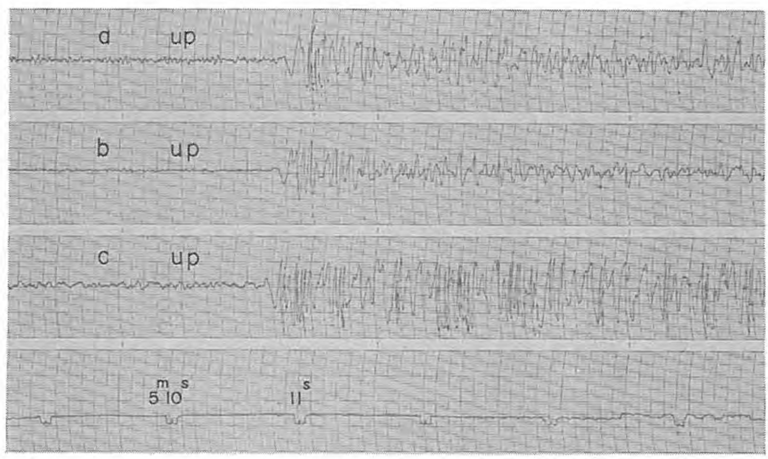

(99)

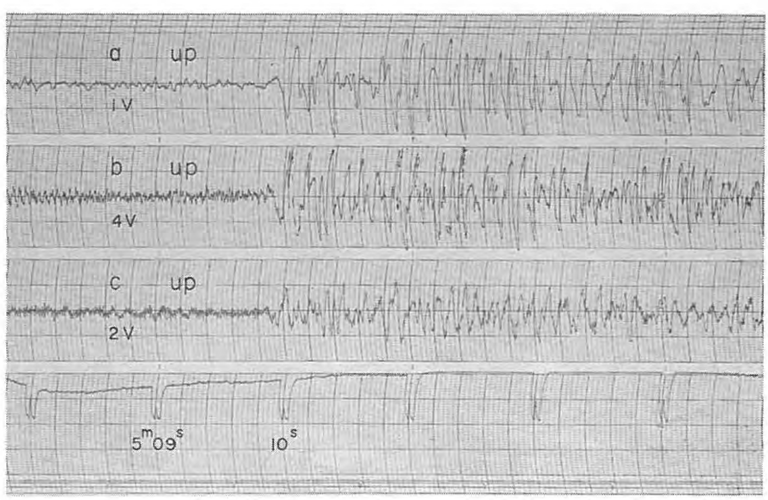

Fig. 5–33 Seismograms obtained (97) at D_1, (98) at D_2 and (99) at D_3 from the shot A–V_2

(100)

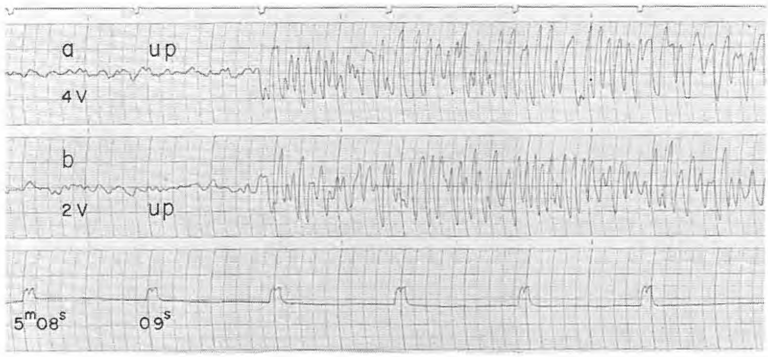

(101)

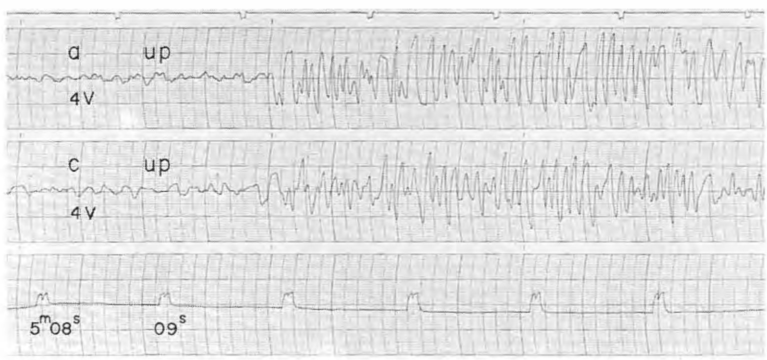

(102)

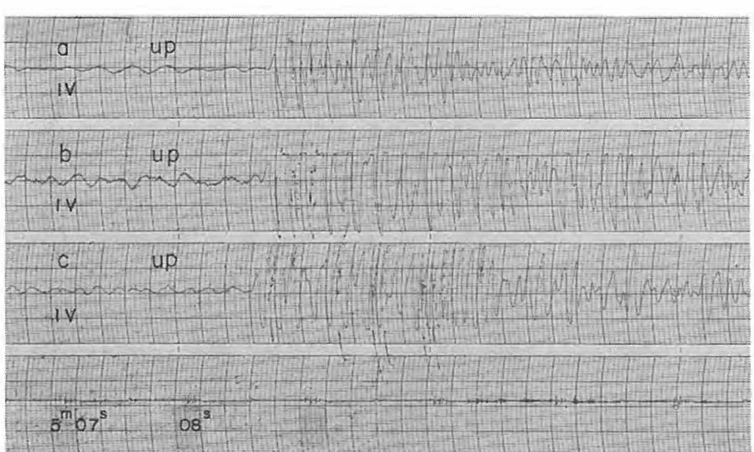

Fig. 5–34 Seismograms obtained (100), (101) at D_4 and (102) at D_5 from the shot A–V_2

(103)

(104)

(105)

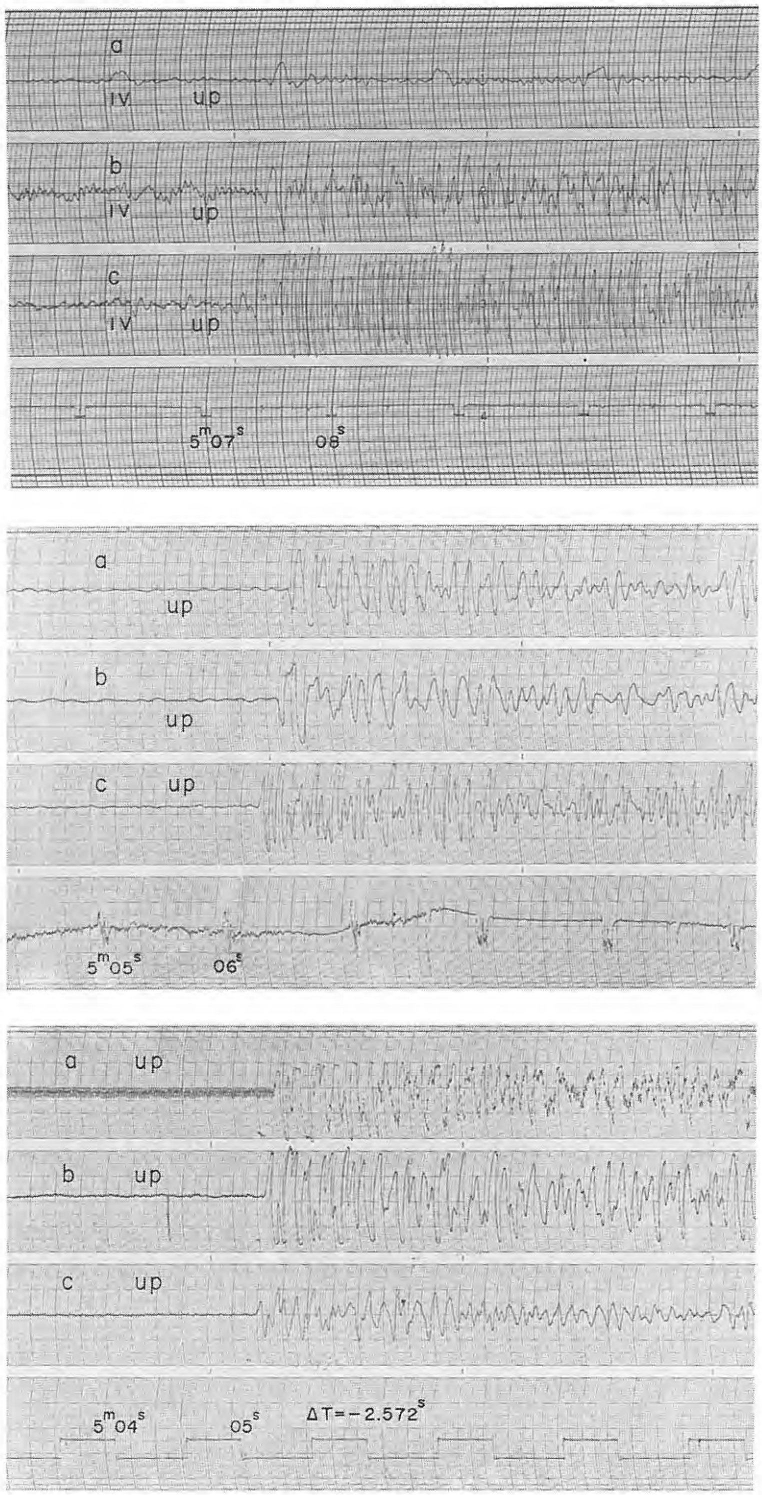

Fig. 5–35 Seismograms obtained (103) at D_6, (104) at D_7 and (105) at D_8 from the shot A–V_2

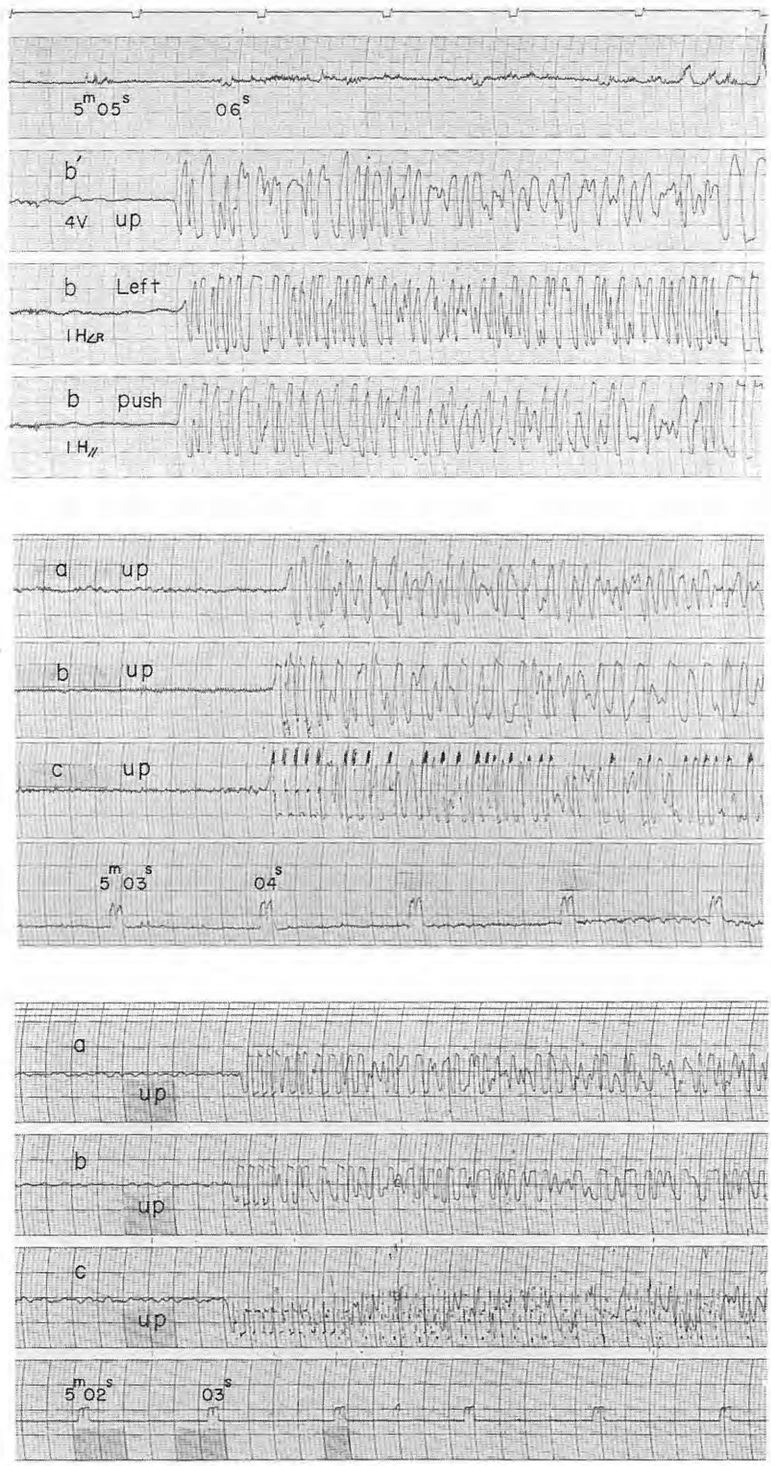

(106)

(107)

(108)

Fig. 5–36 Seismograms obtained (106) at D_8', (107) at D_9 and (108) at D_{10} from the shot A–V_2

(109)

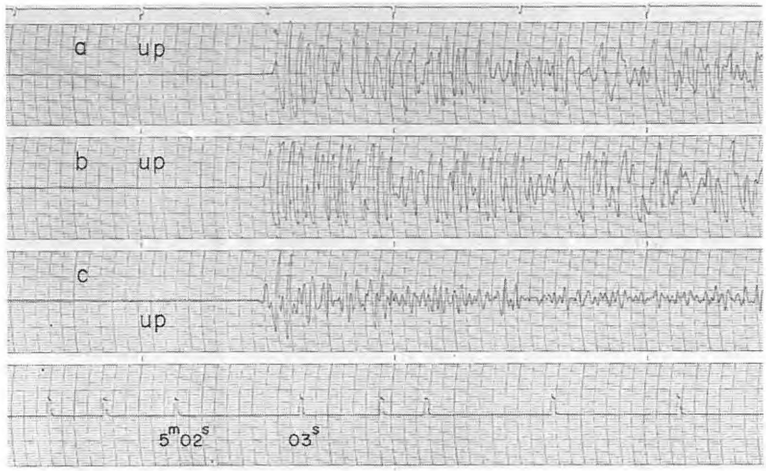

(110)

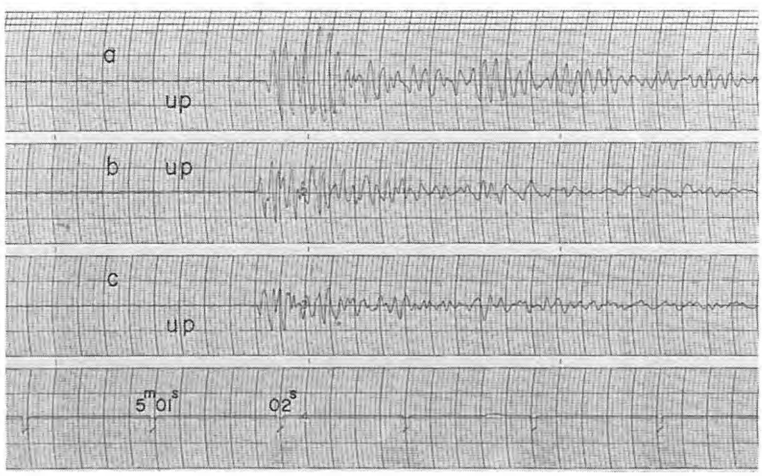

(111)

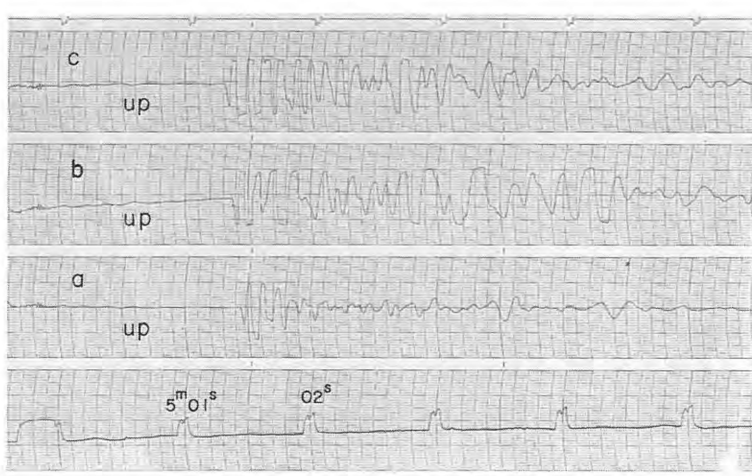

Fig. 5–37 Seismograms obtained (109) at D_{11}, (110) at D_{12} and (111) at D_{13} from the shot A–V_2

(112)

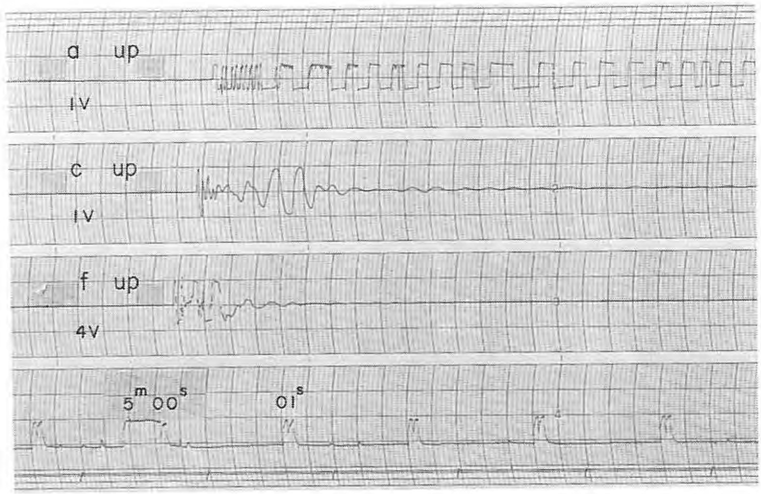

(113)

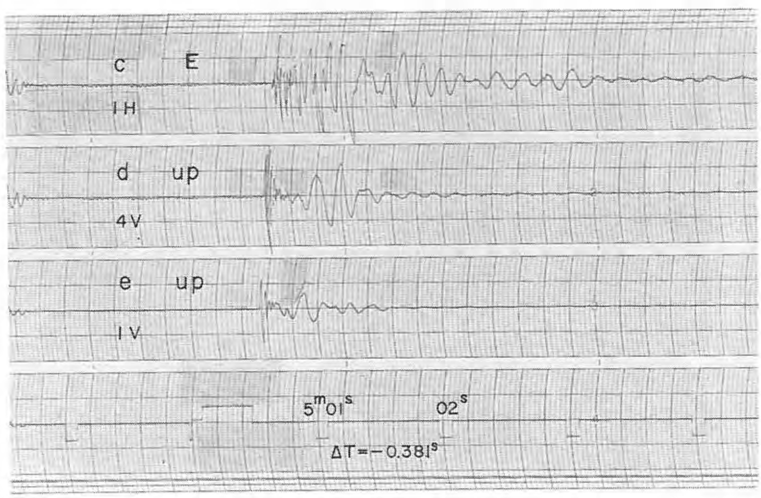

(114)

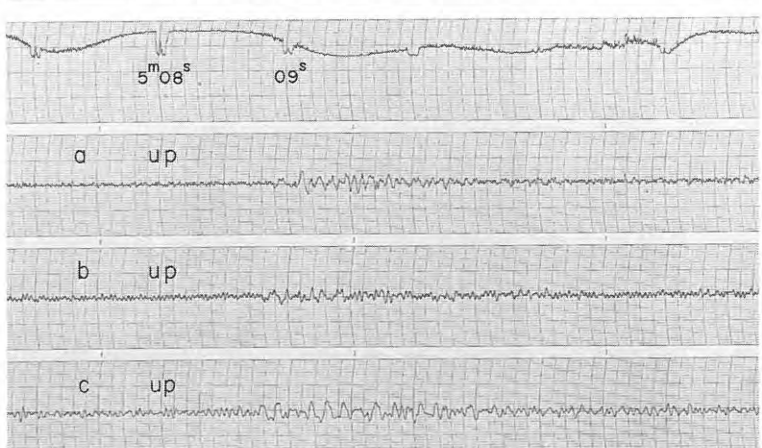

Fig. 5–38 Seismograms obtained (112), (113) at D_{14} from the shot A–V_2, and (114) at D_1 of profile A from the shot B–IV

(115)

(116)

(117)

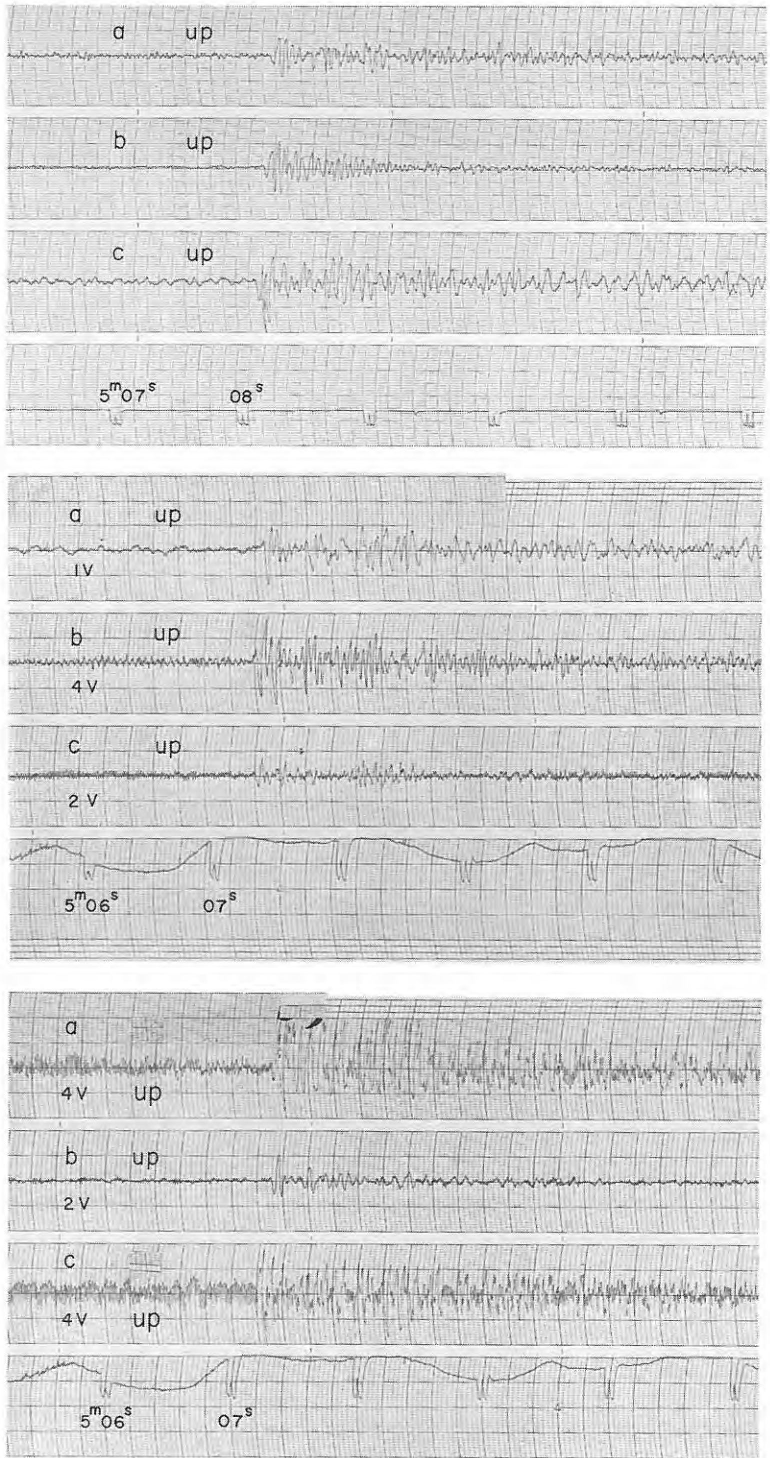

Fig. 5–39 Seismograms obtained (115) at D_2, (116) at D_3 and (117) at D_4 of profile A from the shot B–IV

(118)

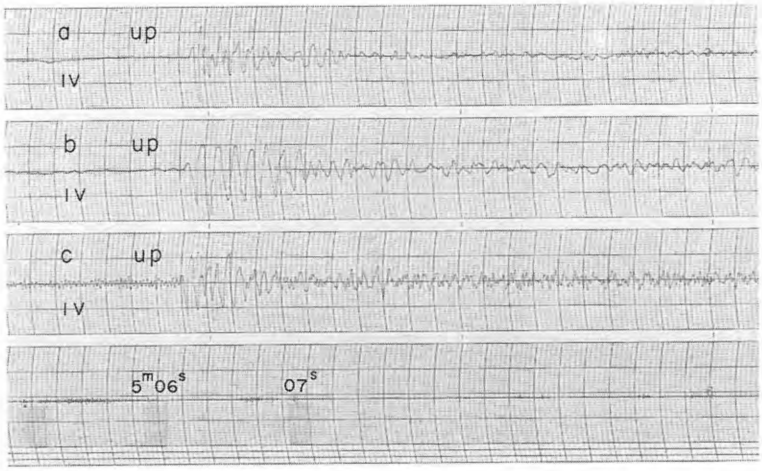

(119)

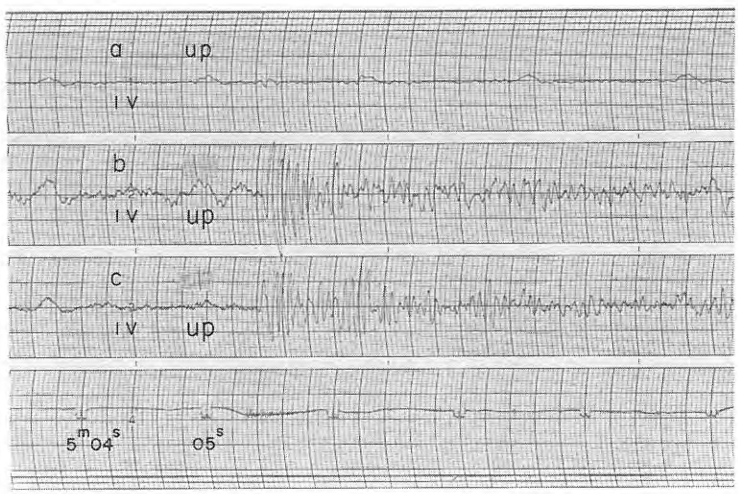

(120)

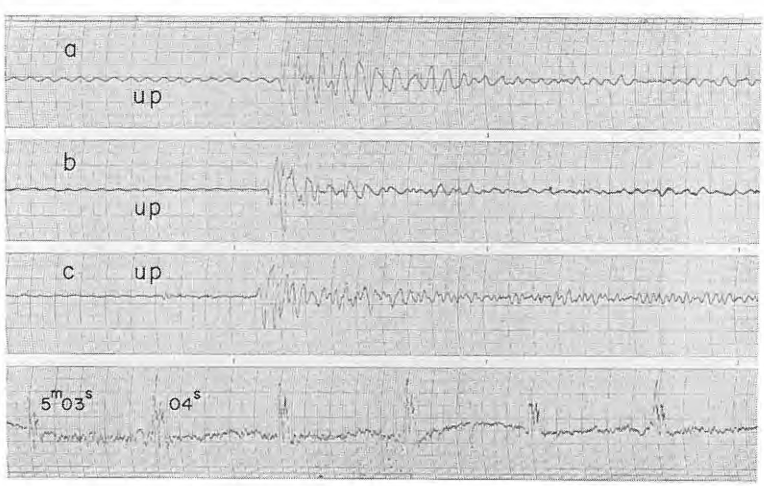

Fig. 5–40 Seismograms obtained (118) at D_5, (119) at D_6 and (120) at D_7 of profile A from the shot B–IV

(121)

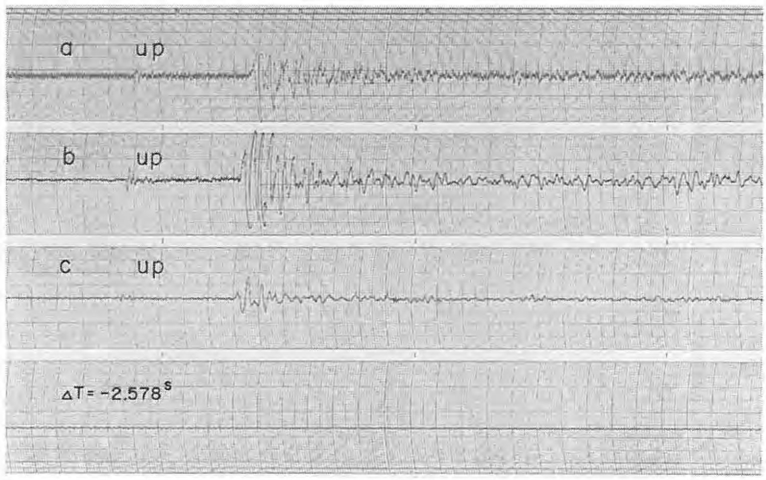

(122)

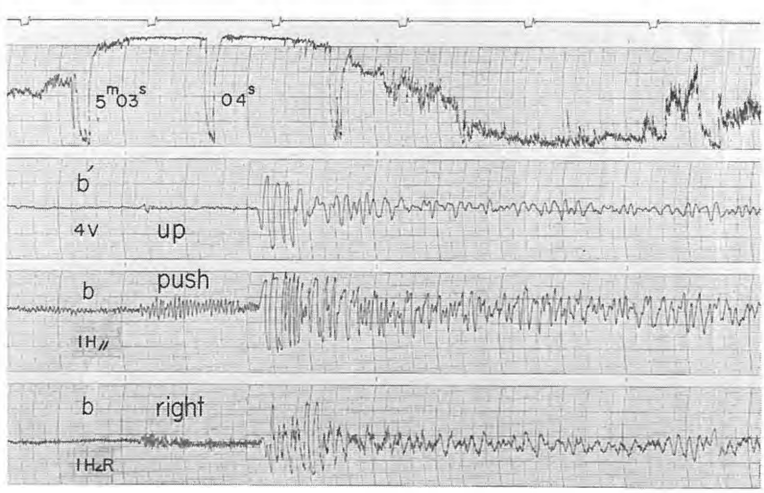

(123)

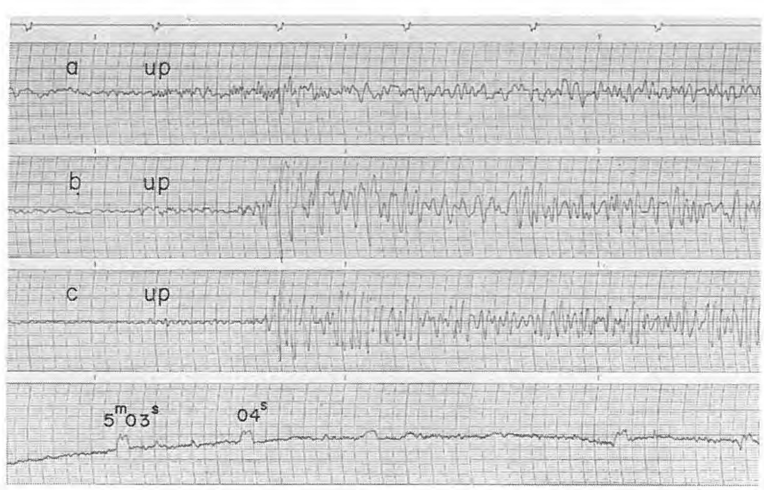

Fig. 5–41 Seismograms obtained (121) at D_8, (122) at D_8' and (123) at D_9 of profile A from the shot B–IV

(124)

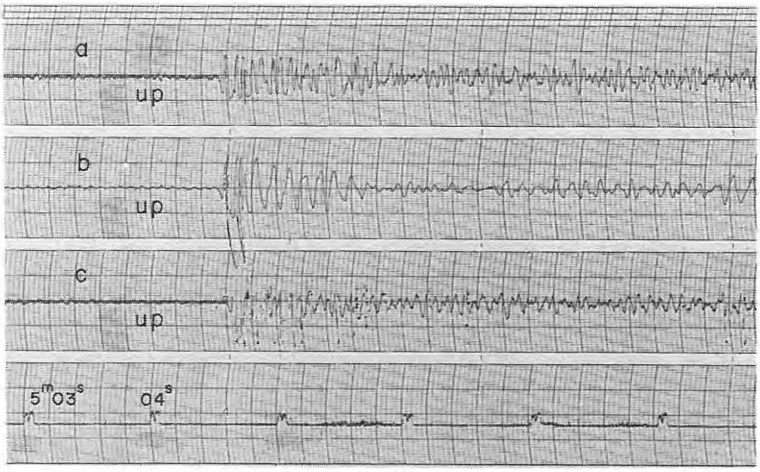

(125)

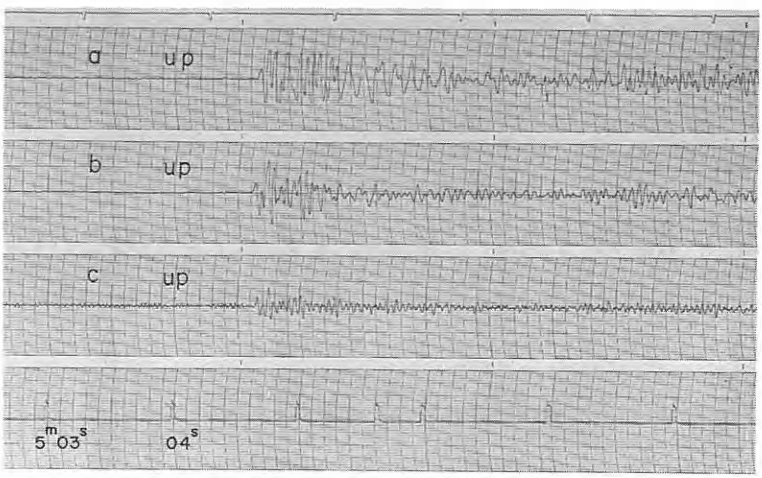

(126)

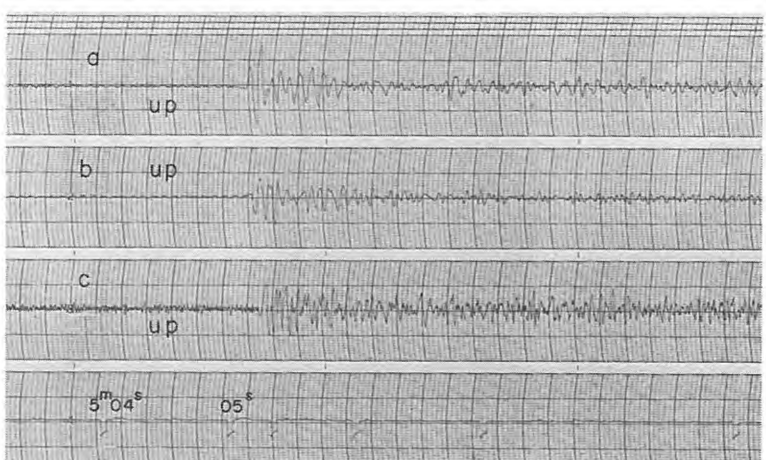

Fig. 5–42 Seismograms obtained (124) at D_{10}, (125) at D_{11} and (126) at D_{12} of profile A from the shot B–IV

(127)

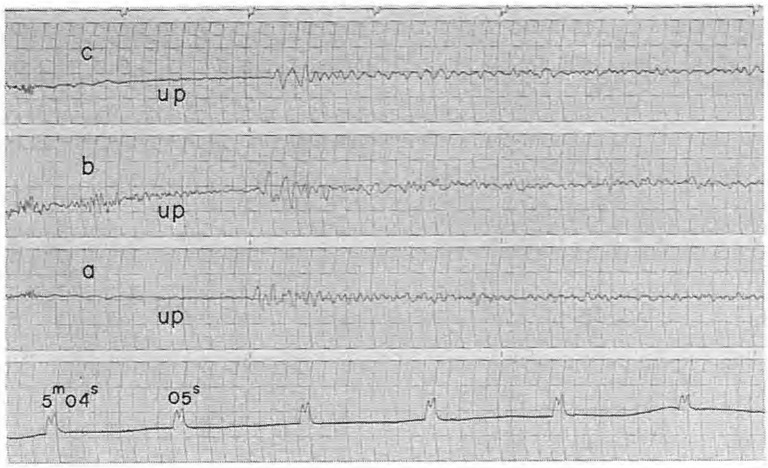

(128)

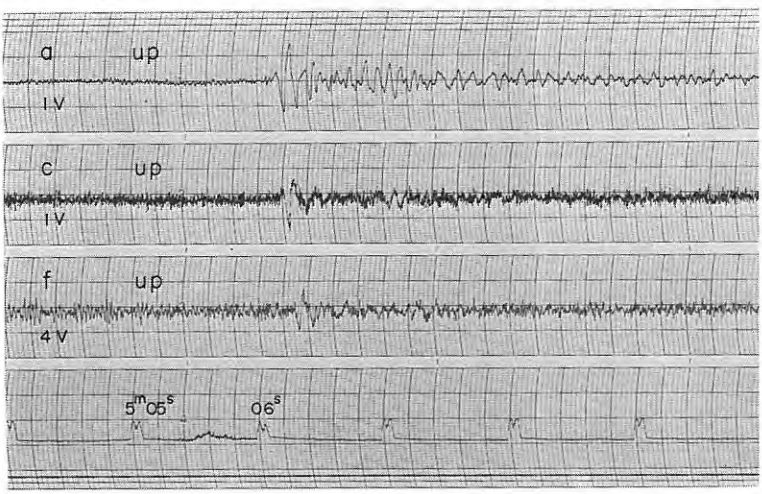

(129)

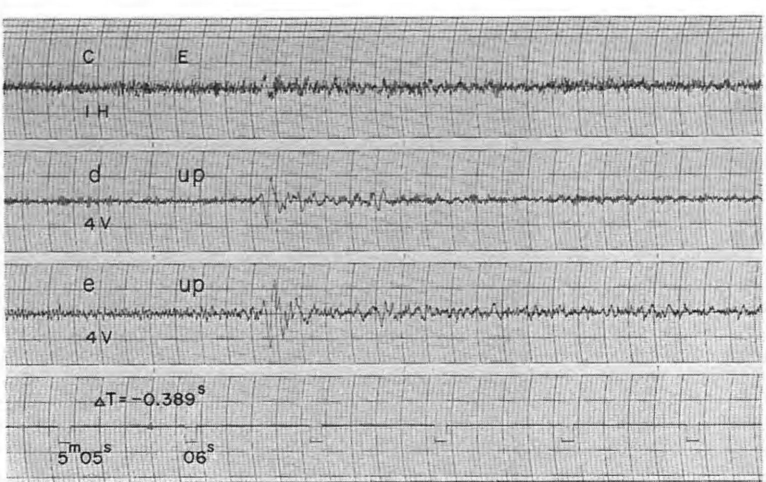

Fig. 5–43 Seismograms obtained (127) at D_{13}, (128), (129) at D_{14} of profile A from the shot B–IV

(130)

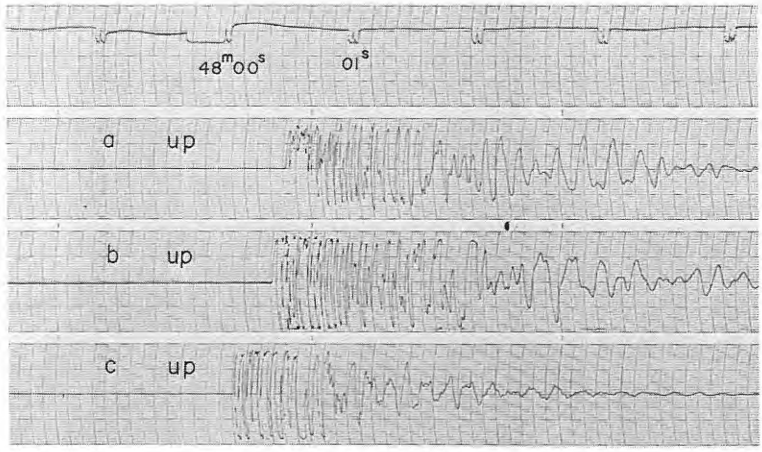

(131)

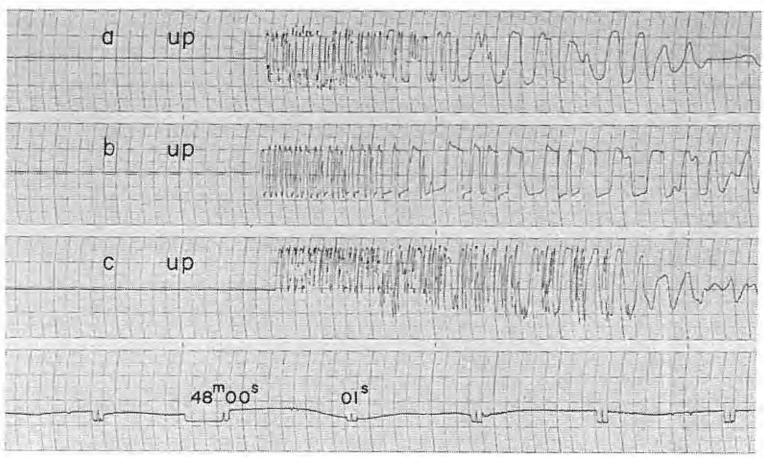

(132)

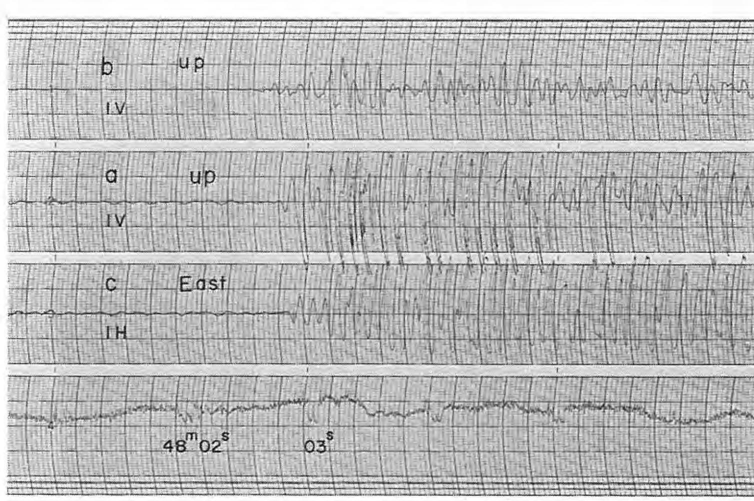

Fig. 5–44 Seismograms obtained (130) at D_1, (131) at D_2 and (132) at D_3 from the shot B–I

(133)

(134)

(135)

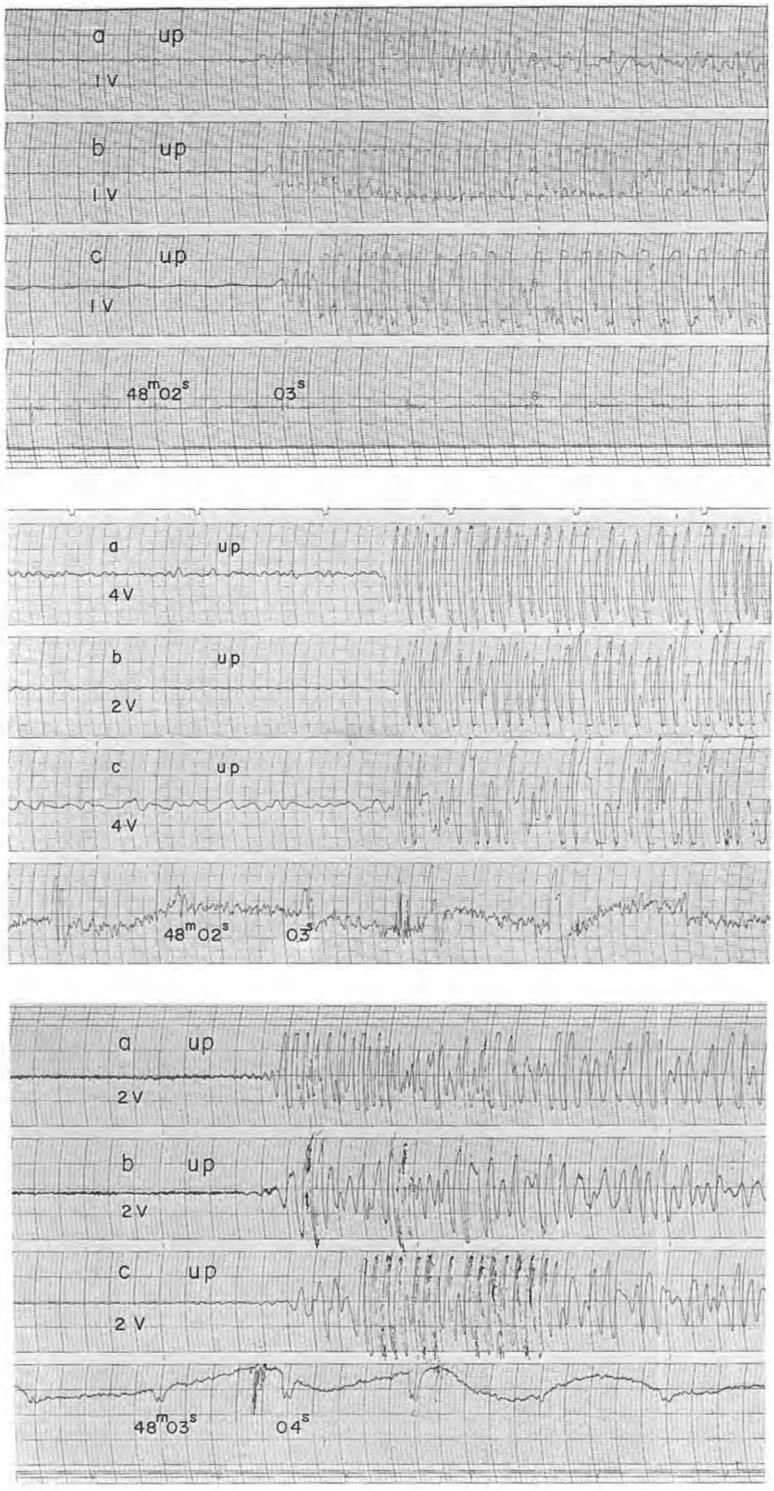

Fig. 5–45 Seismograms obtained (133) at D_4, (134) at D_5 and (135) at D_6 from the shot B–I

(136)

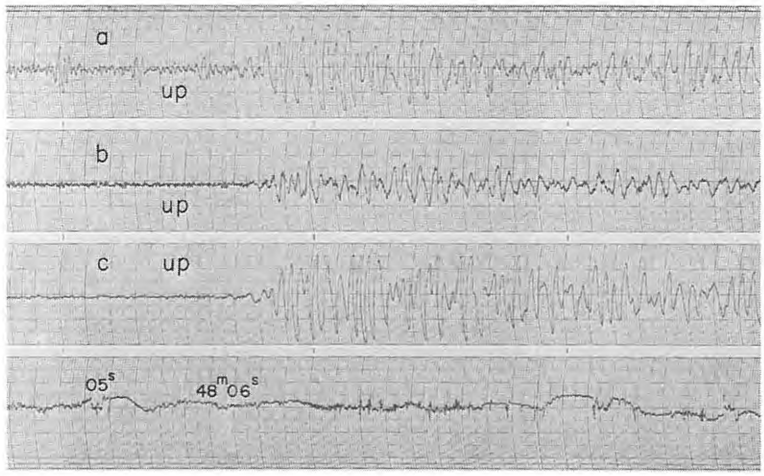

(137)

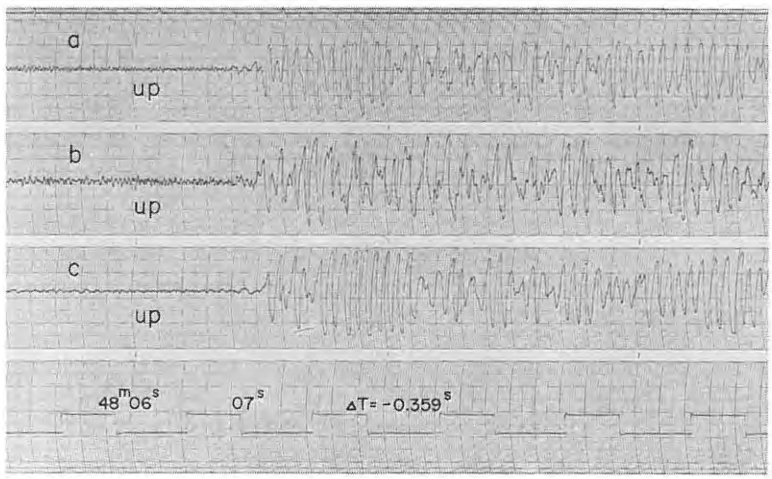

(138)

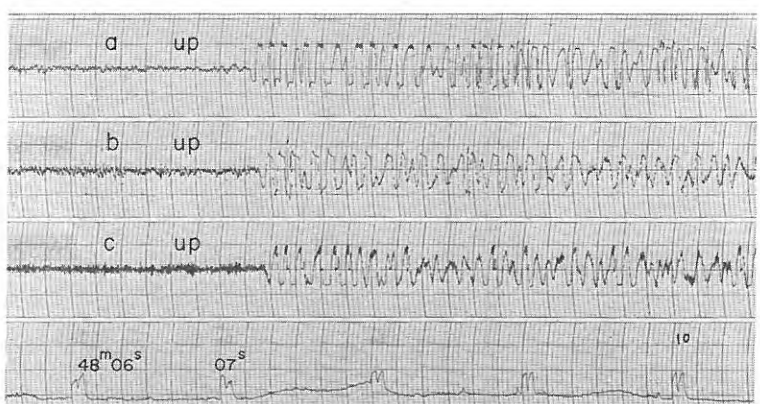

Fig. 5–46 Seismograms obtained (136) at D_7, (137) at D_8 and (138) at D_9 from the shot B–I

(139)

(140)

(141)

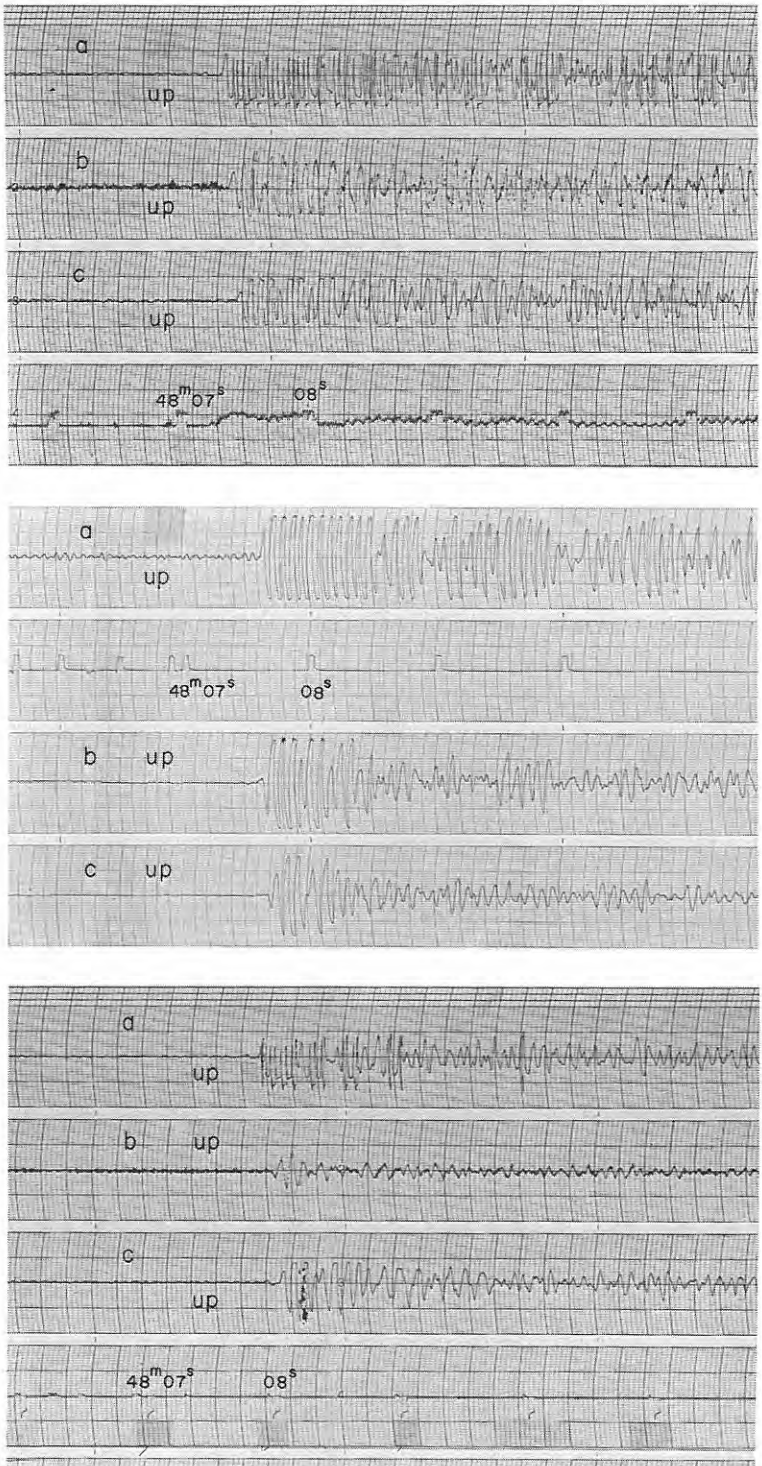

Fig. 5–47 Seismograms obtained (139) at D_{10}, (140) at D_{11} and (141) at D_{12} from the shot B–I

(142)

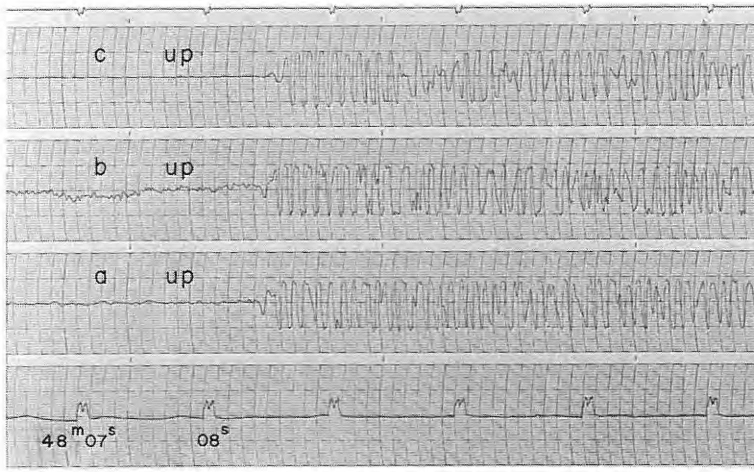

(143)

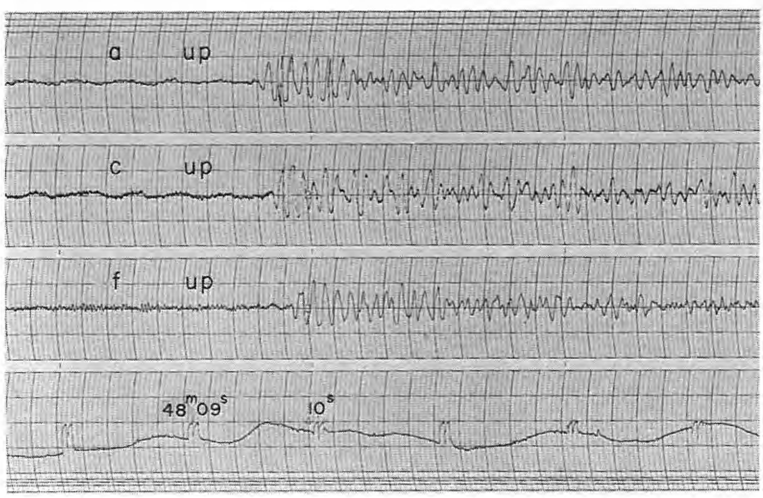

(144)

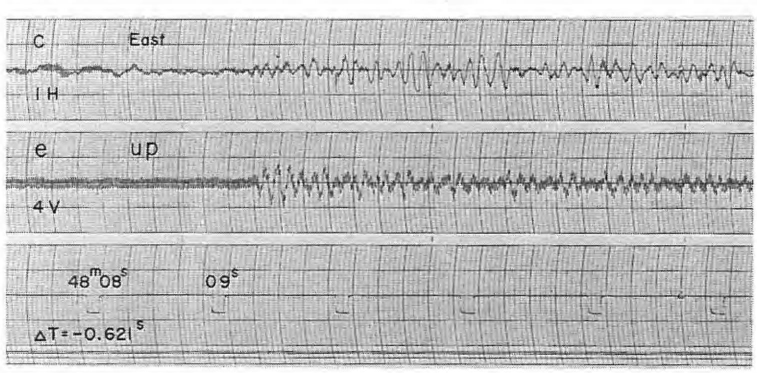

Fig. 5–48 Seismograms obtained (142) at D_{13}, (143), (144) at D_{14} from the shot B–I

(145)

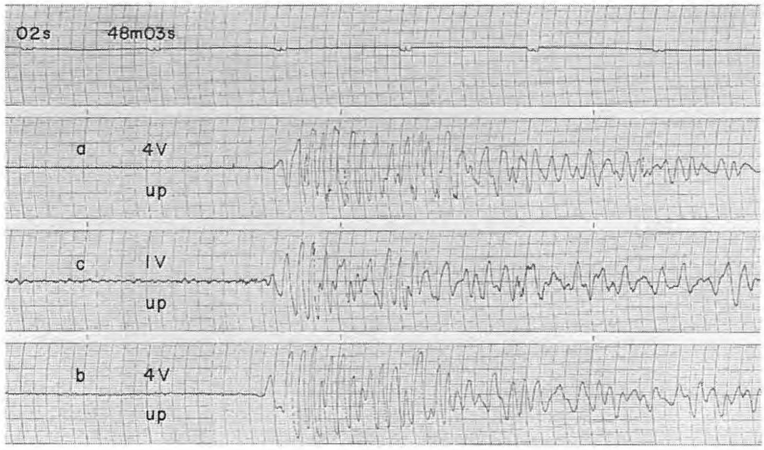

(146)

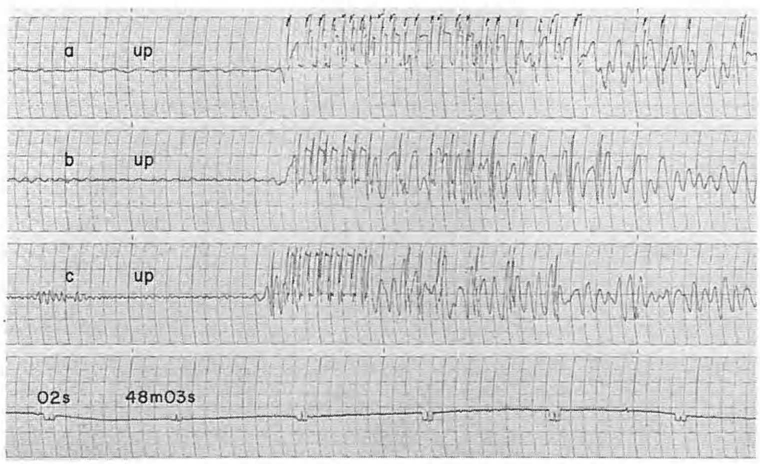

(147)

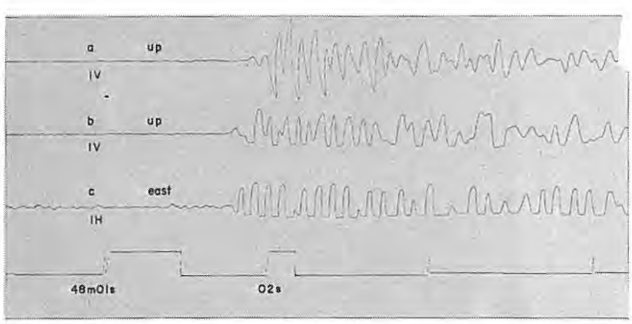

Fig. 5–49 Seismograms obtained (145) at D_1, (146) at D_2 and (147) at D_3 from the shot B–II

(148)

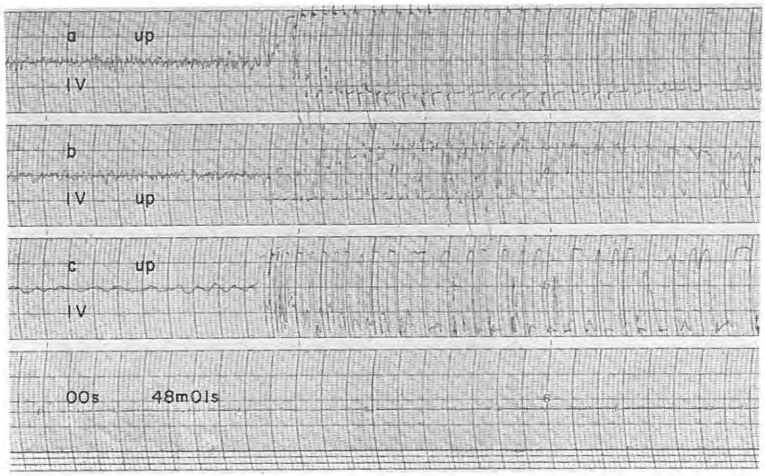

(149)

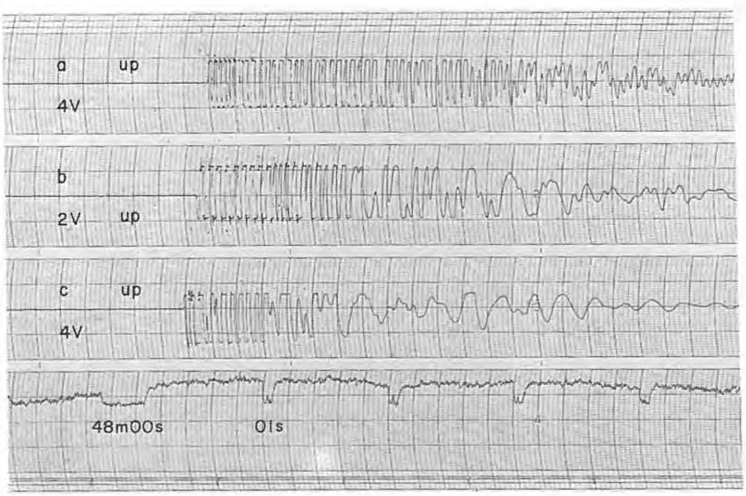

(150)

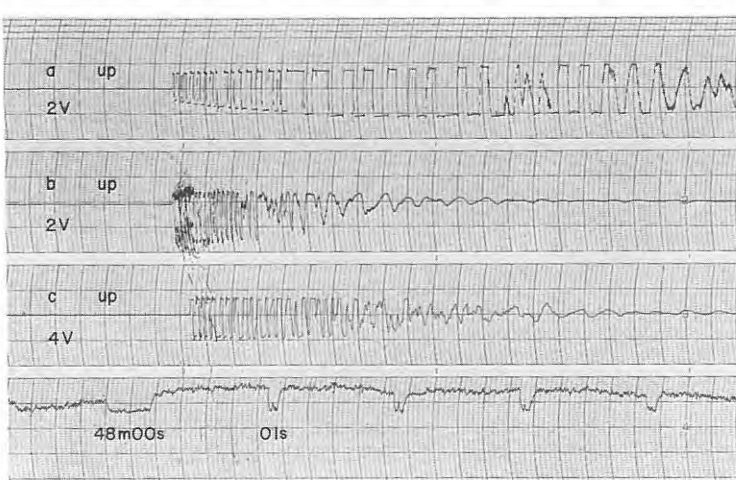

Fig. 5–50 Seismograms obtained (148) at D_4, (149) at D_5 and (150) at D_6 from the shot B–II

(151)

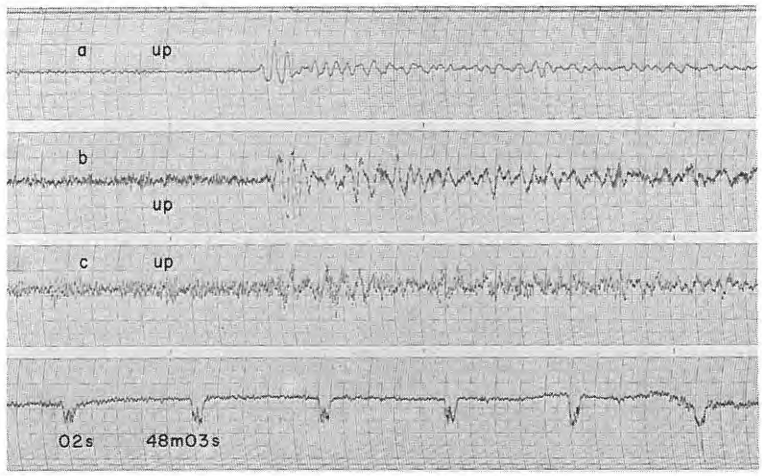

(152)

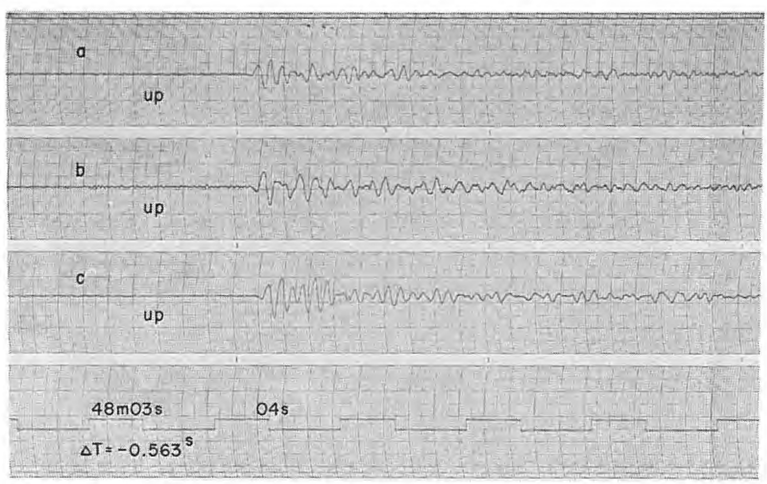

(153)

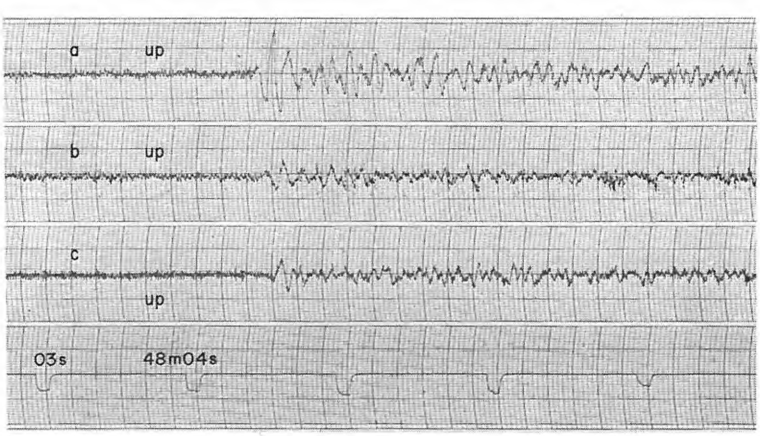

Fig. 5–51 Seismograms obtained (151) at D_7, (152) at D_8 and (153) at D_9 from the shot B–II

(154)

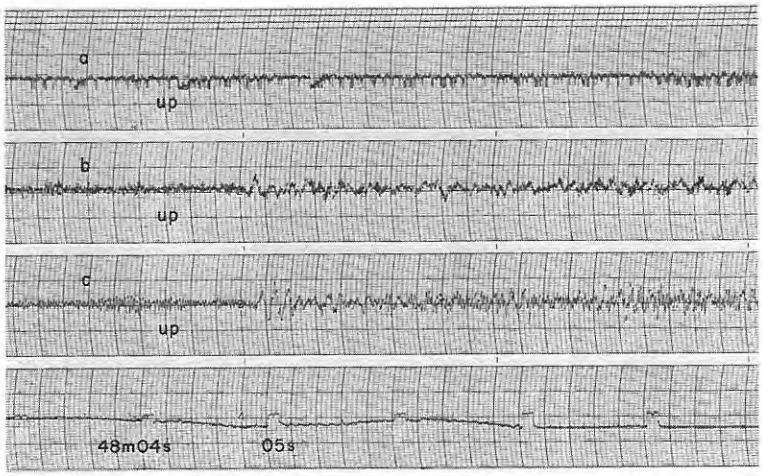

(155)

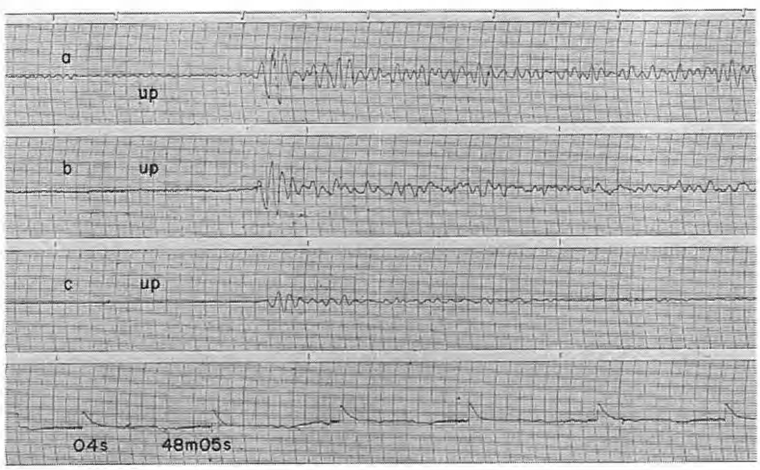

(156)

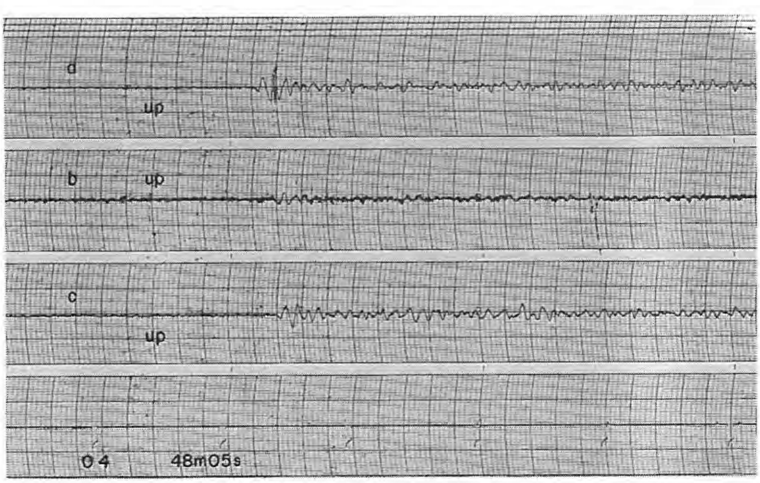

Fig. 5–52 Seismograms obtained (154) at D_{10}, (155) at D_{11} and (156) at D_{12} from the shot B–II

(157)

(158)

(159)

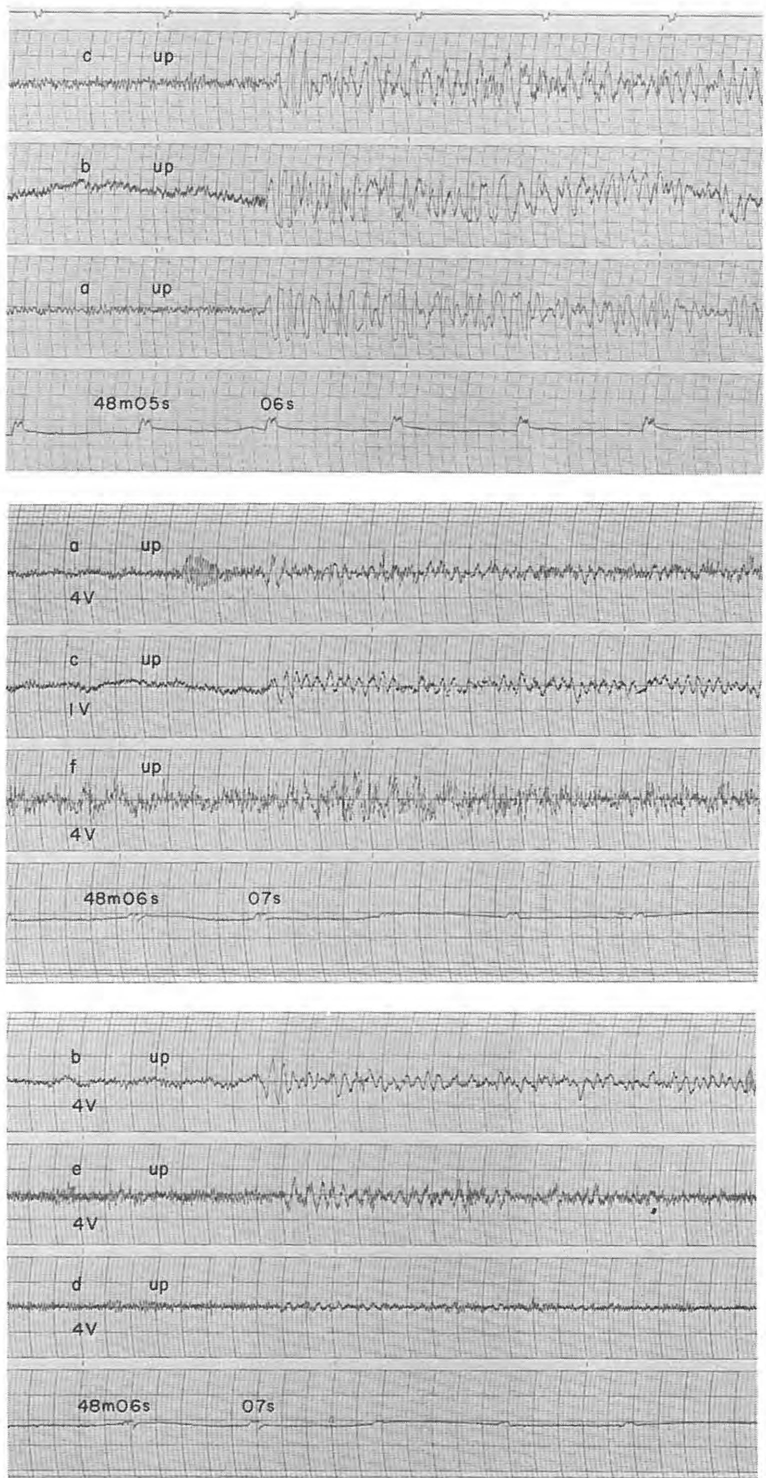

Fig. 5–53 Seismograms obtained (157) at D_{13}, (158), (159) at D_{14} from the shot B–II

(160)

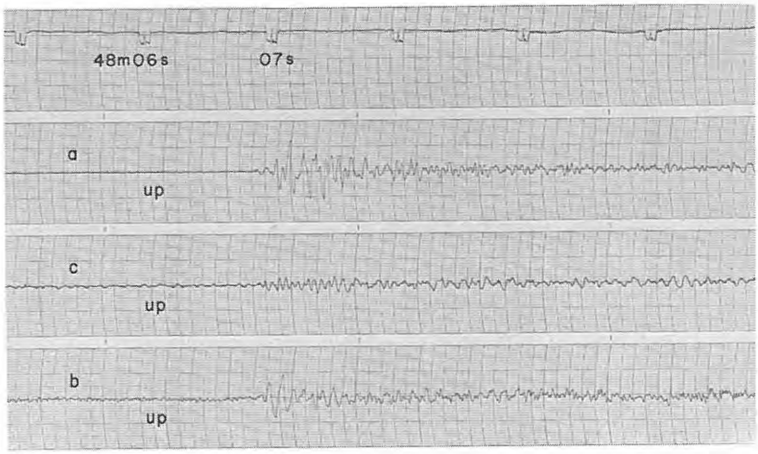

(161)

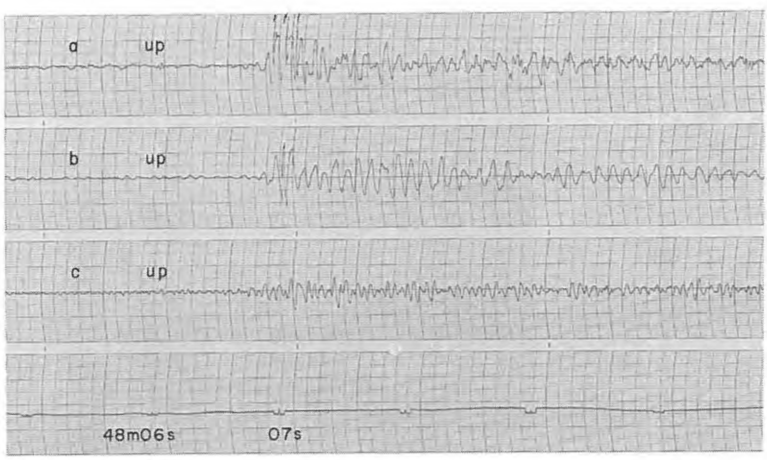

(162)

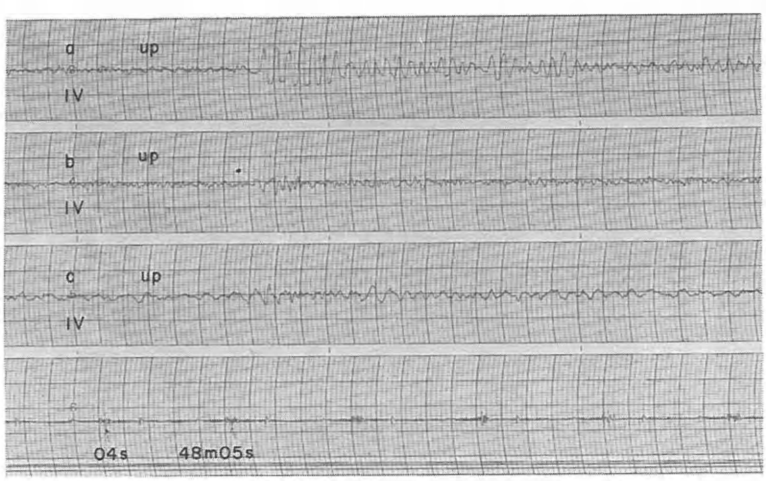

Fig. 5–54 Seismograms obtained (160) at D_1, (161) at D_2 and (162) at D_4 from the shot B–III_1

(163)

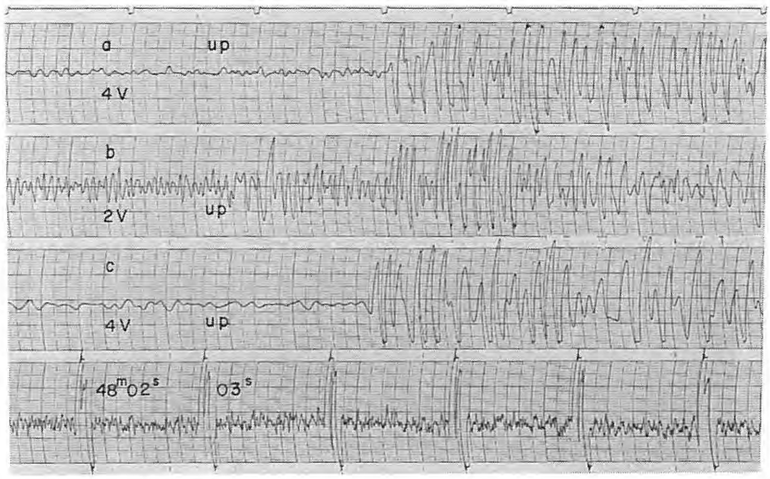

(164)

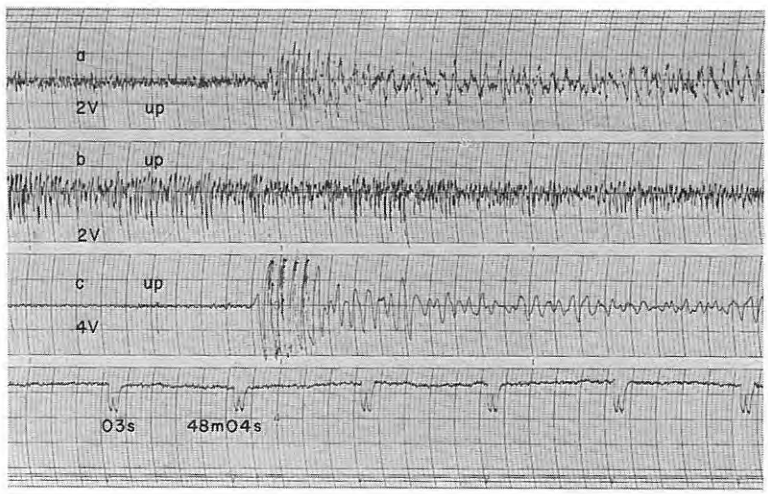

(165)

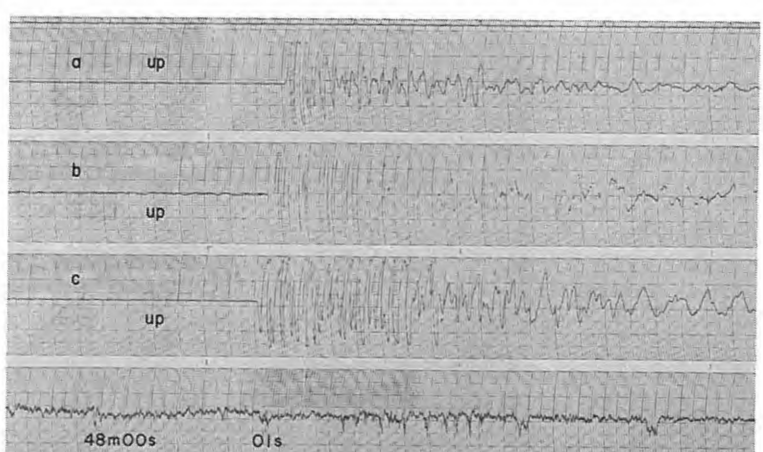

Fig. 5–55 Seismograms obtained (163) at D_5, (164) at D_6 and (165) at D_7 from the shot B–III_1

(166)

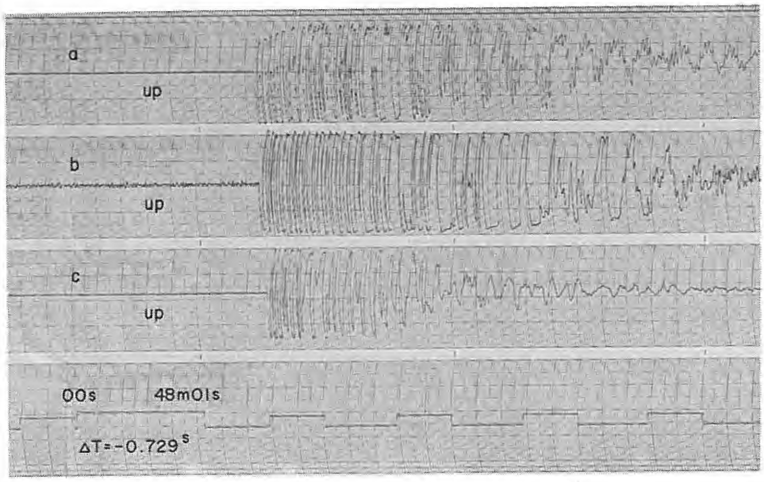

(167)

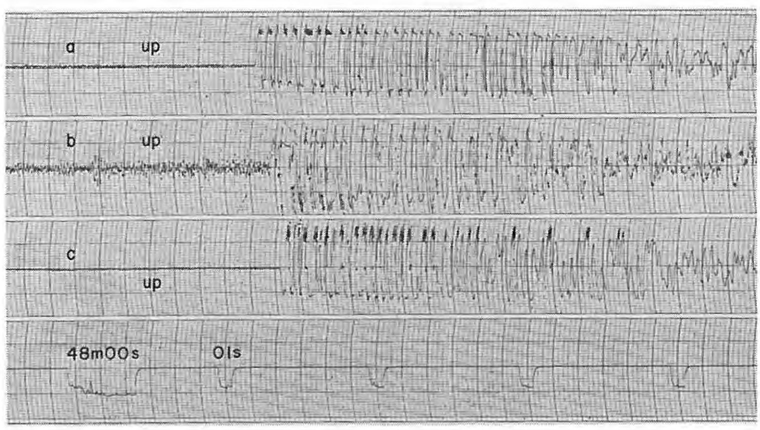

(168)

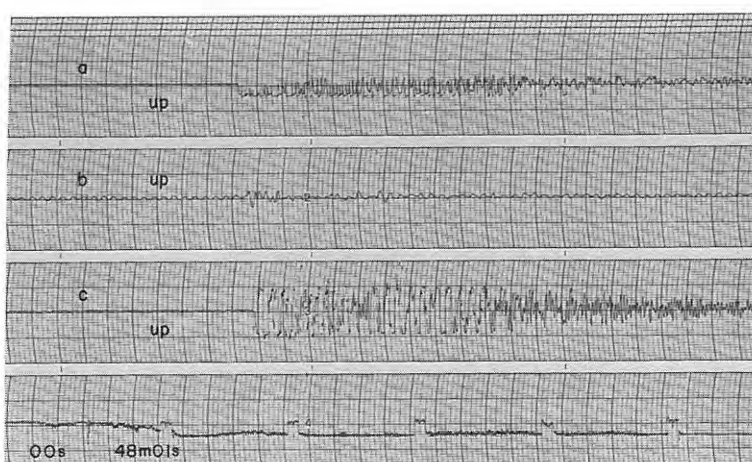

Fig. 5–56 Seismograms obtained (166) at D_8, (167) at D_9 and (168) at D_{10} from the shot B–III_1

(169)

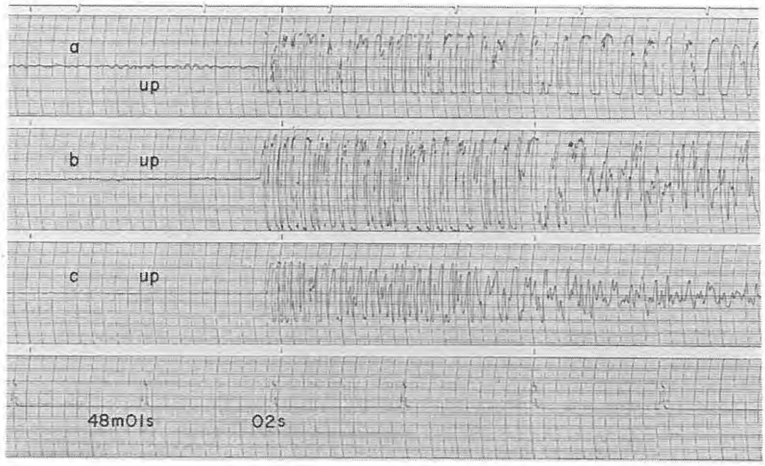

(170)

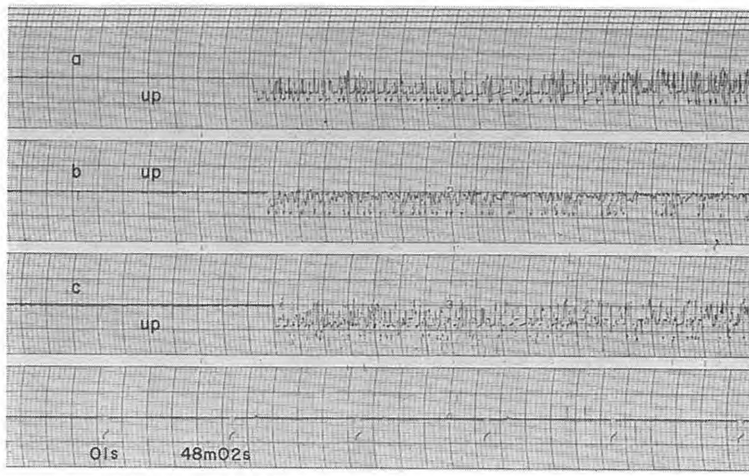

(171)

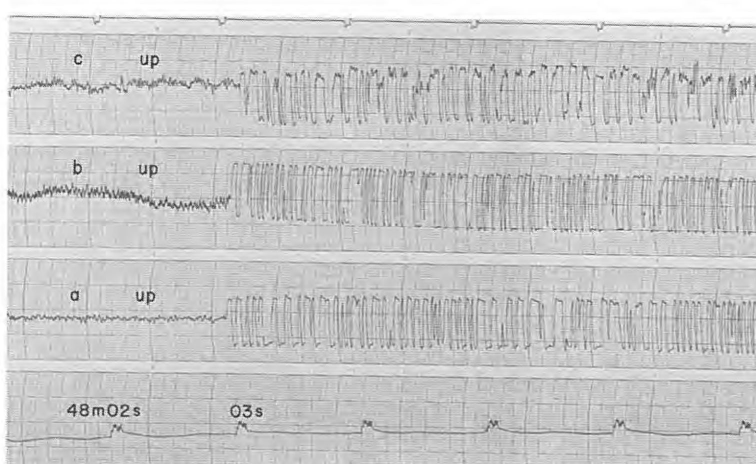

Fig. 5–57 Seismograms obtained (169) at D_{11}, (170) at D_{12} and (171) at D_{13} from the shot B–III_1

(172)

(173)

(174)

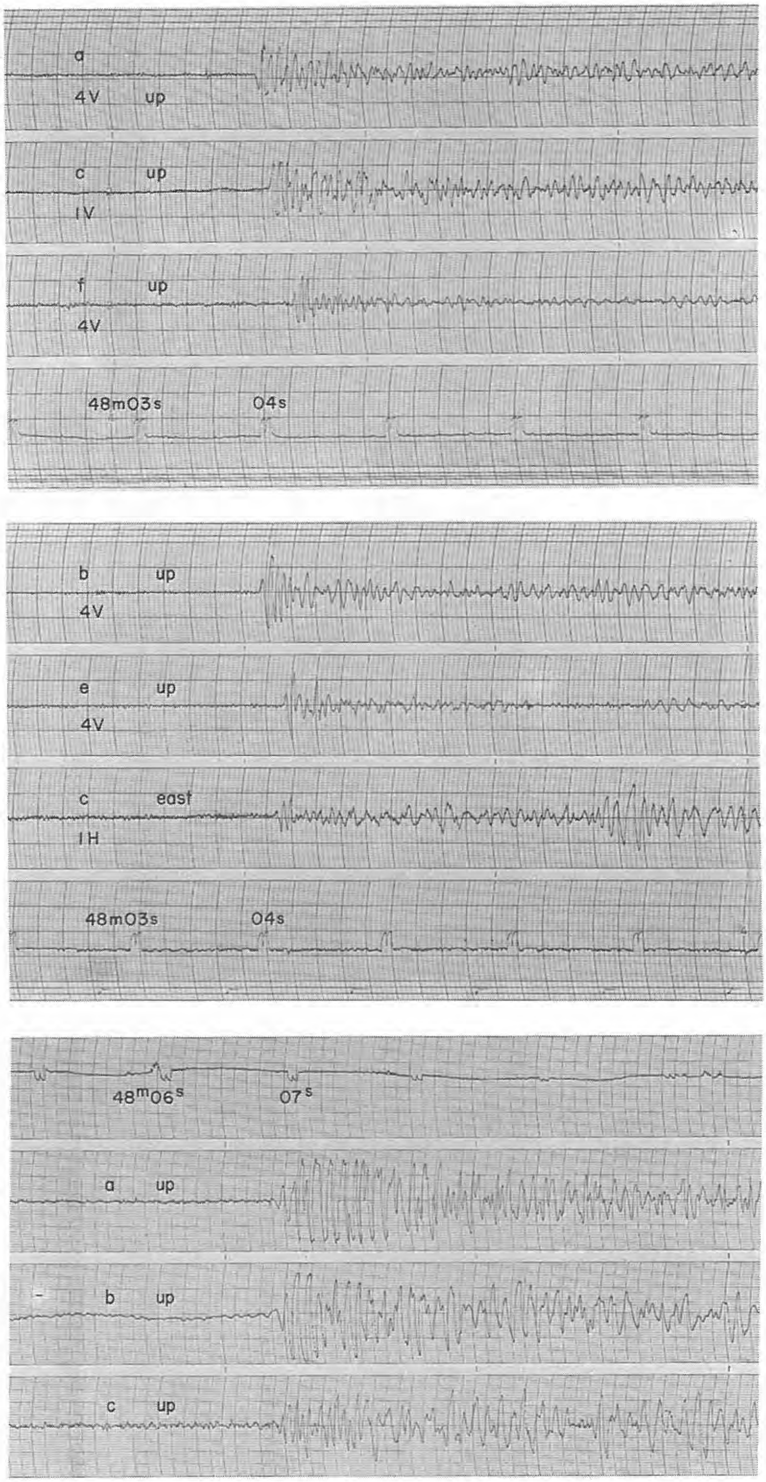

Fig. 5–58 Seismograms obtained (172), (173) at D_{14} from the shot B–III_1, and (174) at D_1 from the shot B–III_2

(175)

(176)

(177)

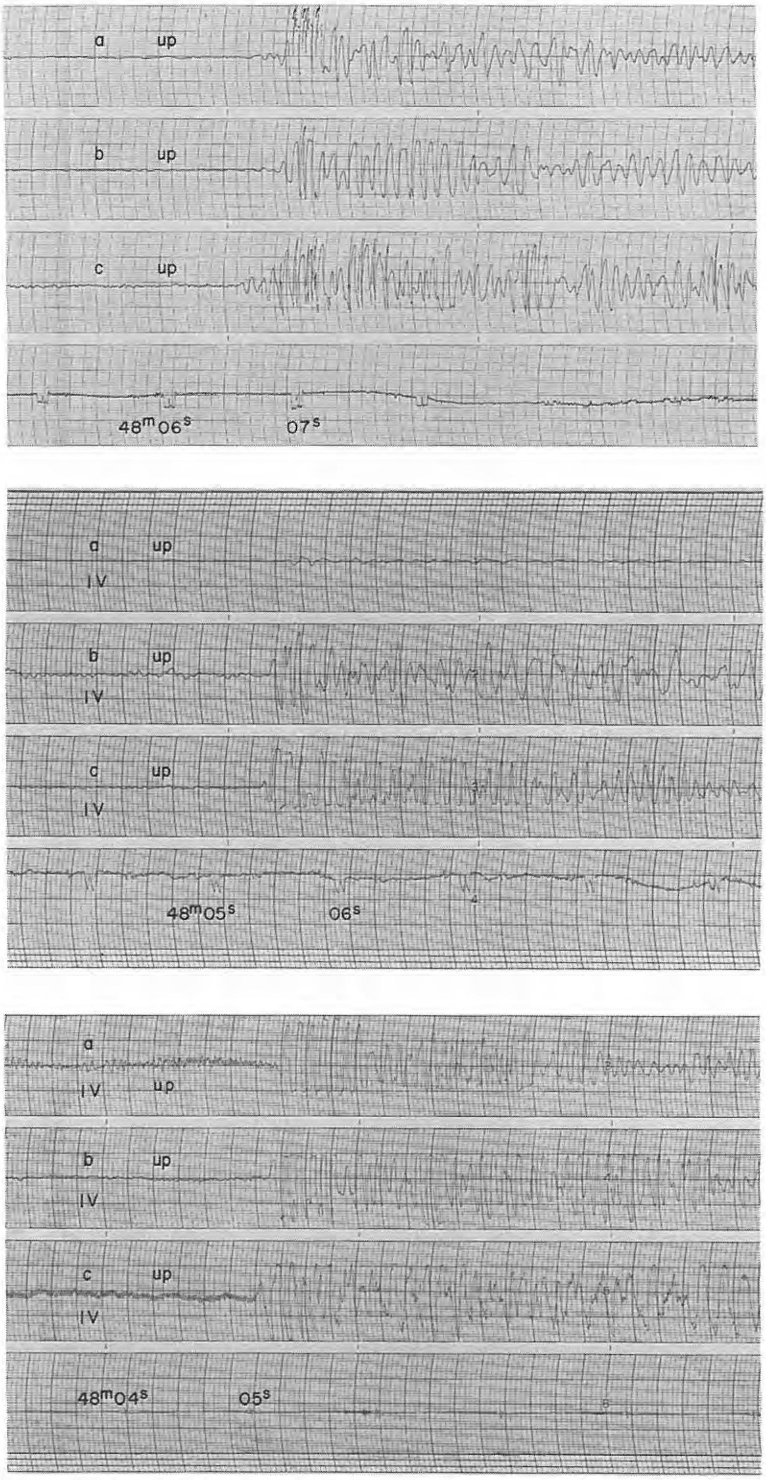

Fig. 5–59 Seismograms obtained (175) at D_2, (176) at D_3 and (177) at D_4 from the shot B–III_2

(178)

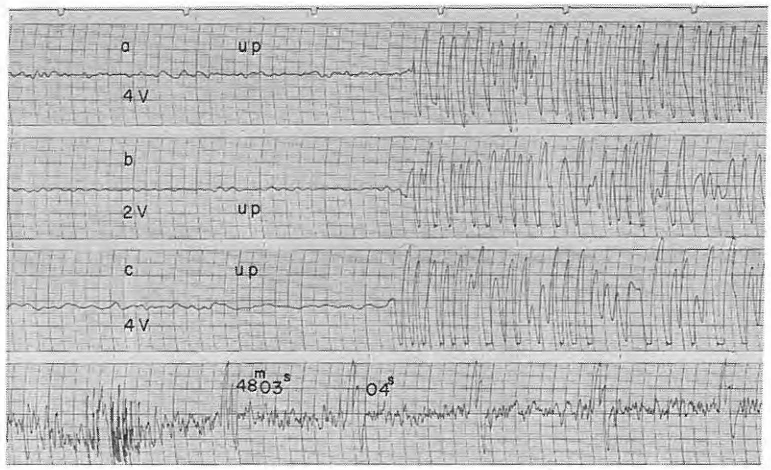

(179)

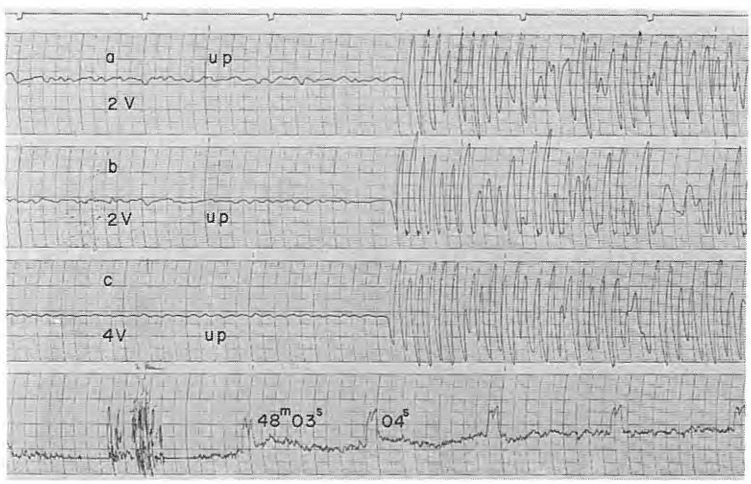

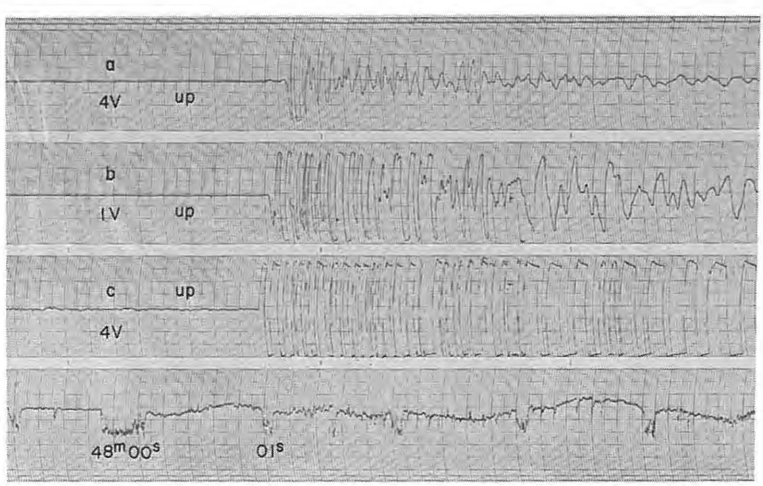

Fig. 5–60 Seismograms obtained (178) at D_5, (179) at D_6 and (180) at D_7 from the shot B–III_2

(181)

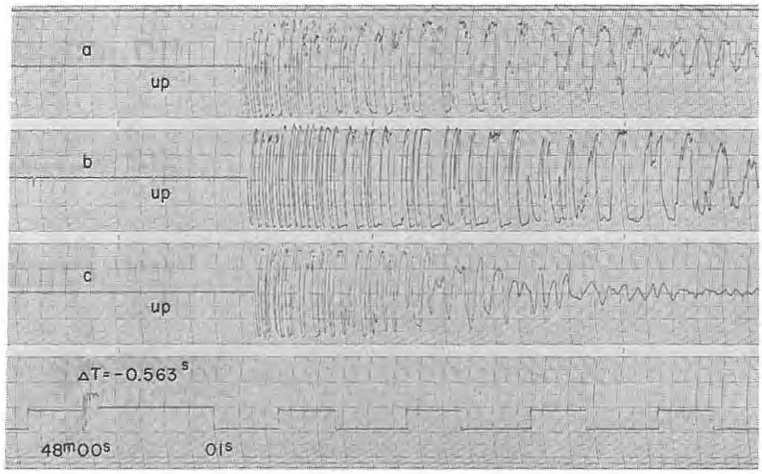

(182)

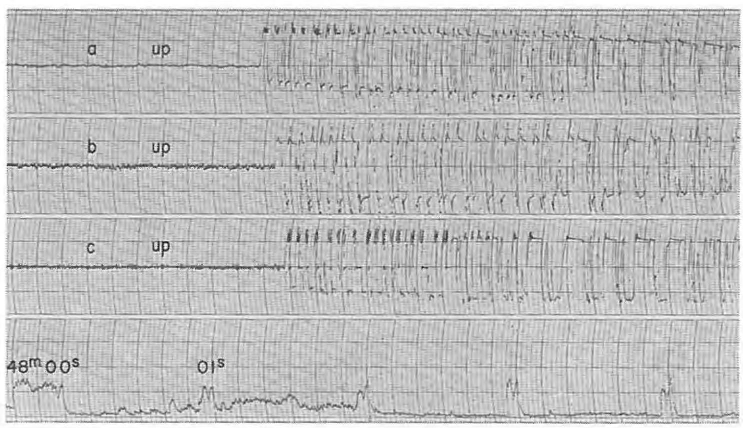

(183)

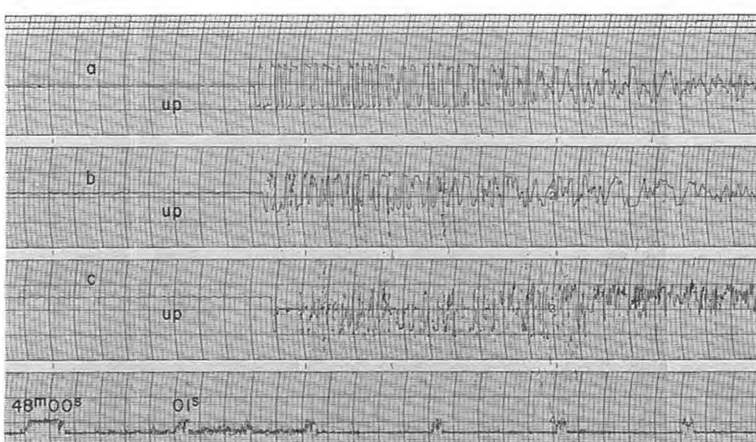

Fig. 5–61 Seismograms obtained (181) at D_8, (182) at D_9 and (183) at D_{10} from the shot B–III_2

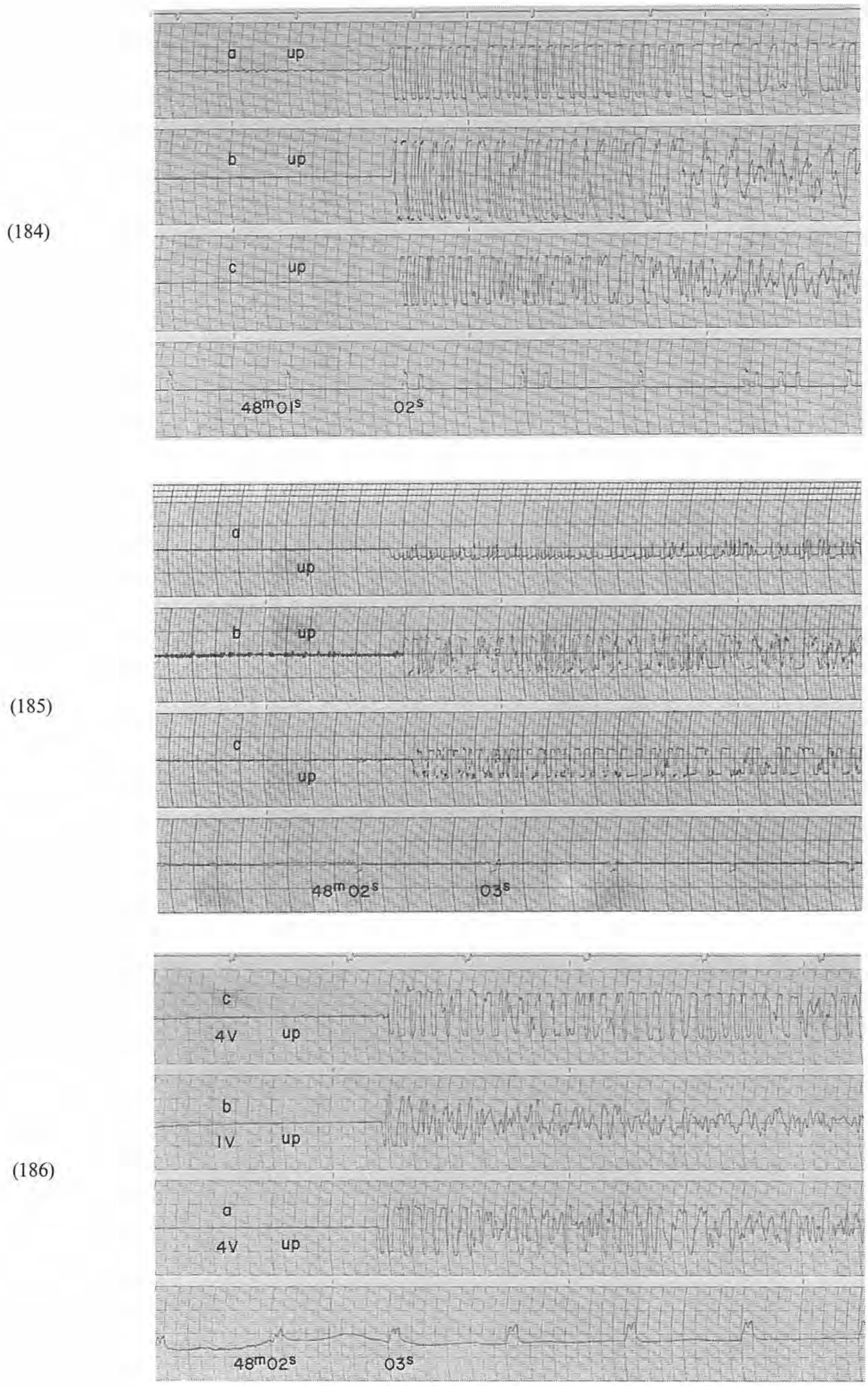

Fig. 5–62 Seismograms obtained (184) at D_{11}, (185) at D_{12} and (186) at D_{13} from the shot B–III_2

(187)

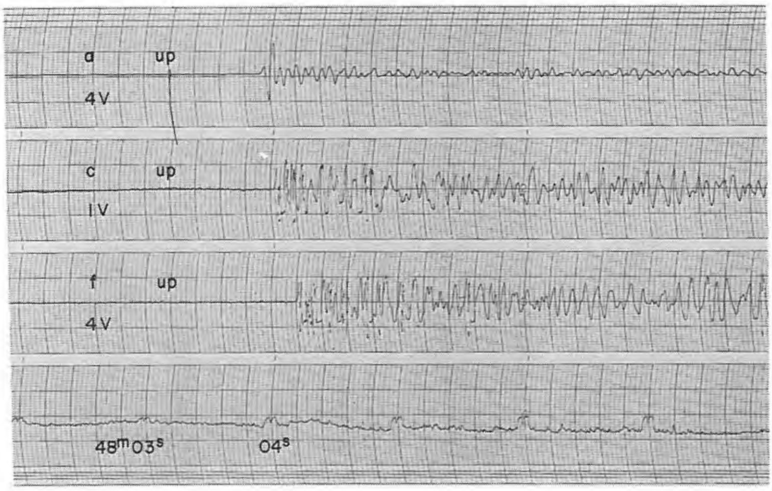

(188)

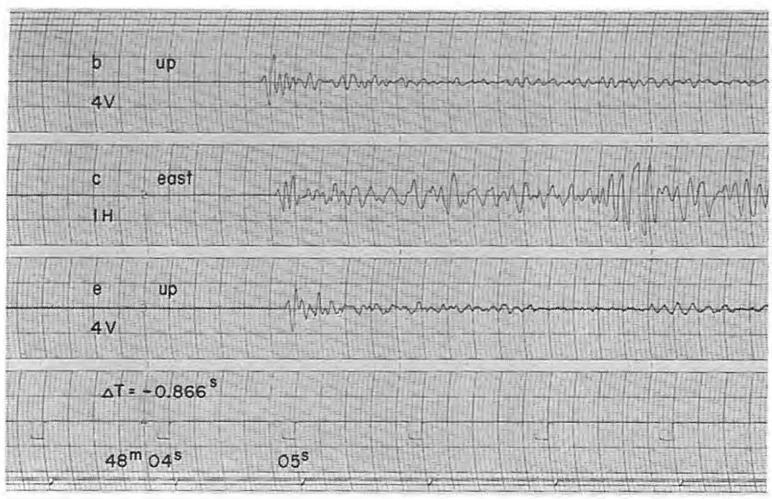

(189)

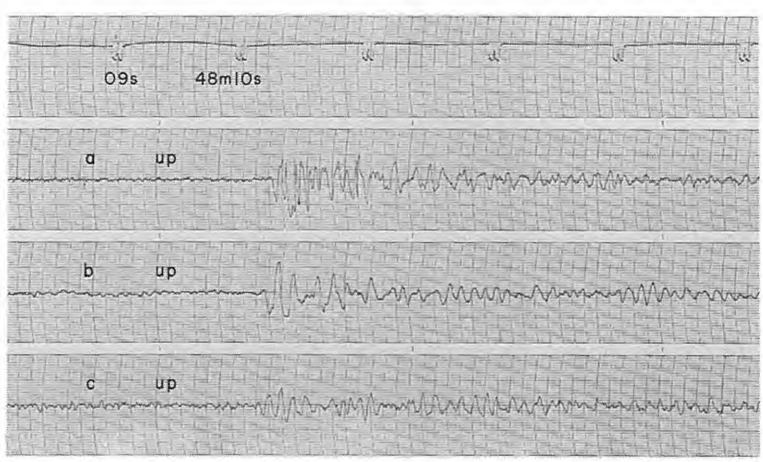

Fig. 5–63 Seismograms obtained (187), (188) at D_{14} from the shot B–III_2, and (189) at D_1 from the shot B–IV

(190)

(191)

(192)

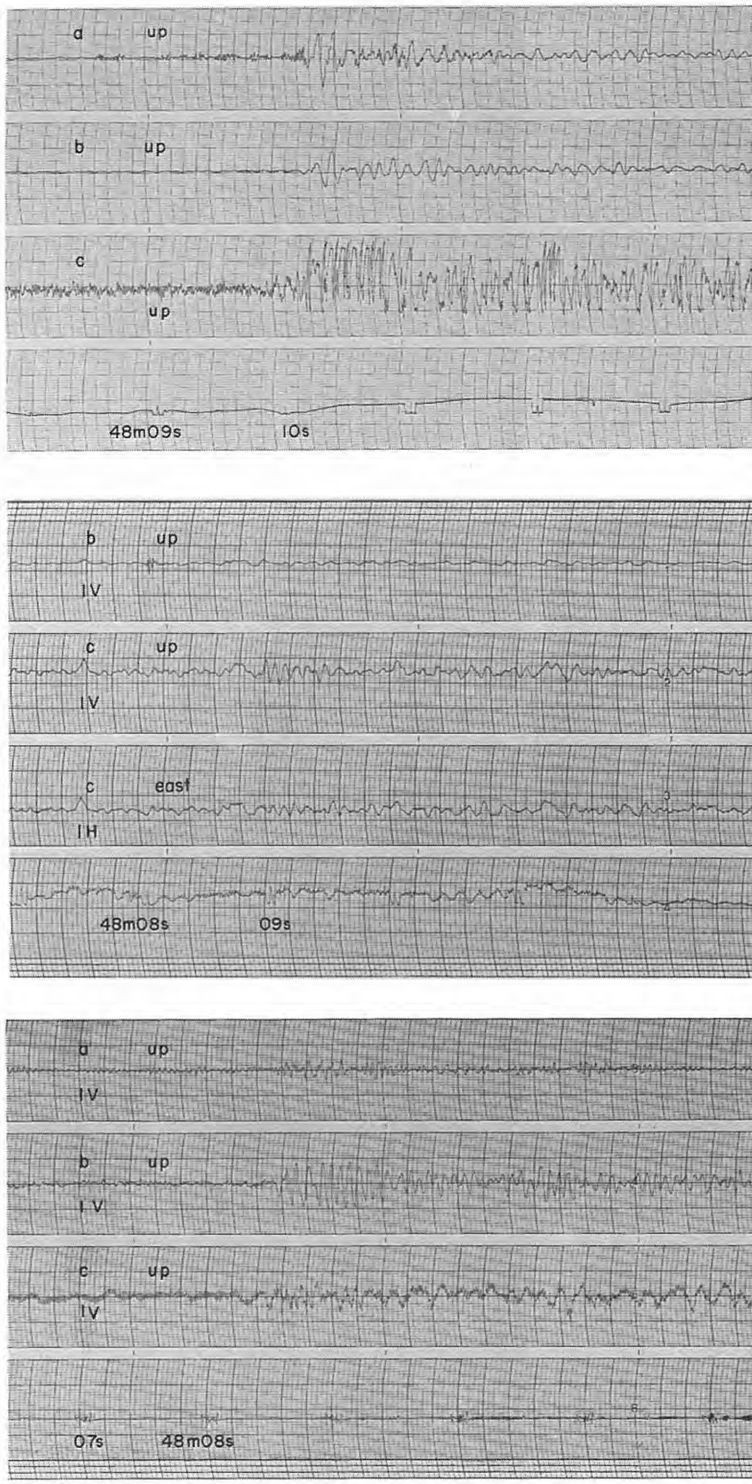

Fig. 5–64 Seismograms obtained (190) at D_2, (191) at D_3 and (192) at D_4 from the shot B–IV

(193)

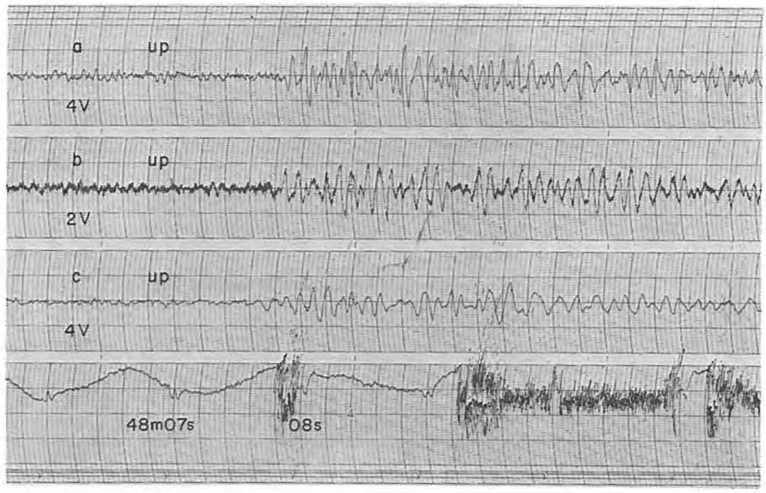

(194)

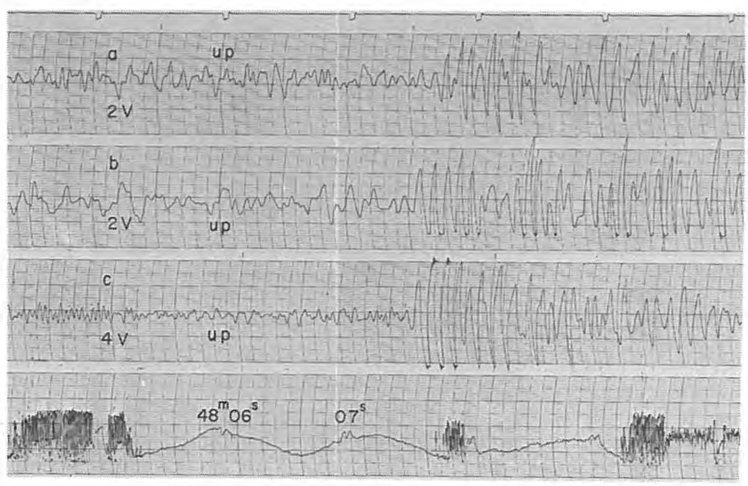

(195)

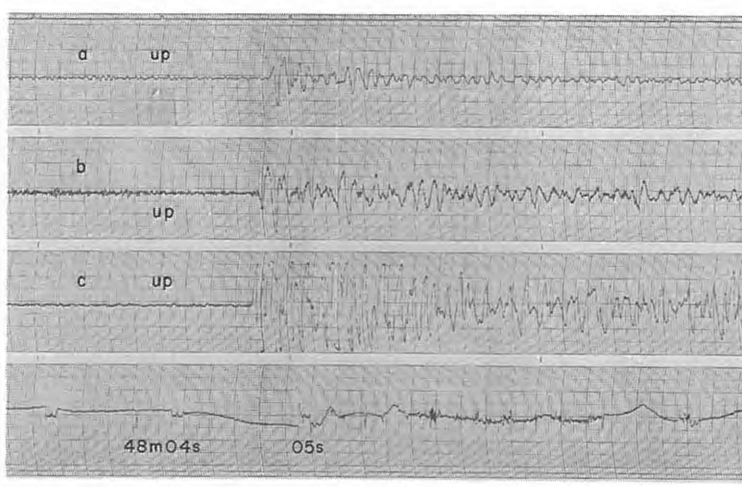

Fig. 5–65 Seismograms obtained (193) at D_5, (194) at D_6 and (195) at D_7 from the shot B–IV

(196)

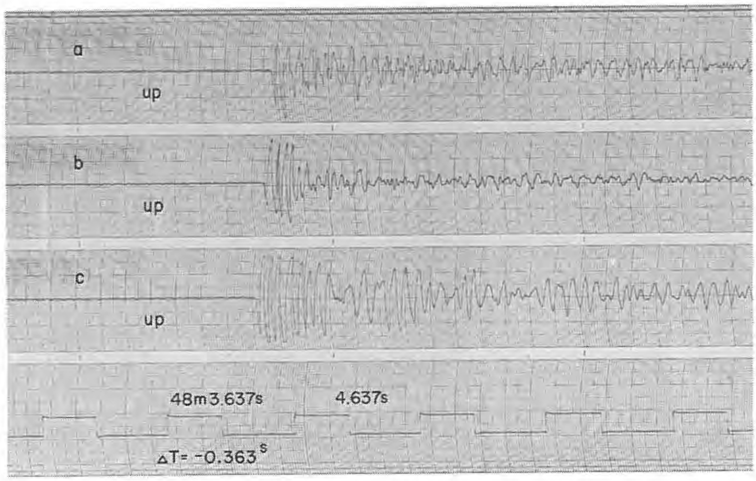

(197)

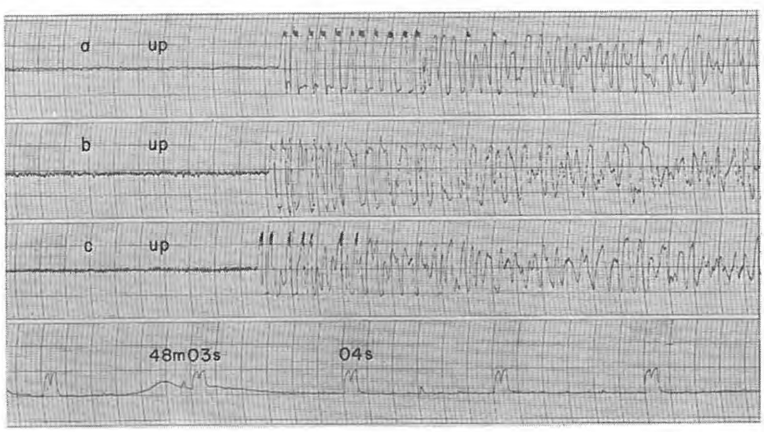

(198)

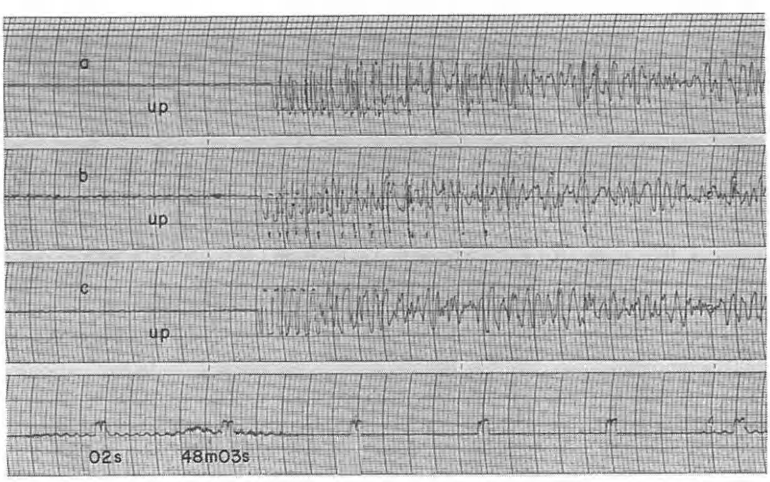

Fig. 5–66 Seismograms obtained (196) at D_8, (197) at D_9 and (198) at D_{10} from the shot B–IV

(199)

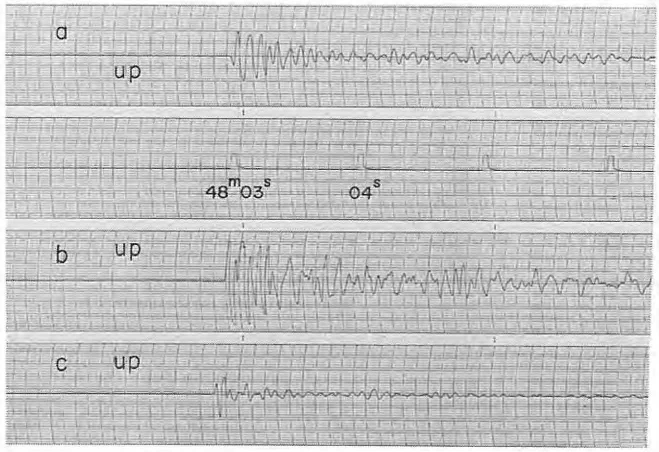

(200)

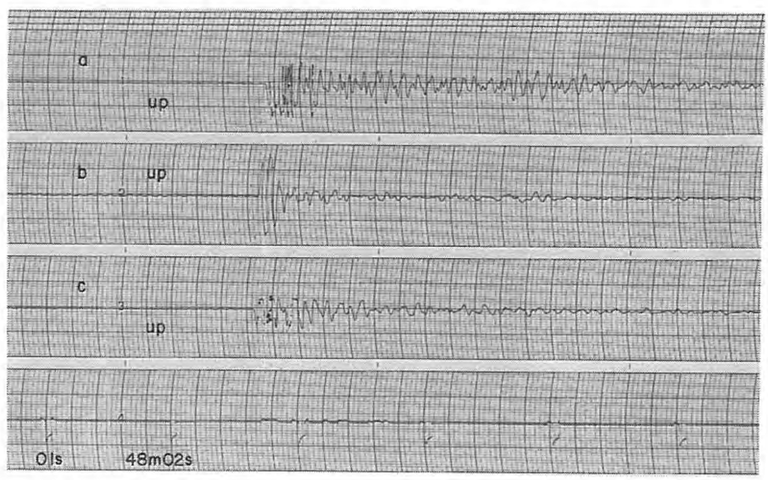

(201)

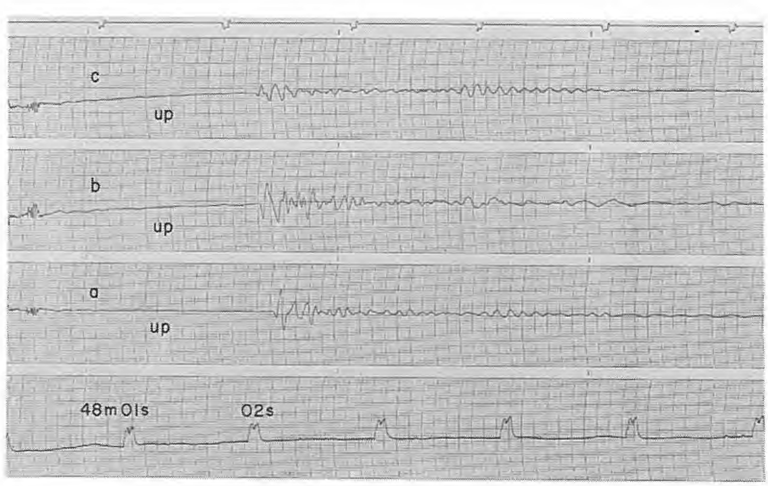

Fig. 5–67 Seismograms obtained (199) at D_{11}, (200) at D_{12} and (201) at D_{13} from the shot B–IV

(202)

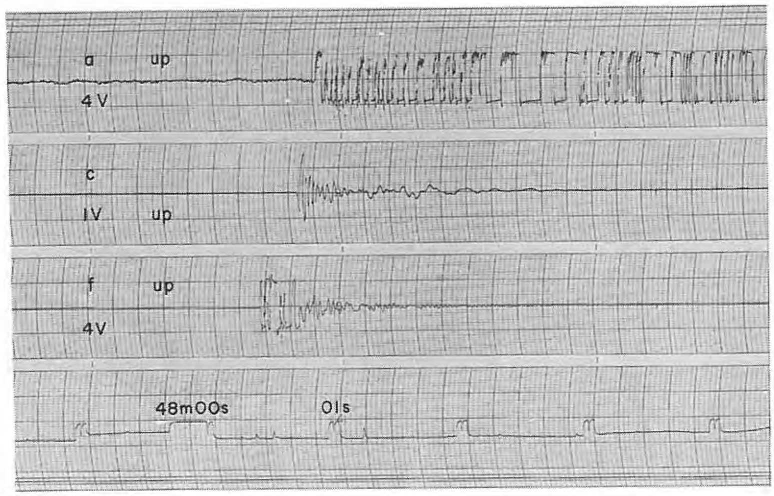

(203)

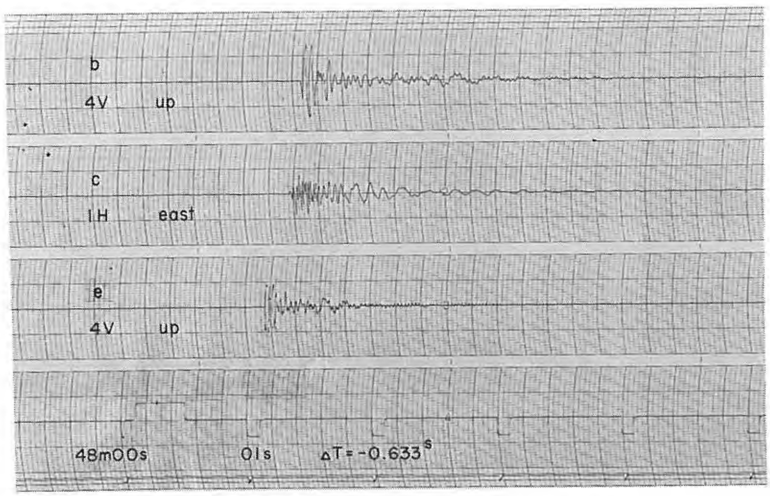

Fig. 5–68 Seismograms obtained (202), (203) at D_{14} from the shot B–IV

(1)

(2)

(3)

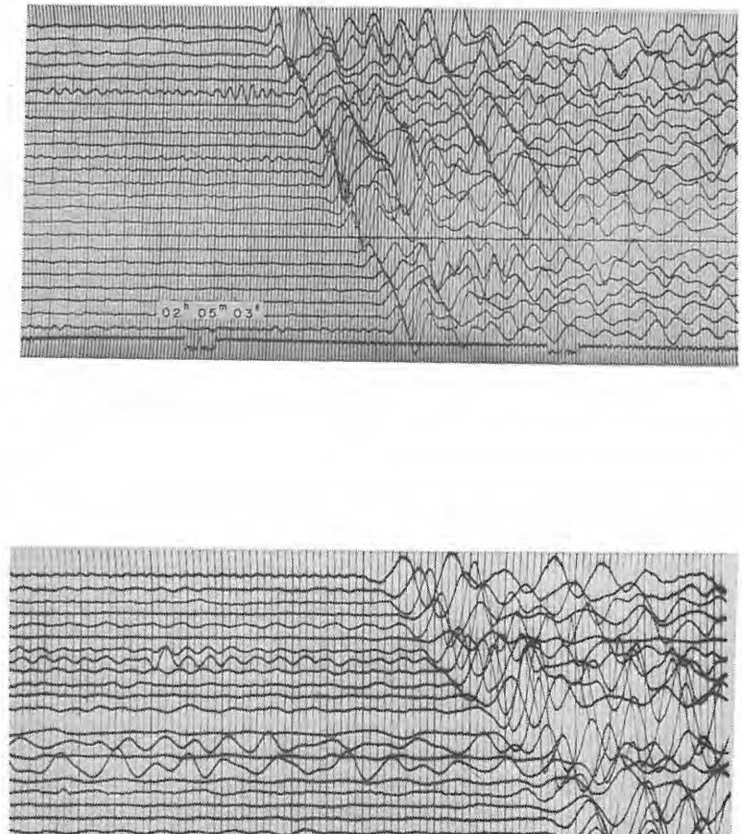

Fig. 6–1 Seismograms obtained (1) at E_1, (2) at E_2 and (3) at E_3 from the shot A–I

(4)

(5)

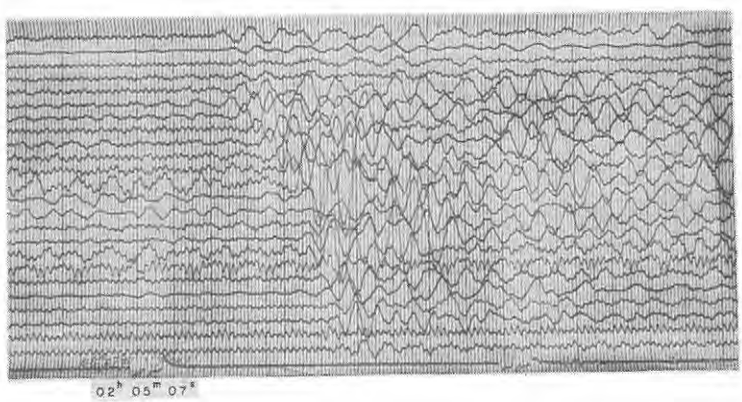

(6)

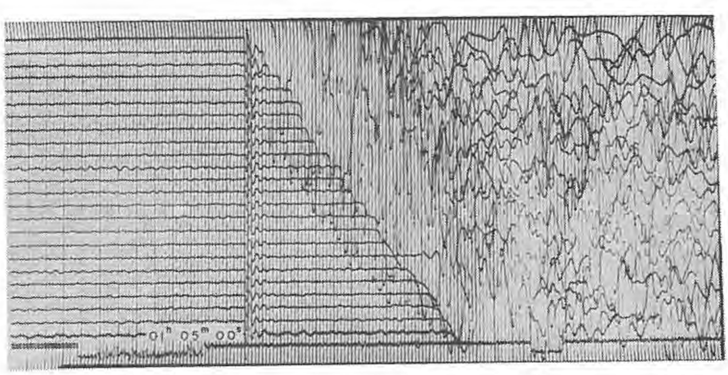

Fig. 6–2 Seismograms obtained (4) at E_4 and (5) at E_5 from the shot A–I, and (6) at E_1 from the shot A–II

(7)

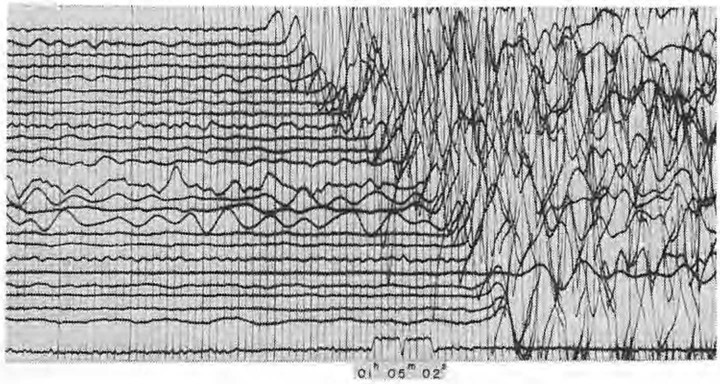

(8)

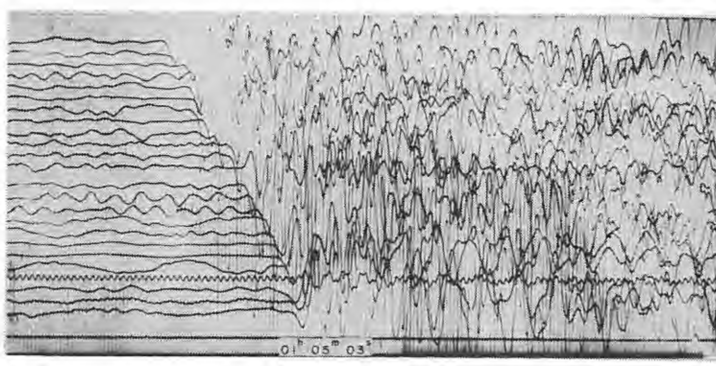

(9)

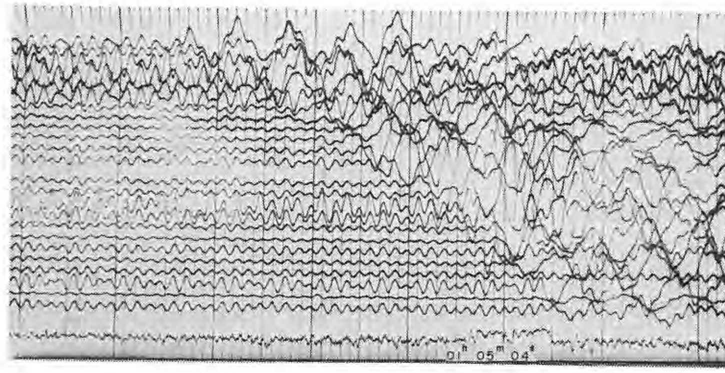

Fig. 6–3 Seismograms obtained (7) at E_2, (8) at E_3 and (9) at E_4 from the shot A–II

(10)

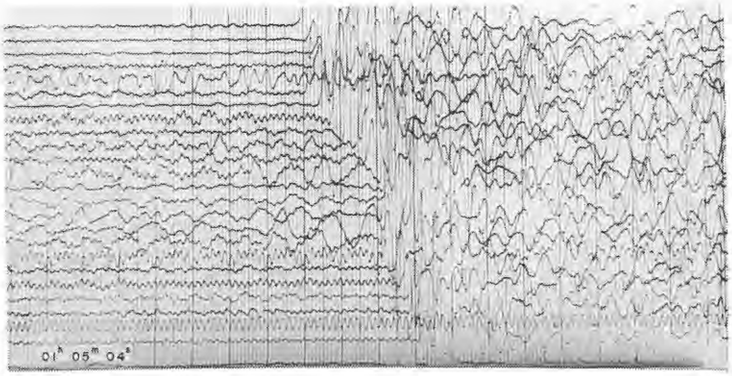

(11)

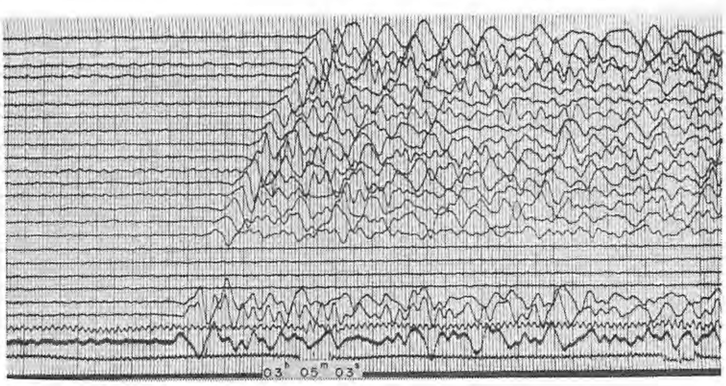

(12)

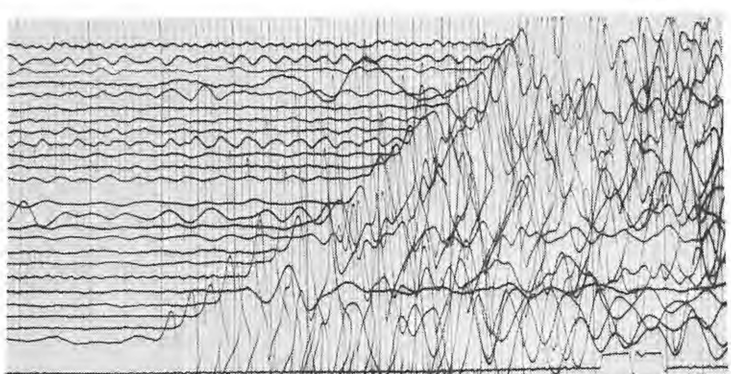

Fig. 6–4 Seismograms obtained (10) at E_5 from the shot A–II, and (11) at E_1 and (12) at E_2 from the shot A–III

(13)

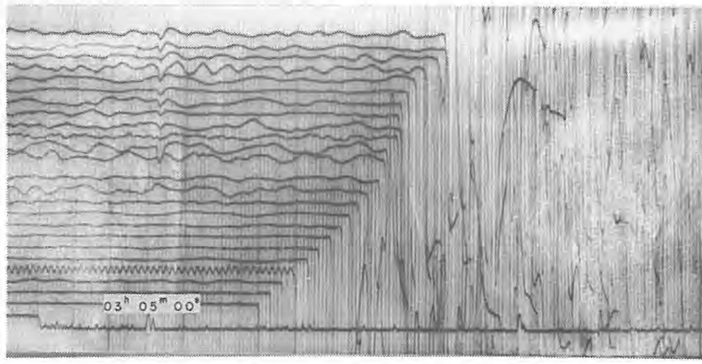

(14)

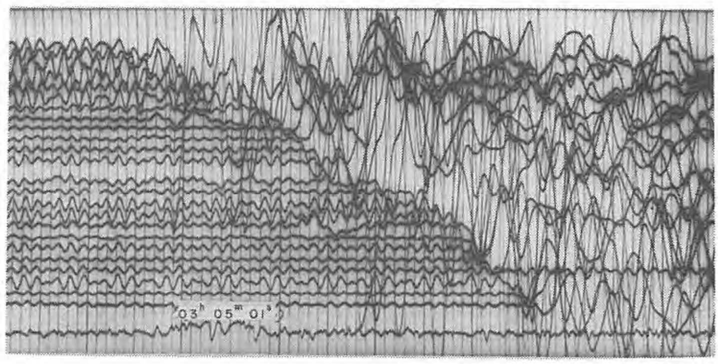

(15)

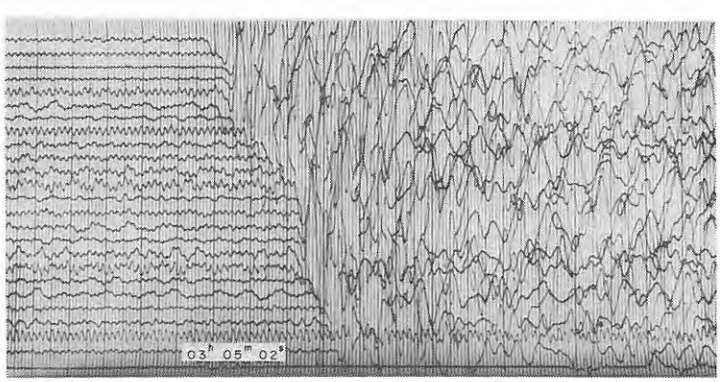

Fig. 6–5 Seismograms obtained (13) at E_3, (14) at E_4 and (15) at E_5 from the shot A–III

(16)

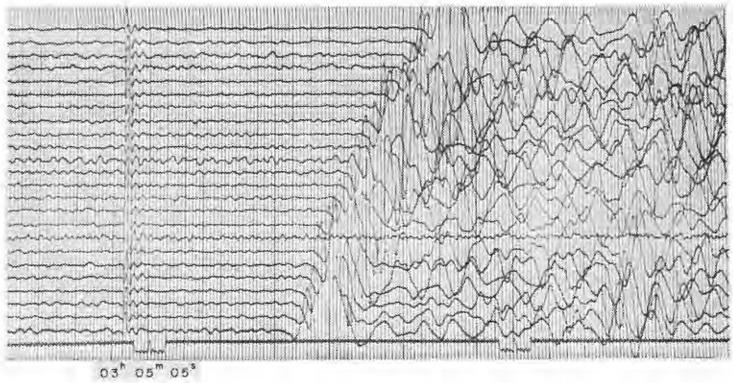

(17)

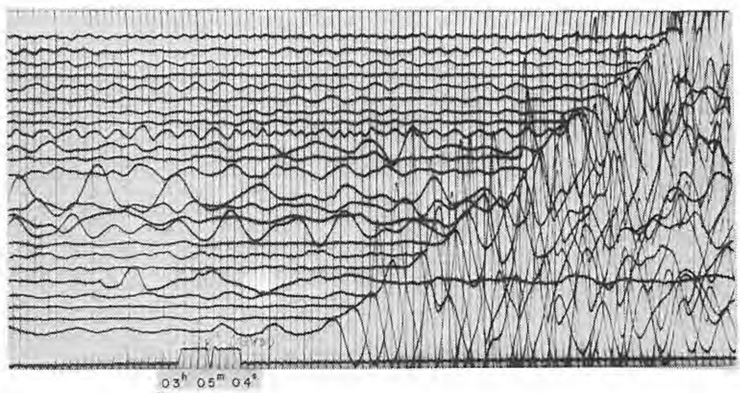

(18)

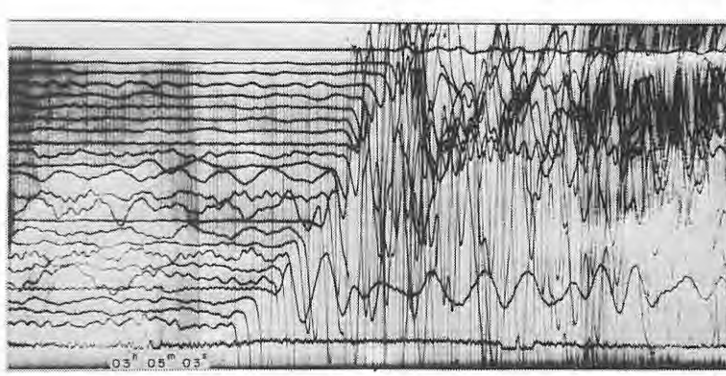

Fig. 6–6 Seismograms obtained (16) at E_1, (17) at E_2 and (18) at E_3 from the shot A–IV_1

(19)

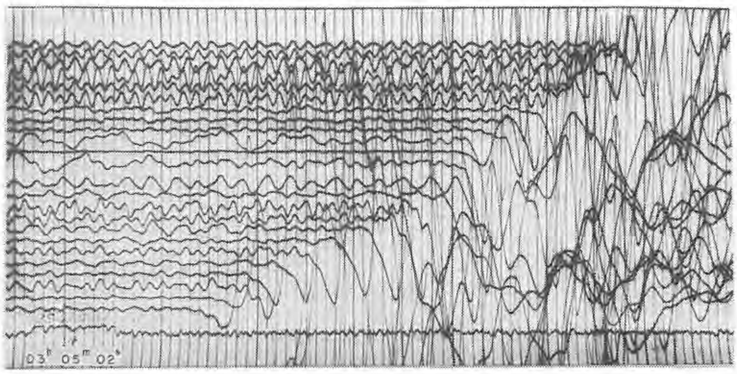

(20)

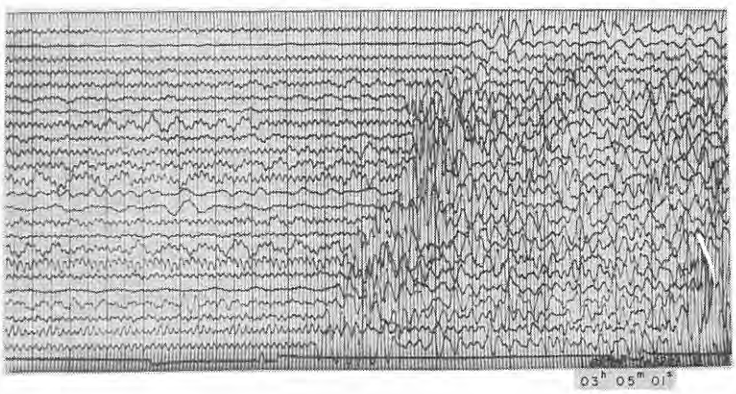

(21)

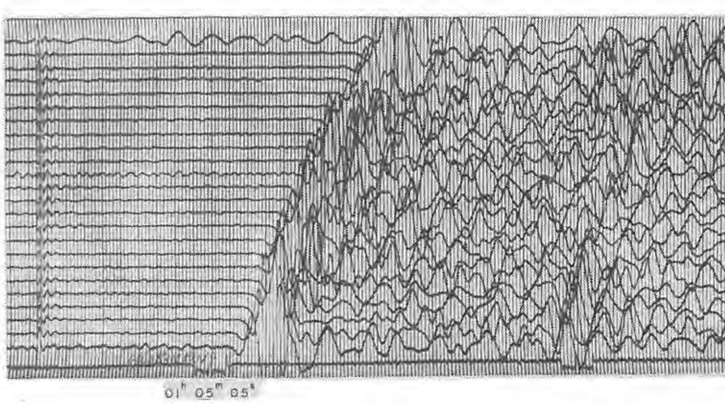

Fig. 6–7 Seismograms obtained (19) at E_4 and (20) at E_5 from the shot A–IV_1, and (21) at E_1 from the shot A–IV_2

(22)

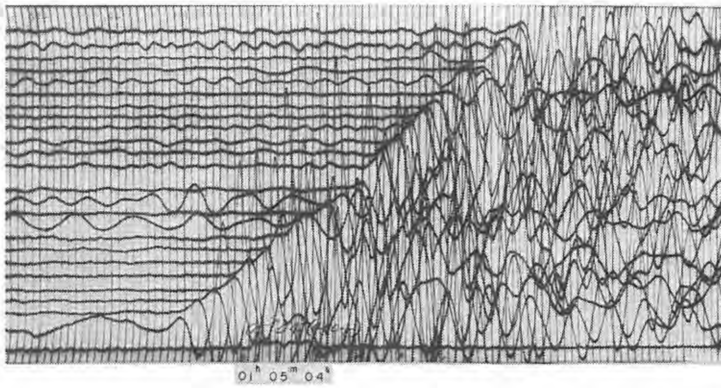

(23)

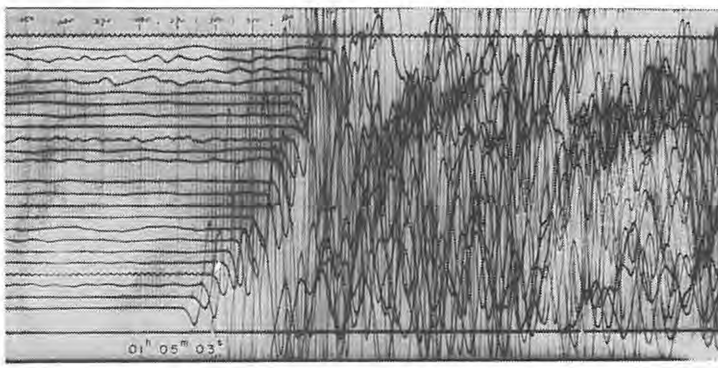

(24)

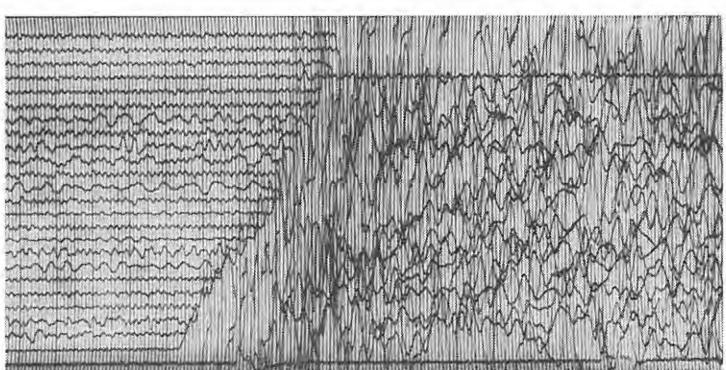

Fig. 6–8 Seismograms obtained (22) at E_2, (23) at E_3 and (24) at E_4 from the shot A–IV_2

(25)

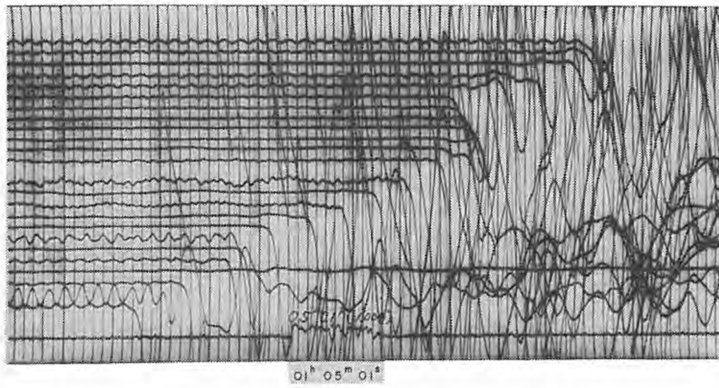

(26)

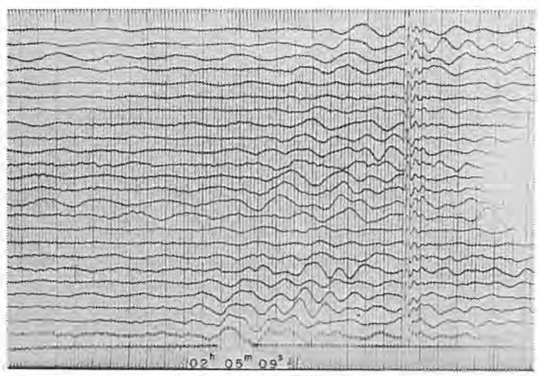

(27)

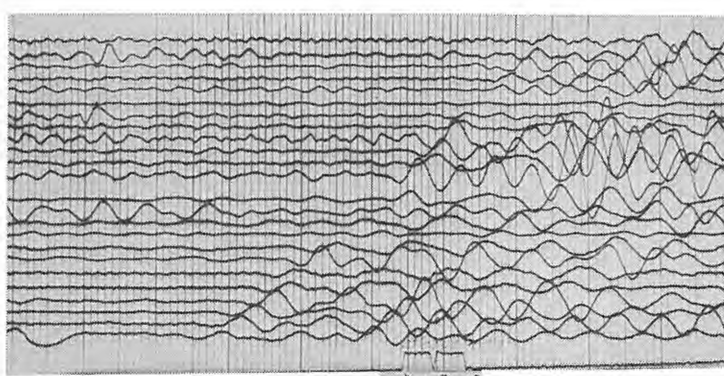

Fig. 6–9 Seismograms obtained (25) at E_5 from the shot A–IV_2, and (26) at E_1 and (27) at E_2 from the shot A–V_1

(28)

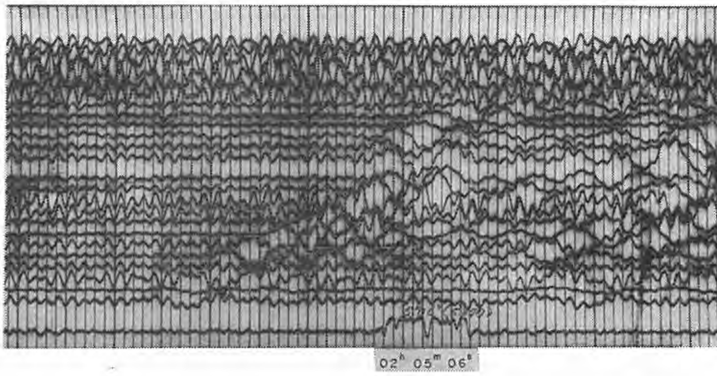

(29)

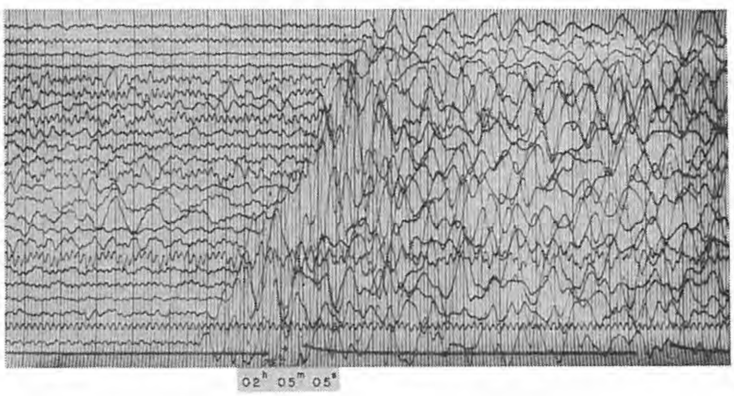

(30)

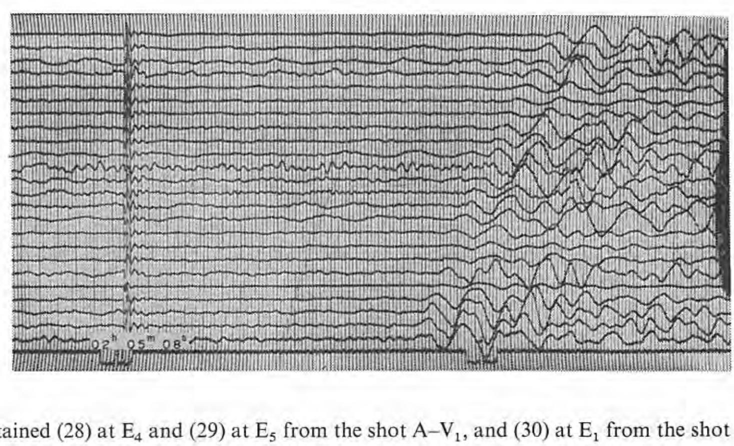

Fig. 6–10 Seismograms obtained (28) at E_4 and (29) at E_5 from the shot A–V_1, and (30) at E_1 from the shot A–V_2

(31)

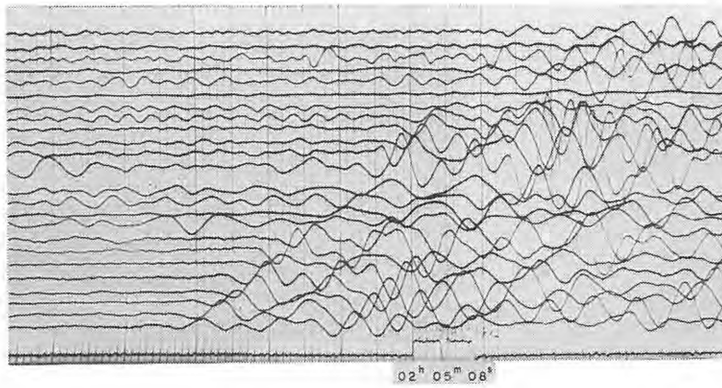

(32)

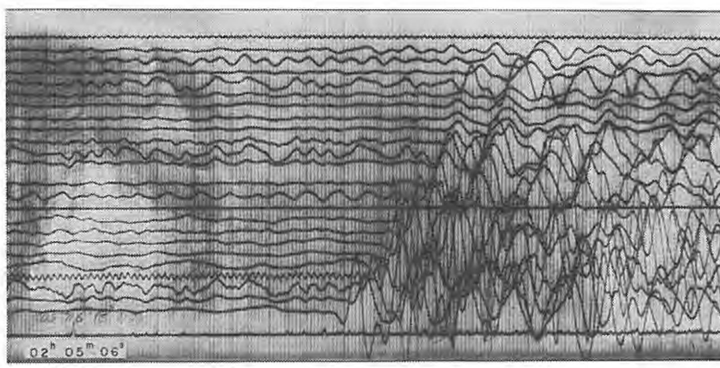

(33)

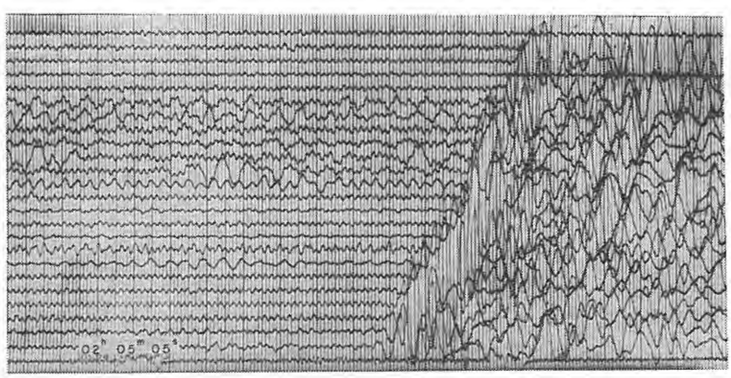

Fig. 6–11 Seismograms obtained (31) at E_2, (32) at E_3 and (33) at E_4 from the shot A–V_2

(34)

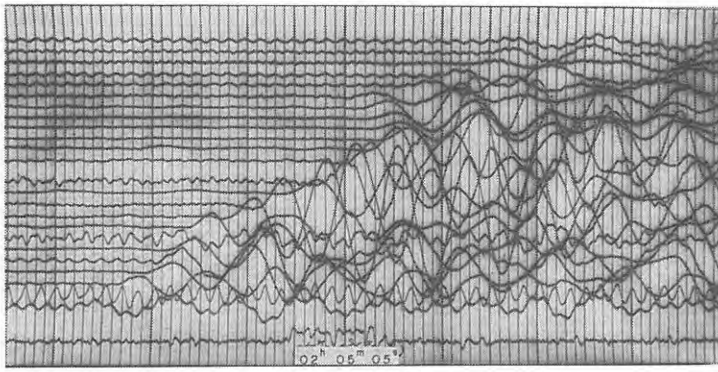

(35)

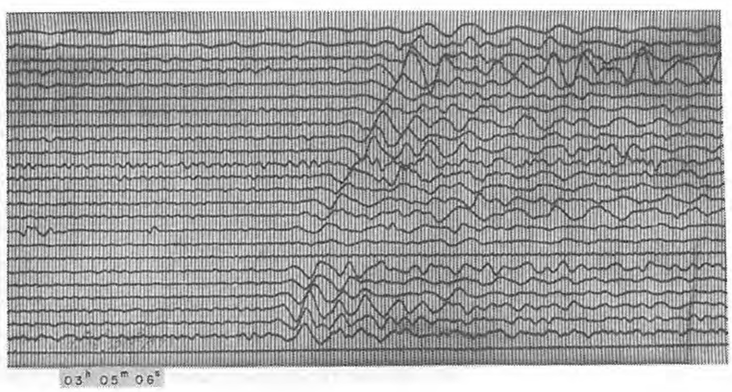

(36)

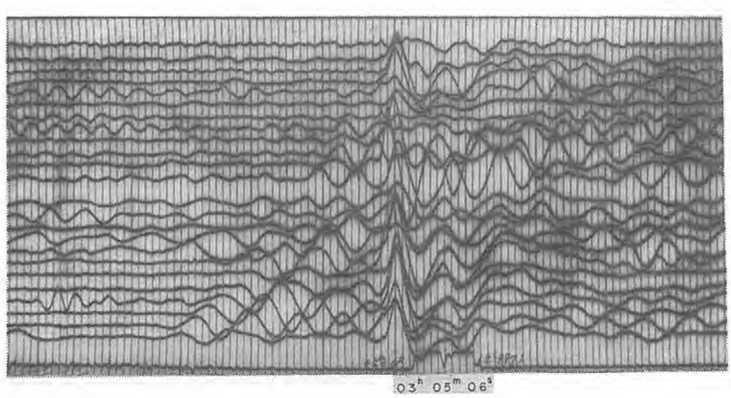

Fig. 6–12 Seismograms obtained (34) at E_5 from the shot A–V_2, and (35) at E_1 (A) and (36) at E_2 (A) from the shot B–IV

(37)

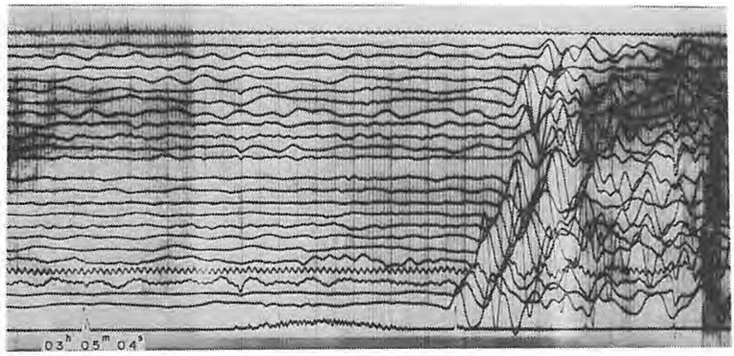

(38)

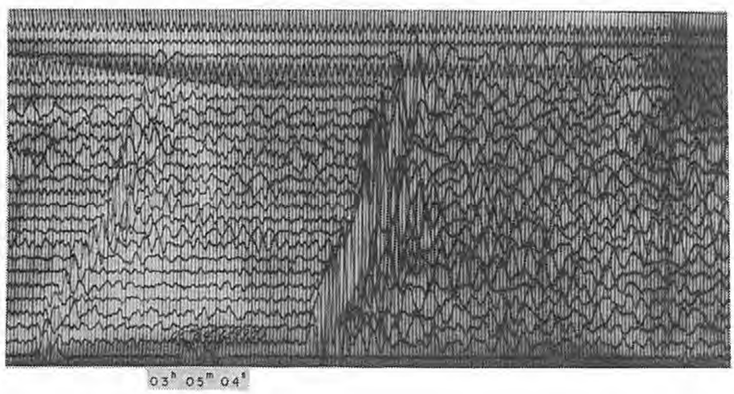

(39)

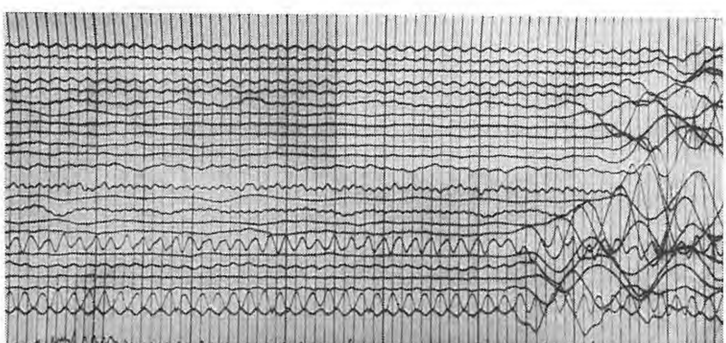

Fig. 6–13 Seismograms obtained (37) at E_3 (A), (38) at E_4 (A) and (39) at E_5 (A) from the shot B–IV

(40)

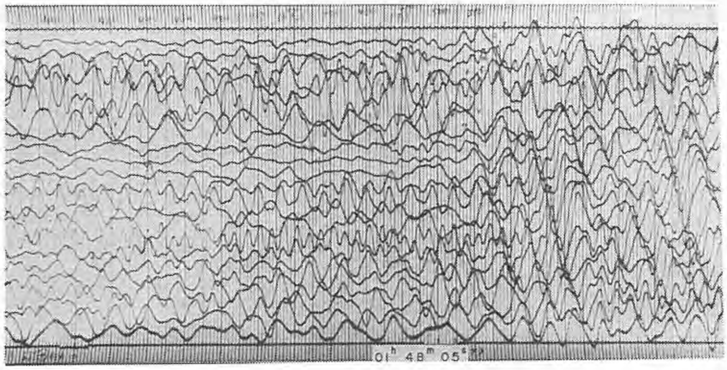

(41)

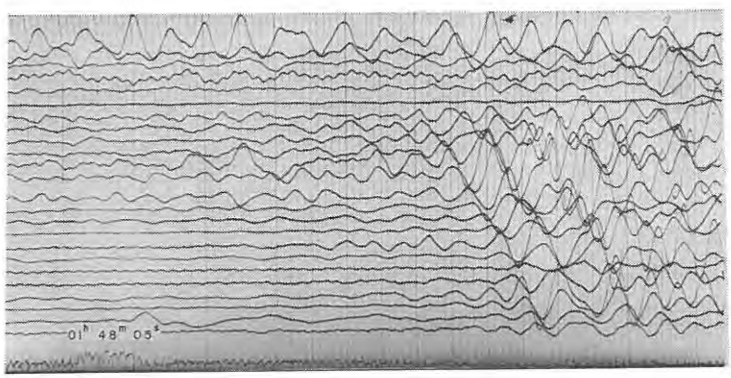

(42)

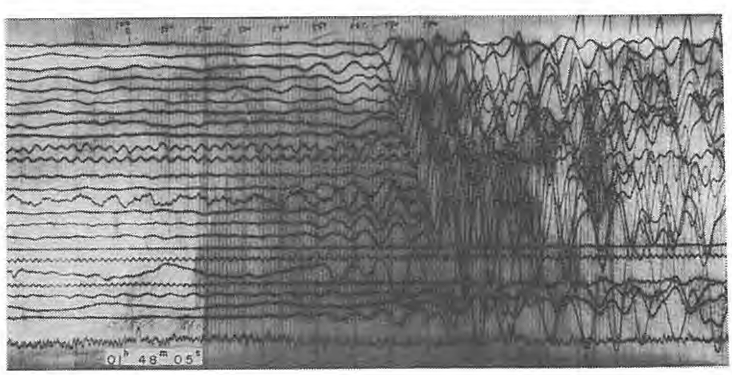

Fig. 6–14 Seismograms obtained (40) at E_1, (41) at E_2 and (42) at E_3 from the shot B–I

(43)

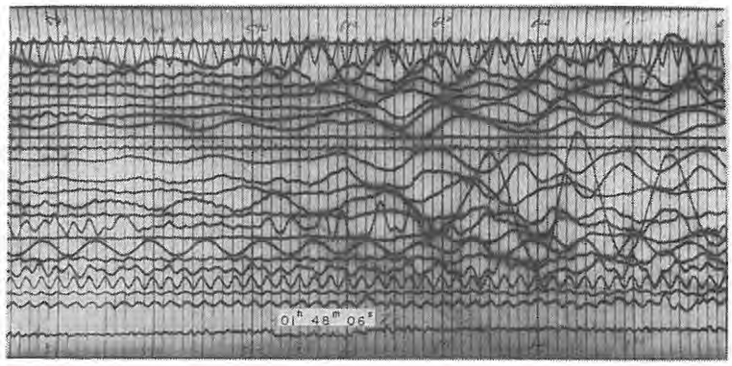

(44)

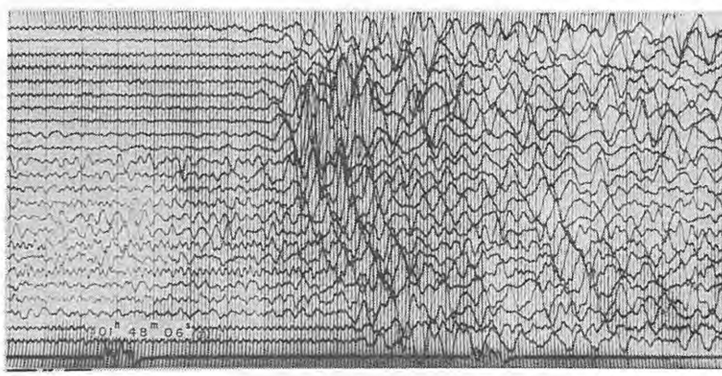

(45)

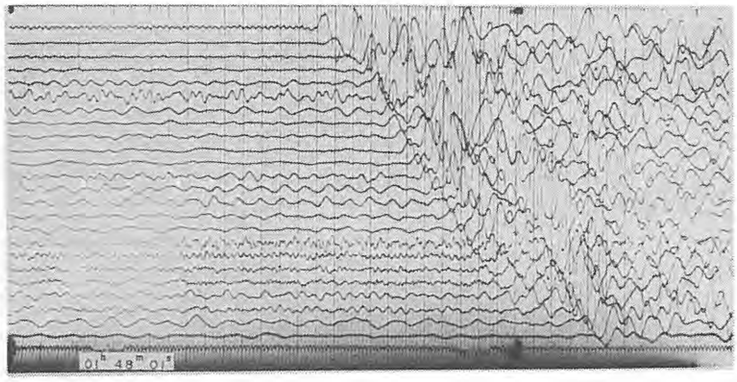

Fig. 6–15 Seismograms obtained (43) at E_4 and (44) at E_5 from the shot B–I, and (45) at E_1 from the shot B–II

(46)

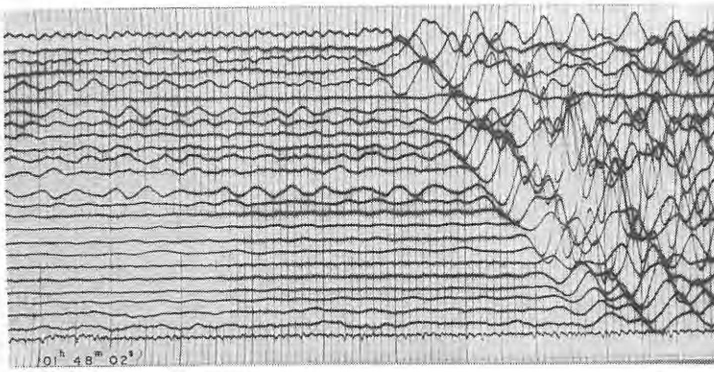

(47)

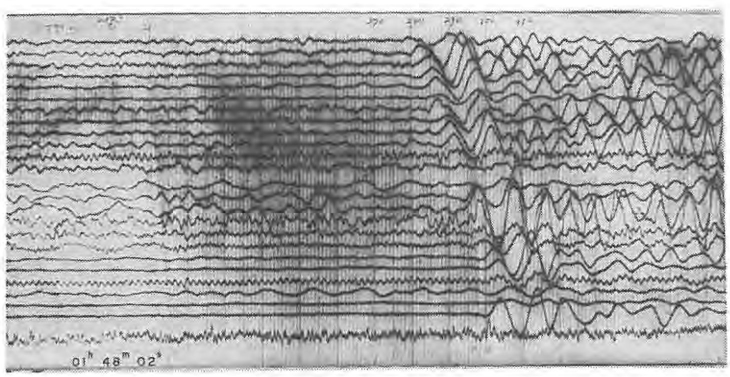

(48)

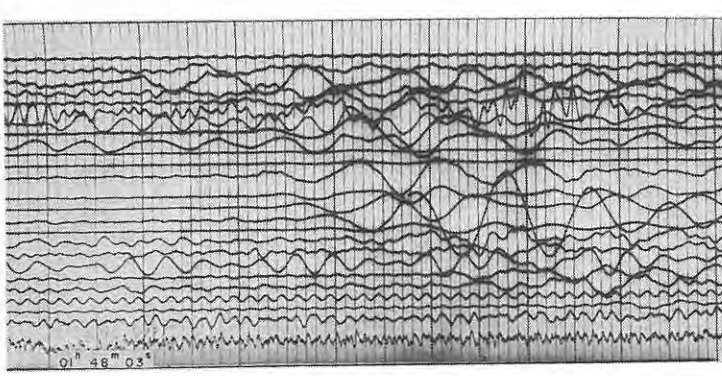

Fig. 6–16 Seismograms obtained (46) at E_2, (47) at E_3 and (48) at E_4 from the shot B–II

(49)

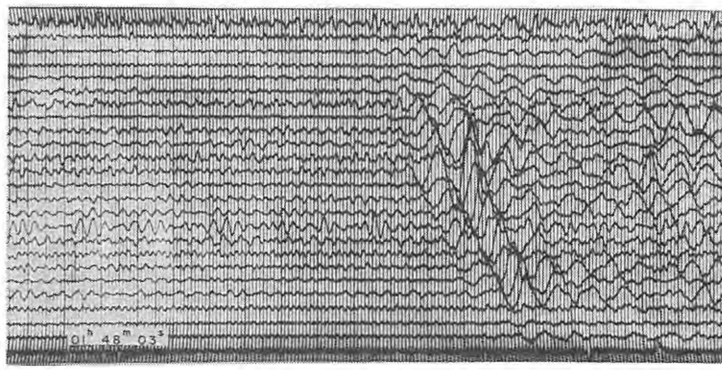

(50)

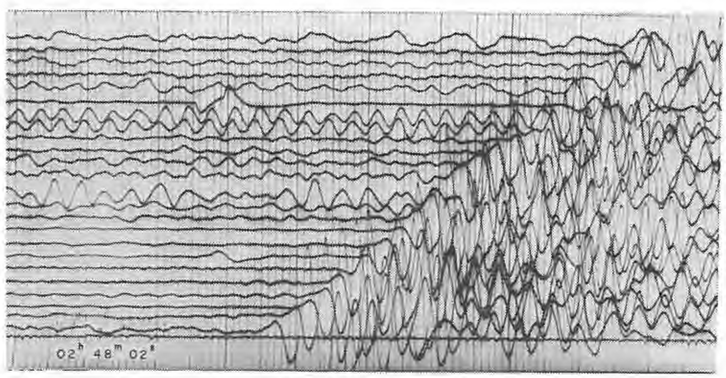

(51)

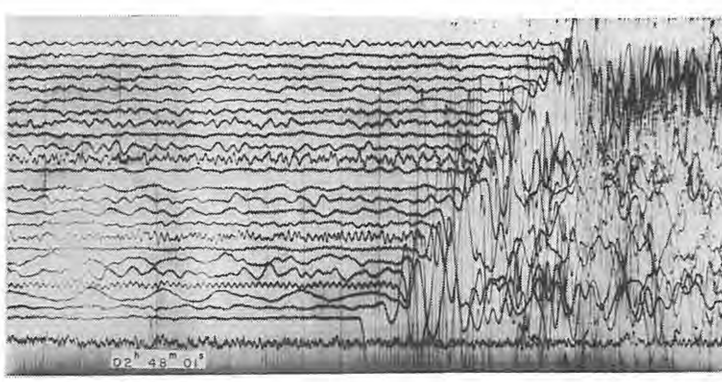

Fig. 6–17 Seismograms obtained (49) at E_5 from the shot B–II, and (50) at E_2 and (51) at E_3 from the shot B–III_1

(52)

(53)

(54)

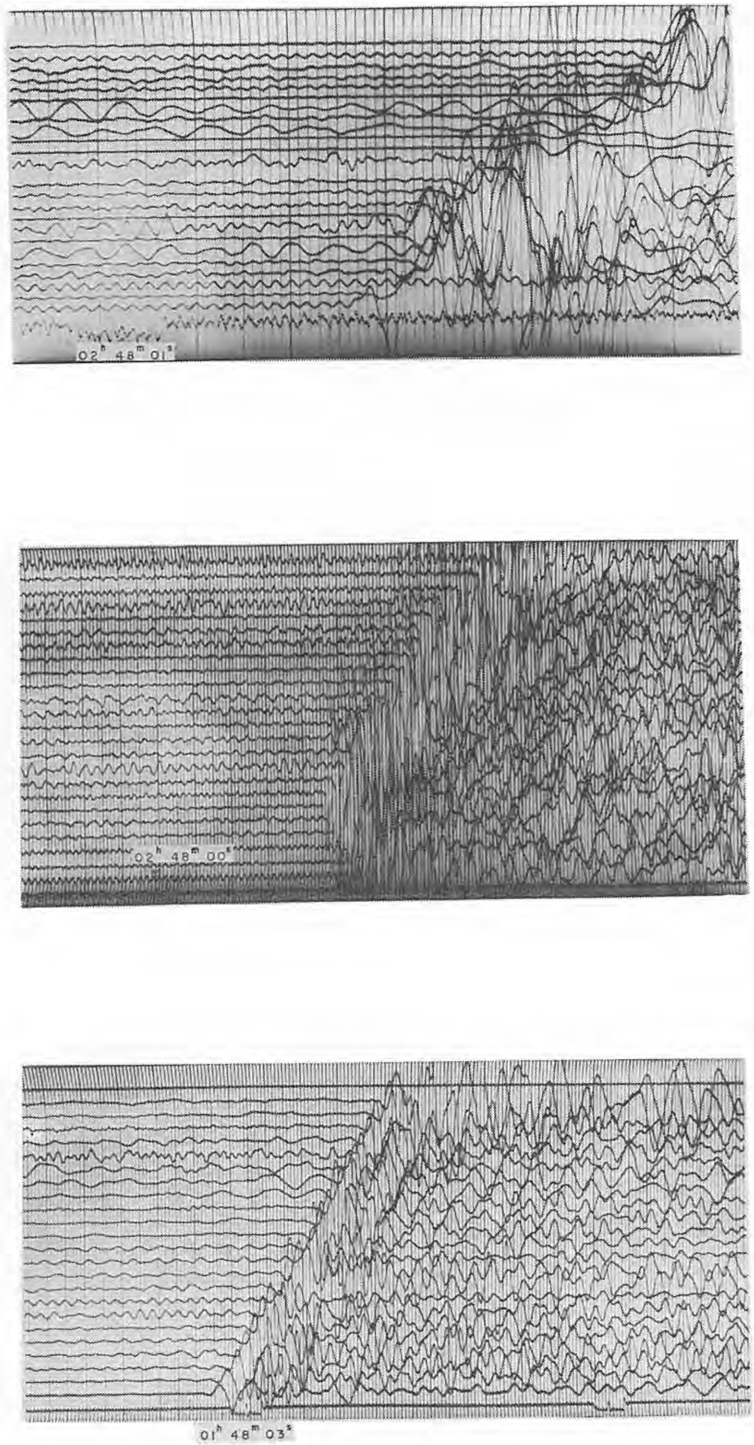

Fig. 6–18 Seismograms obtained (52) at E_4 and (53) at E_5 from the shot B–III_1, and (54) at E_1 from the shot B–III_2

(55)

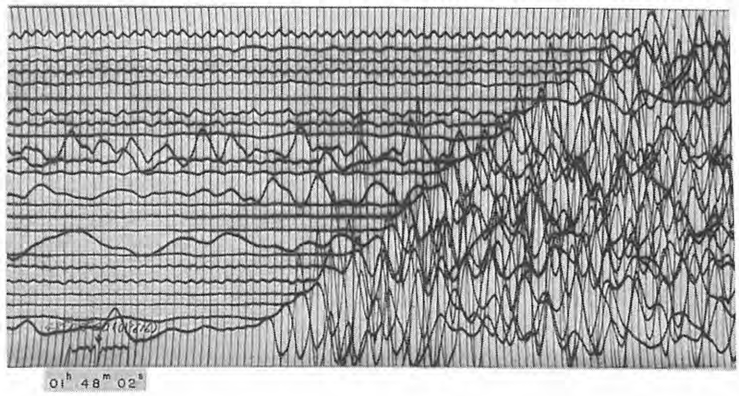

(56)

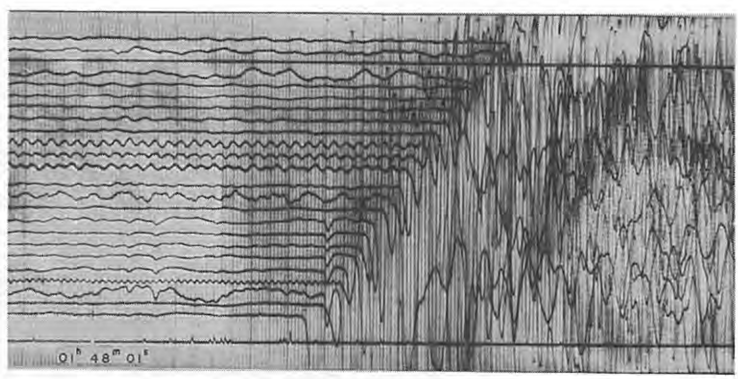

(57)

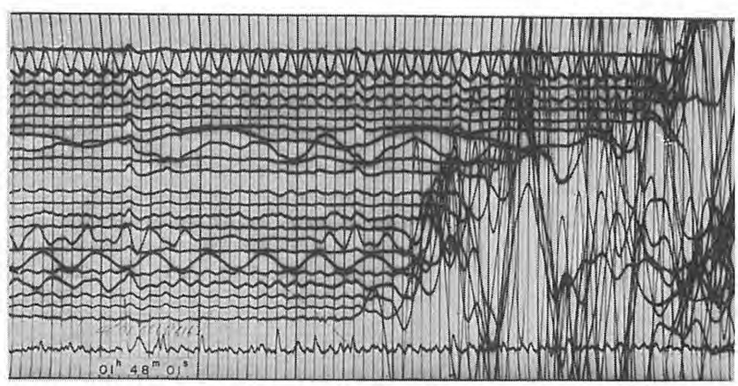

Fig. 6–19 Seismograms obtained (55) at E_2, (56) at E_3 and (57) at E_4 from the shot B–III_2

(58)

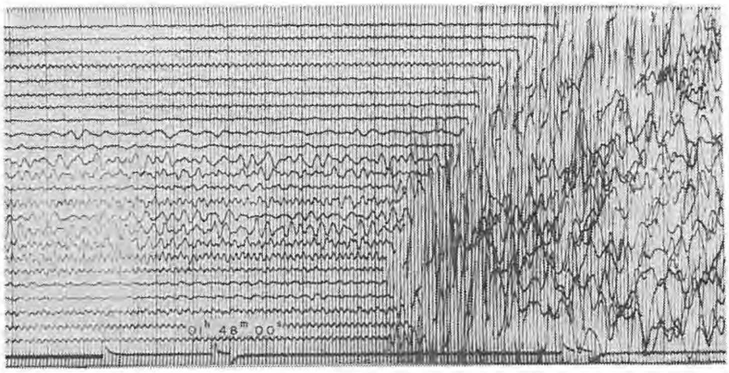

(59)

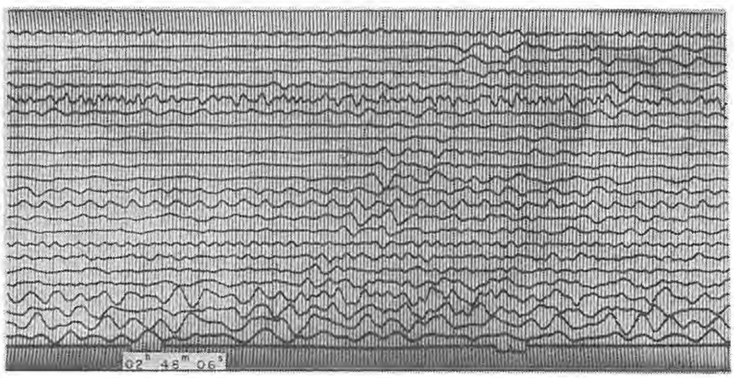

(60)

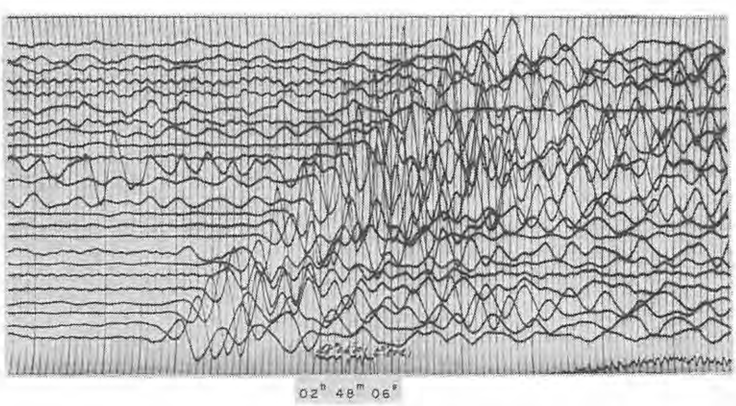

Fig. 6–20 Seismograms obtained (58) at E_5 from the shot B–III_2, and (59) at E_1 and (60) at E_2 from the shot B–IV

(61)

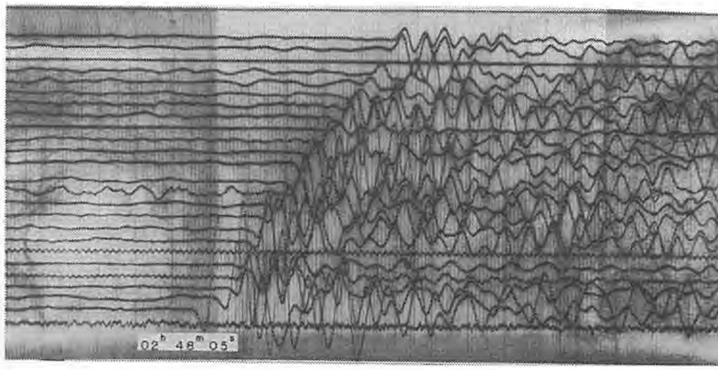

(62)

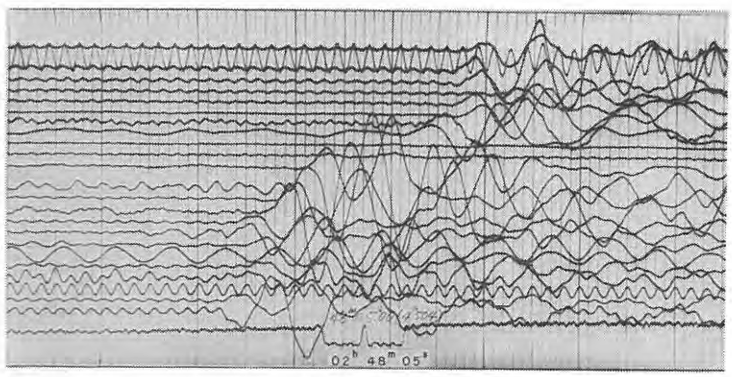

(63)

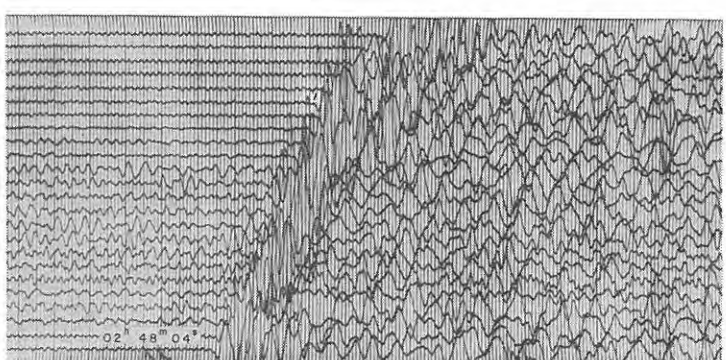

Fig. 6–21 Seismograms obtained (61) at E_3, (62) at E_4 and (63) at E_5 from the shot B–IV

(64)

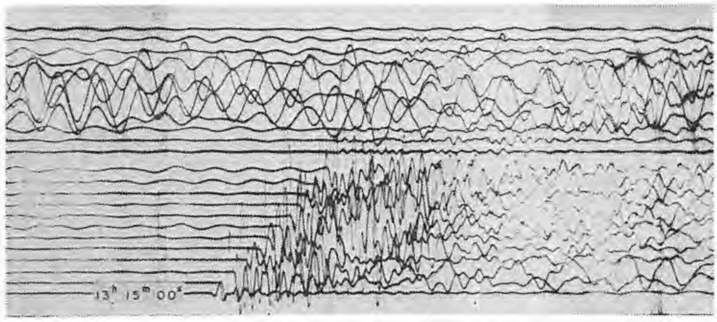

(65)

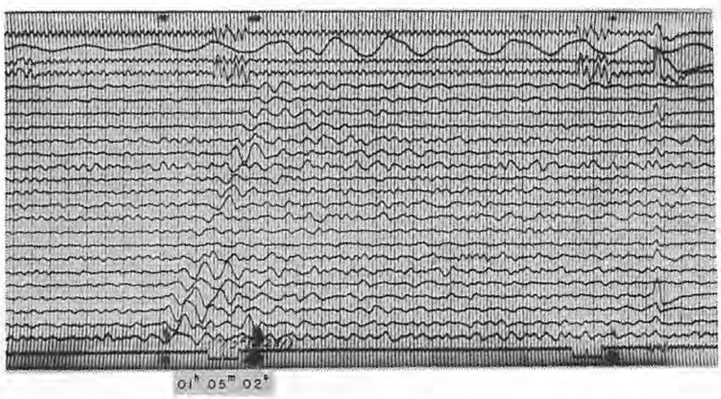

(66)

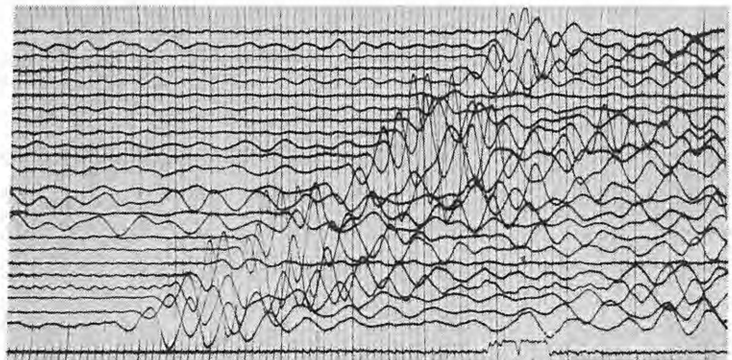

Fig. 6–22 Seismograms obtained (64) at E_3 from the shot A–III, and (65) at E_1 and (66) at E_2 from the shot E_3–W_1

(67)

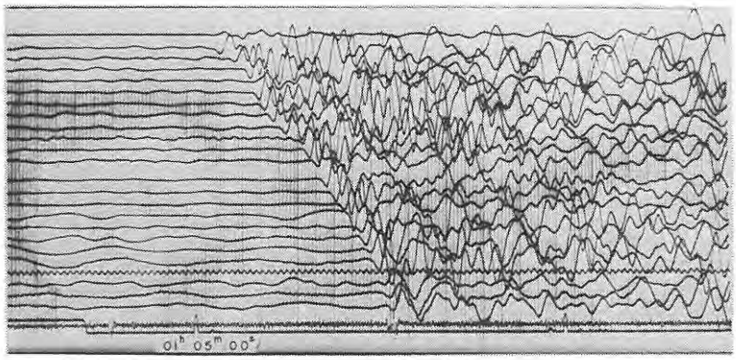

(68)

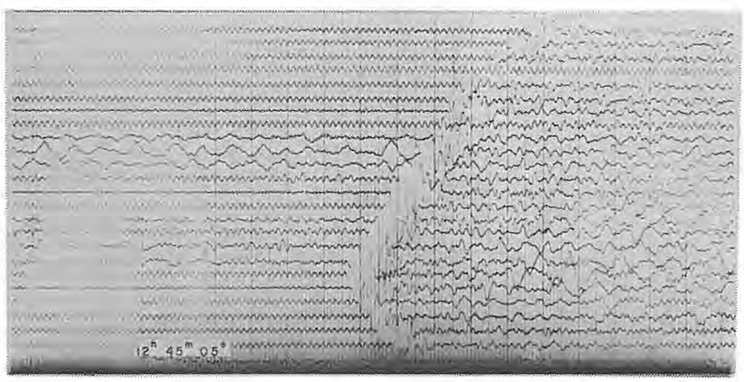

(69)

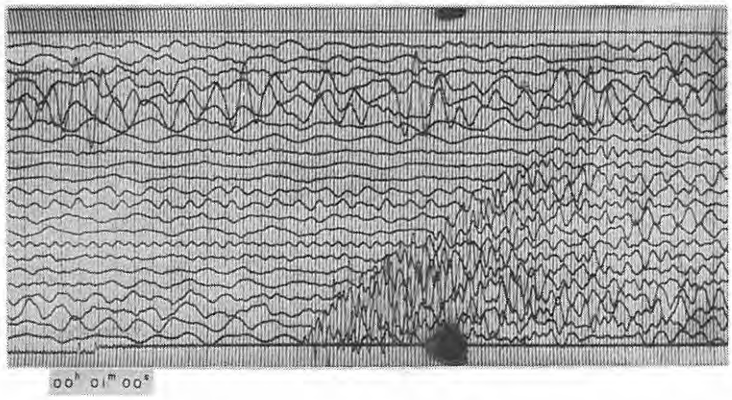

Fig. 6–23 Seismograms obtained (67) at E_3 from the shot E_3–W_1, (68) at E_5 from the shot B–III, and (69) at E_1 from the shot E_2–W_1

(70)

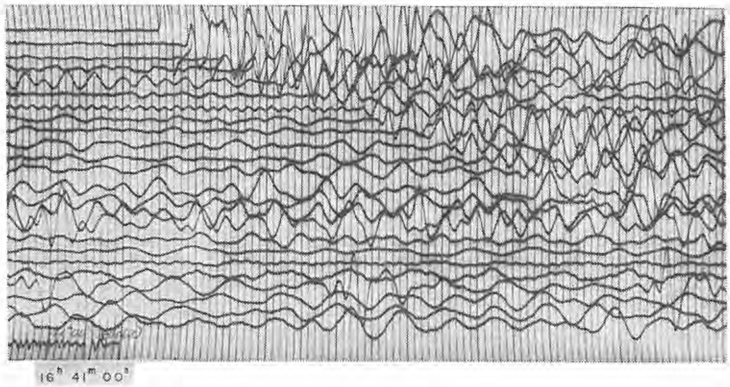

(71)

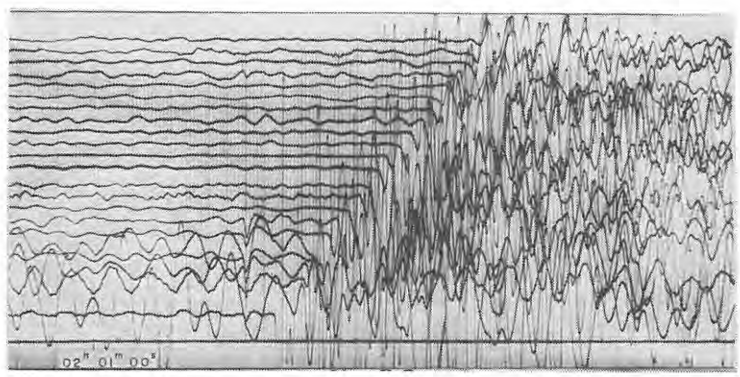

(72)

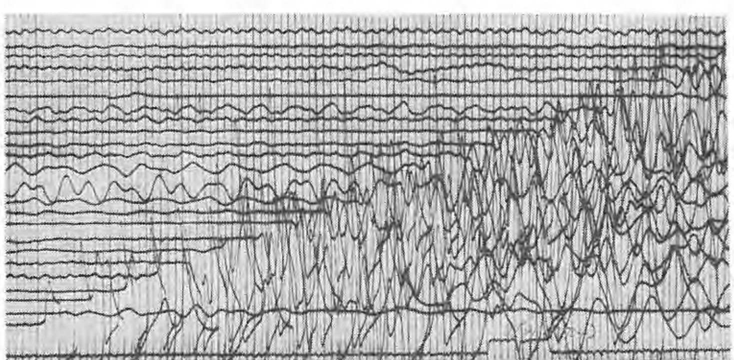

Fig. 6–24 Seismograms obtained (70) at E_2 from the shot E_2–W_1, (71) at E_2 from the shot E_2–W_2, and (72) at E_3 from the shot E_4–W_1

(73)

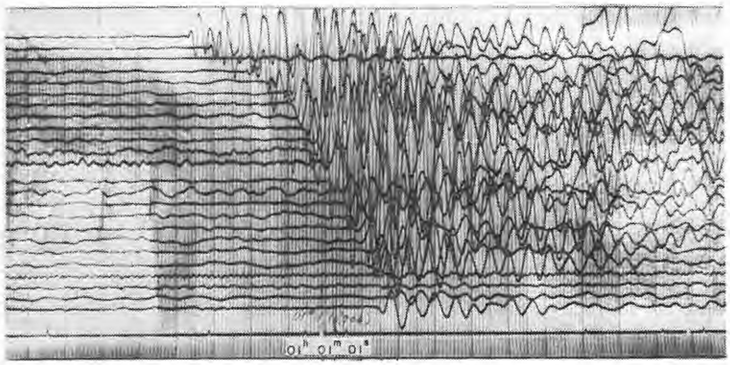

(74)

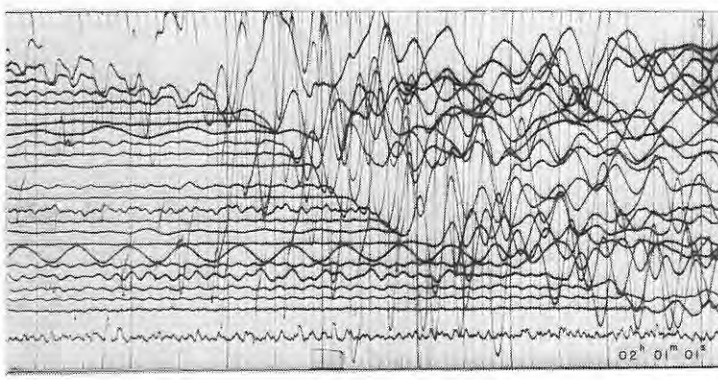

(75)

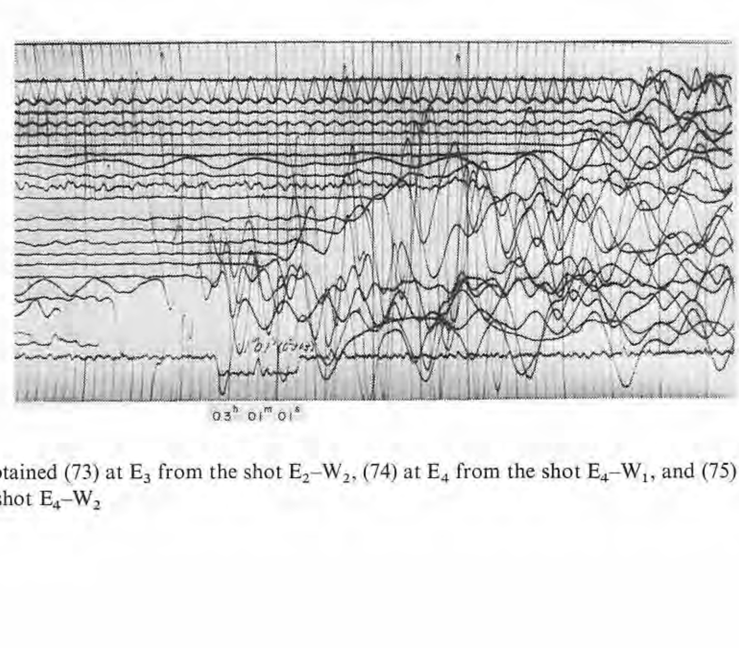

Fig. 6–25 Seismograms obtained (73) at E_3 from the shot E_2–W_2, (74) at E_4 from the shot E_4–W_1, and (75) at E_4 from the shot E_4–W_2

(76)

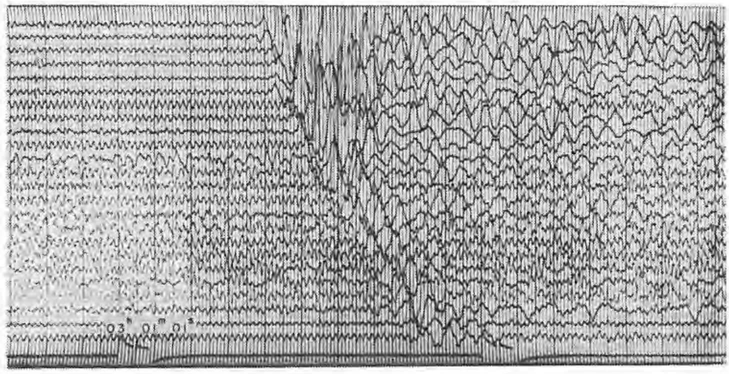

Fig. 6–26 Seismograms obtained (76) at E_5 from the shot E_4–W_2

松代群発地震域における爆破地震動の観測

浅野周三　市川金徳　岡田　広　窪田　将　鈴木宏芳
野越三雄　渡辺偉夫　瀬谷　清　乗富一雄　田治米鏡二

要　　旨

1967年11月14日 ― 12月7日の期間に，衰えたとはいえ活動中の松代群発地震の震源域を含む地域において，A，B 2測線上で爆破地震動の観測が実施された。本実験は，震源決定のための速度情報の追求に加え，活動中の震源域の物理的性状を知ることを目的とし，地質調査所を実施主体とし，国立防災科学技術センター，気象庁，北海道大学，秋田大学，東京大学地震研究所の協力により，磁気録音方式の観測班が14班組織され，各測線上に配置された。24成分地震探鉱器5台（うち2台は磁気録音装置付）による観測，爆破孔作孔，爆破作業および爆破時刻測定，爆破点，観測点の測量は宇部興産株式会社によって請負われた。A測線は地質学上の中央隆起帯の西端近くに設けられ，下高井郡山ノ内町より東筑摩郡四賀村に至る北東，南西の方向をとり，測線長約65.5 km，爆破点を5個所設けた。B測線はA測線と松代町北部で約63°の角度で交叉し，震源域中心部を横断するようにとられ，上水内郡戸隠村から上田市東部に至る約47 kmの測線長があり，爆破点を4個所設けた。薬量は171～499 kgが用いられ，深度30～45 m，内径10 cmの爆破孔，1～4本につめて爆破が実施された。

爆破地震動の観測は，すべてnoiseの少ない深夜に実施された。測線長が長いので，時刻は，爆破点，観測点ともJJY信号を用いた。記録は全体的に良好なものが得られ，とくに磁気録音方式による14班の記録は，ほとんどが明瞭な初動を与えた。よみとりに際してはA，B，Cの3つの階級にわけ，その精度や初動の質の良好度を示した。これらの観測および，その結果，得られた資料について報告する。

なお，この観測は科学技術庁特別研究促進調整費によって実施し得たことを付記して，感謝の意を表する。

550.24:550.348.05(521.52)

PART II

UNDERGROUND STRUCTURE IN THE MATSUSHIRO EARTHQUAKE SWARM AREA AS DERIVED FROM EXPLOSION SEISMIC DATA

By

Shuzo ASANO, Susumu KUBOTA, Hiroshi OKADA, Mitsuo NOGOSHI, Hiroyoshi SUZUKI, Kanenori ICHIKAWA and Hideo WATANABE

Underground Structure in the Matsushiro Earthquake Swarm Area as Derived from Explosion Seismic Data

By

Shuzo ASANO*, Susumu KUBOTA*, Hiroshi OKADA**, Mitsuo NOGOSHI***, Hiroyoshi SUZUKI†, Kanenori ICHIKAWA†† and Hideo WATANABE†††

Abstract

The underground structure in the Matsushiro Earthquake Swarm Area was derived from the data of explosion seismic observations in profiles A and B. First, the number of layers and the velocity in each layer are determined by using the T' curve. Then on the assumption that the dip of each interface is small, the structure of the first approximation was derived. The final models were derived by the method of trial and error so as to reduce (O−C), the difference between observed and calculated travel times.

Profile A

The underground structure consists of the following three layers on the whole:

the first layer:	1.6–2.3 km/s
the second layer:	3.3–4.75 km/s
the third layer:	5.9–6.0 km/s

Furthermore, in each section the following velocities are obtained.

1) The velocities derived from the observations near the shot points are as follows:

A-I	A-II	A-III	A-IV	A-V	
1.6	(<2.0)	2.3	2.3	(<1.9)	km/s

2) I-II

the first layer:	1.6–2.0 km/s
the second layer:	4.5 km/s
the third layer:	6.0 km/s

3) II-III

the first layer:	2.0–2.3 km/s
the second layer:	4.3–4.75 km/s
the third layer:	6.0 km/s

4) III-IV

the first layer:	2.3 km/s
the second layer:	4.3–4.75 km/s
the third layer:	6.0 km/s

5) IV-V

the first layer:	1.9–2.3 km/s
the second layer:	3.3–3.5 km/s
the third layer:	5.9 km/s

Profile B

In this profile the underground structure also consists of three layers, but there is a surface layer in some places.

the surface layer:	0.36–1.2 km/s
the first layer:	1.7–3.2 km/s

* Earthquake Research Institute, University of Tokyo. Asano was also a research associate of Geological Survey of Japan.
** Hokkaido University. Okada was also a research associate of Geological Survey of Japan.
*** Akita University.
† National Research Center for Disaster Prevention.
†† Geological Survey of Japan.
††† Japan Meteorological Agency.

the second layer:	4.0–4.4 km/s
the third layer:	6.0 km/s

The velocities in each section are as follows:

1) I-II

the first layer:	2.1–2.2 km/s
the second layer:	4.0 km/s

2) II-III

the surface layer:	0.36–1.2 km/s
the first layer:	1.7–3.2 km/s
the second layer:	4.0–4.4 km/s
the third layer:	6.0 km/s

3) III-IV

the first layer:	2.4–3.2 km/s
the second layer:	4.4 km/s
the third layer:	6.0 km/s

The underground structures derived by using above velocities are given in Fig. 2 for profile A and in Fig. 8 for profile B.

The underground structure in profile A, which is in the Central Belt of Uplift, one of geological blocks and is parallel to its strike, is relatively simple. Generally speaking, the top of the third layer (with the velocity of 6.0 km/s) is unusually shallow, about 1.5 km from the earth's surface even at the deepest, and has a tendency getting shallower a little toward the southwest. Or it may be said that the depth to the top of the third layer is smaller by 0.3–0.5 km in the portion from the middle of E_2 to D_8 than the other portions. The velocity in the third layer is 6.0 km/s northeast of Matsushiro and 5.9 km/s southwest of Matsushiro. There is a possibility of existence of anomalous structure or a fault between E_4 and E_5 although there are no observation points in this area because of the topography. This anomalous structure may correspond to the low Bouguer anomaly around Mt. Minakami.

The underground structure in profile B, which passes the central part of the epicentral area and crosses the Central Belt of Uplift, is fairly complicated. The velocity in the first layer is 1.7–3.2 km/s and this layer becomes thick abruptly near the Chikuma River toward the northwest. The velocity in the second layer is 4.0–4.4 km/s and it is noteworthy that the thickness of this layer increases by about 3 km almost discontinuously around the middle of E_1 near Nagano City. From another point of view, the top of the third layer becomes very shallow in the central part of the profile and reaches only about 1 km from the earth's surface. This interface becomes deep toward the southeastern end of the profile, so that the deep structure of the Central Belt of Uplift may be defined. At least the layer with the velocity of 6.0 km/s might be related to the formation of the Central Belt of Uplift, or it might be said that this layer played an important role for its formation. This profile passes the foot of Mt. Minakami at D_7 and the underground structure has anomaly near Mt. Minakami which may correspond to low Bouguer anomaly. There is a large possibility that the anomalous structure in this profile is of the same origin with that in profile A since the locations of anomalous structures are close with each other and their manners are quite similar. It is quite interesting that there exists anomalous underground structures in the area where Matsushiro swarm earthquakes occurred most frequently. Also it is interresting to note that there is no layer with the velocity of about 5.5 km/s in the area concerned.

On the other hand comparing the underground structure in this paper with results from other geophysical and geological investigations, several interesting relations are pointed out. That is, most of the swarm earthquakes have their foci within the layer of 6.0 km/s, the agreement between explosion seismic and geological structure is fairly good, especially the deep structure of the Central Belt of Uplift seems to be clarified, the anomalous structure near Mt. Minakami becomes certain and the structure derived from various methods agrees fairly well with each other.

I. Introduction

The Matsushiro Earthquake Swarm has been active for more than three years since August, 1965. The explosion seismic experiment on profiles A and B including the epicentral area (Fig.1) was conducted in the period of November 14—December 7, 1967 when the decreasing tendency of seismic activity has appeared. The purposes of this experiment are not only to obtain the velocity structure around the earthquake swarm area for the hypocenter determination but also to obtain the data on the relation between the underground structure and the earthquake swarm, on the physical status of the hypocentral region, and so on. In a separate paper[1)] the description of this experiment and the basic data obtained such as seismograms, travel times of initial P wave, etc. are presented. In this paper, the method of analysis with these data and the models of underground structure thus derived from these data will be presented.

II. Underground Structure Derived from the Explosion Seismic Data

In this paper, the number of layers and the velocity in each layer are estimated from T' travel time by the method of differences and the thickness of each layer is derived by using velocities thus obtained as usually done in the analysis of seismic prospecting data. The validity of this procedure for this length of profile has not been confirmed yet, but it is worth while applying this procedure.

Since there are five shot points, I-V, in profile A and four, I-IV, in profile B, various T' travel time curves are derived from various combinations of original travel times for each shot. Therefore the abbreviations are made for the sake of simplicity and shown together with those of other quantities in the following:

T(II):	original travel time from shot II,
T_2(III):	travel time of wave refracted through the second layer from shot III,
T'(II−V):	T' travel time derived by combining original travel times from shot II with those from shot V; $T'(\mathrm{II}-\mathrm{V})=T(\mathrm{II})-\frac{1}{2}\{T(\mathrm{II})+T(\mathrm{V})-T_{IIV}\}$ where T_{IIV} is the travel time observed at the shot point II for shot V or vice versa.
v_i:	the velocity in the i-th layer,
H_i:	the thickness of the i-th layer,
d_i:	the depth from the surface to the upper interface of the i-th layer,
T_i:	travel time of refracted wave propagating in the interface between the (i−1)-th and the i-th layers,
T'_i:	T' travel time indicating the true velocity of the i-th layer,
T'_{ij}:	T' travel times resulted from combination of waves of different types, for example, from combination of the refracted waves in the i-th layer and those in the j-th layer
(e_i):	$T_i-T'_i$
θ_{ij}:	the angle of incidence to the i-th layer for refracted waves in the j-th layer,
II−IV:	the section between shot points II and IV.

The assumption of small inclination of each interface, cos $\omega\approx1$ (ω: angle of inclination), is made so that the formula

$$T_n-T_n'=(e_n)=\sum_{i=1}^{n-1}H_i\cdot\frac{\cos\theta_{in}}{v_i} \qquad (1)$$

is applied for estimation of thickness in each layer where $\cos\theta_{in}=\{1-(v_i/v_n)^2\}^{1/2}$. If the T' travel time curve for some observation stations shows only an apparent velocity, the T' travel time curve from the adjacent observation stations indicating a true velocity is extrapolated as done in the usual procedure. Otherwise, T' travel time at each observation station is mainly used for the derivation of underground structure.

In the following, first the velocity for each layer will be determined with T' travel time through each profile and most prohable underground structure will be derived after various models of underground structure are examined based upon the velocity obtained.

II.1 Velocity for each layer in profile A

For the analysis, the *T'* travel time curve is constructed with all possible combinations of shot points through the profile. The important *T'* curves are shown together with the ordinary travel time curve in Fig. 2. In the travel time curve of Fig. 2 for profile A (Fig. 8 for profile B), the distance projected to the line connecting shot point A-I (B-I for profile B) with shot point A-V (B-IV for profile B) and the corresponding corrected travel times are used. It is found through the arrangement of various velocities obtained with these *T'* curves the underground structure in profile A consists of three layers as a whole. That is,

the first layer (surface layer):	1.6–2.3 km/s
the second layer:	3.3–4.75 km/s
the third layer:	5.9–6.0 km/s

The layer with the velocity of about 5.2 km/s seems to exist from parts of *T'* curves between the second and the third layers. However, the existence of this layer is not so certain from the quality of data that this layer is not taken into account in the analysis.

The existence of the second and the third layers are certain over the whole profile, but that of the first layer (the surface layer) depends on the locality. Since the velocity measurement in the surface layers was carried out only in the spread E_3, the structure of the first layer was not derived accurately in some of places other than the spread E_3. Thus this uncertainty in the determination of structure of the first layer affects the derivation of structure deeper than the first layer. Therefore, the structure below the first layer is examined on the several possible assumptions about the structure of the first layer.

Also there are some places where the velocity in the second layer could not be determined accurately. In such places, the examination of structure was made by assuming probable values for the velocity in the second layer.

1) Velocity in the first layer

The observations by three to five geophones were conducted within about 150 m from each shot point. The travel time curves for each shot are shown in Fig. 3. The velocities near shot points A-II and A-V in this figure are almost the same with that of the second layer estimated in the later stage. This implies that the first layer near these shot points is very thin and it is hard to obtain the velocity in the first layer from this observation. Therefore, the velocity obtained by dividing the distances of the nearest observation point from the center of shot holes with corresponding observed travel times is assumed as that in the first layer at each shot point. These values may give the upper limits of the velocities in the first layer.

The travel time curve near the shot point A-III gives a somewhat large value of intercept time in comparison with other curves. This shows that the layer with a velocity smaller than 2.3 km/s is relatively thick. From quantitative examination, the layer with the velocity of 0.94 km/s is about 15 m (intercept time 0.031 sec) in thickness on the second layer with the velocity of 2.3 km/s. The value 0.94 km/s is obtained by dividing the distance of the nearest observation point with the travel time of the initial P wave there. The delay due to this surface layer for possible refracted waves is less than 0.02 sec, which can be neglected by taking the accuracy of identification of initial P waves into account. Therefore, in the later analysis the value of 2.3 km/s is assumed to be the velocity of the first layer near the shot point A-III.

The velocities of the first layer thus obtained are shown as follows:

Shot point:	A-I	A-II	A-III	A-IV	A-V
Velocity in the first layer (km/s):	1.6	(<2.0)	2.3	2.3	(<1.9)

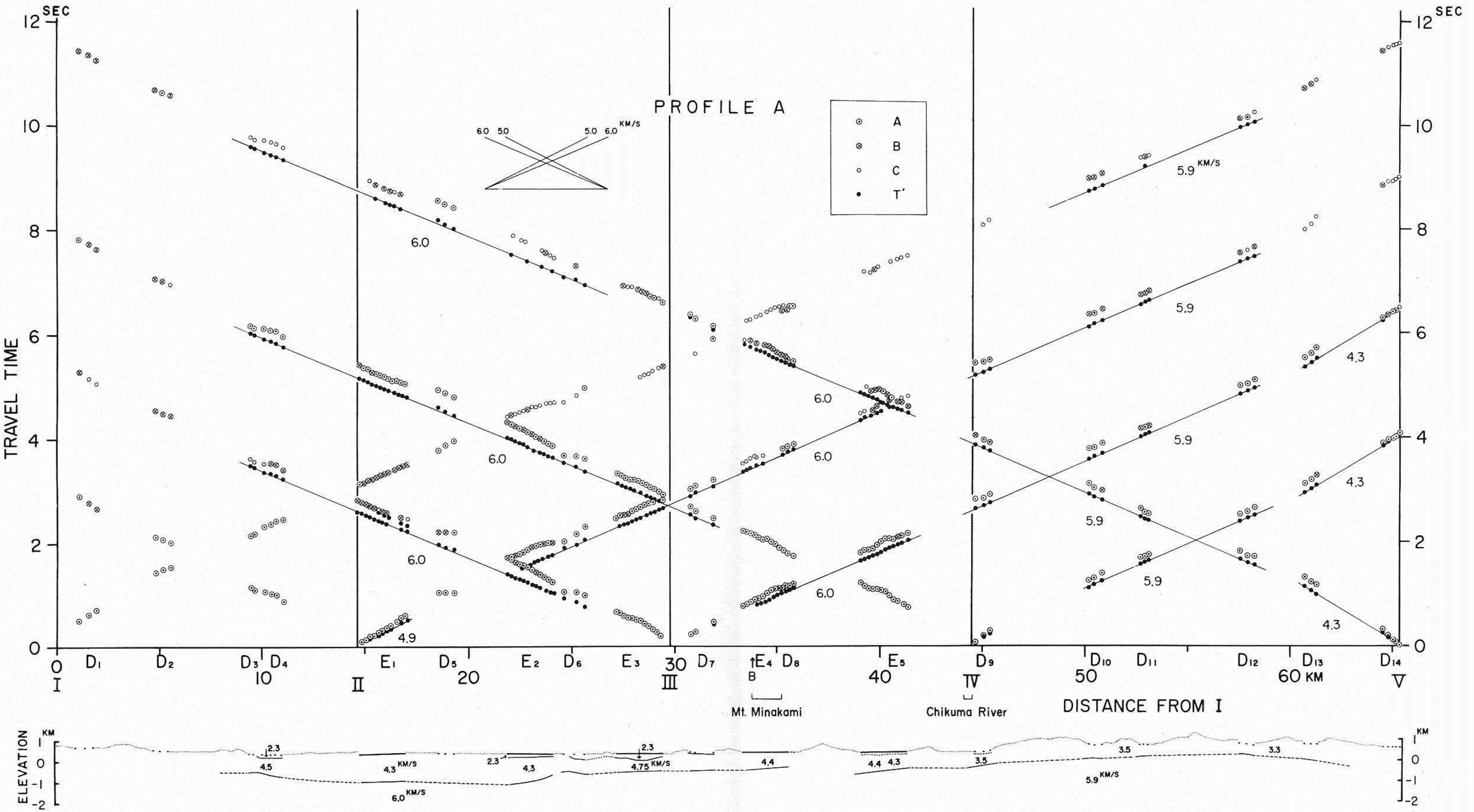

Fig. 2 Travel time curves and the underground structure derived for profile A

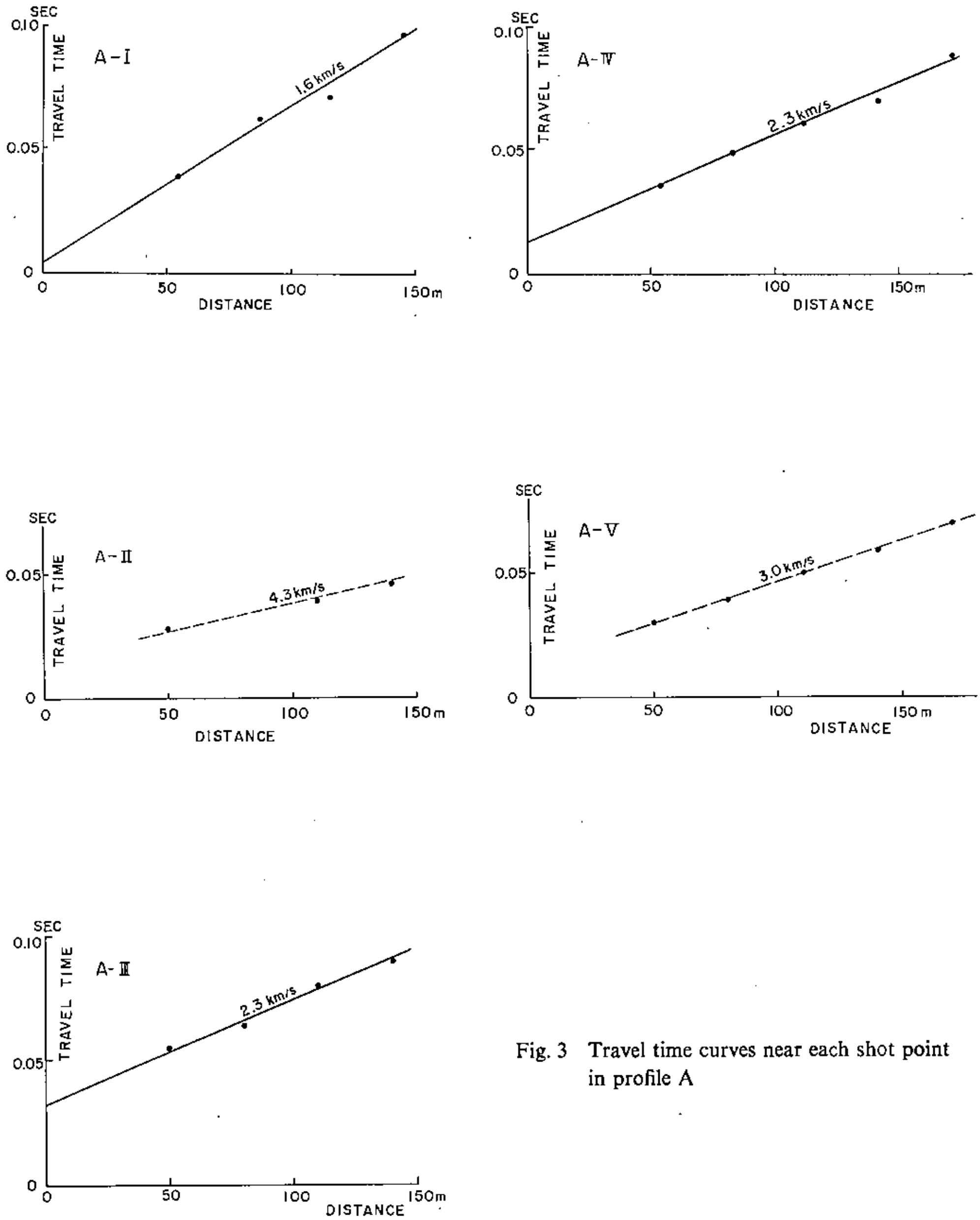

Fig. 3 Travel time curves near each shot point in profile A

2) I-II

T'(I—III) and T'(I—IV) at D_3 and D_4 agree with the extension of corresponding T' at E_1 and E_2 and give the velocity 6.0 km/s. While the gradient of T'(I—II) at D_3 and D_4, 1/(5.2 km/s), differs from that of T'(I—III) and T'(I—IV). Therefore, T(II) at D_3 and D_4 is regarded as travel time of the seismic wave propagating in the layer different from the layer in which the initial P wave travels from shot points III and IV to D_3 and D_4. Also the apparent velocity of T(III) and T(IV) in this section is approximately 6.0 km/s. Thus the velocity 6.0 km/s on the T' curve is interpreted as a true velocity. Then the apparent velocity of 5.2 km/s on T'(I—II) is interpreted as derived from the combination of two true velocities, that is, 6.0 and 4.5 km/s. If the distance of D_3-a, b from the shot point A-II is divided by the corresponding travel time on trial, the velocity 4.5 km/s is obtained and agrees well with the velocity obtained above. While the first layer seems to be very thin near the shot point A-II as mentioned in **1)** of **II.1.** These points show that T(II) at D_3-a, b is T_2(II), travel time of wave refracted at the upper boundary of the second layer, and the first layer at D_3-a, b is very thin. Also from the measurements of surface velocity near the shot points A-I and A-II, the velocity 1.6 km/s near A-I and the value smaller than 2.0 km/s near A-II are obtained.

The underground structure in the range I-II is thus revealed to consist of three layers and the velocity of each layer is as follows:

the first layer:	1.6–2.0 km/s
the sceond layer:	4.5 km/s
the third layer:	6.0 km/s

3) II-III

The T'(I—IV) curve over the whole section and the T'(I—III) curve in this section except for the part of the spread E_3 coincide with the extension of T' curve at D_3 indicating the velocity of 6.0 km/s as pointed out in **2)**. Although T'(I—IV) at the spread E_3 gives the velocity slightly higher than 6.0 km/s, the velocity in the third layer is estimated to be 6.0 km/s in general.

The velocities in the first (surface) layer and in the second layer are determined from T(II) and T'(II—III) at the spread E_1 and from the measurement of surface velocity at the spread E_3.

The travel time curve from the shot for the measurement of surface velocity at the spread E_3 and the results thus obtained are shown in Fig. 4. The velocity 4.75 km/s in the second layer is derived from the T' curve. The velocity in the first layer is 2.3 km/s as mentioned in **1)** of **II.1.** The structure near the surface at the spread E_3 derived is shown in Fig. 4 with the travel time curve. The depth of the upper interface of the second layer is about 350 m, the deepest in the middle of the spread E_3 and about 200 m, the shallowest on both sides of the spread E_3. When the structure of U-type as shown in Fig. 4 is derived, there are two possibilities to introduce this kind of structure by mistake. First, it is possible to misinterprete the real direct wave near the shot point as the wave refracted at the upper interface of the second layer. Second, it is also possible to misinterprete the real refracted wave at the upper interface of the third layer as the wave refracted at the upper interface of the second layer in the distance far from the shot point. The first possibility is rejected since the velocity about 3.2 km/s is obtained from the data near the shot point A-III and the velocity about 3.6 km/s, from the data near the shot point E_3-W_1. These values of velocity support the surface structure in Fig. 4.

As regards the second possibility, the data only at the spread E_3 are not sufficient. Then the T' travel time is computed by combining the observed data from the shot E_3-W_1 at the spread E_2 with those at the spread E_3, which is shown in Fig. 5. Travel times at the spread E_2 are assumed to fit to the extension of travel time curve at the spread E_3 although there might be slight difference in the underground structure at E_2 and E_3. Then if the seismic wave observed at distant points were the refracted wave in the third layer, the value of velocity larger than 4.75 km/s could be obtained from the T' curve. Therefore the second suspicion can be safely rejected because of 4.4 km/s for the T' curve shown in Fig. 5.

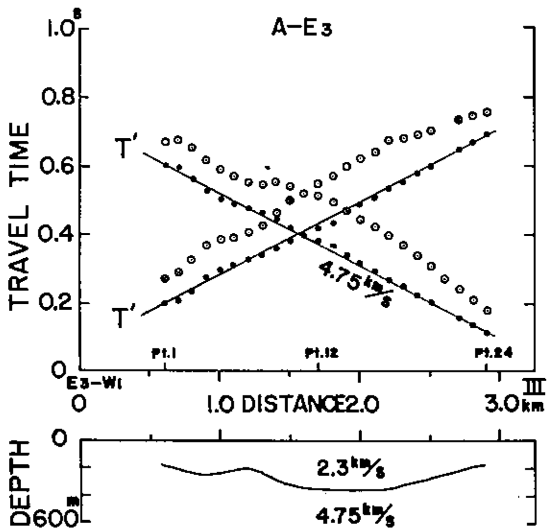

Fig. 4 Travel time curves from the measurement of surface structure at the spread E_3 (above) and the surface structure derived (below).

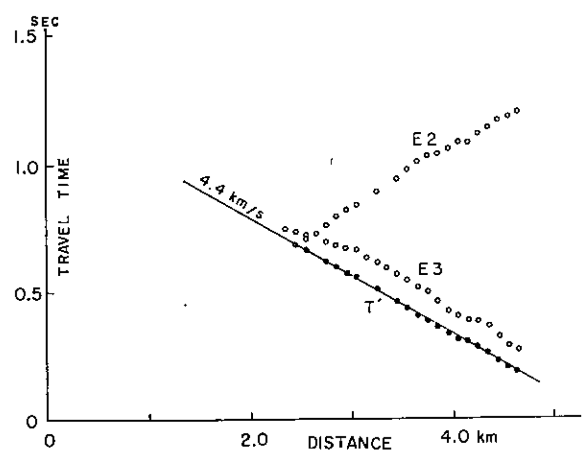

Fig. 5 Travel time curve from the data at E_2 and E_3 for the small shot at E_3–W_1

The value of velocity in the second layer depends on the observation sites. The value 4.3 km/s is obtained at the spread E_1 by combining the apparent velocity of T'(II—III) curve with v_3(=6.0 km/s) and also at the spread E_2 by the travel times from the shot E_3-W_1. While 4.75 km/s is derived at the spread E_3 from the measurement of surface velocity as discussed above.

In summary

the first layer:	2.0–2.3 km/s	(Fig. 3)
the second layer:	4.3–4.75 km/s	
the third layer:	6.0 km/s	

4) III-IV

T'(II–IV), T'(II–V) at observation sites, D_7, E_4 and D_8 and T'(III–V), T'(II–V) etc. at the spread E_5, all these show the gradient 1/(6.0 km/s) in the travel time curves. In the range from D_7 to E_5 the T'(II–V) curve is a straight line with the gradient 1/(6.0 km/s). Thus it is concluded that the velocity in the third layer is 6.0 km/s.

There are no data suitable for estimating the velocity in the second layer in this section, but the apparent velocity of original observed travel time at D_7 from the shot III is 4.7 km/s. Since this value of apparent velocity is almost equal to the velocity in the second layer at the spread E_3, 4.75 km/s, the second layer is assumed to have uniform velocity in the range D_7–E_3. Profile A intersects profile B at a point in the spread E_4. In profile B, there is the measurement of surface velocity at the spread E_4, from which the value 4.4 km/s is obtained for the velocity in the second layer. Therefore, the velocity in the second layer changes between D_7 and E_4.

In this range III-IV no special measurement of surface velocity was carried out. However, since there are systematic variations in whole observed travel times at the spread E_4 and E_5, it is dangerous to neglect the structure of the first layer. However, the lines which fit to the travel time curves observed at the spreads E_4 and E_5 give the small value of intercept time, about 0.02 sec. This implies that the thickness of the first (surface) layer is as a whole very small in this area. Also the time difference between the lines mentioned above and the observed values can explain the systematic variation of travel times mostly as the effect of the structure in the first layer by taking the direction of approach of seismic wave into account. Therefore, to evaluate the depth to the upper interface of the third layer the effect of the first layer can be safely neglected.

In summary

the first layer:	2.3 km/s	
the second layer:	4.3–4.75 km/s	(Fig. 3, Fig. 4)
the third layer:	6.0 km/s	

5) IV-V

T'(IV–V) and T'(III–V) from D_{10} to D_{13}-a give the lines with the gradient of 1/(5.9 km/s) and T'(III–V) at D_9 fits to the extension of the T'(III–V) curve. Therefore, the value of velocity in the third layer is estimated to be 5.9 km/s.

As regards the velocity in the second layer there are no data suitable to estimate its value. However, the line through observed values of the shot A-IV at D_9-b and D_9-c gives 3.5 km/s. Furthermore the value of 3.3 km/s for v_2 is obtained by combining the apparent velocity 4.3 km/s given by T'(IV–V) and T'(III–V) at D_{13}-b, c, D_{14}-a, c, d with the velocity 5.9 km/s in the third layer. This value 3.3 km/s is close to 3.5 km/s at D_9 obtained above. Also the value 3.0 km/s is obtained with observations near the shot point V (Fig. 3). Therefore, the velocity in the second layer is estimated to be 3.3–3.5 km/s except for the region of D_{10}, D_{11} and D_{12}.

Since the observation sites are in the mountains except for the area near D_{14}, it might be unnecessary to take the surface layer with low velocity 1.5–2.0 km/s into account in the analysis.

In summary

the first layer:	1.9–2.3 km/s	(Fig. 3)
the second layer:	3.3–3.5 km/s	
the third layer:	5.9 km/s	

6) Evaluation of error in the analysis*

In this section, the error of the analysis introduced by making use of formula (I) is examined. As mentioned above, the underground structure consists of two or three layers. The depth to the upper interface of the third layer is given in the following.

* Although the same kind of consideration was made by TAZIME[26], the method can not be applied to the present analysis.

Putting

$$\xi = v_1/\cos\theta_{12},\ \eta = v_2/\cos\theta_{23} \text{ and } \zeta = v_1/\cos\theta_{13} \tag{2}$$

into the equation (1),
where

$$\cos\theta_{ij} = \{1-(v_i/v_j)^2\}^{1/2}$$

then

$$\left.\begin{aligned} H_1 &= \xi\cdot(e_2) \\ H_2 &= \eta\cdot(e_3) - \frac{\xi\eta}{\zeta}(e_2) \end{aligned}\right\} \tag{3}$$

where $(e_2)=0$ if there is no surface layer. Then

$$d_3 = H_1 + H_2 = \eta\cdot(e_3)\cdot\left\{1+\xi\cdot\left(\frac{1}{\eta}-\frac{1}{\zeta}\right)\cdot\frac{(e_2)}{(e_3)}\right\} \tag{4}$$

Putting

$$K = 1+\xi\cdot\left(\frac{1}{\eta}-\frac{1}{\zeta}\right)\cdot\frac{(e_2)}{(e_3)}, \tag{5}$$

$$d_3 = \eta\cdot K\cdot(e_3). \tag{6}$$

In the case without the first (surface) layer

$$d_3 = \eta\cdot(e_3) \tag{6'}$$

The effect of the accuracy in the identification of initial P wave and the error in the value of velocity in each layer on the depth d_3 is then examined. The error in (e_i), $\Delta(e_i)$, is expressed from the difinition of (e_i) as follows:

$$\begin{aligned} \Delta(e_i) &= (1/2)\cdot(\Delta T_{iAD}+\Delta T_{iBD}-\Delta T_{iAB}) \\ &< (1/2)\cdot(|\Delta T_{iAD}|+|\Delta T_{iBD}|+|\Delta T_{iAB}|) \end{aligned}$$

where ΔT_{iAD}=error in T_{AD} for the i-th layer
A, B=one of shot points
D=one of observation points, variable between A and B.

In the present case, $\Delta(e_2)<0.013$ sec and $\Delta(e_3)<0.035$ sec for most of data. Through simple transformation from the formula (6),

$$\begin{aligned} \frac{\Delta d_3}{d_3} = &\left(1-\frac{1}{K}\right)\cdot\frac{(e_2)}{(e_3)}\cdot\frac{\Delta(e_2)}{(e_2)}+\frac{1}{K}\cdot\frac{\Delta(e_3)}{(e_3)}+\left\{(K-1)+\frac{\zeta}{\xi}\cdot\frac{(e_2)}{(e_3)}\right\}\cdot\left(\frac{\xi}{v_1}\right)^2\cdot\frac{1}{K}\cdot\frac{\Delta v_1}{v_1} \\ &+\left\{1-(K-1)\left(\frac{\xi}{\eta}\right)^2-\frac{\xi}{\zeta}\cdot\frac{(e_2)}{(e_3)}\right\}\cdot\left(\frac{\eta}{v_2}\right)^2\cdot\frac{1}{K}\cdot\frac{\Delta v_2}{v_2} \\ &-\left\{K+(K-1)\frac{\zeta}{\eta}\right\}\cdot\left(\frac{\eta}{v_3}\right)^2\cdot\frac{1}{K}\cdot\frac{\Delta v_3}{v_3} \end{aligned} \tag{7}$$

In the case of no first layer,

$$\frac{\Delta d_3}{d_3} = \left(\frac{\eta}{v_2}\right)^2\cdot\frac{\Delta v_2}{v_2}-\left(\frac{\eta}{v_3}\right)^2\cdot\frac{\Delta v_3}{v_3}+\frac{\Delta(e_3)}{(e_3)} \tag{8}$$

Since the underground structure in the area concerned consists of three layers and the error in the depth for the case of three layers might be larger than that for the case of two layers, the error in the depth for the case of three layers is examined in the following. The formula (7) is written in the following form:

$$\frac{\Delta d_3}{d_3} = F_1\cdot\frac{\Delta(e_2)}{(e_2)}+F_2\cdot\frac{\Delta(e_3)}{(e_3)}+F_3\cdot\frac{\Delta v_1}{v_1}+F_4\cdot\frac{\Delta v_2}{v_2}+F_5\cdot\frac{\Delta v_3}{v_3} \tag{9}$$

The values of the coefficients $F_1, \ldots, F_5$ of the ratios $\Delta(e_2)/(e_2), \ldots, \Delta v_3/v_3$ are important to the evaluation of error. Substituting the known real values into $F_1, \ldots, F_5$, the following values are obtained:

F_1	F_2	F_3	F_4	F_5
−0.01∼−0.39	1.08∼1.68	0.08∼0.29	1.43∼2.08	−0.52∼−1.20

The value of F_2 and F_4 is larger than other F_i's. Since $\Delta(e_3)/(e_3)<0.1$ and $\Delta v_2/v_2<0.09$ at most of the observation sites, the error Δd_3 caused by $\Delta(e_3)$ and Δv_2 is estimated to be about 35% of the depth d_3 in the worst case. In profile A, it is possible for the velocity of the second layer to have relatively large error since the data on the surface velocity are insufficient except for at the spread E_3. However, the effect of $\Delta(e_3)$ and Δv_2 on the error Δd_3 is less than 20% of d_3 at all observation sites as shown later.

Since F_1, F_3 and F_5 are relatively small, the error Δd_3 caused by $\Delta(e_2)$, Δv_1, and Δv_3 is within 2–3% of d_3 for the present cases.

II.2 Underground structure in profile A

1) I-II

The underground structure derived is fairly uncertain in the area D_1 and D_2 because of insufficient observed data. Therefore, several models for the structure near D_1 are derived on the different assumptions as mentioned below.

In the beginning it is assumed that this area has a relatively uniform two layered structure since there is no shot for a reversed profile around D_1.

From T(III) and T_3'(I−III) or T(IV) and T_3'(I−IV), $(e_3)=0.390$ sec at D_1-a and $(e_3)=0.325$ sec at D_1-c are obtained. The velocity is assumed to be 1.6 km/s for the first layer and to be 6.0 km/s for the third layer as obtained previously. While 4.5 km/s can not be used for the velocity of the second layer from the reason described below. The first layer should become thick from D_1-a to D_1-c by interpreting the apparent velocity 4.0 km/s of T(I) at D_1 as derived from the inclination of the top of the second layer with the velocity of 4.5 km/s. On the contrary the above values of (e_3) give the model in which the first layer should be shallower from D_1-a to D_1-c without introducing large inclination of the top of the third layer. In order to avoid this contradiction, it is necessary to assume an appropriate value for the velocity of the second layer instead of 4.5 km/s. Therefore, the dependence of the depth to the third layer on the velocity of the second layer are examined in the following to make the further consideration easier. From the formula (1)

$$d_3=H_1+H_2=\left\{(e_3)-\left(\frac{\cos\theta_{13}}{v_1}-\frac{\cos\theta_{23}}{v_2}\right)\cdot H_1\right\}\Big/\left(\frac{\cos\theta_{23}}{v_2}\right) \tag{10}$$

where H_1, the thickness of the first layer near D_1, is evaluated approximately by using the intercept time τ of T(I) and the formula

$$H_1=\frac{v_1}{\cos\theta_{12}}\cdot\frac{\tau}{2}-\Delta\cdot\sin\omega_{12} \tag{11}$$

and ω_{12}, the dip of the interface between the first and the second layers, is given by the formula

$$\omega_{12}=\sin^{-1}\frac{v_1}{v_2}-\sin^{-1}\frac{v_1}{v_{2+}}$$

(v_{2+}: the apparent velocity of T(I)). In the upper figure of Fig. 6 are given the values of d_{3a} and d_{3c}, the depth to the top of the third layer at D_1-a and at D_1-c respectively, derived from the formula (10) for various values of v_2. The following values were used for the computation:

$v_1=1.6$ km/s, $v_{2+}=4.0$ km/s, intercept time $\tau=0.240$ sec,

Δ_a(at D_1-a)$=1.070$ km and Δ_c(at D_1-c)$=1.925$ km.

The dip of the interface between the first and the second layers, ω_{12} and that between the second and the third layers, ω_{23} derived from the above results are given in the lower figure of Fig. 6. That is,

$5°>\omega_{12}>-3°$

$9°<\omega_{23}<43°$

for 3.2 km/s $<v_2<$ 4.5 km/s. From this result, it is found that the assumption $\cos\omega\approx 1$ is valid for ω_{12}

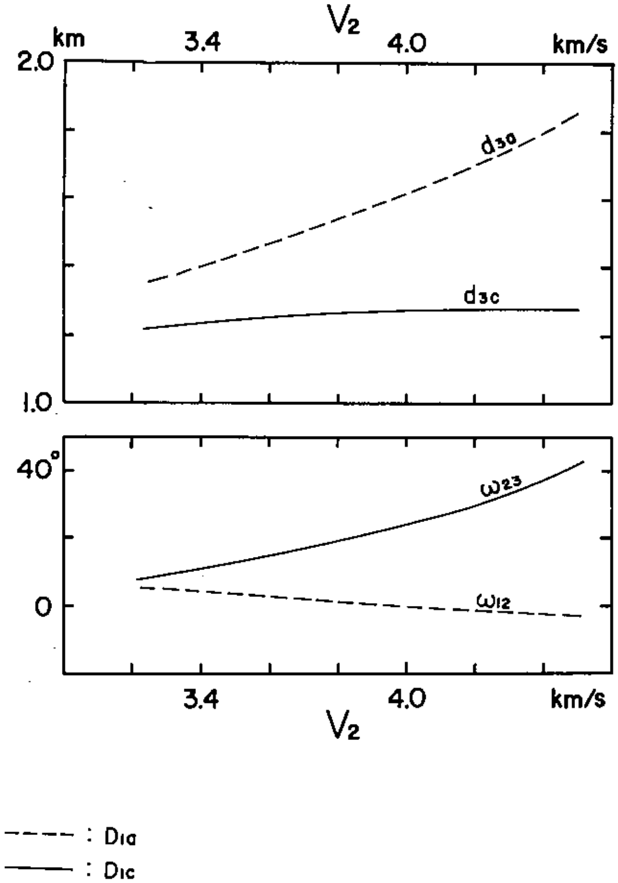

Fig. 6 Depth to the top of the third layer at D_1–a (d_{3a}) and at D_1–c (d_{3c}) and the dip of each interface. v_2 is the velocity in the second layer.

irrespective of the value of v_2 and valid for ω_{23} only for v_2 smaller than 3.5 km/s. That is, the velocity in the second layer is 3.5 km/s at largest on the assumption of two layered structure. The depth to the top of the third layer, d_3, is 1.4 km by using this value as the velocity in the second layer. However, the appropriate velocity of the second layer is found to be 4.5 km/s around D_3 and D_4 as mentioned previously and this value differs much from the corresponding velocity 3.5 km/s at D_1.

Next, the assumption of two layered structure was abandoned to remove the difference of velocity mentioned above. That is, the existence of an additional layer is assumed between the first layer and the layer with the velocity of 4.5 km/s. Then the effect of the velocity and the thickness of this additional layer on the depth to the layer with the velocity of 6.0 km/s was examined. If the velocity and the thickness of the additional layer are designated as $v_{1'}$ and $H_{1'}$ respectively, the depth to the layer with the velocity of 6.0 km/s is given by

$$d_3 = H_1 + H_{1'} + H_2$$

$$= \frac{v_2}{\cos\theta_{23}}\left\{(e_3) - \left(\frac{\cos\theta_{13}}{v_1} - \frac{\cos\theta_{23}}{v_2}\right) \cdot H_1 - \left(\frac{\cos\theta_{1'3}}{v_{1'}} - \frac{\cos\theta_{23}}{v_2}\right) \cdot H_{1'}\right\} \qquad (12)$$

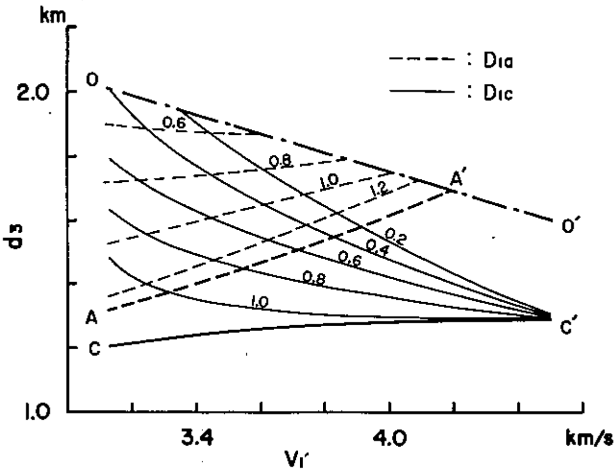

Fig. 7 Depth to the top of the deepest layer, d_3, when an additional layer with the velocity $v_{1'}$ and with the thickness of $H_{1'}$ is introduced. The parameter is $H_{1'}$.

by using (1). H_1 is given by (11). The variation of d_3 with a parameter of $H_{1'}$ due to the value of $v_{1'}$ is shown in Fig. 7. $v_1=1.6$ km/s, $v_2=4.5$ km/s and $v_3=6.0$ km/s are assumed for the computation. The thick dotted line and thick solid line are taken from the results in Fig. 6. The parameter is the value of $H_{1'}$ in km. Furthermore there is the lower limit in the value of $H_{1'}$ depending upon the value of $v_{1'}$ to satisfy the condition that T(I) at D_1-c are travel times of waves refracted at the 1′ layer. The value of the lower limit of $H_{1'}$ is calculated approximately by the formula

$$H_{1'} \geq \frac{v_{1'}}{\cos\theta_{1'2}}\left\{\frac{\Delta_c}{2}\left(\frac{1}{v_{1'}}-\frac{1}{v_2}\right)-\frac{H_1}{v_1}\left(\cos\theta_{12}-\cos\theta_{11'}\right)\right\} \tag{13}$$

In Fig. 7 is shown the maximum value of d_3 which is derived from the formula (13) by using the average value of the thickness of the first layer at D_1-a and D_1-c for H_1. The upper limit of $v_{1'}$ must be taken as 4.5 km/s and its lower limit, about 3.1 km/s, is obtained by putting $\Delta=\Delta_c$ and $H_1=0$ in the formula (11). Therefore, the depth to the fourth layer on the assumption of a three layered structure should have the value within the portion enclosed by the curves OO′ and AA′ in Fig. 7 at D_1-a and within the portion enclosed by the curves OO′ and CC′ at D_1-c. This means that a model can not be derived uniquely from the observed data. Furthermore, two conditions $d_{3_a} \fallingdotseq d_{3_c}$ and $H_{1'_a} \fallingdotseq H_{1'_c}$ at D_1-a as well as at D_1-c should be satisfied for the application of method of differences. However, as seen from Fig. 7, the structure can not be determined uniquely even though these two conditions were taken into account.

Through the above trials, the model with an additional layer between the first and the second layers is more preferable near D_1. The thickness of this layer is estimated to be 0.5–1.0 km, its velocity, 3.2–3.8 km/s and the depth to the deepest layer, 1.2–1.8 km. There is a tendency that this depth becomes larger from D_1-c to D_1-a, that is, the interface between the second and the third layer becomes deep toward the northeast. Since the additional layer seems to taper toward the southwest, the waves travelling through this layer can not be observed in the observation points other than D_1.

For the structure near D_2, the detailed analysis is almost impossible because of insufficient data. However, on the assumption of the two layered structure, that is, $v_1=1.6$ km/s, $v_2=4.5$ km/s and $v_3=6.0$ km/s, the following relation between the thickness of the first layer, H_1, and that of the second layer, H_2, is derived from $(e_3) \fallingdotseq 0.29$ sec at D_2 obtained by T_3(III) and T_3'(I−III):

$H_2=2.03-4.32H_1$, that is, $d_3=H_2+H_1=2.03-3.32H_1$.
Although there are no data at D_2 for determining H_1, it is certain from the above formula that d_3 is less than 2 km though dependent on the value of v_2. The corresponding formula for $v_2=4.3$ km/s is $d_3=1.76-2.74H_1$ and gives the value of d_3 less than 1.8 km.

T(II) at D_3-c, D_4-a, b, c is delayed by about 0.06 sec from the line of T(II) at D_3-a, b. Similarly T(I) and T(III) at D_3-c, D_4-a, b, c are regarded as delayed by about 0.06 sec from the line with the gradient 1/(6.0 km/s) through D_3-a, b. This kind of delay in travel time, the amount of which is same and independent of direction of approach, is mainly caused by the first (surface) layer. The thickness of the first layer at D_3-c, D_4-a, b, c for cases of the velocity 1.6 km/s and 2.0 km/s is obtained as shown below from the amount of delay due to the absence of the first layer at D_3-a, b as mentioned in **II.1, 2.**

(1) for the shot A-II

v_1 \ v_2	4.5 km/s
1.6 km/s	0.10 km
2.0	0.15

(2) for the shot A-III

v_1 \ v_3	6.0 km/s
1.6 km/s	0.10 km
2.0	0.14

The thickness of the second layer is derived from T(I), T(III) and T'(I−III) to be about 0.9 km at D_3-a, b and about 1.0 km at D_4-b, c by taking the thickness of the first layer into account. That is, the depth to the upper boundary of the third layer is about 0.9 km and about 1.1 km at respective sites. If the smaller value 4.3 km/s obtained in the range II-III is also adopted in this range, I-II, for the velocity in the second layer, the depth to the upper boundary of the third layer is on the average 0.75 km at D_3-a, b and 0.88 km at D_4. The difference of these values from the values obtained above is about 0.15—0.22 km which is 17–20% of the depth obtained by taking v_2 as 4.5 km/s.

2) II-III

The velocity in the first layer is estimated from the observations near the shot point A-II to be less than 2.0 km/s. The velocity in the second layer around the spread E_1 is 4.3 km/s as obtained already. Assuming the value 1.8 km/s for the velocity in the first layer and using the intercept time 0.04 sec by the line with the gradient 1/(4.3 km/s) which fits to T(II) at E_1, the thickness of the first layer is derived as about 40 m. The delay in T_3 due to this first layer is less than about 0.02 sec, which is within the error in the identification of most of initial P wave. Therefore the disregard of the first layer does not give significant effect on the evaluation of deeper structures. The thickness of the second layer is derived from T(I), T(III), T(IV), T'(I−III) and T'(I−IV). It is found that the second layer exists with uniform thickness 1.33 km over the spread E_1.

In the range from E_2 to E_3, the first layer with the velocity of 2.3 km/s is about 160 m in thickness at the spread E_2 and 200–350 m in thickness at the spread E_3 from the data of the measurement of surface velocity. Then the thickness of the second layer and the depth to the upper boundary of the third layer are obtained as follows:

(1) E_2

Obs. point	H_2 (km)	d_3 (km)
E_2– 1	1.38	1.54
E_2–19	1.09	1.25
E_2–24	0.79	0.95

(2) E_3

Obs. point	H_2 (km)	d_3 (km)
E_3– 3	0.78	1.12
E_3– 8	0.62	0.85
E_3–16	0.50	0.85
E_3–22	0.61	0.84

As regards the velocity in the second layer, 4.3 km/s is used at the spread E_2 and 4.75 km/s, at the spread E_3 for these computations. Since the velocity in the second layer is determined fairly accurately at the spread E_3 by the measurement of surface velocity, the values of H_2 and d_3 in this spread shown above have a good accuracy. While the values of H_2 and d_3 at the spread E_2 are less reliable than those at E_3 since 4.3 km/s is estimated by the observed travel times at E_2 from the small shot E_3-W_1 for the measurement of surface velocity at E_3 and this shot was not reversed as far as the spread E_2 is concerned. Therefore, assuming 4.75 km/s instead of 4.3 km/s for the velocity in the second layer at E_2, then the following values were obtained:

(3) E_2

Obs. point	H_1 (km)	H_2 (km)	d_3 (km)
E_2– 1	0.45	0.85	1.30
E_2–19	0.38	0.66	1.04
E_2–24	0.30	0.58	0.88

There is only small difference between the values in (1) and (3) by about 17% of the depth in (1).

The underground structure at D_6 is obtained as follows on the assumption v_2=4.75 km/s:

D_6

Obs. point	H_1 (km)	H_2 (km)	d_3 (km)
a	0.00	0.93	0.93
b	0.26	0.65	0.91
c	0.34	0.75	1.09

T(II) and *T*(III) at D_5 show quite peculiar behavior. There is almost no difference of travel times between three observation sites, a, b, c. For shots other than A-II and A-III, there is systematic difference between the three observation points and this fact contradicts the behavior of *T*(II) and *T*(III). Therefore since the desirable data are not available in this area, any complicated structure is not derived to explain the inconsistent observations at D_5. The structure interpolated from those at E_1 and at E_2 is here assumed to exist at D_5.

The depth of the interface between the second and the third layers is about 1.33 km at E_1, about 1.54 km to 0.95 km within E_2 and about 1.12 to 0.84 km at E_3. As a whole there is a tendency for this depth to become smaller toward the southwest.

3) III-IV

The thickness of the first layer at D_7 is about 90 m from the intercept time of travel times from shot A-III. As already mentioned, the thickness of the first layer is negligibly small at E_4. The thickness of the second layer and the depth to the upper interface of the third layer is estimated as follows by taking the above results into account and assuming v_2 at D_7 to be 4.75 km/s and at E_4 to be 4.4 km/s:

	D_7–a	b	c	E_4–3	24
H_2 (km)	1.05	1.00	0.94	0.89	0.73
d_3 (km)	1.14	1.09	1.03	0.89	0.73

The effect of the value of v_2 on H_2 is seen from the comparison of the above table with the table of H_2 below:

v_2	E_4–3	24
4.3 km/s	0.84 km	0.69 km
4.7	1.04	0.85

Even though the velocity in the second layer were changed within some limit, there still exists the tendency for the top of the third layer to become shallower toward the southwest.

There are no data available at the spread E_5 to estimate the detailed structure of the first (surface) layer. A systematic fluctuation of observed travel times within the spread regardless of the location of shot points might be due to the irregularity of thickness of the first layer. As a rough estimation, the lines with the velocity of 4.3 or 4.4 km/s are fitted to T(IV) at E_5 and their intercept times are used to calculate the thickness of the first layer. The intercept time 0.02 sec from the line of 4.3 km/s gives 25 m for the thickness of the first layer and that 0.06 sec from the line of 4.4 km/s gives 78 m, assuming the velocity in the first layer to be 2.3 km/s. From this trial, the first layer is so thin that the disregard of this layer does not give much error in the analysis of deeper structure. This point is also seen from the following computations.

The three cases are examined as follows in the estimation of thickness of the second layer because the velocity in the second layer can not be determined accurately enough.

v_2 (km/s)	4.3	4.4		4.7	
	H_2 (km)	H_2 (km)	d_3 (km)	H_2 (km)	d_3 (km)
E_5– 3	1.06	0.93	1.02	0.85	1.00
E_5–24	0.81	0.66	0.74	0.54	0.69

The above results show that the depth to the upper interface of the third layer, d_3, is insensitive to the change in the value of velocity in the second layer and the change of d_3 due to this kind of ambiguity is at most within 10%. The tendency of d_3 to become smaller from northeast to southwest is ascertained further in this section, but there is an offset of d_3 by about 0.3 km between E_4 and E_5. That is, the top of the third layer is shallower by about 0.3 km in the area between the middle of E_2 and E_4 than in the other part of the profile. The details of the structure between E_4 and E_5 can not be obtained because of insufficiency of data in quality as well as in quantity.

4) **IV-V**

The velocity in the first layer and in the second layer at D_9 are 2.3 km/s and 3.5 km/s respectively. These values are derived from the observations near the shot point A-IV though not accurate enough. Since there are no other data to obtain these velocities more accurately, these values are used to estimate the thickness of the first layer, which is obtained as about 70 m by using the intercept time of the line through the data at D_9-b, c for the shot point A-IV. Then the thickness of the second layer and the depth to the top of the third layer are obtained in the area D_9-D_{11} as follows although the values are not sufficiently reliable because of uncertainty in the value of the velocity in the second layer.

	H_2 (km)	d_3 (km)
D_9	0.65–0.80	0.72–0.87
D_{10}	0.66–0.76	0.66–0.76
D_{11}	0.52–0.62	0.52–0.62

From the present data it is hard to obtain the value larger than 3.5 km/s for the velocity in the second layer. However, the depth to the upper interface of the third layer is computed as follows by assuming v_2 to be 4.3 km/s in order to see the change due to the value of v_2:

	D_9	D_{10}	D_{11}
d_3 (km)	1.0	0.9	0.8

The value of d_3 thus obtained is larger by about 20% than previous results. The above value might give the upper limit of d_3.

In this range as in the other ranges there exists the tendency for the depth to the upper interface of the third layer to become smaller toward the southwest. At D_{12} and D_{13} the value of d_3 is calculated on the assumption for v_2 to be 3.3 km/s.

	H_2 (km)	d_3 (km)
D_{12}	0.63–0.66	0.63–0.66
D_{13}	0.73–0.75	0.73–0.75

Thus the value of d_3 again becomes a little larger at D_{13}. The depth to the top of the third layer can not be computed at D_{14} because of insufficient data, but the extraordinary delay of travel times intrinsic to D_{14} might be caused by the thick first layer as well as the abnormally thick second layer. On the assumption of the two layered model with almost the same velocity structure with that near D_{13}, that is, $v_2=3.3$ km/s, $v_3=5.9$ km/s and of 1.9 km/s for the velocity of the first layer, v_1, the depth to the third layer is represented with the formula

$$d_3=1.26-1.07H_1$$

by using $(e_3)\fallingdotseq 0.31$ sec at D_{14}, where H_1 is the thickness of the first layer. Therefore, d_3 should be less than 1.3 km.

II.3 Velocity for each layer in profile B

The variation of the underground structure along profile B is fairly large as expected from the complexity of observed travel times. Although the surface structures are derived in fairly detail in the central portion of the profile by using the data from the measurements of surface velocity, the accuracy of values for each true velocity, for the thickness of each layer and for the depth to each boundary is considered to be rather lower in profile B because of the complicated structure than in profile A.

The travel time graph of profile B is given in Fig. 8 together with the main T' curves. The underground structure consists of three layers on the whole, but an additional layer is introduced on the surface for some places where the measurements of surface velocity were specially conducted. That is,

the surface layer (absent in some places):	0.36–1.2 km/s
the first layer (surface layer in some places):	1.7 –3.2 km/s
the second layer:	4.0 –4.4 km/s
the third layer:	6.0 km/s

Referring to the terminology in profile A, the layer with the velocity of about 4 km/s is called the second layer and the layer of about 6 km/s, the third layer in spite of the three layered structure if the surface layer mentioned above exists. There is a slight possibility for the layer with the velocity of about 6.3 km/s to exist below the third layer from the travel time curve, but this layer is not taken into account in the present analysis because of the quality of data. In the following the velocities in each section between each shot point are studied as done in profile A.

1) I-II

The velocity in the first layer is 2.1 km/s near the shot point B-I and 1.9–2.0 km/s near the shot point B-II from the observation near each shot point as shown in Fig. 9. The apparent velocity 2.3

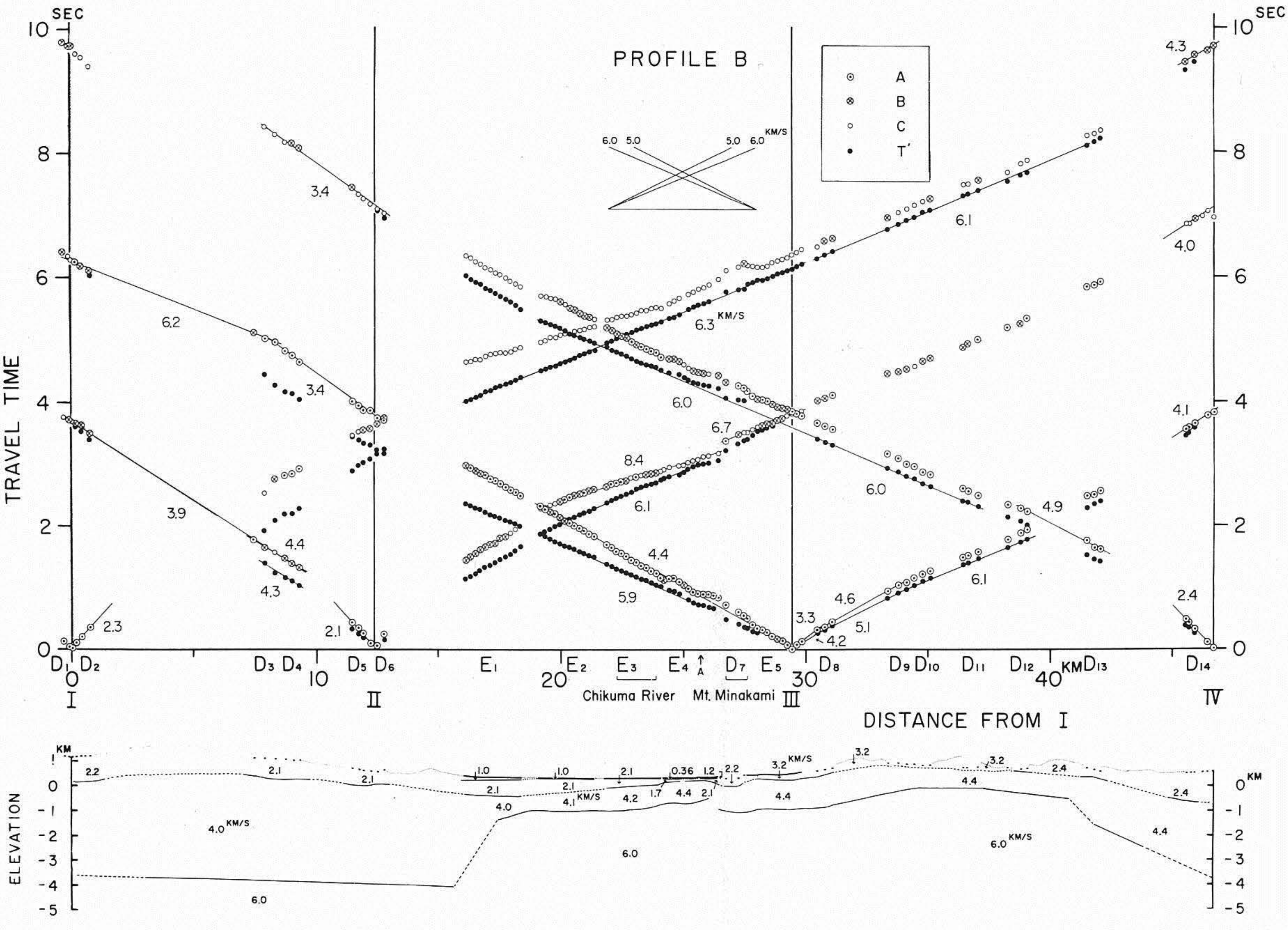

Fig. 8 Travel time curves and the underground structure derived for profile B

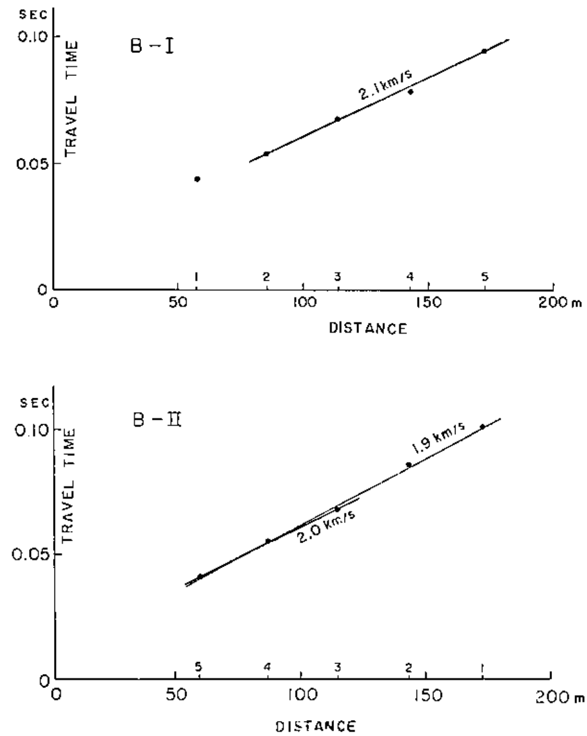

Fig. 9 (a) Travel time curve near the shot point B-I
(b) Travel time curve near the shot point B-II

km/s is obtained from T(I) at D_1 and D_2 and the apparent velocity 2.1 km/s, from T(II) at D_5 and D_6. Thus for v_1 the value of 2.2 km/s is adopted at D_1 and D_2 and the value of 2.1 km/s, in the range from D_3 to D_6.

For the velocity in the second layer the T'(I—II) curve gives 4.3 km/s, but this value is not so accurate since it is determined by only five points. While T(II) at D_3 and D_4 gives the apparent velocity 4.4 km/s, but T(II) at D_1, D_2, D_3 and D_4, 3.9 km/s. In spite of fairly large fluctuation in above two cases, the value 4.0 km/s is tentatively adopted for the velocity of the second layer in this region.

The velocity in the third layer is hard to be estimated only from the data in the section I-II and the inference is made in the later stage from the data of the other sections. Thus the velocities in the first and the second layers are given as follows:

the first layer: 2.1–2.2 km/s
the second layer: 4.0 km/s

2) II-III

In this section geophones of five 24 element seismic prospecting instruments besides D_6 and D_7 were distributed almost continuously and the amount of data on the surface structure is sufficiently large because of four small shots (the shot points: E_2–W_1, E_2–W_2, E_4–W_1 and E_4–W_2 in Fig. 1 (b)) for the measurement of surface velocity structure. First the results from the measurements of surface velocity structure are presented successively from the northwest and then the velocities in the deeper layers are estimated from the travel time curve of the whole section.

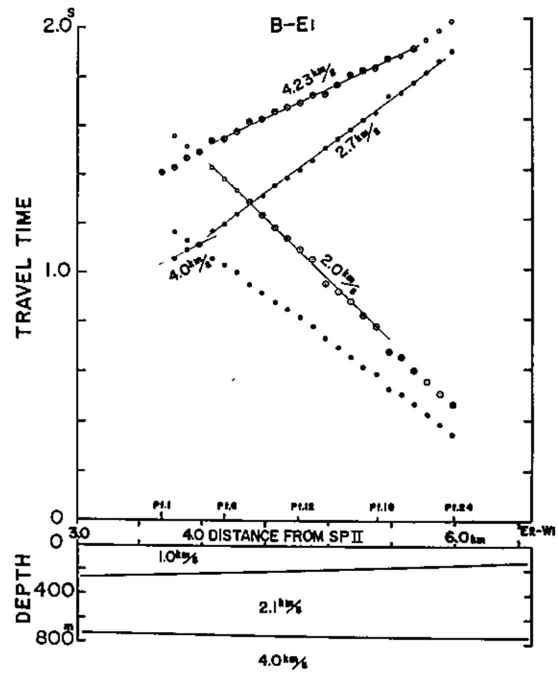

Fig. 10 Travel time curve from the measurement of surface structure at the spread E_I (above) and the surface structure derived (below). Marks for observed data are the same with those in Fig. 8. Closed circle: $T'(II-E_2-W_1)$

The measurement of surface structure at the spread E_I (Fig. 10): The profile in this spread seems to be reversed from the data obtained by the small shot at E_2–W_1 and the large shot at B-II. However, the above data are insufficient for the analysis of the detailed surface structure since the shot point B-II is apart by about 4 km from E_I–1. (Fig. 1 (b)). Computing $T'(II-E_2-W_1)$ from the data of the above two shots, the value 4.0 km/s is obtained for the velocity of the second layer only in the range between E_I–2 and E_I–4. The apparent velocity 4.2 km/s in $T(II)$ can be explained on the interpretation that the top of the second layer becomes shallower toward the southeast. The line with the gradient of 1/(2.7 km/s) fits to $T'(II-E_2-W_1)$ between E_2–5 and E_2–24. If this value of velocity 2.7 km/s on the T' curve results from the true velocities v_1 and 4.0 km/s, then the value of v_1 becomes 2.1 km/s.

Since there are no observation points in the range longer than 600 m between the shot point E_2–W_1 and the observation point E_I–24 (Fig. 1 (b)), the simple division of the distance of E_I–24 from the shot point E_2–W_1 by the corresponding observed travel time gives the velocity 1.4 km/s. This implies that the value of the velocity in the surface layer is 1.4 km/s or less in this vicinity, but the accurate value can not be determined because of shortage of data. The intercept time more than 0.100 sec by the line with the gradient of 1/(2.0 km/s) which fits to $T(E_2$–$W_1)$ can be interpreted by the structure which has the surface layer with the velocity of about 1.0 km/s thickening slightly toward the northwest above the layer with the velocity of 2.1 km/s.

The measurement of surface structure at the spread E_2 (Fig. 11): Despite the good condition with the shots E_2–W_1 and E_2–W_2 at both ends of the spread E_2, the value larger than 4.0 km/s can not be found clearly for the velocity of the second layer in the travel time curve. The value 2.1 km/s is obtained for the velocity of the first layer from the original travel time curve as well as from the T' curve and the existence of very thin surface layer is estimated from the intercept time at the shot point E_2–W_2. The velocity in this surface layer is estimated to be about 1.0 km/s in the same manner at the spread E_1 from the travel times at E_2–24, the nearest observation point to the shot point E_2–W_2.

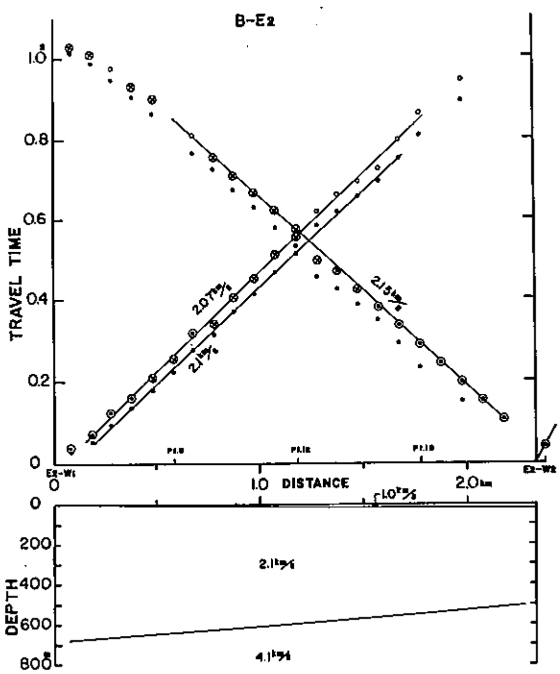

Fig. 11 Travel time curve from the measurement of surface structure at the spread E_2 (above) and the surface structure derived (below). Marks for observed data are the same with those in Fig. 8. Closed circle: $T(E_2\text{–}W_1 - E_2\text{–}W_2)$

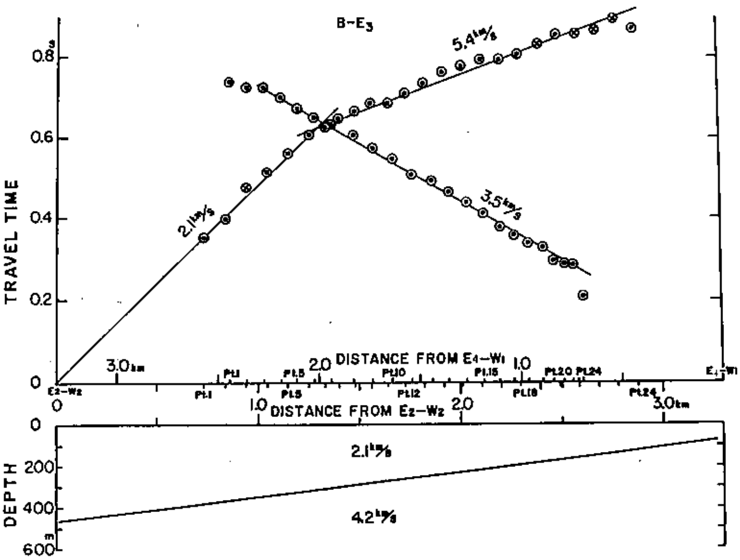

Fig. 12 Travel time curve from the measurement of surface structure at the spread E_3 (above) and the surface structure derived (below). Marks for observed data are the same with those in Fig. 8.

The measurement of surface structure at the spread E_3 (Fig. 12): Since the shot points E_2–W_2 and E_4–W_1 available for the study of surface structure deviate by about 500–700 m from the extension of the spread E_3, the method used to other portions of profile can not be applied because of possibility introducing large error. That is, the real distance and the real travel times are used to construct the travel time curve instead of using the distance projected to the base line B-I–B-IV and of using the travel times corrected the angle between the line connecting the observation point with the shot point and the base line. Therefore, since the seismic waves to one observation point from the two shot points E_2–W_2 and E_4–W_1 propagate different paths, the analysis by the T' curve can not be applied. In the travel time curve thus constructed $T(E_2–W_2)$ gives 2.1 km/s near the shot point and 5.4 km/s in the distance, while $T(E_4–W_1)$ at observation points of E_3 except for E_3–1, E_3–2 and E_3–23 gives 3.5 km/s. The value 2.1 km/s is regarded as the velocity in the first layer and the values 5.4 and 3.5 km/s are interpreted as the apparent velocities due to the deepening of the top of the second layer with the velocity of 4.2 km/s toward the northwest.

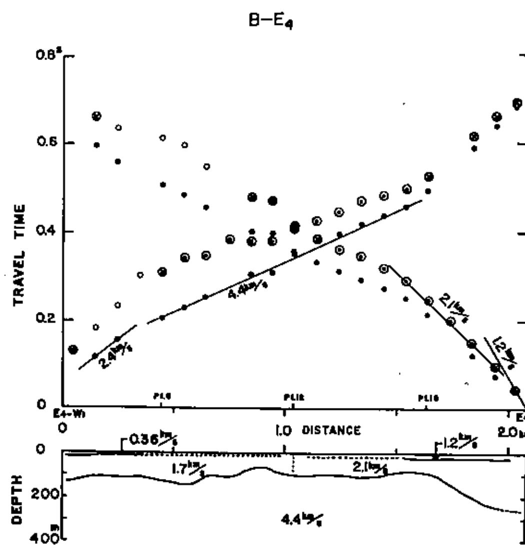

Fig. 13 Travel time curve from the measurement of surface structure at the spread E_4 (above) and the surface structure derived (below). Marks for observed data are the same with those in Fig. 8. Closed circle: $T'(E_4–W_1 – E_4–W_2)$

The measurement of surface structure at the spread E_4 (Fig. 13): First, the velocity of the second layer is estimated to be 4.4 km/s from the T' curve. Next, the velocity in the first layer, 1.7 km/s, is derived by regarding the T' curve between E_4–3 and E_4–4 as the T'_{12} curve combined T_1 with T_2. It is found from $T(E_4–W_1)$ near the shot point that there exists the surface layer with the velocity of 0.36 km/s. In the southeastern half of E_4 the value 2.1 km/s derived from $T(E_4–W_2)$ between E_4–17 and E_4–22 is regarded as the true velocity of the first layer and the value 1.2 km/s obtained by dividing the distance of the observation point E_4–22 from the shot point E_4–W_2 with the corresponding observed travel time is tentatively assumed to be the velocity of the surface layer. Since there are no data for the structure of the surface and the first layers in the central portion of this section, the structure near the shot point E_4–W_1 is assumed to extend to the observation point E_4–12. The southeastern half of E_4 is also assumed to have the same surface structure with that around the shot point E_4–W_2.

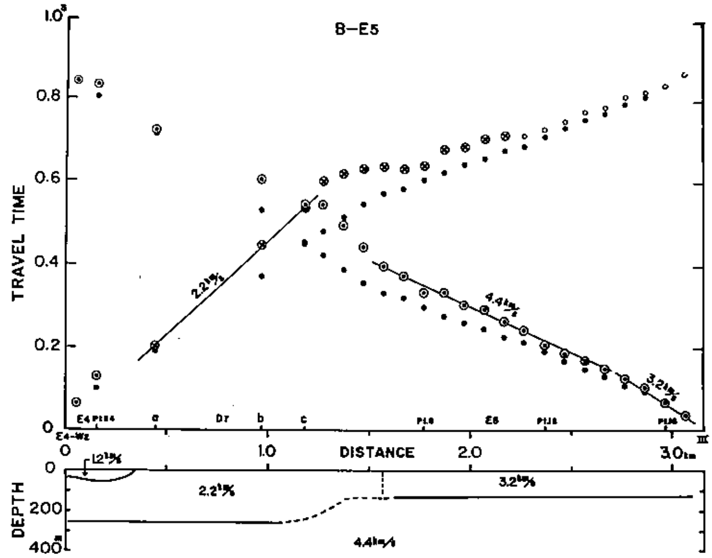

Fig. 14 Travel time curve from the measurement of surface structure at the spread E_5 (above) and the surface structure derived (below). Marks for observed data are the same with those in Fig. 8. Closed circle: T(III—E_4–W_2)

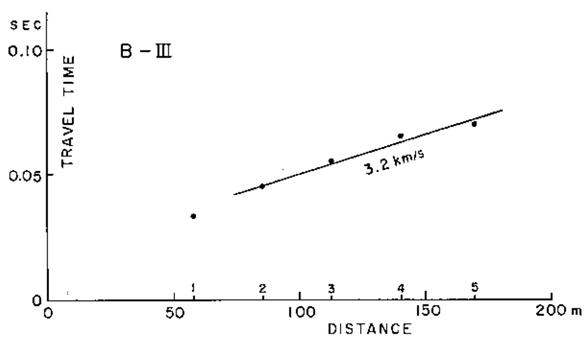

Fig. 15 Travel time curve near the shot point B-III

The measurement of surface structure at D_7 and E_5 (Fig. 14): In this section the observation site D_7 is deviated from the extension of the spread E_5 because of Mt. Minakami and on the whole complicated travel times are observed. Above all, the seismograms obtained from the shot E_4–W_2 are not good in the distant half of E_5 for the accurate analysis of the travel times, although this section of the profile is reversed with the shot B-III. The apparent velocity 2.2 km/s is derived from $T(E_4–W_2)$ at D_7 and is regarded as the velocity in the first layer. The apparent velocity 3.2 km/s is found from T(III) between E_5–16 and E_5–20 and is interpreted to be the velocity of the first layer in the vicinity of B-III since the observations near B-III give the same value of the velocity as shown in Fig. 15. The line with the velocity of 4.4 km/s fits to T(III) between E_5–4 and E_5–16 though not so certain and this value 4.4 km/s is regarded as the velocity of the second layer.

So far the results from the measurement of surface structure for each spread having been presented, the velocities thus derived are summarized as follows:

spread	E_1	E_2	E_3	E_4	D_7–E_5
the surface layer	1.0(?)	1.0(?)	—	0.36–1.2	—
the first layer	2.1	2.1	2.1	1.7–2.1	2.2–3.2
the second layer	4.0	?	4.2	4.4	4.4

(unit: km/s)

Now, attention is paid to the travel times in the whole section, II-III. The apparent velocity 4.4 km/s appears in T(III) from E_2 to E_5, but in the travel times T(II) for the corresponding reversed profile the apparent velocity 8.4 km/s is found between E_2 and E_4 and 6.7 km/s, at E_5. Therefore, the velocity 4.4 km/s must be interpreted, except for the portion near the shot point B-III, as the apparent velocity by T_3(III), travel times of waves propagating through the third layer from B-III, although the first apparent velocity 4.4 km/s is very close or equal to the velocity of the second layer in the above table. That is, the apparent velocities 4.4 km/s from T(III), 8.4 km/s from T(II), etc. is explained by the structure with the top of the third layer becoming deep toward the northwest. From the T'(II−III) curve between E_2 and E_4 the value 6.1 km/s is also obtained. In the same portion, 5.9 km/s, 6.0 km/s and 6.3 km/s are derived from T'(I−III), T'(I−IV) and T'(I−IV) respectively. The last value 6.3 km/s may give the velocity of the layer deeper than the third one and is disregarded in the present analysis because of the quality of data as mentioned previously. Therefore the average velocity 6.0 km/s of the former three values is regarded as the velocity of the third layer in this analysis.

In summary,

the surface layer:	0.36–1.2 km/s
the first layer:	1.7 –3.2 km/s
the second layer:	4.0 –4.4 km/s
the third layer:	6.0 km/s

3) **III-IV**

The T'(III−IV) curve in the northwestern portion of this section is composed of three lines with the velocities 4.2 km/s, 5.1 km/s and 6.1 km/s from the shot point B-III to the southeast in turn. Therefore, the underground structure in this section is assumed to consist of three layers. If the value 6.1 km/s is interpreted as the velocity of the third layer and the values 5.1 km/s and 4.2 km/s result from the combination of travel times of the second layer with those of the third layer and from the combination of travel times of the first layer with those of the third layer respectively, the true velocity of the second layer is 4.4 km/s and that of the first layer is 3.2 km/s as those in the range II-III.

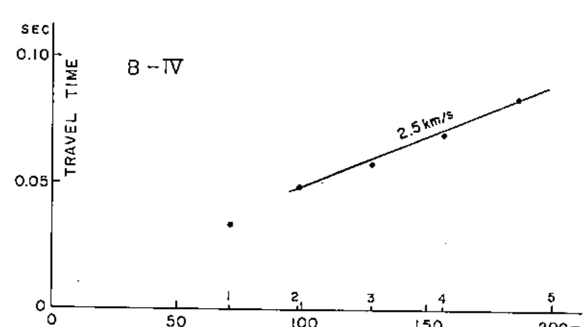

Fig. 16 Travel time curve near the shot point B-IV

For the velocity of the third layer the value 6.0 km/s is derived from T'(II−IV) and 6.1 km/s, from T'(I−IV). However, the value 6.0 km/s is assumed to be the velocity of the third layer since there is no basis for the velocity of the third layer to be larger in this section than in other sections and the deviation of observed values from the line 6.0 km/s fitted to T'(II−IV) is smallest. T'(II−IV) is used to obtain the depth to the top of the third layer.

Next the velocity around the southeastern end in this section is examined. Since the pronounced systematic delays are found in observed travel times from all shots at D_{13} and D_{14}, it is certain that there exists a thick layer with a low velocity in this portion of the profile. Therefore, the velocity 2.4 km/s obtained from T(IV) at D_{14} is regarded as the velocity of the first layer. The observed data near the shot point B-IV also support this interpretation since the velocity 2.5 km/s is obtained under the very thin surface layer from those data as shown in Fig. 16. The values for the second and the third layers in this area are assumed to be equal to those in the northwestern part of the area. Finally in this section,

the first layer:	2.4-3.2 km/s
the second layer:	4.4 km/s
the third layer:	6.0 km/s

II.4 Underground structure in profile B

First the method of differences is mainly applied to estimate the underground structure as in profile A. However, the two assumptions in this method, that the refracted waves travel along the interface and that the irregularity of the interface is not large, are sometimes violated because of the complicated structure in this profile. In this case, the difference in travel times between the observed and the calculated values from the underground structure derived first is sometimes very large. Then the method of trial and error is graphically applied to the model of structure, which is modified so as to make (O−C) as small as possible. When the velocity can not be determined only from the data in the section concerned as in the case of the third layer in the range I-II, the depth corresponding to the combination of assumed velocities is computed.

The results of estimation in the range II-III with a fairly large amount of data obtained for the surface structure are presented in the first place and those in I-II where the data for the third layer are insufficient, lastly. In addition to the terminology in the previous parts of this paper, the quantities for the surface layer have the suffix 0.

1) II-III

First, the structure shallower than the second layer are derived from the data of each spread and then the structures of deeper part, from the travel time curve of the whole section as done in **II.3.**

Surface structure at the spread E_1 (Fig. 10): Because of the absence of observation points in the distance of 4 km between the shot point B-II and E_1–1 and the simple travel time curve, the structure down to the second layer is obtained on the assumption of the linear boundary instead of the detailed analysis. First, the thickness of the surface layer with the velocity of 1.0 km/s near the shot point E_2–W_1 is 85 m by using the intercept time 0.150 sec of $T(E_2–W_1)$. Now, if the value of the velocity 2.0 km/s predominant in $T(E_2–W_1)$ is regarded as the apparent velocity of waves propagating in the first layer with the velocity of 2.1 km/s, the top of the first layer must become deep toward the northwest by the angle 1.6° and the surface layer is 170 m in thickness at E_1–1. The apparent velocity 4.23 km/s in T(II) is explained by the top of the second layer with the velocity of 4.0 km/s being deep toward the southeast with the angle of 0.3° to the earth's surface. The values of d_2, the depth to the top of the second layer, are 730 m around E_1–1 and 750 m near E_1–24. The values presented above are generally a function of v_0, the velocity of the surface layer. Since the value of v_0 can not be determined accurately and varies about 1.0 km/s to the maximum 1.4 km/s, the dependence of quantities other than v_0 upon the value of v_0 is shown in the following table which gives the extent of error included in the present analysis. (The dip of the interface is taken positive when the interface becomes shallow to the southeast.)

v_0	H_0 at E_1–1	The dip of the top of the first layer	d_2 at E_1–1	The dip of the top of the second layer
0.8 km/s	126 m	+1°11′	708 m	−0°26′
1.0	165	+1 34	734	−0 16
1.2	214	+2 02	757	−0 07
1.4	275	+2 37	784	+0 13

From this table, the dip of the top of the first layer is influenced by the value of the velocity in the surface layer and the change by 0.4 km/s in v_0 gives the difference of 50 m in the depth to the top of the second layer, d_2. However, the upper interface of the second layer is almost horizontal for any value of v_0 in the table, because the change in the thickness of the surface layer is cancelled by that in the thickness of the first layer.

Surface structure at the spread E_2 (Fig. 11): The thickness of the surface layer with the velocity of 1.0 km/s is derived to be 22 m from the intercept time at the shot point E_2–W_2. From the more detailed inspection on the travel time curve, the value 2.07 km/s is obtained in $T(E_2–W_1)$ for the average apparent velocity of the first layer and the value 2.15 km/s, in $T(E_2–W_2)$. Therefore, the surface layer above the first layer with the velocity of 2.11 km/s tapers to the northwest by the average angle of 35′, so that there is no surface layer near the shot point E_2–W_1 and the first layer outcrops there. This interpretation agrees with almost no intercept time of $T(E_2–W_1)$ at the shot point E_2–W_1.

The velocity in the second layer can not be determined with sufficient accuracy because of weak initial P's in the seismograms at distant points. However, if the initial P's at the distant points (observation points E_2–20 in $T(E_2–W_1)$ and E_2–1, E_2–2 in $T(E_2–W_2)$ are regarded as those of waves propagating in the second layer and the velocity around 4.0 km/s for the second layer is assumed, the intercept time of this line is not less than 0.400 sec. Then the depth to the top of the second layer is deeper than 500 m. The depth to the top of the second layer at each point is estimated from the structure at the spreads E_1 and E_3 by taking the above estimation into account. That is, the extension of the upper interface of the second layer at E_3, which becomes deep to the northeast, roughly coincides with the top of the second layer at E_1, the depth of which is about 700 m. As there is a portion of E_2 where the top of the second layer is less than 500 m as it is, this interface is modified slightly to that with the angle of 4.5° which is 500 m in depth at E_2–24 and 680 m in depth at E_2–1 so as to be compatible with those at E_1 and E_3. The value of velocity 4.1 km/s, which is the intermediate value of those at E_1 and E_3, is adopted for the second layer in the above computation but the alteration by 0.1 km/s in the velocity causes that by only 5% in H_2.

Surface structure at the spread E_3 (Fig. 12): The surface layer is neglected to be considered even though any existing, since there are no observation points near the shot points.

The thickness of the first layer is 470 m at the shot point E_2–W_2 and 80 m at the shot point E_4–W_1 by using the intercept time. It is 380 m around E_3–1 although the fact that this portion is not reversed literally gives some inaccuracy and 150 m around E_3–24. Thus the top of the second layer with the velocity of 4.2 km/s becomes deep to the northwest with the angle of about 7°.

Surface structure at the spread E_4 (Fig. 13): The analysis of travel times at this spread is carried out by using the T' curve since there are shots at the both ends of spread, seismograms obtained are good and the structure is supposed to be fairly complicated from the travel time curve.

First, the thickness of the surface layer with the velocity of 0.36 km/s in the northwestern part is obtained by regarding $T(E_4\text{–}W_1)$ from E_4–2 to E_4–5 as T_1, travel times of waves travelling through the first layer. Since only T'_2 and $T_{1,2}'$ are present in the T' curve, the line with the gradient of 1/(1.7 km/s) through the intersection point of $T_{1,2}'$ with the ordinate at E_4–W_1 (0.06 sec) is assumed to be T_1' (Tazime et al.)[27]. Then the thickness of the surface layer, H_0, is obtained from the equation (1) and is 11–18 m from E_4–2 to E_4–5. This procedure can not be applied in the farther southeastern part than E_4–6 and the surface layer is assumed to exist with the thickness of 15 m from E_4–6 to E_4–11. If there is no surface layer in this portion, the thickness of the first layer is increased by about 80 m.

The thickness of the surface layer with the velocity of 1.2 km/s in the southeastern part is obtained similarly by using $T(E_4\text{–}W_2)$ from E_4–17 to E_4–22. The value of H_0 thus obtained is 18–29 m and the same thickness with that at E_4–17 (18 m) is assumed for the surface layer to exist until E_4–13. Without the surface layer, the thickness of the first layer is increased by 32 m.

Next, the thickness of the first layer at each observation point is derived from $(T_2\text{–}T_2')$ on the interpretation that $T(E_4\text{–}W_2)$ from E_4–1 to E_4–17 is T_2. In the portion between E_4–1 and E_4–4, T_2' is extended from the central part of E_3 since T_2' is absent in this part. The depth to the top of the second layer with the velocity of 4.4 km/s thus obtained is about 100 m except around E_4–10 and E_4–11 and has a tendency of increasing to the northwest as shown in Fig. 13. The thickness of the first layer in the southeastern half of the spread is calculated by subtracting the delay time due to the surface layer from $(T_2 - T_2')$. The depth to the top of the second layer, d_2, thus obtained is about 100 m from E_4–13 to E_4–19 and is getting larger abruptly from E_4–20 until it is about 250 m at E_4–22.

Surface structure at the spread D_7–E_5 including a part of E_4 (Fig. 14): As mentioned in 2) of **II.3**, the precise analysis can not be carried out because of complicated travel times, but the underground structure is tried to derive on the assumption of two layered model in which the velocities in the first layer are 2.2 km/s around D_7 and 3.2 km/s near the shot point B-III and the velocity in the second layer is 4.4 km/s.

$T(E_4\text{–}W_2)$ at D_7–a, b, c fits to the line with the gradient of 1/(2.2 km/s), the intercept time of which is zero sec. Therefore, the three geophones are set directly on the layer with the velocity of 2.2 km/s. Observed travel times at E_4–23 and E_4–24 are fairly delayed and this may give the explanation that these observation points are located on the same surface layer with that of 1.2 km/s present in the southeastern part of E_4. The thickness of the surface layer in this part is obtained to be 37 m at E_4–23 and 54 m at E_4–24 by assuming the difference between the travel times T(III) at E_4–23, 24 and the extension of those at D_7–a, b, c to be the delay time due to the surface layer for the refracted wave from the second layer. The first layer with the velocity of 3.2 km/s in the southeastern part of E_5 is 126 m in thickness from the intercept time 0.050 sec. This first layer is assumed to exist until E_5–4 and to be replaced in the farther northwest (in the range including E_5–4∼1 and D_7–c∼a) by the first layer with the velocity of 2.2 km/s. Regarding T(III) from E_5–15 to D_7–a as the travel times of the refracted wave from the second layer, T_2, the thickness of the first layer in D_7–a∼E_5–3 is obtained as follows (that is, this computation is done by assuming the difference between observed travel times T(III) and the line with the gradient of 1/(4.4 km/s) which gives half of the intercept time (0.025 sec) on the shot point A-III to be the delay time due to the first layer.):

Observation point	D_7–a	b	c	E_5–1	2	3
Thickness of the first layer (m)	247	244	211	267	196	127

Thus the depth to the second layer increases abruptly from E_5–2 to the northwest and is about 250 m at D_7–a connected to the structure at the southeastern end of E_4.

Next the depth to the top of the third layer, d_3, is derived from the equation (1). Of four T' curves available in this section, (II-III), T'(II−IV) is most reliable to obtain the depth d_3 since seismograms from shot B-II are as a whole better than those from shot B-I and the fluctuation of T'(II−IV) is relatively small. However, T'(I−III) is used at the spread E_1 for this purpose since T'(II) does not give the travel times of the refracted waves in the layer with the velocity of 6.0 km/s.

The underground structure in this section thus derived is shown in Fig. 8. In this figure the interface of the portion, where the extent of irregularity of the interface derived is too large for its depth and the method of differences fails to be valid for such structure, is shown after slight smoothing. The depth to the top of the third layer is about 1.9 km in the northwestern part of E_1 and decreases to the southeast until it is about 1.4 km at the southeastern end of E_1. (In more detail page 192 should be referred to.) The depth at the spread E_2 is smaller by 0.3–0.4 km than at E_1 and is 1.3∼1.4 km almost through the spread. Then the top of the third layer becomes shallower gradually from the northwest to the southeast until it is about 0.7 km in the southeastern portion of E_4. In this range the top of the third layer becomes shallower almost uniformly with the angle of about 8°.

The observed travel times at D_7 which is located at the foot of Mt. Minakami show peculiarity for some shots. The depth to the upper interface of the third layer is about 1.3 km from T'(II−IV). Comparing this depth with that at E_4, there exists an offset by at least 0.5–0.6 km between D_7 and E_4 as seen in Fig. 8. In the travel time curve, especially in T(I) the existence of the similar offset is suggested between D_7 and E_4, while this kind of anomaly is not seen in T(III) of waves travelling this region from the southeast. These features in observed travel times can be explained qualitatively from the model shown in Fig. 8. The top of the third layer is roughly horizontal from D_7 to E_5 and 1.3–1.4 km in depth.

2) III-IV

In this section there is no measurement for the surface structure and the thickness of the first layer is estimated or assumed in most parts from the data available. The final form of the top of the third layer in this range, especially in the southeastern part, is determined by graphical calculation of travel times.

In T(III) between E_5–20 and D_9, first the apparent velocity 3.3 km/s and then 4.6 km/s are observed. If this value 4.6 km/s is regarded as the apparent velocity of refracted waves in the layer with the velocity of 4.4 km/s, the depth to the top of the second layer is 0.21 km at the shot point B-III from the intercept time 0.090 sec of T(III) and decreases toward the southeast with the dip of 2.6° to the earth's surface. In more detail the thickness of the first layer at each point is calculated as follows by the difference between observed travel times T(III) and the line with the gradient of 1/(4.4 km/s) giving the intercept time 0.045 sec at the shot point B-III.

Observation point	E_5–20	D_8–a	b	c	D_9–a
H_1 (km)	0.21	0.19	0.15	0.14	0.07

The first layer, 70 m in thickness, is assumed to exist until D_{12}-a by taking H_1 at D_9-a into account because of absence of T_2 in the range farther southeast of D_9. The depth to the top of the third layer between E_5–20 and D_{12}-a is calculated from T(II)–T'(II−IV). Thus it is about 1.3 km from E_5–20 to E_5–24, about 1.5 km at D_8, 1.4∼1.1 km at D_9 and about 1.1 km from D_{10}-a to D_{12}-a.

In the southwestern part of this section, that is, the southwestern end of profile B, the line with the gradient of 1/(4.9 km/s) fits to T(IV) between D_{12}–b and D_{13}–c and gives the intercept time 0.68 sec at the shot point B-IV. Then assuming that the first layer with the velocity of 2.4 km/s at D_{12} and

D_{13} extends with the same dip to D_{14}–f as done previously, the following values are obtained for the thickness of the first layer. (Although the values are derived at each point, only some are presented.)

Observation point	D_{12}–b	D_{13}–b	D_{14}–a	D_{14}–f
H_1 (km)	0.35	0.53	0.89	0.97

In this table, it is noteworthy that the thickness of the first layer increases fairly abruptly at D_{12}-b by about 300 m in comparison with that in $D_9 \sim D_{12}$-a. If the depth to the top of the third layer is derived from T(II)–T'(II–IV) by using the thickness of the first layer obtained above, the top of the third layer becomes shallow by 400 m southwest of D_{12}–b on the contrary to the result for the first layer. This is not only unexpected from the travel times but also fairly artificial. Also to explain the delay present uniformly in T(I), T(II) and T(III) at D_{14}, an abnormally thick second layer should be introduced at D_{14} because of too thin first layer in the above model. Therefore, the modification of the model is made by the following procedure. There are many possible models of the structure in $D_{13} \sim D_{14}$ since D_{14} is located at the end of the profile and there are no observation points for 3.5 km between D_{13} and D_{14}. Although the first layer is assumed to hold its tendency continuously between D_{12} and D_{14} in the first model, a model with an offset between D_{13} and D_{14} gives the same travel times with those in the first model on the same interpretation that T(IV) gives T_1 at D_{14}–f$\sim$a and T_2 between D_{13}–c and D_{12}–b. Then the decrease in H_1 at D_{12} and D_{13} and the increase in H_1 at D_{14} by the same amount cause the more increase in the depth d_3 at D_{12} and D_{13} and the decrease in d_3 at D_{14}. This change is expected to improve the model. The change in H_2 due to that in H_1 is evaluated by using the formula derived below.

$$(T-T')-H_1 \cdot \frac{\cos\theta_{13}}{v_1} = H_2 \cdot \frac{\cos\theta_{23}}{v_2},$$

$$\text{then } \frac{\partial H_2}{\partial H_1} = -\frac{\cos\theta_{13}/v_1}{\cos\theta_{23}/v_2} = -2.46 \quad \text{and} \quad \frac{\partial(H_1+H_2)}{\partial H_1} = -1.46.$$

Thus H_1 is reduced by 0.40/1.46=0.27 km to eliminate the difference of 0.40 km in d_3 between D_{12}–a and D_{12}–b. That is, the model of the second approximation derived from reducing H_1 by 0.27 km between D_{12}–b and D_{13}–c and increasing it by the same amount at D_{14} is given below.

Observation point	D_{12}–b	D_{13}–b	D_{14}–a	D_{14}–f
H_1 (km)	0.08	0.26	1.16	1.24
H_2 (km)	1.04	1.04	1.23	1.50
d_3 (km)	1.12	1.30	2.39	2.74

However, from graphical calculations of travel times based on this model (O–C)'s such as $-0.07 \sim -0.10$ sec at $D_{10} \sim D_{11}$ and about -0.15 sec at D_{14} result for T(III) and $-0.10 \sim -0.15$ sec at observation sites farther northwest of D_{12}, for T(IV). Therefore, the thickness of the second layer is reduced by 0.2 km between D_{10} and D_{12} and it is increased by 1.0 km at D_{14} to improve the large (O–C)'s. The final model of the underground structure is shown in Fig. 8. The depth to the top of the third layer is about 1.3 km in E_4–20$\sim E_4$–24, 1.5 km at D_8, 1.2$\sim$1.0 km at D_9, almost horizontal in $D_{10} \sim D_{11}$ and increases again from D_{12} until D_{13}. Farther southeast it increases fairly abruptly by 1.0 km at D_{13} and reaches 2.2 km from the earth's surface (that is, 1.5 km below the mean sea level) deepening with the dip of about 25° toward the southwest. This amount of dip, 25°, is necessary to explain the apparent velocity, about 4.1 km/s, obtained at D_{14}–a$\sim$f from observation of the shots other than B-IV. Although the offset at D_{13} is shown by a dotted line, the steep dip (45°) of the offset is the minimum value to satisfy the observed travel times at D_{13} and D_{14} simultaneously.

3) I-II

First, the thickness of the first layer (v_1=2.1~2.2 km/s) is derived on the assumption of one layered model since the velocity of the third layer can not be found in T(I) and T(II). T_2' is constructed by fitting the line with the gradient of 1/(4.0 km/s) to the data at D_3 and D_4. The thickness of the first layer obtained from T–T' is about 1.0 km at D_1 and D_2, about 0.70 km at D_3 and D_4, about 0.65 km at D_5 and about 0.50 km at D_6. Since T(I) and T(II) do not give T_3, the information on the velocity in the third layer should be obtained from T(III) and T(IV). T(IV) is roughly parallel to T(III), but T(III) is chiefly used in this analysis because there is a possibility that the information on the layer below the third one may be included in T(IV) as mentioned previously and also seismograms in this section from the shot B-IV are poor on the whole.

Now, T(III) (as well as T(IV)) gives very low apparent velocity 3.4 km/s at D_4, D_5 and D_6 and the apparent velocity 6.2 km/s at D_1, D_2 and D_3. This may be interpreted as the top of the third layer to become deep abruptly around E_1 and then extend almost horizontally to the northwest of D_4. The offset of the first approximation is estimated as described in the following.

First, the average value of T–T' is obtained as about 1.3 sec by extending T'(I–III) to D_4~D_1. Combining this value with H_1 already derived (for example, 0.70 km at D_3), d_3 which is the sum of H_1 and H_2 is computed as 6.0 km. Therefore, the interface between the layers with the velocity of 4.0 km/s and 6.0 km/s can be assumed to be located at the depth of 5.0 km below the mean sea level, since the surface elevation in this section is 1.0–1.1 km above the mean sea level. There exists an offset of several km in the top of the third layer between E_1 and D_6 in this model, which has too large irregularity to be analysed by the method of differences. Therefore, successive modification of the model is carried out by calculating travel times graphically.

First, the shape of the offset is examined in the range D_6~E_1. Judging from the structure of the first approximation and the apparent velocity, T(III) and T(IV) in D_4~D_6 are safely regarded as travel times of waves diffracted from the edge of the shallow third layer at E_1 into the second layer instead of those of waves refracted from the third layer at D_6. According to the computed travel times corresponding to T(III), it is concluded that the top of the third layer increases its depth discontinuously under E_1–15 and waves should diffract from the corner to D_4~D_6. Although the description was done as if the third layer extending to the northwestern end of E_1, (see page 190), there is no necessity to alter the shallow structure in E_1–15~E_1–1 due to the modification explained above since the P waves to E_1–15~E_1–1 are refracted around the point below E_1–15 into the second layer even in the former model. Furthermore, it is evident that the top of the third layer should become deep with the dip larger than at least 50° to the northwest for the waves diffracted from the above corner to be observed as the initials at D_3~D_6. In the following examination this dip is tentatively assumed to be 57°.

After the form of the top of the third layer was elaborated, the differences between observed travel times and calculated ones, (O–C)'s, are –0.190 sec at D_3 and –0.200~–0.300 sec at D_1 and D_2 for the model of the first approximation (in which the depth to the top of the third layer is 5.0 km below the mean sea level). Thus it is found that the depth to the top of the third layer is too large and this top becomes shallower a little toward the northwest with the dip of 2.2° from the apparent velocity at D_1~D_3. The method of trial and error is applied to obtain (O–C) less than 0.050 sec since there are no simple methods to obtain the correction to the depth of the first approximation. The underground structure thus derived is given in Fig. 8. That is, for v_3=6.0 km/s the depth to the top of the third layer is 4.0 km below the mean sea level at the shot point B-II and decreases with the dip of 2.2° toward the northwest. Its extension reaches 3.7 km below the mean sea level at the shot point B-I. This model gives the difference of about 2.8 km in the depth to the top of the third layer in the area E_1–1~12.

Now the effect of the values of v_2 and v_3 on the underground structure is examined in the following. There is a possibility for v_2 to be as much as about 4.3 km/s in this section as mentioned in **II.3.** For the value 4.3 km/s, the changes in H_1 and in the dip of the top of the third layer are so small that the effect can be disregarded (change in H_1: $+1\%$; change in the dip: $+0.1°$), while the value of d_3 changes by 0.700 km, that is, the increase in d_3 due to the change in v_2 is 18 %. Therefore, the amount of the offset at E_1 becomes 3.5 km as shown in Fig. 17. Since there are no data on T_3 from the northwest in I-II, there is no method suitable to determine v_3 and the value 6.0 km/s has been assumed for v_3 so far to derive the underground structure by referring to the values in the other sections. Here, the changes of the underground structure are examined in two cases of 5.5 km/s and 6.5 km/s for v_3. Assuming these values of v_3 are applied at the northwest of E_1, the position of the interface between the second and the third layers is obtained again by the method of trial and error. The results are also shown by dotted lines in Fig. 17 and summarized as follows:

(1) The case $v_3=5.5$ km/s

d_3 at the shot point B-II:	3.7 km below the mean sea level
d_3 at the shot point B-I:	2.2 km below the mean sea level
the angle of dip:	$+6.5°$

(2) The case $v_3=6.5$ km/s

d_3 at the shot point B-II:	4.2 km below the mean sea level
d_3 at the shot point B-I:	4.7 km below the mean sea level
the angle of dip:	$-2.2°$

The plus sign in the angle of dip implies that the interface becomes shallower toward the northwest and the minus sign, deeper toward the northwest. The amount of the offset at E_1 for both cases is the same with that for the case of 6.0 km/s, that is, 2.8 km. The change in the depth between D_6 and E_1 is not large for other possible values, while the dip becomes unreasonably large for some of v_3. Thus, the underground structure derived on the assumption of 6.0 km/s for v_3 has been supported from the above trials.

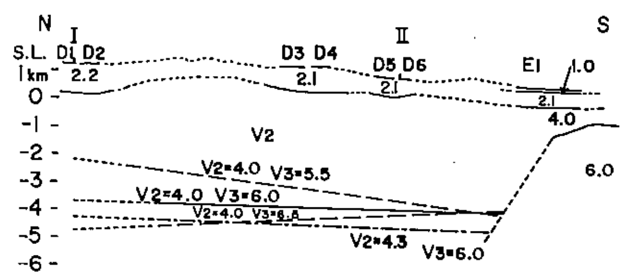

Fig. 17 Various models in the section between B–I and E_1

III. Some Remarks on the Relation between the Underground Structures Derived from the Present Experiment and the Results from Other Geophysical and Geological Investigations

In this section the underground structures derived from the explosion seismic data are going to be compared with the results obtained by other geophysical and geological investigations and some related considerations will be given.

1) The location of hypocenters

The Matsushiro Earthquake Swarm has not ceased its activity yet although more than three years have passed and the decreasing tendency of seismic activity has appeared. During this long period of activity, in addition to the Japan Meteorological Agency, Earthquake Research Institute, University of Tokyo, and almost all kinds of related universities and institutions made use of this opportunity to carry out various kinds of seismological observations. Of these investigations, the location of hypocenters of felt earthquakes determined by the temporary net of Earthquake Research Institute is presented in Fig. 18[5]. Comparing this figure with the underground structures shown in Figs. 2 and 8, several interesting points are observed. The first remarkable point is that almost all earthquakes have occurred in the layer with the velocity of 6 km/s, furthermore, they have confined their hypocenters to the shallower part of this layer as shown in the structure of Fig. 8. Next, since the locations of hypocenters in Fig. 18 are projected to the vertical plane roughly parallel to profile A, Fig. 18 is compared with the structure of profile A (Fig. 2). It is noticed from this comparison that the top of the layer with the velocity of 6.0 km/s becomes shallower toward the southwest, while the focal depth has a tendency to become large as a whole toward the southwest. This fact presents the data for the question whether this discrepancy would be caused by the structure of the factors

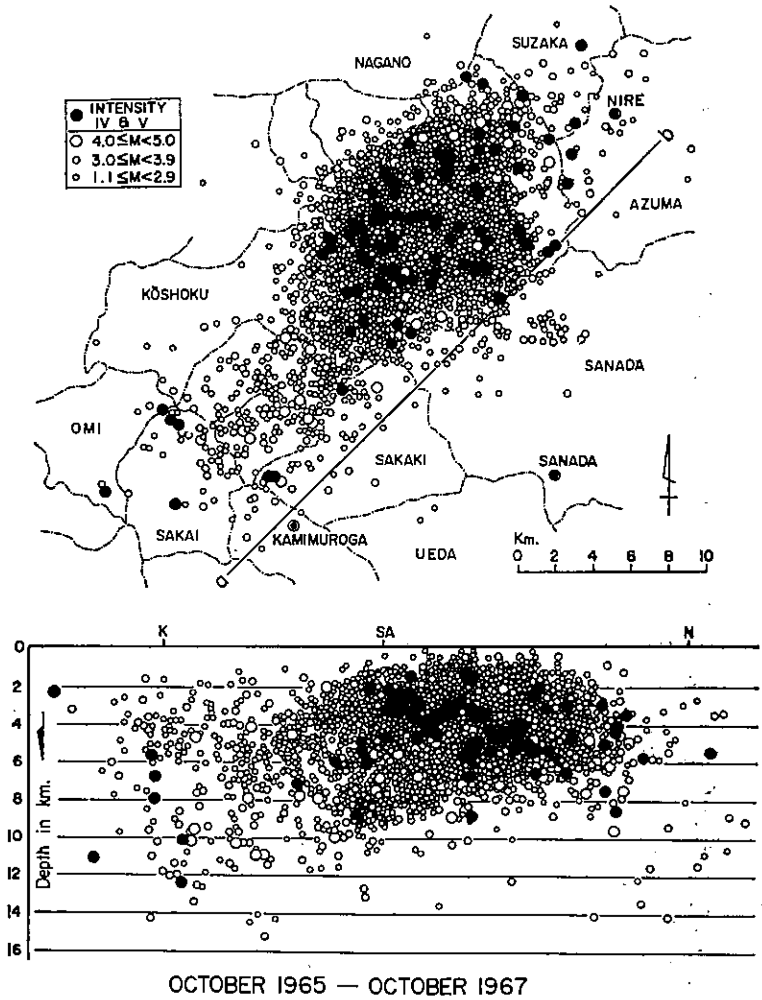

Fig. 18 Distribution of hypocenters of the felt earthquakes in the period October 1965–October 1967. a–b: Plane of projection, K: Kamimuroga, N: Nire, SA: Sanada (After HAGIWARA and IWATA).

generating swarm earthquakes or whether this discrepancy would indicate that the structure of strength including inhomogeneity might differ from the velocity structure, etc.

Furthermore, one of the reasons why there are little earthquakes northwest of the Chikuma River may be attributed to the underground structure with the fault-like deepening of the third layer (the layer of 6.0 km/s). However, the locations of hypocenters shown in Fig. 18 were determined without accurate information on the velocity structure. Therefore it is worth while examining those locations of hypocenters by taking the underground structure into account. It is interesting to see the change in the locations of hypocenters through above procedure and to see whether the relation between the underground structure and the locations of hypocenters becomes clearer or not.

2) The velocity of seismic waves by the observations of natural earthquakes and the locations of hypocenters by the tripartite observations

The velocity information derived from the data of tripartite observations and from the data of mobile observations is examined by the structure shown in Figs. 2 and 8.

First, according to the results reported by HAMADA and HAGIWARA[8] from the data of the tripartite observations at Hoshina the minimum value of the apparent velocity obtained is 5.0 km/s and this value is adopted to determine hypocenters on the assumption of uniform structure. Hoshina is located on a little east of the spread E_3 of profile A near the mountain and the measurement of surface structure at E_3 gives the value 4.75 km/s for the velocity of the second layer. Since almost all earthquakes occurred in the third layer (with the velocity of 6.0 km/s), the value 5.0 km/s used to determine hypocenters may be fairly good approximation on the average although the length of path in each layer should be taken into account in the accurate procedure. Also HAMADA and HAGIWARA[9] obtained from the data of the tripartite observations at Sanada that the minimum value of the apparent velocity is 4.5 km/s, the maximum frequency of that is at 5.0 km/s and from the dependence of the apparent velocity on the azimuth it is possible for the upper layer to become thick in the direction of S35°E. Since Sanada temporary observatory is close to D_{13} in profile B, the last result is fairly pertinent to the structure in Fig. 8. At Sanada as well as at Hoshina, the initial wave is the direct wave travelling through the layers with velocities 2.4, 4.4 and 6.0 km/s. The results mentioned above on the apparent velocity can be also understood qualitatively from the structure shown in Fig. 8. The minimum apparent velocity obtained from the tripartite observations at Kamimuroga is 5.0 km/s[20] and it is found that there are systematic differences between the hypocenters determined by the data of the tripartite observations at Sanada and at Kamimuroga and those determined by the temporary stations surrounding the epicentral area[9, 20]. The existence of these systematic differences are similarly found at Kamimuroga, and this may imply that these observation sites similarly deviate from the strike of the underground structure.

Furthermore from the tripartite observations at Asakawa apart from the Central Belt of Uplift the hypocenters are obtained as deviated about 30° clockwise from Asakawa[3]. At Asakawa the minimum apparent velocity is 4.0 km/s which is used to determine the hypocenters. Asakawa is near D_5 and D_6 in profile B and the minimum apparent velocity smaller than at other stations such as Hoshina, Kamimuroga, etc. may be due to the existence of the thick first layer with the velocity of 2.1 km/s.

HAMADA[7] concluded from the relation between Omori's constant K and hypocentral distance that K for the wave propagating toward the southwest is larger than K for the wave propagating toward the northeast, the fact that the value of K is closely related to the direction of propagation indicates the complicated structure shallower than several km and on the average the velocity is larger in the southwest than in the northeast. These results are reasonable from the underground structure shown in Figs. 2 and 8 together with the results that the apparent velocity 6 km/s is obtained quite frequently at Kamimuroga where $S-P$ time is large, while the apparent velocity obtained at Asakawa is small in spite of large $S-P$ time. For example, since in profile A the top of the layer with the velocity of 6.0 km/s becomes deep toward the northeast, the velocity appears to be smaller in the northeast than in the southwest.

Asano and others[2] carried out observations at five temporary stations in the distance range 15–55 km in the northeastern direction almost parallel to profile A and its extension and obtained the apparent velocity 5.13 km/s on the average. It is estimated that there exists the layer with the velocity of 5.13 km/s in thickness of about 9 km above the layer with the velocity of 6.0 km/s by using the small travel times observed at the distant two observation stations. This estimation is based on the assumption of the velocity structure derived from the Miboro explosions. However, according to the structure in Figs. 2 and 8 there exist anomalous underground structures in this district in which there is no layer with the velocity of 5.5 km/s, the layer with the velocity of 4.5–4.8 km/s is thin and the top of the layer with the velocity of 6.0 km/s is shallow. In order to get more correct information the data should be re-examined by taking these points into account. However, it is reasonable that the apparent velocity 5.1 km/s is derived from the observations of the direct wave.

The minimum apparent velocity derived by Hori[10] from the tripartite observation near D_4 and D_5 in profile A is 4.8 km/s and the value 5.5 km/s is most frequently observed. These results can be explained by the underground structure.

There is one profile of Research Group for Explosion Seismology[29] passing this region in the case of Miboro explosions. The crustal structure derived has a fairly thick layer with the velocity of 5.5 km/s[15]. However, there is no doubt that the structure obtained by this experiment is of quality better than that derived from the data of the Miboro explosions since the shot and observation points are more dense in this experiment and the quality of data is also on the average better in this experiment. Therefore, the structure derived by Mikumo and others[15] should be re-examined by taking the abnormal structure in this district into account if it is necessary.

Nagumo and others[18] obtained the value 3.2 km/s for the velocity of black shale and the value 3.8 km/s for the velocity of porphyry mass by the seismic prospecting with the span of 30–50 m in the pit of the Seismological Observatory, Japan Meteorological Agency. The value of 4.4 km/s is obtained in this area by the experiment in the present paper. The slight difference between the velocities may be due to the difference of scales in the experiments as well as to the different locations between two experiments.

Also Takahashi and others[25] obtained the value 4.1 km/s for the velocity of Bessho Formation at the depth 150–200 m from the velocity logging in the bore hole with the depth of 200 m near Mt. Minakami and the value is very close to the value derived from the experiment of the present paper.

3) Earthquake generating force

According to the investigation on the mechanism of the Matsushiro earthquakes from the distribution of push and pull of initial P waves by Ichikawa[11] and the Party for Seismographic Observation of Matsushiro Earthquakes and the Seismological Section[28], it is found that the distribution of push and pull from almost all Matsushiro earthquakes is of quadratic type, the direction of principal pressure of the Matsushiro earthquakes agrees with that of very shallow earthquakes having occurred in the past in this district, which is roughly east-west. The agreement between these results and the direction of crustal deformation is most remarkable[13] and furthermore, the comparison of these results with the underground structure as shown in Figs. 2 and 8, especially in Fig. 8, is quite interesting from the stand point of physical process of the Matsushiro earthquakes.

4) Other geophysical results

The existence of close correlations between the seismic activity and the crustal movement is one of the most established facts in the Matsushiro Earthquake Swarm. The narrow area including Mt. Minakami uplifted by about 40 cm within the first month of the third stage (August-December, 1966) [30] and there happened to record or observe sudden change in the tilting and the extension of ground surface[6],[13]. This means that the upheaval occurred in the Central Belt of Uplift as its name and the correspondence between the shallower part of the top of the third layer in profile B and the uplifted part is quite interesting. Also it is quite noteworthy that the shallower portion of the upper boundary of the layer with the velocity of 6.0 km/s between D_8 and E_2 in profile A is closely related to the part of ground upheaval in 1966 between Yashiro and Suzaka[30].

The surveys such as with electrical, gravimetric methods were carried out by the Geological Survey of Japan. The agreement between the structure estimated with the electrical method[21] and the corresponding part of structure in profile B is quite good. Especially in the structure of Fig. 8 the layer with the velocity of about 2 km/s becomes thick from Mt. Minakami toward the northeast across the Chikuma River and there is sudden change in the thickness of this layer near the Chikuma River. These features also resulted from the survey by the electrical method. According to the distribution of Bouguer anomaly derived from the gravity survey, the decrease of Bouguer anomaly by 15–20 mgal in the northwestern part supports the underground structure of profile B[23]. The distribution of Bouguer anomaly along profile A has a tendency to increase slightly in a large scale toward the southwest although it is disturbed by the local anomaly and this tendency coincides with that of the top of the third layer in Fig. 2.

In addition to the agreement between the results from the above different methods, there is also the coincidence between the result by the airborne magnetic survey[24] and by the seismic method. There is a change of the pattern in the distribution of magnetic anomaly around Matsushiro, that is, there is positive anomaly in the southwest of Matsushiro and negative anomaly in the northeast of Matsushiro. The existence of a boundary near Matsushiro is also seen in the distribution of Bouguer anomaly and there is a possibility that this boundary corresponds to that between 5.9 km/s and 6.0 km/s in profile A. Also the strike of NE–SW shown in the distribution of magnetic anomaly as well as in that of gravity anomaly agrees with the features of the underground structure in Figs. 2 and 8.

5) Geological results

Extensive geological investigations were concentrated to the relation between swarm earthquakes and geology (MORIMOTO and others[16], SAWAMURA and others[22], NAKAMURA and TSUNEISHI [19], MURAI[17], MATSUDA[14]). From the comparison of the underground structure in Figs. 2 and 8 with the geology in this area it is clearly seen that the Central Belt of Uplift as named by IIJIMA[12] is exhibited quite well in the structure derived only from the seismic method. In the structure of profile B there is an offset by about 3 km between observation sites E_1 and D_6 if the layer with the velocity of 4 km/s is assumed to exist directly above the layer with the velocity of 6.0 km/s. This offset may give the western end of the Central Belt of Uplift. Also the structures in Figs. 2 and 8 show that not only the surface layers but also the deeper structures might have played an important role in formation of the Central Belt of Uplift and this is closely connected with the geological history (IIJIMA[12]). Whether the layer deeper than that of 6.0 km/s is also related to the formation of the Central Belt of Uplift or not is an interesting subject to be investigated in near future, also probably relating to the cause of the Matsushiro Earthquake Swarm. The travel times observed at observation points near Mt. Minakami show quite peculiar behavior, but detailed minor structure has not been elaborated because of the quality of data.

Since profile A is in the Central Belt of Uplift, the underground structure in this profile is simpler than that in profile B as expected. The dependence of velocity about 4.0 km/s on the locality might be caused by the differences in the constituent rocks with the intrusion of volcanic rocks. Also it is ascertained that the Central Belt of Uplift extends farther southwestward passing the Chikuma River.

It is interesting to correlate the velocity of seismic waves with the rocks in the actual layer by comparing the structure in Figs. 2 and 8 with the geology. It is well known that the structure derived from the seismic method is only connected with elastic properties and the layers with the same elastic parameters as a gross in spite of different constituents can not be distinguished by the seismic method. In addition to the above feature because of the resolving power in the refraction method it is hard to find one to one correspondence between the layers determined by the seismic method and those by the geology. However, since there exist good correlations between the features of structure derived from the seismic method and of geological one, it is worth while trying to find the correspondences. The layer with the velocity of about 2 km/s corresponds to the sedimentary layer formed in the era from the late Miocene to the Quaternary, although the same layer around Mt. Iizuna near D_3 and D_4 in profile B may be composed of volcanic rocks. The layer with the velocity of about 4 km/s corresponds chiefly to the sedimentary layer of sea origin (Bessho Formation, Uchimura Formation, etc.) in the era of Neogene, mainly before the middle Miocene, locally with intrusion of porphyry mass, diorite, etc. The layer with the velocity of 3.3 km/s in the southwestern portion of profile A may be correlated to the sedimentary layer newer than the middle Miocene. The layer with the velocity of 6.0 km/s is the basement in this district and is considered to consist of Miocene granitic rocks in the elevated part and Palaeozoic rocks or corresponding metamorphic rocks or granitic rocks of the Mesozoic era in the deeper part.

IV. Conclusions

Explosion seismic studies of the Matsushiro Earthquake Swarm area were carried out in two profiles A and B to investigate the deep underground structure including hypocentral regions of these swarm earthquakes, the activity of which becomes weaker at present and the results of these studies are presented in Figs. 2 and 8. This kind of study in the active epicentral area was conducted for the first time not only in Japan but also in the world.

Profile A is set up roughly parallel to the strike of the Central Belt of Uplift and within this geological block crossing the epicentral area in the direction of NE–SW. The underground structure in this profile is fairly simple as expected and it is found that the top of the third layer with the velocity of 6.0 km/s is very shallow on the whole and there is a tendency for this top to deepen a little in the northeast and to become shallow in the southwest. Also the top of the layer with the velocity of 6.0 km/s is shallower from the middle of the spread E_2 (near Suzaka) to D_8 (near Matsushiro) by 0.3–0.5 km than in other portions of the profile. The depth to the top of the third layer from the earth's surface is 0.9–1.2 km around Nakano, 1.0–1.5 km around Suzaka, 0.7–0.9 km around Matsushiro, and 0.7 km farther south around Sakai. The velocity in the third layer is 6.0 km/s in the northeastern portion of Matsushiro and 5.9 km/s in the southwestern portion of Matsushiro. The velocity in the first layer is 1.6–2.3 km/s and the thickness of the first layer is largest at the spread E_3 around Kawada. The velocity in the second layer varies from 3.3 to 4.75 km/s depending upon the locations and is smallest in the southwest. Since there is no observation point between E_4 and E_5 because of topography, the details of the structure are not certain. However, it is noteworthy that there exists a kind of anomaly or discontinuity, which might be related to the anomaly such as Bouguer near Mt. Minakami although profile A runs a little apart from Mt. Minakami.

In profile B crossing the Central Belt of Uplift through the epicentral area in the NW–SE direction the underground structure obtained is fairly complicated. The velocity in the first layer is 1.7–3.2 km/s except for the thin surface layer present locally and it is notable that this first layer becomes thick almost discontinuously from the vicinity of the Chikuma River toward the northwest. The velocity of the second layer is 4.0–4.4 km/s. Attention must be paid to the almost discontinuous thickening of the second layer toward the northwest in the middle of the spread E_1 near Nagano City, where the increase of depth to the upper boundary of the third layer occurs by about 3 km on the assumption of the second layer existing directly above the third layer with the velocity of 6.0 km/s. This means from another point of view that the top of the third layer becomes shallower almost discontinuously in the central portion of the profile, only about 1 km from the earth's surface near the intersection with profile A and getting shallower further at D_{11} roughly parallel to the topography.

There is a tendency for the first layer with the velocity of 2.4 km/s to become thick toward farther south, and the top of the third layer becomes deeper abruptly by about 1 km at D_{13}. This structure is considered to define that of the Central Belt of Uplift. It should be pointed out that at least the layers including the layer with the velocity of 6.0 km/s might contribute to the formation of this geological block or there is a possibility for the layer with the velocity of 6.0 km/s to have played an important role to the upheaval. Furthermore, it is notable that there exists a fault or a kind of anomalous structure near Mt. Minakami in this profile. At present it can not be concluded from the results of two profiles whether or not this extraordinary feature in profile B comes from the same origin which introduced an anomalous structure in profile A. However, since the offset is quite similar in manner, in quantity and in location between the two profiles, there is a large possibility for these two features to be of same origin. At any rate, it is interesting to note that the location of these anomalous structure is in the region where swarm earthquakes occurred most frequently.

In addition to the above anomalous structure, attention must be paid to the absence of the layer with the velocity of about 5.5 km/s.

So far the underground structure derived exclusively from the explosion seismic data has been summarized. Comparing the present structure with results from other kinds of data, the several important points are summarized in the following. It becomes clear that most of swarm earthquakes occur in the layer with the velocity of 6.0 km/s, the correspondence between the present structure and the structure estimated from the geological investigation is fairly good. Also the deep structure of the so-called Central Belt of Uplift is obtained in more detail and the existence of anomalous structure near Mt. Minakami becomes fairly certain. Furthermore, the agreement between results derived from different methods such as explosion-seismic, gravity, electric, airborne magnetic, geodetic is excellent although mostly qualitative. According to HAGIWARA[4)], results from all kinds of observations can be tentatively explained on the idea that the Matsushiro Earthquake Swarms have occurred due to the intrusion of water of deep origin into the body under the large pressure in the east-west direction. The results obtained by the present study may also support this explanation.

One of the original objectives in the present explosion seismic studies is to offer the information necessary to determine the hypocenters. Once the fairly detailed underground structures have derived, it should be investigated how the distribution of hypocenters is affected by the information on the underground structure and how accurately the hypocenters can be determined under the best circumstances with good network and information on the structure. Furthermore, there are many future problems from the standpoint of understanding the physical processes included in the Matsushiro Earthquake Swarm such as whether the layer deeper than the layer of 6.0 km/s is related to the upheaval, that is, the investigation on the deep structure of the Central Belt of Uplift, the investigation on the abnormal structures between E_4 and E_5 in profile A and around E_4 and D_7 in profile B near Mt. Minakami, the re-examination of gravity data and so on. Also it is interesting to drill holes at appropriate places since the top of the layer with the velocity of 6 km/s is found to be shallow.

In conclusion, the authors express hearty gratitude to the scientists and technicians who participated in this experiment for advices, encouragements and placing the data at author's disposal. The authors' thanks are also due to Dr. K. NAKAMURA for his discussions. The authors are much obliged to Misses M. KUBOTA, S. INOUE, M. IMAI and Messrs. I. OGINO, M. SAKA, Y. ICHINOSE for assistance in computations, in typewriting the manuscript and in preparing figures.

References

1) ASANO, S., ICHIKAWA, K., OKADA, H., KUBOTA, S., SUZUKI, H., NOGOSHI, M., WATANABE, H., SEYA, K., NORITOMI, K. & TAZIME, K. (1969): Explosion seismic studies of the Matsushiro Earthquake Swarm Area, Part 1 Explosion seismic observations in the Matsushiro Earthquake Swarm Area, *Spec. Rep. Geol. Survey of Japan*, no. 5.

2) ASANO, S., OHTA, Y., YANAGISAWA, M., ICHINOSE, Y. & MAEDA, Y. (1966): Observations of the Matsushiro Earthquake Swarm at five temporary stations (Part 1), *Bull. Earthq. Res. Inst. Univ. of Tokyo*, vol. 44, p. 1771～1792 (in Japanese).

3) GENERAL SEISMOMETRY LABORATORY (1967): High sensitivity tripartite observation of Matsushiro Earthquakes; observations at Kamimuroga, Kawanishi Village and at Asakawa, Nagano City (Part 4), *Read at the* 450-th *Monthly Meeting of Earthquake Research Institute, Univ. of Tokyo, Feb. 28.*

4) HAGIWARA, T. (1967): General description of the Matsushiro Swarm Earthquakes, *Zisin*, Ser. II, vol. 20, no. 4, p. 192～200 (in Japanese).

5) HAGIWARA, T. & IWATA, T. (1968): Summary of the seismographic observation of Matsushiro Swarm Earthquakes, *Bull. Earthq. Res. Inst. Univ. of Tokyo*, vol. 46, p. 485～515.

6) HAGIWARA, T., YAMADA, J. & HIRAI, M. (1966): Observation of tilting of the earth's surface due to Matsushiro Earthquakes, Part 1, *Bull. Earthq. Res. Inst. Univ. of Tokyo*, vol. 44, p. 351～361.

7) HAMADA, K. (1968): Ultra micro-earthquakes in the area around Matsushiro, *Bull. Earthq. Res. Inst. Univ. of Tokyo*, vol. 46, p. 271～318.

8) HAMADA, K. & HAGIWARA, T. (1966): High sensitivity tripartite observation of Matsushiro Earthquakes. Part 1, *Bull. Earthq. Res. Inst. Univ. of Tokyo*, vol. 44, p. 1213～1238.

9) HAMADA, K. & HAGIWARA, T. (1967): High sensitivity tripartite observation of Matsushiro Earthquakes. Part 4, *Bull. Earthq. Res. Inst. Univ. of Tokyo*, vol. 45, p. 159～196.

10) HORI, M. (1967): Matsushiro Earthquake Swarm and its peripheral seismicity, *Bull. Earthq. Res. Inst. Univ. of Tokyo*, vol. 45, p. 489～503 (in Japanese).

11) ICHIKAWA, M. (1967): Statistical study of the focal mechanism of Matsushiro Earthquake Swarm, *Zisin*, Ser. II, vol. 20, p. 116～127 (in Japanese).

12) IIJIMA, N. (1962): Volcanostratigraphy and petrology of the eastern part of Fossa Magna (Part 1), *Bulletin of the Faculty of Education of Shinshu University, Natural Science*, no. 12, p. 86～133 (in Japanese).

13) KASAHARA, K. & OKADA, A. (1966) (1966) (1967) (1968): Electro-optical measurement of horizontal strains accumulating in the swarm earthquake area, *Bull. Earthq. Res. Inst. Univ. of Tokyo*, (1), vol. 44, p. 335～350; (2), vol. 44, p. 1715～1733; (3), vol. 45, p. 225～239; (4), vol. 46, p. 651～661.

14) MATSUDA, T. (1967): Geological aspect of the Matsushiro Earthquake Fault, *Bull. Earthq. Res. Inst. Univ. of Tokyo*, vol. 45, p. 537～550 (in Japanese).

15) MIKUMO, T., ŌTSUKA, M., UTSU, T., TERASHIMA, T. & OKADA, A. (1961): Crustal structure in Central Japan as derived from the Miboro explosion-seismic observations. Part 2. On the crustal structure, *Bull. Earthq. Res. Inst. Univ. of Tokyo*, vol. 39, p. 327～349.

16) MORIMOTO, R., MURAI, I., MATSUDA, T., NAKAMURA, K., TSUNEISHI, Y. & YOSHIDA, S. (1966): Geological consideration on the Matsushiro Earthquake Swarm since 1965 in Central Japan, *Bull. Earthq. Res. Inst. Univ. of Tokyo*, vol. 44, p. 423～445 (in Japanese).

17) MURAI, I. (1967): Fracture analysis of the seismic area where the Matsushiro Earthquake Swarm has been occurring, *Bull. Earthq. Res. Inst. Univ. of Tokyo*, vol. 45, p. 505～536 (in Japanese).

18) Nagumo, S., Takahashi, H. & Hasegawa, K. (1967): Elastic wave velocity measurement in the pit of the Matsushiro Seismological Observatory, *Notes of Cooperative Research for Disaster Prevention*, no. 5, p. 49～55 (in Japanese).

19) Nakamura, K. & Tsuneishi, Y. (1967): Ground cracks at Matsushiro probably of underlying strike-slip fault origin, II-The Matsushiro Earthquake Fault, *Bull. Earthq. Res. Inst. Univ. of Tokyo*, vol. 45, p. 417～471.

20) Ohtake, M., Chiba, H. & Hagiwara, T. (1967): Ultra micro-earthquake activity at the southwestern border of the area of Matsushiro Earthquakes. Part 1, *Bull. Earthq. Res. Inst. Univ. of Tokyo*, vol. 45, p. 861～886.

21) Ono, Y. (1967): Electrical sounding at Matsushiro Earthquake district (Report 1), *Notes of Cooperative Research for Disaster Prevention*, no. 5, p. 23～27 (in Japanese).

22) Sawamura, K., Kakimi, T., Sogabe, M., Kobayashi, I. & Hase, H. (1967): Geology and geological structure of the Matsushiro seismic area, *Notes of Cooperative Research for Disaster Prevention*, no. 5, p. 3～11 (in Japanese).

23) Seya, K. (1967): Gravity survey in the Matsushiro Earthquake Swarm Area, *Notes of Cooperative Research for Disaster Prevention*, no. 5, p. 13～22 (in Japanese).

24) Takagi, A., Kato, Y. & Muroi, I. (1968): Features of some earthquake areas from the results of airborn magnetic survey, *Read at the annual meeting of Seismological Society of Japan, June 26.*

25) Takahashi, H., Takahashi, M. & Suzuki, H. (1967): Studies on the underground structure of the Matsushiro Earthquake Area by test boring, *Notes of Cooperative Research for Disaster Prevention*, no. 5, p. 57～81 (in Japanese).

26) Tazime, K. (1968): Refraction shooting at the projected place for the large bridge on the Bay of Akkeshi in Hokkaido (continued), *Geophysical Exploration*, vol. 21, p. 193～198 (in Japanese).

27) Tazime, K., Okada, H., Hamada, K. & Kubota, S. (1961): Seismic Prospecting at the projected places for the Dam at Shizunai and Shimo-shizunai in Hokkaido, *Geophysical Bulletin of the Hokkaido Univ.*, vol. 8, p. 11～35 (in Japanese).

28) The Party for Seismographic Observation of Matsushiro Earthquakes and the Seismological Section (1966): Matsushiro Earthquakes observed with a temporary seismographic network. Part 2, *Bull. Earthq. Res. Inst. Univ. of Tokyo*, vol. 44, p. 1689～1714.

29) The Research Group for Explosion Seismology (1961): Crustal structure in Central Japan as derived from the Miboro explosion-seismic observations. Part 1. Explosions and seismic observations, *Bull. Earthq. Res. Inst. Univ. of Tokyo*, vol. 39, p. 285～326.

30) Tsubokawa, I., Okada, A., Tajima, H., Murata, I., Nagasawa, K., Izutsuya, S. & Ito, Y. (1967): Levelling resurvey associated with the area of Matsushiro Earthquake Swarms. (1), *Bull. Earthq. Res. Inst. Univ. of Tokyo*, vol. 45, p. 265～288 (in Japanese).

爆破地震動観測資料より得られた
松代群発地震域の地下構造

浅野周三　窪田　将　岡田　広　野越三雄
鈴木宏芳　市川金徳　渡辺偉夫

要　　旨

松代群発地震域の速度構造を得るなどの目的をもって実施されたA, B 2測線における爆破地震動の観測資料を用いて地下構造を求めた。解析には T' 曲線を作って速度および層数を求め，境界面の傾きが小さいとして，第1近似の構造を推定し，走時の観測値と図式に計算した値との差，(O−C)を求め，trial and error method で (O−C) が小さくなるように修正する手続をとった。

A 測線

A 測線においては，3層構造であり

第1層（最表層）　1.6—2.3 km/s
第2層　3.3—4.75 km/s
第3層　5.9—6.0 km/s

さらに各区間で細かく見ると，

1）爆破点近傍の観測より得られた第1層の速度は

A-Ⅰ	A-Ⅱ	A-Ⅲ	A-Ⅳ	A-Ⅴ	
1.6	(<2.0)	2.3	2.3	(<1.9)	km/s

2）Ⅰ—Ⅱ

第1層　1.6—2.0 km/s
第2層　4.5 km/s
第3層　6.0 km/s

3）Ⅱ—Ⅲ

第1層　2.0—2.3 km/s
第2層　4.3—4.75 km/s
第3層　6.0 km/s

4）Ⅲ—Ⅳ

第1層　2.3 km/s
第2層　4.3—4.75 km/s
第3層　6.0 km/s

5）Ⅳ—Ⅴ

第1層　1.9—2.3 km/s
第2層　3.3—3.5 km/s
第3層　5.9 km/s

B 測線

全体として3層構造であり，ところにより，最表層が存在する。

最表層　0.36—1.2 km/s
第1層　1.7—3.2 km/s
第2層　4.0—4.4 km/s
第3層　6.0 km/s

各区間別に見ると

1） Ⅰ—Ⅱ

第1層	2.1—2.2 km/s
第2層	4.0 km/s

2） Ⅱ—Ⅲ

最表層	0.36—1.2 km/s
第1層	1.7—3.2 km/s
第2層	4.0—4.4 km/s
第3層	6.0 km/s

3） Ⅲ—Ⅳ

第1層	2.4—3.2 km/s
第2層	4.4 km/s
第3層	6.0 km/s

以上の速度を用いて求められた地下構造はA測線については Fig. 2 に，B測線については Fig. 8 に示されている。

A測線は，地質学上の中央隆起帯内に，その走向にほぼ平行に設けられており，構造は比較的簡単である。すなわち，第3層 (6 km/s 層) の上面は大変浅く，一番深いところでも地表より 1.5 km であり，南西に向かって少し浅くなる傾向がある。E_2 の中頃より D_8 までの区間でこの面が 0.3～0.5 km，他の部分より浅くなっているともみられる。速度については，松代の北東では 6.0 km/s，南西では 5.9 km/s である。また，E_4 と E_5 の間には地形のために観測点がおけなかったが，この付近に地下構造に異常あるいは断層が存在する可能性があり，皆神山近くの低い Bouguer 異常と対応するかも知れない。

B測線は，震央域の中心を通って中央隆起帯を横切っており，構造は複雑である。第1層の速度は 1.7～3.2 km/s で，千曲川の近くで北西に向かつてほとんど不連続的に厚くなっている。第2層の速度は 4.0～4.4 km/s であり，長野市付近の E_1 の中間より北西に向かって 3 km 程度急激に厚くなっていることは注目すべきことである。別の見方では，第3層の上面が測線中央部できわめて浅くなっており，地表からわずかに 1 km 程度に達する。さらに測線南東部では深くなっており地質学上の中央隆起帯の深部構造を与えるといえる。中央隆起帯は少なくとも 6 km/s の層までは，その形成に関係があった，あるいはこの層が重要な役割を演じたといえるかも知れない。この測線は D_7 において皆神山を迂回しているが，この付近の構造は異常の存在を示しており，重力の結果とよく対応している。A測線での異常と場所も近く，異常の傾向が似ているので，同じ原因による可能性は大きい。地震がもっとも頻発した地域にこのような異常が存在することはきわめて興味深い。また，5.5 km/s 程度の速度の層が存在しない点でも調査地域の構造は異常といえる。

一方，他の地球物理学的，地質学的研究結果と比較すると，今回得られた地下構造は，それらの解釈を与え，大変興味ある事柄を示す。群発地震はほとんどが 6 km/s の層の中に起っていること，地質学的な構造との対応がよいこと，とくに中央隆起帯の深部構造を与えること，皆神山付近の構造の異常が明らかになったこと，いろいろな方法による構造の情報とよく調和していることなどが重要な点であろう。

地質調査所特別報告

第 1 号

門倉三能，大橋敏男，伊原敬之助，木村六郎，佐藤戈止，赤木　健：関東地震調査報告 第 1，1925

第 2 号

門倉三能，小倉　勉，清野信雄：関東地震調査報告　第 2，1925

第 3 号

新潟地震調査研究グループ：新潟地震調査研究報告，1966

第 4 号

須貝貫二，佐藤　茂，牧野登喜男：新潟地震予察報告，1966

SPECIAL REPORT, GEOLOGICAL SURVEY OF JAPAN

No. 1

KADOKURA, M., OHASHI, T., IHARA, K., KIMURA, R., SATO, H. & AKAGI, T.: Reports on the Kwanto Earthquake, September 1923, Part I, 1925 (in Japanese)

No. 2

KADOKURA, M., OGURA, T. & KIYONO, N.: Reports on the Kwanto Earthquake, September 1923, Part II, 1925 (in Japanese)

No. 3

Research Group of Niigata Earthquake: Report of the Geological Survey on the Niigata Earthquake, 1966 (in Japanese with English abstract)

No. 4

SUGAI, K., SATO, S. & MAKINO, T.: Report of a Preliminary Survey on the Niigata Earthquake, 1966 (in Japanese with English abstract)

ASANO, S.
& others

Explosion Seismic Studies of the Matsushiro Earthquake Swarm Area Part I
Explosion Seismic Observations in the Matsushiro Earthquake Swarm Area

Shuzo ASANO & others

Special Report, Geological Survey of Japan, No. 5, p. 1～162, 1969
291 illus., 26 tab.

Explosion seismic observations in the Matsushiro Earthquake Swarm Area were conducted in the period of November 14-December 7, 1967 for two profiles A and B. One of the purposes of this experiment is to obtain the velocity structure in the swarm area. Fourteen parties with magnetic tape recorders and five parties with 24 element seismic prospecting instruments were distributed in each profile. Most of seismograms obtained are fairly good.

550.343:550.348.436.098.62(521.52)

ASANO, S.
& others

Explosion Seismic Studies of the Matsushiro Earthquake Swarm Area Part II
Underground Structure in the Matsushiro Earthquake Swarm Area as Derived from Explosion Seismic Data

Shuzo ASANO & others

Special Report, Geological Survey of Japan, No. 5, p. 163～203, 1969
21 illus.

The underground structure in the Matsushiro Earthquake Swarm Area was derived from explosion seismic data in profiles A and B by the method of differences. This structure is compatible with results obtained by other geophysical and geological methods.

550.24:550.348.05(521.52)

昭和44年10月4日　印刷
昭和44年10月9日　発行

工業技術院地質調査所

印刷者　小宮山一雄
東京都新宿区天神町78
印刷所　小宮山印刷工業株式会社

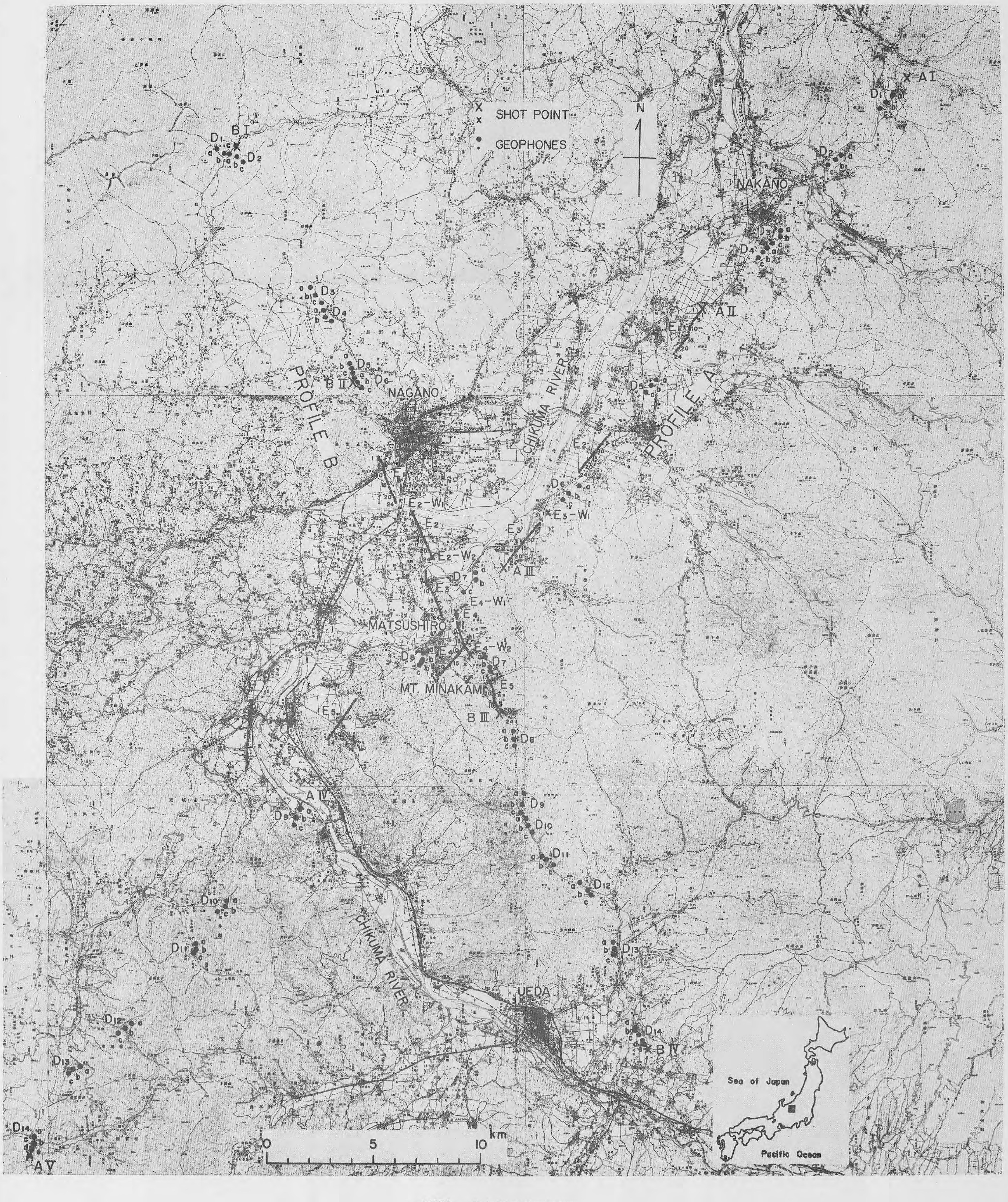

PART I Fig. 2 Shot and observation points

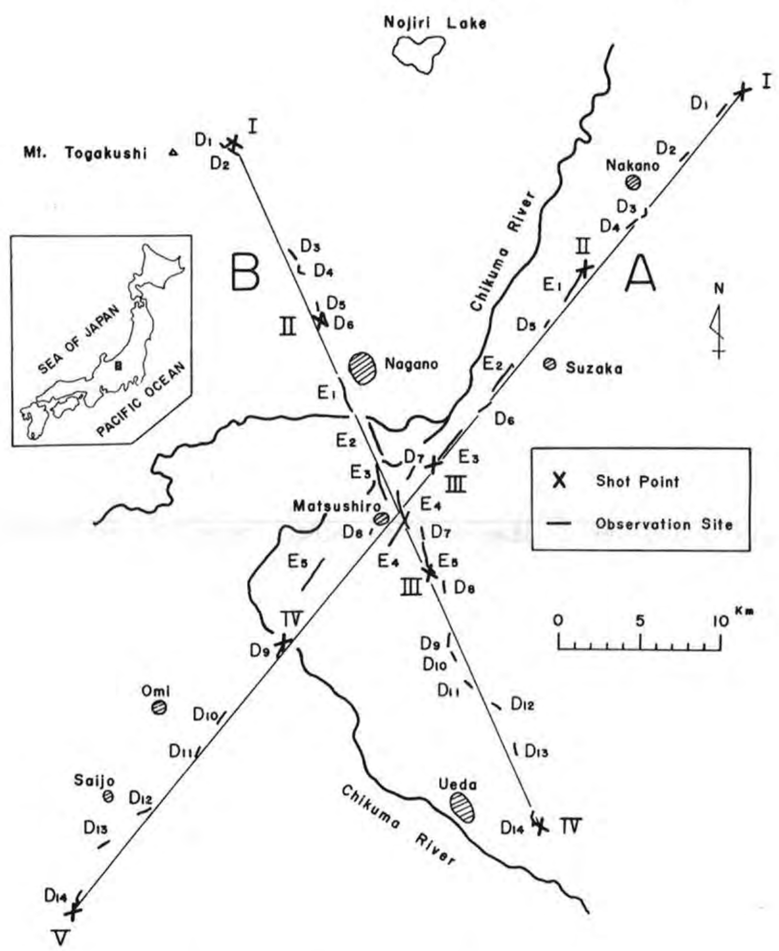

PART II Fig. 1 (a) Shot and observation points

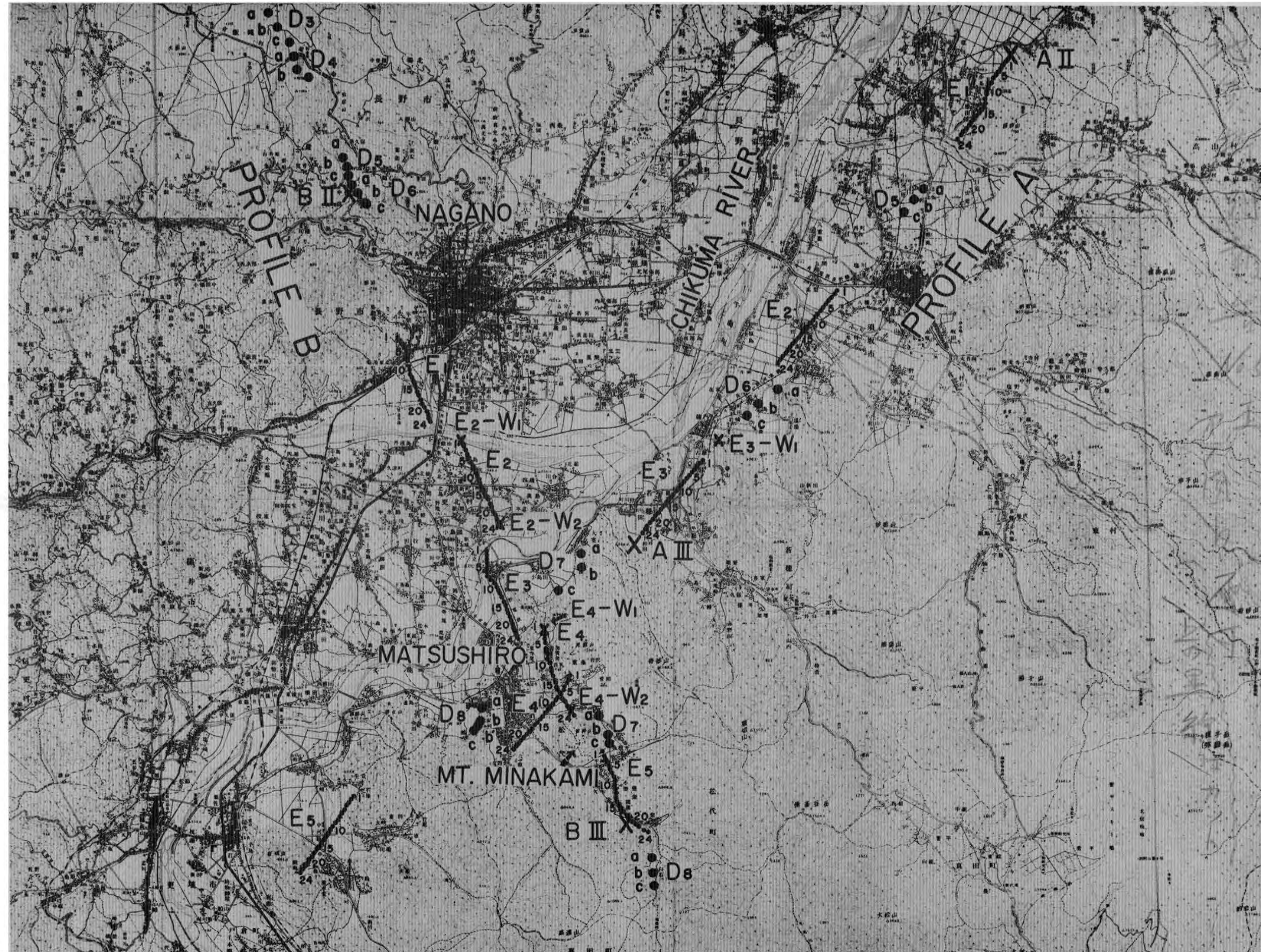

PART II Fig. 1 (b) A part of shot and observation points